UNIVERSITÀ DEGLI STUDI DI TRENTO

*Department of*
*Physics*
*Trento, Italy*

*School of Mathematics,*
*Statistics & Physics*
*Newcastle upon Tyne, UK*

# Dynamical excitations in low-dimensional condensates:

## sound, vortices and quenched dynamics

Fabrizio Larcher

Thesis submitted for the degree of
Doctor of Philosophy

under the joint supervision of
Prof. Franco Dalfovo
Prof. Nikolaos P. Proukakis

April 2018

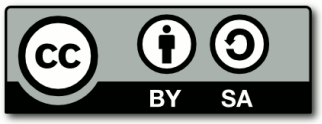

**Abstract**

The dynamics of systems out of equilibrium, such as the phase transition process, are very rich, and related to largely scalable problems, from very small ultracold gases to large expanding galaxies. Quantum low-dimensional systems show interesting features, notably different from the canonical three-dimensional case. Bose-Einstein condensates are very good platforms to study macroscopic quantum phenomena. These three points describe well the motivation behind the study presented in this work.

In this thesis, some dynamical problems of trapped and uniform condensates are studied, both at zero and finite temperature. In particular, we focus on the analysis of the propagation of linear and nonlinear excitations in a quasi-1D and in quasi-2D systems. In the first case, we are able to correctly describe the dynamics of a solitonic vortex in an elongated condensate, as measured by Serafini *et al.* [Phys. Rev. Lett. **115**, 170402 (2015)]. In the second case, we reproduce the decay rate of a phase-imprinted soliton (collaboration with Birmingham), and assess its dependence on the temperature. We also replicate the propagation speed of sound waves over a wide range of temperatures as in Ville *et al.* [arXiv:1804.04037] (collaboration with Collège de France). The result of this analysis is included in Ota *et al.* [arXiv:1804.04032], which is currently under revision.

In uniform low-dimensional systems Bose-Einstein condensation is technically not possible, and in two dimensions it is replaced by the Berezinskii-Kosterlitz-Thouless superfluid phase transition. We study its critical properties by analysing the spontaneous generation of vortices during a quench, produced via the Kibble-Zurek mechanism. This procedure predicts, for any dimension, the scaling for the density of defects formed during a fast transition, when the system is not adiabatically following the control parameter, and regions of phase inhomogeneity are formed. We address the role of reduced dimensionality on this process. All finite temperature simulations are performed by means of the stochastic (projected) Gross-Pitaevskii equation, a model fully incorporating density and phase fluctuations for weakly interacting Bose gases.

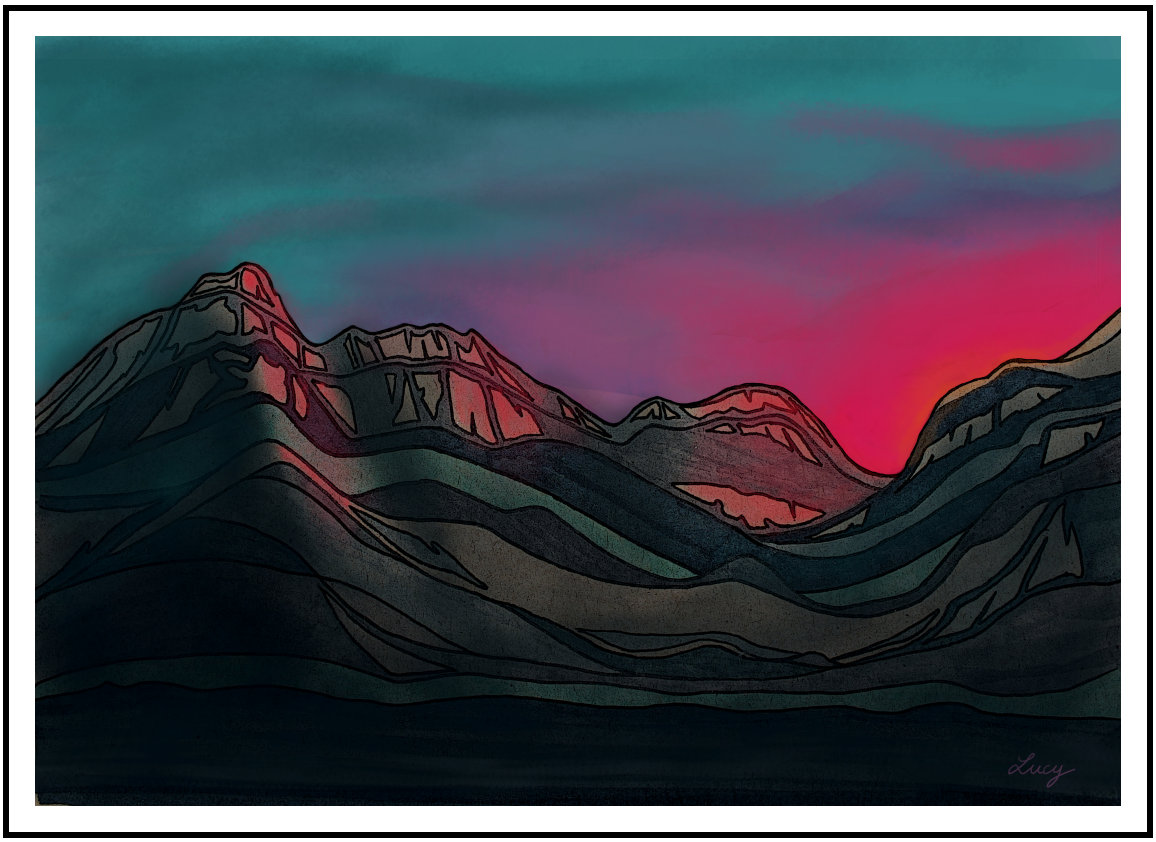

*A Caterina, donna straordinaria.*

*"Peregrinaggio di tre giovani figliuoli del re di Serendippo"* (The Three Princes of Serendip) is an old fairy tale published by a Venetian editor, in 1557. The editor claimed that the story arrived in his hands from a Persian writer and translator, Cristoforo Armeno, who was a narrator of the culture of ancient Iran in Italy and in Europe. The story goes that three princes from Serendip, the ancient Persian name for Sri Lanka, were wandering in a foreign country, being tested by their father on their worthiness to succeed him. By means of their spirit of observation, cleverness and, ultimately, unexpected luck, they were able to gather a large fortune and the favour of the Persian emperor, and they came home, safe and sound, to their satisfied king. Their adventures were the inspiration for Horace Walpole to coin the expression "serendipity", meaning the luck to make fortunate discoveries by following unforeseen paths.

Scientists often find themselves wandering in the foreign country of research, and they can only succeed in finding their way, by replicating the virtues of the good princes. It is not always an easy journey, and there are many dead ends. However, it becomes much easier (and funnier) when it is faced together with good companions. This is the reason why I would like to acknowledge some of the people that shared these years with me, and without whom this work would not exist.

Let me start by thanking my two supervisors, Franco Dalfovo and Nick Proukakis,

for their constant scientific and human support. Despite the complications of distance and regulations, your supervision has always been fully careful, and essential in getting to this final stage. I would also like to thank Jean Dalibard and Jérôme Beugnon, for allowing me to spend a very interesting stage at the Collège de France, and for their kindness and support during my stay. I would like to mention Nadine Meyer and Giovanni Barontini for the use of their data in this work, and Gabriele Ferrari and Giacomo Lamporesi, for their attention and courtesy during our collaboration, and beyond that.

These years also brought me in a lot of interesting discussions with many researchers, and I would like to particularly thank Lev Pitaevskii, Sandro Stringari, Carlo Barenghi, Boris Malomed, and Leticia Cugliandolo.

Having spent my PhD in between different countries, I had the pleasure to meet a great variety of people. A special thanks goes to my dear Geordie companions: Paolo Comaron and Luca Galantucci, with whom I had the pleasure to spread some Italian culture in the far North, Thomas Bland, and his lovely feathered spear, Klejdia Xhani and Donatello Gallucci. A special mention goes to Kean Loon Lee and I-Kang Liu, for helping me out and for many nice chats. I would like to acknowledge the Rubidium team at Collège de France, and especially Jean-Loup Ville and Raphaël Saint-Jalm. A big hurray goes to all the guys at the BEC lab in Trento.

Then, of course, there is life outside physics. I would like to thank all my friends, for their constant support and love: Zeno and Francesco, who are more than brothers; Lorenzo, Michele, Martino and Simone, real friends without whom I would not be here, my dear housemates of all time, my fellow singers of the University Choir; then Diana, Simone, Stefano and Luca, and all my dearest friends from Bolzano, scattered around the globe. A special thank and a hug to Lucia, for having realised the amazing painting of my “Serendipity”, and for her friendship.

Infine, il più grande ringraziamento va alla mia famiglia, a mia madre Mariateresa ed a mio padre Renato, che mi sostengono attraverso tutte le questioni più importanti della vita, con amore e dedizione, e che mi sono di ispirazione ogni giorno.

# Contents

# Introduction

In the last decades, ultracold atomic gases have proven to be a versatile toolbox for investigating fundamental problems in many-body physics[1–3]. The high controllability of the trapping potentials, and the possibility to tune important properties such as the inter-atomic interactions, allow to study a great variety of configurations and phenomena. Among these, low-dimensional systems have recently acquired a widespread interest in the community, particularly concerning two aspects: the study of phase transitions and their dynamical behaviour. Phase transitions are a phenomenon that goes beyond the boundaries of a single physical system and can be found at very different scales, both at a classical and at a quantum level: from microscopic ultracold atomic gases, condensed matter systems and photonic devices, to huge galaxy clusters[4]. The dimensionality of the sample can have a strong effect in limiting the kind of phase transitions allowed to occur in it. Moreover, the dynamical properties of systems in reduced dimensions can also show interesting new features, when compared to the canonical three-dimensional case. Let us start by briefly introducing some historical steps leading to the notorious Bose-Einstein condensation.

## A long journey: Bose-Einstein condensation

Bose-Einstein condensation (BEC) is a clear example of serendipity[5]: enriching new physics can arise from unexpected paths. It is nowadays regarded as one of the great manifestations of the quantum nature of the microscopic world, despite having been first postulated in 1924, one year before Werner Heisenberg and Erwin Schrödinger gave the first formulation of quantum mechanics[1]. Satyendra Bose was having some

[1] Even more so, Schrödinger first met the concept of "de Broglie wavelength" in Einstein's paper about BEC, hence one could say that the concept of *wavefunction* itself was pushed by Bose-Einstein condensation, and not the other way around!


[1] F. Dalfovo et al. In: *Rev. Mod. Phys.* 71 (1999), pp. 463–512.

[2] I. Bloch, J. Dalibard, and W. Zwerger. In: *Rev. Mod. Phys.* 80 (2008), pp. 885–964.

[3] S. Giorgini, L. P. Pitaevskii, and S. Stringari. In: *Rev. Mod. Phys.* 80 (2008), pp. 1215–1274.

[4] A. A. Starobinsky. In: *Physics Letters B* 117.3 (1982), pp. 175–178.

[5] M. Delbruck. In: *J. Chem. Ed.* 57.7 (1980), p. 467.

difficulties in getting his work on the quantum statistics of photons accepted, and sent the English manuscript to Albert Einstein to get his opinion. Einstein was highly impressed by the work of the brilliant Indian physicist, and translated it himself to German in order to have it published[6] in "Zeitschriff für Physik", at the time the most important journal for physics. He then further developed the ideas of that paper in two consecutive publications[7,8], so to also include some concepts that a young Louis de Broglie had just developed in his PhD thesis: matter particles can behave as waves, and thus they should obey the same statistics. Initially the paper produced little effect, and was almost forgotten, but after the discovery of superfluidity in liquid helium (Pëtr Kapitza[9], 1938) Fritz London[10] realised that it might have been related to Bose-Einstein condensation, and that Einstein's relation for the transition temperature of the ideal gas, $T_{\mathrm{BEC}}$, was a close estimation of the observed superfluid transition temperature. This revamped the interest in this topic, especially from a theoretical point of view: Lev Landau[11] (1941) formulated the two-fluid model for superfluidity, Nikolay Bogoliubov[12] (1947) the first microscopic theory for interacting Bose gases, Oliver Penrose (1951) and Lars Onsager (1956) connected[13] the BEC with the occurrence of off-diagonal long-range ordering. Experiments on superfluid liquid helium showed indeed a good agreement with Landau's prediction for the excitation spectrum, and were able to measure the condensate fraction by means of the momentum dis-

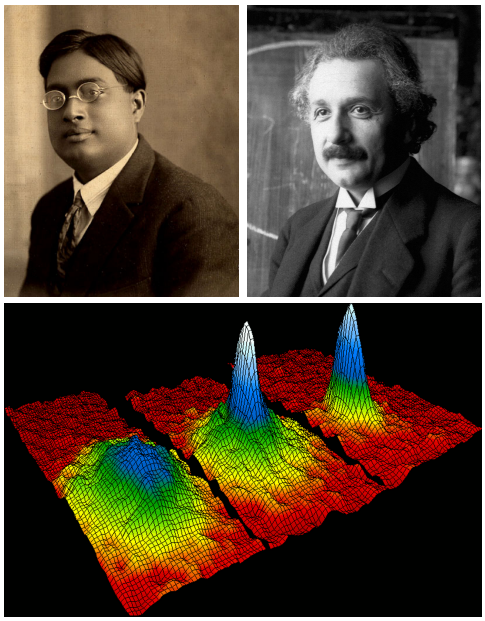

Bose, Einstein and the condensation.[2]

[2] Incidentally, a great name for a folk rock band.

[6] Bose. In: *Zeitschrift für Physik* 26.1 (1924), pp. 178–181.
[7] A. Einstein. In: *Sitz. der Preus. Akad. der Wiss.* (1924).
[8] A. Einstein. In: *Sitz. der Preus. Akad. der Wiss.* (1925).
[9] P. Kapitza. In: *Nature* 141 (1938), p. 74.
[10] F. London. In: *Nature* 141 (1938), p. 643.
[11] L. D. Landau. In: *Phys. Rev.* 60 (1941), pp. 356–358. (original Rus.) Zh. Eksp. Teor. Fiz. 11 (1941) p. 592.
[12] N. N. Bogoliubov. In: *J. Phys U.S.S.R.* 11.1 (1947), p. 23.
[13] O. Penrose and L. Onsager. In: *Phys. Rev.* 104 (1956), pp. 576–584.

tribution. Onsager[14] (1949) and Richard Feynman[15] (1955) further predicted the existence of vortices with quantised circulation, which were later discovered by Henry Hall and Joe Vinen[16] in 1956.

On the experimental side, Bose-Einstein condensation remained a chimera for a long time. The connection of condensation with helium superfluidity was fruitful but non-conclusive: due to the strong interactions between helium atoms, a complete condensation can not occur in such a system, and only a small fraction of the atoms is condensed at low temperature. Einstein predicted condensation for non-interacting particles, thus prompting the research for weakly interacting gases that could be effectively trapped and cooled down. The first suggestions came from Charles Hecht[17], pointing out the small interactions of spin-polarised hydrogen at low temperatures. This stimulated several experiments throughout the 70s and 80s (e.g. Isaac Silvera and Jook Walraven[18]), but, however close to the required degeneracy, this was not reached until 1998 by Thomas Greytak and Daniel Kleppner[19]. A noteworthy contribution to the field has been carried out by the study of laser cooling by Stephen Chu, Claude Cohen-Tannoudji and William Phillips over three decades[3], but the major breakthrough finally came by applying a series of different techniques at the same time. Indeed, by combining laser cooling and evaporation, the groups of Eric Cornell and Carl Wieman[20] at JILA, and of Wolfgang Ketterle[21] at MIT, were finally able to reach the required densities and temperature for the condensation in 1995, seventy years after its first formulation. For this achievement they shared the Nobel Prize in Physics in 2001. These first realisations usually involved the alkali atoms, given their energetic internal structure, suitable for trapping and cooling, but condensation has been achieved also in other systems, including fermionic gases[22], magnons[23], photons[24] and exciton-polaritons[25].

[3] Nobel Prize in Physics 1997.

[14] L. Onsager. In: *Il Nuovo Cimento* 6 (1949), pp. 279–287.

[15] R.P. Feynman. *Chapter II Application of Quantum Mechanics to Liquid Helium.* Ed. by C. J. Gorter. Vol. 1. Supplement C. Elsevier, 1955, pp. 17–53.

[16] H. E. Hall and W. F. Vinen. In: *Proceedings of the Royal Society of London A: Mathematical, Physical and Engineering Sciences* 238.1213 (1956), pp. 215–234.

[17] C. E. Hecht. In: *Physica* 25.7 (1959), pp. 1159–1161.

[18] Isaac F. Silvera and J. T. M. Walraven. In: *Phys. Rev. Lett.* 44 (1980), pp. 164–168.

[19] Dale G. Fried et al. In: *Phys. Rev. Lett.* 81 (1998), pp. 3811–3814.

[20] M. H. Anderson et al. In: *Science* 269.5221 (1995), pp. 198–201.

[21] K. B. Davis et al. In: *Phys. Rev. Lett.* 75 (1995), pp. 3969–3973.

[22] C. A. Regal, M. Greiner, and D. S. Jin. In: *Phys. Rev. Lett.* 92 (2004), p. 040403.

[23] Fang Fang et al. In: *Phys. Rev. Lett.* 116 (2016), p. 095301.

[24] J. Klaers et al. In: *Nature* 468 (2010), p. 545.

[25] J. Kasprzak et al. In: *Nature* 443 (2006), p. 409.

**Phenomenology of Bose-Einstein condensation.** Particle indistinguishability lies at the foundations of quantum mechanics, and ultimately determines its statistical nature. The Heisenberg uncertainty principle, i.e. the impossibility to know simultaneously the position and the momentum of a particle, negates the deterministic approach allowed by classical mechanics. Particles can no longer be seen as discrete entities but in certain regimes show wave-like properties, and collective behaviours. Their quantum mechanical description has to be inherently statistical, and it is hence implemented by means of a *wavefunction*, whose square modulus describes the probability density for the particles. In a many-body system, two outcomes are possible when exchanging two particles: either the wavefunction maintains its sign (and is therefore *symmetric* under particle exchange), or it changes it (*antisymmetric*). In the first case the particles are called *bosons* and have integer spin, while in the second they are referred to as *fermions*, with half-integer spin. The antisymmetry of the wavefunction implies that two fermions cannot share the same quantum state, and cannot be described by the same wavefunction. This is known as the Pauli exclusion principle for fermions, and has no counterpart for bosons: they can lie in the same quantum state, with no limitations.

The quantum nature of a Bose gas becomes apparent in certain regimes. Two length scales play an important role in the definition of the transition. In three dimensions these are:

- the average distance between the particles $n^{-1/3}$, given in terms of the inverse density of the system $n = N/V$, where $N$ is the number of atoms and $V$ is their volume;
- the thermal de Broglie wavelength, which, for a particle of mass $m$ and temperature $T$ is
$$\lambda_T = \sqrt{\frac{2\pi\hbar^2}{m k_{\mathrm{B}} T}}, \tag{1}$$
where $\hbar$ is the reduced Planck constant and $k_{\mathrm{B}}$ is the Boltzmann constant.

In our everyday experience, the values of the temperature and of the masses of common objects are such that $\lambda_T$ is effectively very small. In this regime, when $\lambda_T \ll n^{-1/3}$, the particles see each other as discrete classical objects. Both fermions and bosons will distribute according to the classical Boltzmann statistics. However, decreasing the temperature means to increase the value of $\lambda_T$, meaning that eventually one can reach a phase in which $\lambda_T \geqslant n^{-1/3}$. This is the so-called *quantum degenerate* regime, in which the notion of a particle trajectory is not defined, and indistinguishability plays an important role.

The result of the work of Bose and Einstein is the formulation of the Bose-Einstein statistics for a gas of bosons

$$n(E_s) = \frac{1}{e^{(E_s-\mu)/k_\mathrm{B}T} - 1} \tag{2}$$

in terms of the energy $E_s$ of the single particle state $s$, the chemical potential $\mu$ and the temperature $T$. A notable consequence of the statistics defined in equation (2) is that, in three dimensions, it naturally predicts a macroscopic occupation of a single particle state at low temperature, in the thermodynamic limit (see Appendix C). This accumulation of particles in a single mode of the system is the essence of Bose-Einstein condensation. For a free ideal Bose gas, the particles condense in the zero momentum state, corresponding to the state at minimum energy. The critical point for this transition is determined[26], in three dimensions and in free space, by the condition

$$n\lambda_T^3 \geq \zeta(3/2), \tag{3}$$

where $\zeta(3/2) \simeq 2.612$ is the Riemann zeta function. The *phase-space density* $n\lambda_T^3$ effectively represents the number of particles lying in a volume set by the de Broglie wavelength. The above criterion can be reformulated in terms of a critical temperature

$$T_c = \frac{2\pi\hbar^2}{mk_\mathrm{B}} \left( \frac{n}{\zeta(3/2)} \right)^{2/3}, \tag{4}$$

which determines the fraction of atoms in the lowest energy level, the so-called *condensed fraction*

$$n_0 = \frac{N_0}{N} = 1 - \left( \frac{T}{T_c} \right)^{3/2}. \tag{5}$$

In typical experimental systems, the atoms are confined in a magneto-optical trap (MOT), combining the use of magnetic trapping and laser cooling techniques to reach condensation. One of the most common configurations for the trapping potential is the harmonic confinement

$$V_\mathrm{tr} = \frac{1}{2} m(\omega_x x^2 + \omega_y y^2 + \omega_z z^2) \tag{6}$$

being $(\omega_x, \omega_y, \omega_z)/2\pi$ the trapping frequencies in the three directions. The non-uniformity of the system causes a redefinition of the critical quantities, and the critical temperature is

$$T_c^\mathrm{ho} = \frac{\hbar}{k_\mathrm{B}} (\omega_x\omega_y\omega_z)^{1/3} \left( \frac{N}{\zeta(3)} \right). \tag{7}$$

[26] L. Pitaevskii and S. Stringari. *Bose-Einstein Condensation and Superfluidity.* Oxford University Press, 2016.

The typical values of the critical temperatures for experimentally achievable number of atoms in the trap is of the order of $10^{-7}$ K. Such extreme conditions explain the difficulty in realising the technology needed to reach condensation. Moreover, at such low temperatures, the stable thermodynamic phase is the solid state. To maintain the system in a gaseous form, it is therefore necessary to use low densities of the order of $10^{-14}$ cm$^{-3}$, to avoid the clustering of atoms. Being so dilute means that the distance between the atoms is rather large, and the details of the interatomic potential at short scales become negligible. Furthermore, the high-energy scattering processes, involving high angular momenta, are suppressed by the low temperature in the system. It is therefore possible to describe the interaction among the atoms as an effective contact potential, parametrised by a single quantity, the *s-wave* scattering length $a$ (see more on that in Chapter 1).

An important remark is that the above discussion is only valid in three dimensions. In a system of reduced dimensionality, the Mermin-Wagner-Hohenberg theorem prevents the formation of a true BEC. The thermal fluctuations become more relevant in reduced dimensions, and are able to destroy the long-range coherence of the system at any finite temperature. However, a two-dimensional infinite system can still exhibit a superfluid phase transition, the celebrated Berezinskii-Kosterlitz-Thouless (BKT) phase transition. A detailed discussion about the BKT transition and its consequences is reported in Chapter 4.

## Thesis outline

The purpose of this work, and of my PhD, is to understand some of the aspects related to the dynamical properties of low-dimensional Bose-Einstein condensates, at equilibrium and when driven across a phase transition. The thesis is structured as follows:
Part I is dedicated to the study of zero temperature systems.

- *Chapter* 1: Description of the Gross-Pitaevskii equation. Solitonic solution and its properties. Superfluidity and hydrodynamic equations. Bogoliubov approach to first-order excitations in a Bose-Einstein condensate.

- *Chapter* 2: Description of the experimental setup in [27]. Theoretical description of the motion of solitonic vortices in a cigar-shaped BEC, and modifications due to the particle reduction. Comparison with the experiment and further results on vortex interactions.

[27] S. Serafini et al. In: *Phys. Rev. Lett.* 115 (2015), p. 170402.

Part II is dedicated to the study of finite temperature systems.

- *Chapter* 3: Description of the theoretical framework for the stochastic Gross-Pitaevskii equation and the stochastic projected Gross-Pitaevskii equation. Numerical implementation for the two models and details on analysis of the results: Penrose-Onsager diagonalisation and computation of the order parameter.

- *Chapter* 4: Description of the Berezinskii-Kosterlitz-Thouless phase transition for two-dimensional systems, and of its principal properties. Introduction to the Kibble-Zurek mechanism for fast quenches across a continuous phase transition. Numerical results for the thermal equilibrium of a two-dimensional system with periodic boundary conditions. Analysis on the critical point for the transition. Dynamical scalings for the correlation length in an instantaneous quench in temperature and chemical potential. Slow quenches in the two parameters and scaling for the number of defects. Interaction quench and dynamical scaling for the correlation length.

- *Chapter* 5: Description of two experiments concerning the dynamics of excitations in low-dimensional atomic gases. Decay of a phase-imprinted grey soliton in a quasi-2D elongated condensate, for different temperatures. Theoretical background for the propagation of sound in a two-dimensional system. Description of the experiment at the Collège de France on the measurement of the speed of sound across the BKT phase transition. Numerical analysis and comparison with the experimental results.

Finally, some general conclusions are drawn, followed by some useful appendices and the references.

## Collaborations

Science, however historically driven by influential polymaths and creative flairs, is nowadays a collaborative effort. In the endeavour of my PhD, I enrolled in a joint programme between Università degli Studi di Trento and Newcastle University, co-supervised by Prof. Franco Dalfovo on the Italian side and by Prof. Nick Proukakis on the British side. I also had the opportunity to do a research stage of one month at the Collège de France in Paris, under the supervision of Prof. Jean Dalibard. I have directly collaborated with three experimental groups. Chapter 2 is the result of a collaboration with the experimental group at the BEC Center in Trento, coordinated by Gabriele Ferrari and Giacomo Lamporesi. The first experiment described in Chapter 5 has taken place at the University of Birmingham, in the group of Prof. Kai Bongs, directed

by Nadine Meyer and Giovanni Barontini. The second part of Chapter 5 describes an experiment at the Collège de France, coordinated by Jérôme Beugnon and Sylvain Nascimbène. The following analysis has been carried out with Miki Ota, Lev Pitaevskii and Sandro Stringari in Trento. In these years I met numerous researchers and shared fruitful discussions related with topics addressed in this thesis. In particular, I would like to mention Carlo Barenghi and Luca Galantucci, for discussions on Chapter 2, and Leticia Cugliandolo and Boris Malomed, who gave their insight on the analysis in Chapter 4.

# Part I

# Zero-temperature analysis

# Chapter 1

# Gross-Pitaevskii theory

In this first chapter we present some theoretical tools needed to describe Bose-Einstein condensates at zero temperature. We start from the notorious Gross-Pitaevskii equation, then we introduce some important remarks on the excitations for these systems. We describe the solitonic solutions of the Gross-Pitaevskii equation and review their main properties. We address the concept of superfluidity and quantised vorticity and we briefly present the hydrodynamic equations for a condensate. Finally we review the Bogoliubov approach for the computation of the first-order phononic excitations.

## 1.1 The Gross-Pitaevskii equation

The Gross-Pitaevskii equation (GPE) is a very successful tool to describe a dilute quantum gas of bosons at zero temperature. It was independently formulated by Eugene P. Gross[28] and Lev P. Pitaevskii[29] in 1961, and is a mean field approximation of the complete field equation. Below we report a short derivation of the equation; an alternative approach can be found in the Les Houches lectures of Yvan Castin[30], which also cover other theoretical aspects of Bose-Einstein condensation. Bose-Einstein condensation is a phenomenon concerning a large number

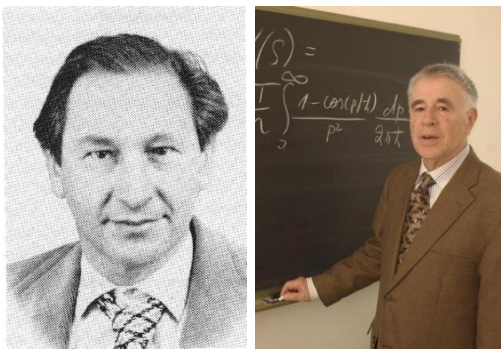

Gross and Pitaevskii

[28] E. P. Gross. In: *Il Nuovo Cimento* 20 (1961), pp. 454–457.

[29] L. P. Pitaevskii. In: *Soviet Physics JETP-USSR* 13.2 (1961). (original Rus.) Zh. Eksp. Teor. Fiz. 40 (1961) p. 646.

[30] Y. Castin. "Bose-Einstein Condensates in Atomic Gases: Simple Theoretical Results". In: *Coherent atomic matter waves*. Ed. by R. Kaiser, C. Westbrook, and F. David. 2001, p. 1.

of bosons, at very low energy. Let us then consider a gas of $N$ bosons, interacting via a two-body isotropic potential $\hat{V}_{\text{int}}$, hence only depending on the interparticle distance, such that its functional representation is $V_{\text{int}}(|\mathbf{r}_i - \mathbf{r}_j|) = V_{\text{int}}(|\mathbf{r}_j - \mathbf{r}_i|)$. In the space of the spatial coordinate $\mathbf{r}$ we therefore require the matrix elements of the two-particle operator to be

$$\langle \mathbf{r}_i \mathbf{r}_j | \hat{V}_{\text{int}} | \mathbf{r}'_i \mathbf{r}'_j \rangle = \delta(\mathbf{r}_i - \mathbf{r}'_i)\delta(\mathbf{r}_j - \mathbf{r}'_j) V_{\text{int}}(|\mathbf{r}_i - \mathbf{r}_j|). \tag{1.1}$$

In the Fock space, the interaction potential operator is represented as

$$\hat{V}_{\text{int}} = \frac{1}{2} \int d\mathbf{r} \int d\mathbf{r}' \hat{\Psi}^\dagger(\mathbf{r}, t) \hat{\Psi}^\dagger(\mathbf{r}', t) V_{\text{int}}(|\mathbf{r} - \mathbf{r}'|) \hat{\Psi}(\mathbf{r}', t) \hat{\Psi}(\mathbf{r}, t) \tag{1.2}$$

and the time-dependent Hamiltonian in coordinate representation is written in the second quantisation formalism as

$$\begin{aligned} \hat{H}(t) = &\int d\mathbf{r}\, \hat{\Psi}^\dagger(\mathbf{r}, t) \left( -\frac{\hbar^2 \nabla^2}{2m} + V_{\text{tr}}(\mathbf{r}, t) \right) \hat{\Psi}(\mathbf{r}, t) \\ &+ \frac{1}{2} \int d\mathbf{r} \int d\mathbf{r}'\, \hat{\Psi}^\dagger(\mathbf{r}, t) \hat{\Psi}^\dagger(\mathbf{r}', t) V_{\text{int}}(|\mathbf{r} - \mathbf{r}'|) \hat{\Psi}(\mathbf{r}', t) \hat{\Psi}(\mathbf{r}, t), \end{aligned} \tag{1.3}$$

where $V_{\text{tr}}$ is the trapping potential for the atoms, and $m$ is their mass.
If we consider a very low temperature, it is sufficient to ensure that the condition

$$n|a|^3 \ll 1 \tag{1.4}$$

holds, for the low-energy $s$-wave collisions to dominate the atomic interactions. Here we defined $n = N/V$ the gas density and $a$ the $s$-wave scattering length. Atoms can then be considered as point-like particles colliding elastically, and one can exclusively consider the contact potential

$$V_{\text{int}}(|\mathbf{r} - \mathbf{r}'|) = g\delta(\mathbf{r} - \mathbf{r}'), \tag{1.5}$$

where $\delta$ is the Dirac delta, and we identify the coupling constant $g$ as

$$g = \frac{4\pi\hbar^2 a}{m}. \tag{1.6}$$

By substituting (1.5) into (1.3), and integrating out the $\mathbf{r}'$ coordinate we get

$$\hat{H}(t) = \int d\mathbf{r}\, \hat{\Psi}^\dagger(\mathbf{r}, t) \hat{H}_0 \hat{\Psi}(\mathbf{r}, t) + \frac{g}{2} \int d\mathbf{r}\, \hat{\Psi}^\dagger(\mathbf{r}, t) \hat{\Psi}^\dagger(\mathbf{r}, t) \hat{\Psi}(\mathbf{r}, t) \hat{\Psi}(\mathbf{r}, t), \tag{1.7}$$

where we defined the Hamiltonian of an ideal gas confined in a trap $V_{\rm tr}$

$$\hat{H}_0 = \left( -\frac{\hbar^2 \nabla^2}{2m} + V_{\rm tr}(\mathbf{r}, t) \right). \tag{1.8}$$

The Heisenberg equation determines the time evolution of the operator $\hat{\Psi}(\mathbf{r}, t)$:

$$i\hbar \frac{\partial \hat{\Psi}(\mathbf{r}, t)}{\partial t} = \left[ \hat{\Psi}(\mathbf{r}, t), \hat{H}(t) \right]. \tag{1.9}$$

By means of the (equal-time) bosonic commutation relations

$$\begin{aligned} \left[ \hat{\Psi}(\mathbf{r}), \hat{\Psi}(\mathbf{r}') \right] &= \left[ \hat{\Psi}^\dagger(\mathbf{r}), \hat{\Psi}^\dagger(\mathbf{r}') \right] = 0; \\ \left[ \hat{\Psi}(\mathbf{r}), \hat{\Psi}^\dagger(\mathbf{r}') \right] &= \delta(\mathbf{r} - \mathbf{r}'), \end{aligned} \tag{1.10}$$

where

$$[\hat{A}, \hat{B}]\phi = \hat{A}(\hat{B}\phi) - \hat{B}(\hat{A}\phi), \tag{1.11}$$

one can simplify the expression (1.9) and get

$$i\hbar \frac{\partial \hat{\Psi}(\mathbf{r}, t)}{\partial t} = \left( -\frac{\hbar^2 \nabla^2}{2m} + V_{\rm tr}(\mathbf{r}, t) \right) \hat{\Psi}(\mathbf{r}, t) + g \hat{\Psi}^\dagger(\mathbf{r}, t) \hat{\Psi}(\mathbf{r}, t) \hat{\Psi}(\mathbf{r}, t). \tag{1.12}$$

The main concept of Bose-Einstein condensation concerns the macroscopic occupation of the same quantum state by a large number of identical bosons. One can therefore separate the Bose field operator in terms of a highly populated term $\psi(\mathbf{r}, t) = \langle \hat{\Psi}(\mathbf{r}, t) \rangle$ and a fluctuation term $\delta\hat{\Psi}(\mathbf{r}, t)$:

$$\hat{\Psi}(\mathbf{r}, t) = \psi(\mathbf{r}, t) + \delta\hat{\Psi}(\mathbf{r}, t). \tag{1.13}$$

The complex function $\psi(\mathbf{r}, t)$ is defined as the mean value of the field operator, and its square modulus fixes the condensate density through the relation $n(\mathbf{r}, t) = |\psi(\mathbf{r}, t)|^2$. It is thus a classical field, and represents the order parameter of the BEC phase transition. At $T = 0$ it is possible to neglect the fluctuations in the expansion (1.13), and equation (1.12) becomes

$$\boxed{i\hbar \frac{\partial}{\partial t} \psi(\mathbf{r}, t) = \left( -\frac{\hbar^2 \nabla^2}{2m} + V_{\rm tr}(\mathbf{r}, t) + g|\psi(\mathbf{r}, t)|^2 \right) \psi(\mathbf{r}, t),} \tag{1.14}$$

which is the celebrated Gross-Pitaevskii equation (GPE).

The corresponding energy functional can be recovered by applying (1.13) to the

Hamiltonian (1.7), while discarding the fluctuations $\delta\hat{\Psi}(\mathbf{r},t)$, and it is

$$E(t) = \int d\mathbf{r} \left( -\frac{\hbar^2}{2m}|\nabla\psi(\mathbf{r},t)|^2 + V_{\rm tr}(\mathbf{r},t)|\psi(\mathbf{r},t)|^2 + \frac{g}{2}|\psi(\mathbf{r},t)|^4 \right). \tag{1.15}$$

In the common case in which the potential is constant in time $V_{\rm tr}(\mathbf{r},t) = V_{tr}(\mathbf{r})$, the GPE admits stationary solutions, meaning wave functions with constant norm. The time evolution of the condensate is dictated by

$$\psi(\mathbf{r},t) = \psi_0(\mathbf{r})e^{-i\frac{\mu}{\hbar}t}, \tag{1.16}$$

and the GPE reduces to its stationary version

$$\boxed{\left( -\frac{\hbar^2\nabla^2}{2m} + V_{\rm tr}(\mathbf{r}) + g|\psi_0(\mathbf{r})|^2 \right)\psi_0(\mathbf{r}) = \mu\psi_0(\mathbf{r}).} \tag{1.17}$$

In equation (1.17), $\psi(\mathbf{r})$ minimizes the expectation value of the Hamiltonian, under the constraint that the number of atoms $N$ is conserved and

$$\int d\mathbf{r}|\psi(\mathbf{r})|^2 = N. \tag{1.18}$$

Then, the Lagrange multiplier $\mu$ can be identified with the chemical potential of the system. In the limit in which the interactions dominate over the kinetic energy effects, one can apply the simple reasoning of discarding the first term in equation (1.17), and perform the so-called *Thomas-Fermi approximation*, for which

$$|\psi_{\rm TF}(\mathbf{r})|^2 = \frac{1}{g}\left(\mu - V_{\rm tr}(\mathbf{r})\right)\Theta(R_{\rm TF} - |\mathbf{r}|). \tag{1.19}$$

This approximation is valid when the number of atoms is large and the density varies smoothly in space over the relevant length scales. Here $\Theta(x)$ is the Heaviside theta function, ensuring that the sign of the density remains positive, and $R_{\rm TF}$ is the Thomas-Fermi radius, representing the boundary of the condensate. In the noteworthy case of a harmonic confinement, where

$$V_{\rm tr}(\mathbf{r}) = \frac{1}{2}m(\omega_x^2x^2 + \omega_y^2y^2 + \omega_z^2z^2), \tag{1.20}$$

the Thomas-Fermi density profile takes the shape of an inverted parabola and the radii in the three directions are

$$R_i = \sqrt{2\mu/m\omega_i^2}. \tag{1.21}$$

Instead, if the density varies on short length scales, the first term in the stationary

Gross-Pitaevskii equation (1.17), the so-called *quantum pressure*, is not negligible. In this case it is convenient to introduce a new quantity: the healing length. For simplicity, let us consider the one-dimensional version of the equation (1.14):

$$i\hbar\frac{\partial}{\partial t}\psi(x,t) = \left(-\frac{\hbar^2}{2m}\frac{\partial^2}{\partial x^2} + V_{\rm tr}(x) + g_{\rm 1D}|\psi(x,t)|^2\right)\psi(x,t), \tag{1.22}$$

where $g_{\rm 1D}$ is the properly rescaled effective one-dimensional interaction strength, obtained with a procedure analogous to the one for $g_{\rm 2D}$ in Chapter 3. Consider then a condensate confined in a static box with infinitely hard walls. At the walls the wavefunction (and the density) must vanish, while in the centre of the box the density approaches its bulk value. One can compute the length over which the density "heals", and rises from zero to its uniform value. This is the so-called *healing length* $\xi$, and can be computed from eq. (1.22). Far from the wall, the wave function is determined by the competition between the kinetic energy and the interaction energy. If we suppose that the two compensate each other over the spatial scale $\xi$, we have that $\hbar^2/2m\xi^2 = ng$, hence

$$\xi = \sqrt{\frac{\hbar^2}{2mng}} = \frac{1}{8\pi na}. \tag{1.23}$$

### 1.1.1 Solitons in a Bose-Einstein condensate

An interesting class of solutions of the one-dimensional Gross-Pitaevskii equation (1.22) is represented by the so-called *solitons*. The concept of soliton is ubiquitous in physics. It basically consists of a localized self-reinforcing solitary wave, at rest or moving at constant speed, maintaining its shape in time. Solitons can also collide with each other without any substantial change, apart from a phase shift. Their existence is directly related to the self-focussing non-linearity of the GPE, which compensates the dispersive quantum pressure term arising from the kinetic energy. Two kind of solitons may exist: *grey* solitons represent a density depletion with respect to the unperturbed value, while *bright* solitons correspond to a density enhancement.

Let us now investigate the uniform case $V_{\rm tr}(x) = 0$, and a solution for (1.22) travelling at a constant speed $v$. Since the soliton has a finite size, far from its core the density should approach its unperturbed uniform value $n$. Following the treatment given by Stringari and Pitaevskii[26], we will search for stationary solutions of the kind

$$\psi_0(x) = \sqrt{n}f(x,\xi), \tag{1.24}$$

[26] L. Pitaevskii and S. Stringari. *Bose-Einstein Condensation and Superfluidity.* Oxford University Press, 2016.

where $f(x,\xi)$ is a dimensionless function with properties

$$\lim_{x\to\pm\infty} f(x,\xi) = 1 \quad \text{and} \quad \lim_{x\to\pm\infty} \partial_x f(x,\xi) = 0. \tag{1.25}$$

The full solution is therefore

$$\psi(x,t) = \sqrt{n} f(\zeta) e^{-i\frac{\mu}{\hbar}t}, \tag{1.26}$$

where $\zeta = (x - vt)/\xi$ and $\mu = ng$. By substituting (1.26) into (1.22) one gets

$$2iS\frac{\partial f}{\partial \zeta} = \frac{\partial^2 f}{\partial \zeta^2} + (1 - |f|^2)f, \tag{1.27}$$

where we substituted $dt = -\dfrac{\xi}{v} d\zeta$ and defined

$$S \equiv \frac{mv\xi}{\hbar} = \frac{v}{\sqrt{2}c}, \tag{1.28}$$

where $c$ is the sound speed (see eq. (1.61)). Multiplying (1.27) by $f^*$ and subtracting its complex conjugate one gets

$$2iS\left(\frac{\partial f}{\partial \zeta} f^* + \frac{\partial f^*}{\partial \zeta} f\right) - \frac{\partial^2 f}{\partial \zeta^2} f^* + \frac{\partial^2 f^*}{\partial \zeta^2} f = 0, \tag{1.29}$$

which can be simplified by recalling the Leibniz rule for the derivative of a product as

$$\frac{\partial}{\partial \zeta}\left(2iS|f|^2 - \frac{\partial f}{\partial \zeta} f^* + \frac{\partial f^*}{\partial \zeta} f\right) = 0. \tag{1.30}$$

The parenthesis in (1.30) is therefore a constant, which we will impose to be $2iS$:

$$2iS(1 - |f|^2) + \frac{\partial f}{\partial \zeta} f^* - \frac{\partial f^*}{\partial \zeta} f = 0. \tag{1.31}$$

Let us keep this equation aside for a moment. In general $f = f_R + i f_I$ is a complex function. By decomposing $f$ into (1.27), and by only taking the imaginary part of the resulting equation, one gets

$$2S\frac{\partial f_R}{\partial \zeta} = \frac{\partial^2 f_I}{\partial \zeta^2} + (1 - f_R^2 - f_I^2) f_I. \tag{1.32}$$

Eq. (1.32) can be simplified by only considering solutions with constant $f_I$:

$$2S\frac{\partial f_R}{\partial \zeta} = (1 - f_R^2 - f_I^2) f_I. \tag{1.33}$$

This last equation coincides with (1.31) by identifying

$$f_I = \sqrt{2}S = v/c, \tag{1.34}$$

and becomes

$$\sqrt{2}\frac{\partial f_R}{\partial \zeta} = 1 - f_R^2 - \frac{v^2}{c^2}, \tag{1.35}$$

whose solution is

$$f_R(\zeta) = \sqrt{1-\frac{v^2}{c^2}}\tanh\left(\frac{\zeta}{\sqrt{2}}\sqrt{1-\frac{v^2}{c^2}}\right). \tag{1.36}$$

Thus, the solitonic solution for the Gross-Pitaevskii equation is

$$\boxed{\psi_{\rm S}(x-vt) = \sqrt{n}\left(i\frac{v}{c} + \sqrt{1-\frac{v^2}{c^2}}\tanh\left(\frac{x-vt}{\sqrt{2}\xi}\sqrt{1-\frac{v^2}{c^2}}\right)\right)e^{-i\frac{\mu}{\hbar}t}}. \tag{1.37}$$

The density profile $n(x-vt) = |\psi_{\rm S}(x-vt)|^2$ has a minimum in the centre of the soliton corresponding to $n(0) = nv^2/c^2$. This value drops to zero whenever $v = 0$, i.e. in the presence of a static defect, which, having a complete density depletion, is evocatively called *black soliton*. The width of the soliton is determined by the healing length $\xi$, amplified by a factor $1/\sqrt{1-v^2/c^2}$ proportional to the velocity.

A peculiar aspect of solitons is the phase jump occurring at the position of the defect. From (1.37) one can compute that

$$\begin{aligned}\Delta\theta(\psi_{\rm S}) &= \pi - 2\arctan\left(\frac{v/c}{\sqrt{1-v^2/c^2}}\right)\\ &= 2\arccos\left(\frac{v}{c}\right).\end{aligned} \tag{1.38}$$

In the case of a black soliton, the wave function then becomes purely real

$$\psi_{\rm DS} = \sqrt{n}\tanh\left(\frac{x}{\sqrt{2}\xi}\right), \tag{1.39}$$

and the phase jump assumes its maximum value $\pi$.

Another interesting aspect to investigate is the soliton energy, which can be computed as the difference between the grand canonical energies in the presence and in the absence of the soliton

$$E_{\rm S} = \int_{-\infty}^{\infty} dx\left(\frac{\hbar^2}{2m}\left|\frac{d\psi_{\rm S}}{dx}\right|^2 + \frac{g}{2}\left(|\psi_{\rm S}|^2 - n\right)^2\right), \tag{1.40}$$

whose result is

$$E_{\mathrm{S}} = \frac{4}{3}\hbar c n \left(1 - \frac{v^2}{c^2}\right)^{3/2}. \tag{1.41}$$

When considering small velocities, and large depletions, eq. (1.41) can be rewritten as

$$E_{\mathrm{S}} \sim \frac{4}{3}\hbar c n - \frac{1}{2}\frac{4\hbar n}{c} v^2. \tag{1.42}$$

Equation (1.42) is remarkable. It tells us that the soliton behaves as a particle of negative mass $m_s = -4\hbar n/c$. Then, being a (quasi)particle with negative kinetic energy, the faster the defect the *less* energetic it is. Therefore, any dissipative effect, such as collisions with thermal excitations, will result in an acceleration of the soliton, corresponding to a decrease in the density depletion, eventually leading to its disappearance for $v \to c$.

### 1.1.2 Superfluidity and hydrodynamic approach

One of the most striking properties of Bose-Einstein condensation is that it strictly connects to *superfluidity*. By superfluidity, one generally means a set of macroscopic phenomena in quantum fluids determined by a peculiar dynamical condition: the system exhibits zero viscosity, and the velocity field is irrotational. The consequences of these facts are quite remarkable, as they allow the presence of persistent mass currents, the possibility of having stationary equilibrium states in rotating vessels and the quantisation of the vorticity.

**Quantised vortices.** The formal link between superfluidity and BEC can be understood from the phase of the order parameter $\psi$. Consider a uniform system, with $V_{\mathrm{tr}} = 0$. At equilibrium, the solution of equation (1.17) is given by the uniform relation

$$\psi(\mathbf{r}, t) = \psi_0 = \sqrt{n} e^{-i\mu t/\hbar}, \tag{1.43}$$

where $n$ is a constant density independent of the position. If we now consider instead a moving frame at constant velocity $\mathbf{v}$, the order parameter takes the form

$$\psi_0 = \sqrt{n} e^{iS(\mathbf{r},t)} \tag{1.44}$$

where

$$S(\mathbf{r}, t) = \frac{1}{\hbar}\left[m\mathbf{v}\cdot\mathbf{r} - \left(m\frac{v^2}{2} + \mu\right)t\right] \tag{1.45}$$

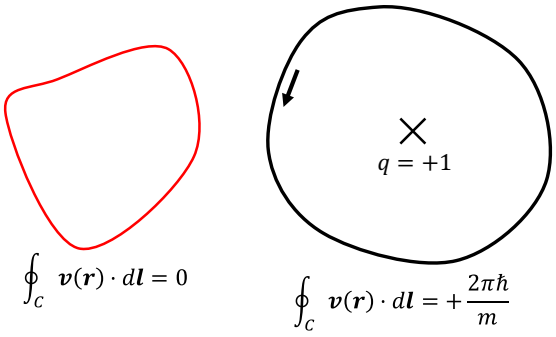


Figure 1.1: Circulation of the velocity $\mathbf{v}(\mathbf{r}) = \hbar/m\boldsymbol{\nabla}S$ associated to the classical field $\psi(\mathbf{r}) = \sqrt{n}e^{iS(\mathbf{c})}$. The value of the circulation does not depend on the contour chosen, unless it crosses a point of zero density (identified as the vortex).

is the *phase* of the condensate. The velocity can be therefore identified with the gradient of the phase

$$\mathbf{v}(\mathbf{r}, t) = \frac{\hbar}{m}\boldsymbol{\nabla}S(\mathbf{r}, t). \tag{1.46}$$

The velocity (1.46) describes the collective motion of many particles in the same quantum state, and since it is defined as the gradient of a scalar function, it is by construction irrotational:

$$\boldsymbol{\nabla} \times \mathbf{v} = 0. \tag{1.47}$$

In order for the wavefunction (1.44) to be single-valued, the change in phase around any closed contour $C$ must be an integer multiple of $2\pi$:

$$\oint_C \boldsymbol{\nabla}S \cdot d\mathbf{l} = 2\pi s \quad s \in \mathbb{Z}. \tag{1.48}$$

This also means that the velocity circulation satisfies the Onsager-Feynman[14,15] quantisation condition

$$\oint_C \mathbf{v} \cdot d\mathbf{l} = s\left(\frac{2\pi\hbar}{m}\right) \quad s \in \mathbb{Z}, \tag{1.49}$$

which implies that the circulation of the fluid is also quantised in units of $(\hbar/m)$. Hence, the system will only present vortices with quantised circulation, which can only be generated and annihilated via recombination processes between pairs of opposite charge (for more on that, see Chapter (4)). This is drastically different from a classical fluid, where the energy of a vortex can dissipate leading to its eventual disappearance.

[14] L. Onsager. In: *Il Nuovo Cimento* 6 (1949), pp. 279–287.

[15] R.P. Feynman. *Chapter II Application of Quantum Mechanics to Liquid Helium.* Ed. by C. J. Gorter. Vol. 1. Supplement C. Elsevier, 1955, pp. 17–53.

The velocity around a single vortex core is given by

$$\mathbf{v}(r,\theta) = s\left(\frac{\hbar}{mr}\right)\hat{\boldsymbol{\theta}} \quad s \in \mathbb{Z}, \tag{1.50}$$

where $r$ is the radius distance from the core, and $\hat{\boldsymbol{\theta}}$ is the azimuthal unit vector.

It is worth stressing that in three dimensional systems, vortices appear as lines where the system density goes to zero. These lines are constrained to be locally perpendicular to the system borders, if present, and thus they can be bent in non-uniform fluids such as trapped ultracold gases (see more on this in Chapter 2). As their classical counterparts, they can present long-wavelength helical excitations, the so-called Kelvin waves[31–33].

**Hydrodynamic equations.** By means of the phase $S$ and the velocity $\mathbf{v}$ defined above, one can show that the macroscopic dynamics of the condensate is well described by the hydrodynamic equations for an irrotational non-viscous fluid. By substituting (1.44) into (1.14), and by discarding[1] the quantum pressure term $\nabla^2\sqrt{n}$, one gets the following coupled hydrodynamic equations

$$\frac{\partial n}{\partial t} + \boldsymbol{\nabla}\cdot(\mathbf{v}n) = 0 \tag{1.51}$$

$$m\frac{\partial \mathbf{v}}{\partial t} + \boldsymbol{\nabla}\left(V_{\mathrm{tr}} + gn + \frac{mv^2}{2}\right) = 0. \tag{1.52}$$

## 1.2 Zero temperature excitations: Bogoliubov approach

**Excitation spectrum.** One can compute the first-order excitations on top of a stationary solution of the Gross-Pitaevskii equation by substituting

$$\psi(\mathbf{r},t) = (\psi_0(\mathbf{r}) + \delta\psi(\mathbf{r},t))e^{-i\frac{\mu}{\hbar}t}, \tag{1.53}$$

into (1.14), which gives

$$i\hbar\frac{\partial}{\partial t}\delta\psi(\mathbf{r},t) = \left[-\frac{\hbar^2}{2m}\nabla^2 + V_{\mathrm{tr}}(\mathbf{r}) + 2g|\psi_0(\mathbf{r})|^2 - \mu\right]\delta\psi(\mathbf{r},t) + g\psi_0^2(\mathbf{r})\delta\psi^* \tag{1.54}$$

[1] This implies a limitation of the description of the system to scales larger than the healing length $\xi$.

[31] W. Thomson (Lord Kelvin). In: *Philos. Mag.* 10 (1880), p. 155.
[32] V. Bretin et al. In: *Phys. Rev. Lett.* 90 (2003), p. 100403.
[33] Alexander L. Fetter. In: *Phys. Rev. A* 69 (2004), p. 043617.

where we have neglected all the terms in $\delta\psi^2$. We can rewrite (1.54) in a system of linear equations by applying the Bogoliubov transformation:

$$\delta\psi(\mathbf{r},t) = \sum_k (u_k(\mathbf{r})e^{-i\omega_k t} + v_k^*(\mathbf{r})e^{i\omega_k t}) \tag{1.55}$$

where $k$ marks the different modes of frequency $\omega_k$. This allows us to write a linear system of two coupled equations for the functions $u_k(\mathbf{r})$ and $v_k(\mathbf{r})$, known as the zero-temperature Bogoliubov equations[2]

$$\begin{bmatrix} \hat{A}(\mathbf{r}) & \hat{B}(\mathbf{r}) \\ -\hat{B}^*(\mathbf{r}) & -\hat{A}^*(\mathbf{r}) \end{bmatrix} \begin{bmatrix} u_k(\mathbf{r}) \\ v_k(\mathbf{r}) \end{bmatrix} = \hbar\omega_k \begin{bmatrix} u_k(\mathbf{r}) \\ v_k(\mathbf{r}) \end{bmatrix} \tag{1.56}$$

where we defined

$$\begin{aligned} \hat{A}(\mathbf{r}) &= -\frac{\hbar^2\nabla^2}{2m} + V_{\mathrm{tr}}(\mathbf{r}) + 2g|\psi_0(\mathbf{r})|^2 - \mu \\ \hat{B}(\mathbf{r}) &= g\psi_0^2(\mathbf{r}). \end{aligned} \tag{1.57}$$

For a uniform system, where $V_{\mathrm{tr}}(\mathbf{r}) = 0$, the Bogoliubov functions have the form

$$u_k(\mathbf{r}) = u_k e^{i\mathbf{k}\cdot\mathbf{r}} \quad \text{and} \quad v_k(\mathbf{r}) = v_k e^{i\mathbf{k}\cdot\mathbf{r}}, \tag{1.58}$$

thus representing the amplitudes of plane waves of wavevector $\mathbf{k}$. Equation (1.55) then means that the excitations are represented by quasi-particles composed of counter-propagating plane waves (see below). Since in the uniform system (1.19) implies that $\mu = g|\psi_0|^2$, we can rewrite (1.56):

$$\begin{bmatrix} \left(-\frac{\hbar^2\mathbf{k}^2}{2m} + g|\psi_0|^2 - \hbar\omega_k\right) & g\psi_0^2 \\ g(\psi_0^*)^2 & \left(-\frac{\hbar^2\mathbf{k}^2}{2m} + g|\psi_0|^2 + \hbar\omega_k\right) \end{bmatrix} \begin{bmatrix} u_k \\ v_k \end{bmatrix} = 0. \tag{1.59}$$

This equation can be solved by simply imposing the determinant to be zero, and results in the well known $T = 0$ Bogoliubov excitation spectrum for the uniform case

$$\boxed{\hbar\omega_k = \sqrt{\frac{\hbar^2k^2}{2m}\left(\frac{\hbar^2k^2}{2m} + 2gn_0\right)}}. \tag{1.60}$$

The Bogoliubov dispersion relation (1.60) shows a peculiar twofold behaviour. In the low momentum regime it is linear, thus leading to a phonon-like relation

$$\hbar\omega_k = \hbar ck \qquad \text{where } c = \sqrt{\frac{gn_0}{m}} \text{ is the } \textit{Bogoliubov speed of sound.} \tag{1.61}$$

[2] These are analogue to the Bogoliubov-de Gennes equations for superconductivity [34].

In the large momentum regime, instead, the spectrum becomes the one of a free particle, plus a mean field contribution $\hbar\omega_k = \hbar^2 k^2/2m + gn_0$.

**Bogoliubov quasiparticles.** It is possible to show[26] that the phonon-like excitations, recovered by linearising the Gross-Pitaevskii equation as performed above, correspond to the Bogoliubov quasi-particles which diagonalise the Hamiltonian (1.3) of a weakly interacting Bose gas of $N$ particles in a uniform potential $V_{\text{tr}}(\mathbf{r}) = 0$, i.e.

$$\hat{H} = \int d\mathbf{r} \left( \frac{\hbar^2}{2m} \nabla\hat{\Psi}^\dagger(\mathbf{r})\hat{\Psi}(\mathbf{r}) \right) + \frac{1}{2} \int d\mathbf{r}\, d\mathbf{r}'\, \hat{\Psi}^\dagger(\mathbf{r})\hat{\Psi}^\dagger(\mathbf{r}')V_{\text{int}}(\mathbf{r}-\mathbf{r}')\hat{\Psi}(\mathbf{r})\hat{\Psi}(\mathbf{r}'), \quad (1.62)$$

where $V_{\text{int}}(\mathbf{r}-\mathbf{r}')$ is the general form of the two-body interaction potential as in (1.1). By assuming that the gas lies in a uniform three-dimensional box of size $L^3$, one can expand the field operators $\hat{\Psi}$ in the plane wave basis

$$\hat{\Psi}(\mathbf{r}) = \frac{1}{\sqrt{L^3}} \sum_{\mathbf{p}} \hat{a}_{\mathbf{p}} e^{i\mathbf{p}\cdot\mathbf{r}/\hbar} \quad (1.63)$$

where $\hat{a}_{\mathbf{p}}$ is the operator annihilating a particle in a plane wave state of momentum $\mathbf{p}$, obeying the bosonic commutation relations

$$\left[\hat{a}_{\mathbf{p}}, \hat{a}^\dagger_{\mathbf{p}'}\right] = \hat{a}_{\mathbf{p}}\hat{a}^\dagger_{\mathbf{p}'} - \hat{a}^\dagger_{\mathbf{p}'}\hat{a}_{\mathbf{p}} = \delta_{\mathbf{p},\mathbf{p}'}. \quad (1.64)$$

By the substitution of (1.63) into (1.62) one gets

$$\hat{H} = \sum_{\mathbf{p}} \frac{p^2}{2m} \hat{a}^\dagger_{\mathbf{p}}\hat{a}_{\mathbf{p}} + \frac{1}{2L^3} \sum_{\mathbf{p}_1,\mathbf{p}_2,\mathbf{q}} V_q \hat{a}^\dagger_{\mathbf{p}_1+\mathbf{q}}\hat{a}^\dagger_{\mathbf{p}_2-\mathbf{q}}\hat{a}_{\mathbf{p}_1}\hat{a}_{\mathbf{p}_2}, \quad (1.65)$$

where

$$V_q = \int d\mathbf{r}\, V_{\text{int}}(\mathbf{r}) e^{-i\mathbf{p}\cdot\mathbf{r}/\hbar}. \quad (1.66)$$

By the same considerations as above, one could exclusively consider a contact potential as in equation (1.5), which means to effectively keeping the sole constant term $V_0 = g$ in the above equation. This allows one to rewrite

$$\hat{H} = \sum_{\mathbf{p}} \frac{p^2}{2m} \hat{a}^\dagger_{\mathbf{p}}\hat{a}_{\mathbf{p}} + \frac{g}{2L^3} \sum_{\mathbf{p}_1,\mathbf{p}_2,\mathbf{q}} \hat{a}^\dagger_{\mathbf{p}_1+\mathbf{q}}\hat{a}^\dagger_{\mathbf{p}_2-\mathbf{q}}\hat{a}_{\mathbf{p}_1}\hat{a}_{\mathbf{p}_2}. \quad (1.67)$$

[26] L. Pitaevskii and S. Stringari. *Bose-Einstein Condensation and Superfluidity.* Oxford University Press, 2016.

By splitting the operator for the ground state $\hat{a}_0$ from the ones for the excited states $\hat{a}_{\mathbf{p}}$ one gets

$$\hat{H} = \frac{g}{2L^3}\hat{a}_0^\dagger\hat{a}_0^\dagger\hat{a}_0\hat{a}_0 + \sum_{\mathbf{p}\neq 0}\frac{p^2}{2m}\hat{a}_{\mathbf{p}}^\dagger\hat{a}_{\mathbf{p}} + \frac{g}{2L^3}\sum_{\mathbf{p}\neq 0}\left(4\hat{a}_0^\dagger\hat{a}_{\mathbf{p}}^\dagger\hat{a}_0\hat{a}_{\mathbf{p}} + \hat{a}_{\mathbf{p}}^\dagger\hat{a}_{-\mathbf{p}}^\dagger\hat{a}_0\hat{a}_0 + \hat{a}_0^\dagger\hat{a}_0^\dagger\hat{a}_{\mathbf{p}}\hat{a}_{-\mathbf{p}}\right). \tag{1.68}$$

The last term of the above equation only includes operators in $\mathbf{p} \neq 0$ which appear quadratically; the terms only having one operator in $\mathbf{p}$ are forbidden due to momentum conservation. The factor 4 accounts for the four different possible combinations of $\mathbf{p}_1, \mathbf{p}_2$ and $\mathbf{q}$ leading to the resulting term in $\mathbf{p}$.

The crucial point is now to follow the Bogoliubov prescription and replace the operators $\hat{a}_0^\dagger$ and $\hat{a}_0$ with a $c$-number

$$\hat{a}_0 = \sqrt{N_0}, \tag{1.69}$$

representing the occupation of the lowest single-particle state. Once again, this approximation corresponds to neglecting the short-range details of the interaction potential. The first term of (1.68) can be computed in terms of the normalisation condition

$$\hat{a}_0^\dagger\hat{a}_0 + \sum_{\mathbf{p}\neq 0}\hat{a}_{\mathbf{p}}^\dagger\hat{a}_{\mathbf{p}} = N, \tag{1.70}$$

which leads, neglecting higher order terms, to

$$\hat{a}_0^\dagger\hat{a}_0^\dagger\hat{a}_0\hat{a}_0 \simeq N^2 - 2N\sum_{\mathbf{p}\neq 0}\hat{a}_{\mathbf{p}}^\dagger\hat{a}_{\mathbf{p}}. \tag{1.71}$$

In the other terms of equation (1.68) we can instead perform the approximate substitution $\hat{a}_0 = \sqrt{N}$, where we assume that the system is very cold and that the occupation of the zero-momentum state is macroscopic. The Hamiltonian (1.68) then becomes

$$\hat{H} = \frac{1}{2}gnN + \sum_{\mathbf{p}}\frac{p^2}{2m}\hat{a}_{\mathbf{p}}^\dagger\hat{a}_{\mathbf{p}} + \frac{1}{2}gn\sum_{\mathbf{p}\neq 0}\left(2\hat{a}_{\mathbf{p}}^\dagger\hat{a}_{\mathbf{p}} + \hat{a}_{\mathbf{p}}^\dagger\hat{a}_{-\mathbf{p}}^\dagger + \hat{a}_{\mathbf{p}}\hat{a}_{-\mathbf{p}}\right), \tag{1.72}$$

where $n = N/L^3$ is the density, and the last term of the Hamiltonian is composed by the self interaction of the excited states, the simultaneous creation of excited states of opposite momentum and their simultaneous annihilation, respectively. Equation (1.72) can be diagonalised by performing the linear transformation in the creation and annihilation operators

$$\hat{a}_{\mathbf{p}} = u_p\hat{b}_{\mathbf{p}} + v_{-\mathbf{p}}\hat{b}_{-\mathbf{p}}^\dagger, \quad \text{and} \quad \hat{a}_{\mathbf{p}}^\dagger = u_p\hat{b}_{\mathbf{p}}^\dagger + v_{-\mathbf{p}}\hat{b}_{-\mathbf{p}}, \tag{1.73}$$

known as the Bogoliubov transformation. The operators $\hat{b}_{\mathbf{p}}$ and $\hat{b}^{\dagger}_{\mathbf{p}}$ obey the same bosonic commutation relations as the original fields. This implies a constraint on the two amplitudes $u_{\mathbf{p}}$ and $v_{-\mathbf{p}}$

$$|u_{\mathbf{p}}|^2 - |v_{-\mathbf{p}}|^2 = 1, \tag{1.74}$$

which means that they can be rewritten as

$$u_{\mathbf{p}} = \cosh(\alpha_{\mathbf{p}}) \quad \text{and} \quad v_{-\mathbf{p}} = \sinh(\alpha_{\mathbf{p}}). \tag{1.75}$$

The value of $\alpha_{\mathbf{p}}$ can be chosen so to suppress the non-diagonal terms $\hat{b}^{\dagger}_{\mathbf{p}}\hat{b}^{\dagger}_{-\mathbf{p}}$ and $\hat{b}_{\mathbf{p}}\hat{b}_{-\mathbf{p}}$ of the Hamiltonian (1.72), by imposing the condition

$$\frac{gn}{2}(|u_{\mathbf{p}}|^2 + |v_{-\mathbf{p}}|^2) + \left(\frac{p^2}{2m} + gn\right) u_{\mathbf{p}} v_{-\mathbf{p}} = 0, \tag{1.76}$$

which translates into

$$\coth(2\alpha_{\mathbf{p}}) = -\frac{1}{gn}\left(\frac{p^2}{2m} + gn\right). \tag{1.77}$$

This condition allows to determine uniquely the coefficients

$$u_{\mathbf{p}}, v_{\mathbf{p}} = \pm\sqrt{\frac{1}{2\epsilon(\mathbf{p})}\left(\frac{p^2}{2m} + gn\right) \pm \frac{1}{2}}, \tag{1.78}$$

being

$$\epsilon(\mathbf{p}) = \sqrt{\frac{p^2}{2m}\left(\frac{p^2}{2m} + 2gn\right)} \tag{1.79}$$

which recovers relation (1.60) for the Bogoliubov excitation spectrum. By substituting equations (1.73) and (1.78), the Hamiltonian (1.72) is diagonalised into

$$H = E_0 + \sum_{\mathbf{p}\neq 0} \epsilon(\mathbf{p}) \hat{b}^{\dagger}_{\mathbf{p}} \hat{b}_{\mathbf{p}}, \tag{1.80}$$

where

$$E_0 = \frac{1}{2}gnN + \frac{1}{2}\sum_{\mathbf{p}\neq 0}\left(\epsilon(\mathbf{p}) - gn - \frac{p^2}{2m} + m\frac{(gn)^2}{p^2}\right) \tag{1.81}$$

is the ground state energy. Its zero-order value can be computed by simply assuming that all the states with $\mathbf{p} \neq 0$ are suppressed due to the low temperature, and consists in the first term $\frac{1}{2}gnN$. The first-order correction has been computed[35,36] to be

$$E_0 = \frac{1}{2}gnN\left(1 + \frac{128}{15\pi}\sqrt{na^3}\right). \tag{1.82}$$

[35] T. D. Lee and C. N. Yang. In: *Phys. Rev.* 105 (1957), pp. 1119–1120.

[36] T. D. Lee, Kerson Huang, and C. N. Yang. In: *Phys. Rev.* 106 (1957), pp. 1135–1145.

The chemical potential in the first order correction then becomes

$$\mu = \frac{\partial E_0}{\partial N} = gn\left(1 + \frac{32}{3\pi}\sqrt{na^3}\right). \tag{1.83}$$

Equations (1.82) and (1.83) are known as Lee-Huang-Yang relations.

## 1.3 Chapter summary

In this chapter we briefly introduced some of the theoretical tools we are going to use throughout the thesis. We reviewed the Gross-Pitaevskii equation and the Thomas-Fermi approximation for its solution in the low-temperature stationary state. We looked at a distinctive class of dynamical solutions for the equation, the solitons, and we described some of their properties. We introduced the concepts of superfluidity in a BEC, and of quantisation of vorticity, and we sketched the hydrodynamic equations for a condensate. We finally studied the Bogoliubov approach for the first-order excitations in the system. We will make use of some of these concepts in the following chapter, describing the dynamics of a defect in an elongated quasi-1D condensate.

# Chapter 2

# Vortices in elongated Bose-Einstein condensates

This chapter reports the theoretical description of an experiment realised at the laboratory of ultracold atoms of the INO-CNR BEC Center in Trento[1], in collaboration with Franco Dalfovo and myself. The experiment concerned the study of the real-time dynamics of randomly generated vortices in a large, elongated sodium BEC. The vortices were produced by the Kibble-Zurek mechanism, and their motion was followed in time by means of a stroboscopic technique. The vortex precession motion showed good agreement with the theory. This work was published[27] in *Physical Review Letters*.

## 2.1 Description of the experiment

The experiment was performed in a cigar-shaped sodium BEC, confined in a magnetic harmonic trap with frequencies $\omega_x = \omega_y = \omega_\perp = 2\pi(131\text{Hz})$, and $\omega_z = 2\pi(13\text{Hz})$, hence giving an aspect ratio of approximately 10. This geometry was chosen in order to probe the role of anisotropy in the motion of the vortices, spontaneously generated by the Kibble-Zurek mechanism (KZM)[2]: if, during the evaporation, the temperature is varied quickly enough when crossing the phase transition critical point, the system will exhibit phase defects, which will eventually decay into a number of vortices with random position and orientation. The average number of vortices scales as an inverse power law of the quench time $\tau_q$. At the end of the evaporation procedure the number of atoms in the condensate was around $10^7$ at 200 nK. It is important to clarify that, even though the system is quite elongated, it is still represented by a three-dimensional de-

[1] `bec.science.unitn.it`

[2] For more on this, see Chapter 4.

[27] S. Serafini et al. In: *Phys. Rev. Lett.* 115 (2015), p. 170402.

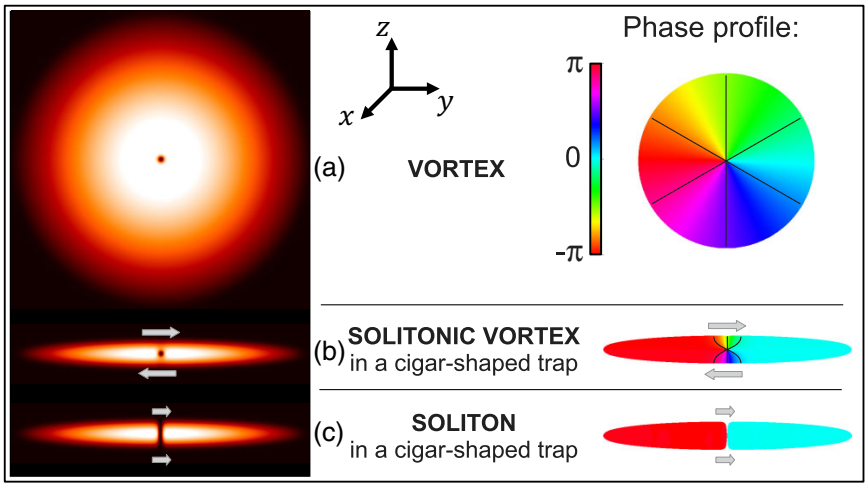


Figure 2.1: [Figure from [37]] Schematic representation of a solitonic vortex, showing the theoretical solutions of the trapped densities (left) and phase profiles (right) for a vortex in an isotropic harmonic potential (a), a solitonic vortex in an elongated geometry (b) and a soliton (c).

scription, and that the phase transition associated with it is the canonical second-order Bose-Einstein condensation.

As opposed to a completely destructive absorption technique, such as the one used in a previous work[37], here a different approach was used, similar to the one used by the group of D. Hall[38]. This consists in a stroboscopic imaging process, which is a quasi non-destructive protocol that allows to follow the real-time dynamics of a *single* sample. For an initial atom number in the trap $N_0$, by shining a microwave pulse on the BEC, it is possible to outcouple a small fraction of the atoms $\Delta N/N_0 \sim 4\%$ into an anti-trapped state. This "extraction" happens homogeneously across the condensate, and the atoms resemble the distribution of the whole system. They are subsequently expanded for a short period of time ($\sim$ 13 ms) and are observed with an imaging laser, leaving the ones in the condensate unperturbed. The resulting optical densities are fitted to a Thomas-Fermi profile[1], which is then subtracted in order to get the residual density. This procedure can be repeated up to 20 times with fixed time steps $\Delta t$ and $\Delta N$, only slightly affecting the dynamics of the system, provided that $\Delta N/N(t)$ is small enough. This way, it is possible to produce "movies" of the motion of the defects in time. Vortices appear as dark stripes in the expanded cloud, because of the distinctive features of the kind of defect that is created in this configuration: the *solitonic vortex*. The difference with the canonical vortex in a bulk lies in the peculiar distribution of

[37] S. Donadello et al. In: *Phys. Rev. Lett.* 113 (2014), p. 065302.
[38] D. V. Freilich et al. In: *Science* 329.5996 (2010), pp. 1182–1185.
[1] F. Dalfovo et al. In: *Rev. Mod. Phys.* 71 (1999), pp. 463–512.

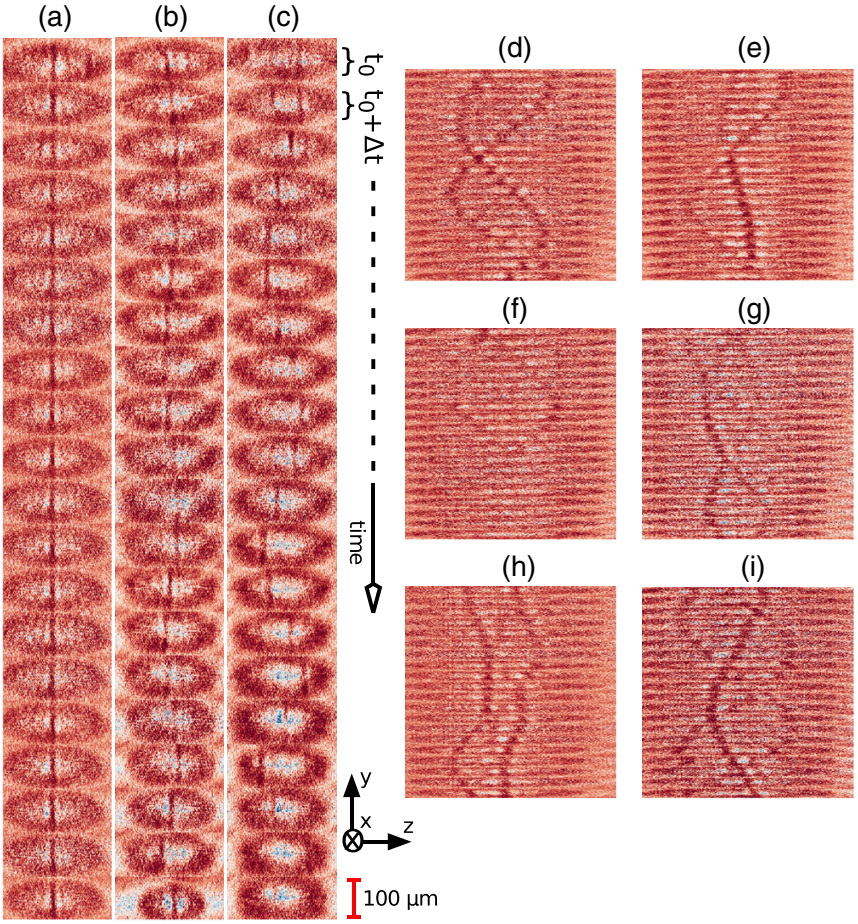


Figure 2.2: [Figure from [27]] (a)-(c) Example sequences of 20 consecutive images of the density distribution of the extracted atoms, only presenting one defect. The time interval between two shots is $\Delta t = 84$ ms, and each picture is taken after 13 ms of expansion. In particular, (a) shows a static vortex, while (b) and (c) show vortices with a different amplitude of the precessing motion. (d)-(i) Sequences with multiple vortices, with $\Delta t = 28$ ms. The time axis of these frames has been squeezed to enhance visibility.

the phase gradient around the vortex core, which is modified by the presence of the BEC boundary. The presence of a virtual vortex on the opposite side of the edge of the condensate causes the lines of equal phase to bend, thus making the regions close to the border the ones where the majority of the flow is concentrated. This causes a planar density depletion in an elongated condensate, and combined with the almost constant phase on two large patches on the side of the vortex core, resembles the features of a soliton (Figure 2.1). It is important to note that with this method it is not possible to estimate the orientation of the vortical line in the $x - y$ plane, as this would require

a different approach in the phase analysis (and was only realised in a later work[39]). Figure 2.2 shows some example trajectories for various numbers of solitonic vortices. From them it is possible to extract the axial position of the vortex $z(t)$ as a function of time.

## 2.2 Motion of a vortex in an elongated BEC

This section reports the theoretical analysis of the motion of a solitonic vortex in the elongated configuration presented above. This analysis is based on the superfluid hydrodynamic approach developed by Pitaevskii[40], and generalised to the case of solitonic vortices as in a paper of Ku *et al.*[41]. Consider a cigar-shaped BEC with isotropic strong confinement in the $x$ and $y$ direction, corresponding to a Thomas-Fermi radius $R_\perp \ll R_z$ much smaller than the one in the loosely confined $z$ direction. Let us further assume that the vortex line is perfectly straight and aligned along $x$, and that, given that the *local density approximation* (LDA) holds, the vortex core size is $\xi \ll R_\perp$, so that $\log(R_\perp/\xi) \gg 1$ and the logarithm is approximately constant. Here the size of the vortex is assumed to be the condensate healing length $\xi = \sqrt{\hbar^2/2mng}$. Let us finally consider the position of the vortex in the $y$-$z$ plane to be $\mathbf{r} = (y_0, z_0)$.

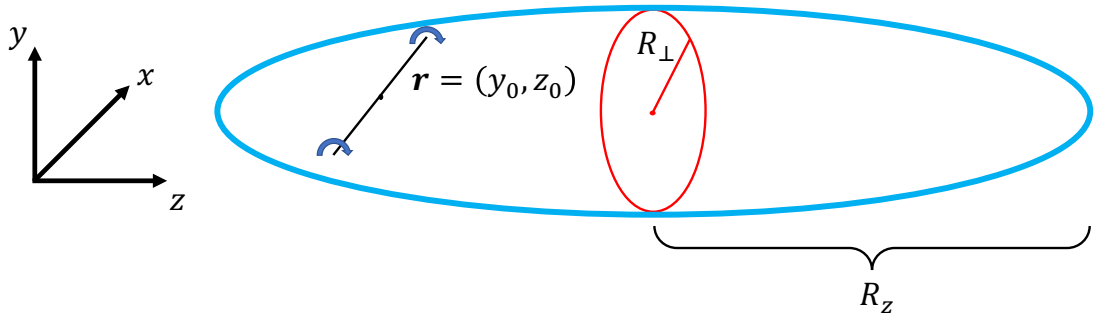


We will assume that the energy of the vortex is dominated by the kinetic energy of its flow field $\mathbf{v} = (\hbar/m_B)\boldsymbol{\nabla}\phi$, where $m_B$ is the mass of the boson (for a BEC this is simply the mass of the atoms $m$, whereas for fermions $m_B = 2m$), and

$$\phi = \arctan\left(\frac{y - y_0}{z - z_0}\right) \tag{2.1}$$

is the phase profile in the vicinity of the vortex core. The vortex presence is only going to affect a density region of dimension $\sim \pi R_\perp^2$ around its core. Hence the defect energy

[39] S. Serafini et al. In: *Phys. Rev. X* 7 (2017), p. 021031.
[40] L. P. Pitaevskii. In: *ArXiv e-prints* (2013). arXiv: 1311.4693 [cond-mat.quant-gas].
[41] M. J. H. Ku et al. In: *Phys. Rev. Lett.* 113 (2014), p. 065301.

is

$$E_V = \int d^3\,\mathbf{r}\frac{1}{2}mn(x,y,z)v^2 = \frac{1}{2}\frac{\hbar^2 m}{m_B^2}\int d^3\,n(x,y,z)(\boldsymbol{\nabla}\phi)^2. \tag{2.2}$$

Now, consider the following:

- compute the term $(\boldsymbol{\nabla}\phi)^2$:

$$\begin{aligned}\boldsymbol{\nabla}\phi\cdot\boldsymbol{\nabla}\phi &= \left(\frac{\partial\phi}{\partial x}\right)^2 + \left(\frac{\partial\phi}{\partial y}\right)^2 + \left(\frac{\partial\phi}{\partial z}\right)^2 \\ &= \left(\frac{z-z_0}{(z-z_0)^2+(y-y_0)^2}\right)^2 + \left(\frac{y-y_0}{(z-z_0)^2+(y-y_0)^2}\right)^2 \\ &= \frac{1}{(z-z_0)^2+(y-y_0)^2};\end{aligned} \tag{2.3}$$

- the volume of integration $\int d^3r$ is a cylinder of height $R_\perp$ and base $\pi R_\perp^2$, excluding the central region of the vortex core of size $\pi\xi^2$;

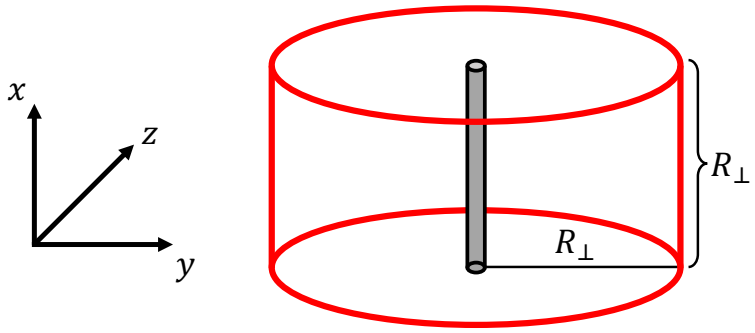


- local density approximation: the expression for the energy can be recovered as the one computed with a uniform density equal to its value near the vortex,

$$n(x,y,z) = n(x,y_0,z_0). \tag{2.4}$$

Thus, we can compute

$$\begin{aligned}E_V &= \frac{1}{2}\frac{\hbar^2 m}{m_B^2}\int_{-R_\perp}^{R_\perp} dx \int_\xi^{R_\perp} dr\, r \int_0^{2\pi} d\theta\, \frac{1}{r^2} n(x,y_0,z_0) \\ &= \frac{1}{2}\frac{\hbar^2 m}{m_B^2}\underbrace{\int_{-R_\perp}^{R_\perp} dx\, n(x,y_0,z_0)}_{\text{two-D column density } n_{2\mathrm{D}}}\, 2\pi \int_\xi^{R_\perp} dr\, \frac{1}{r} \\ &= \pi\hbar^2\frac{m}{m_B^2} n_{2\mathrm{D}}(y_0,z_0)\log\left(\frac{R_\perp}{\xi}\right).\end{aligned} \tag{2.5}$$

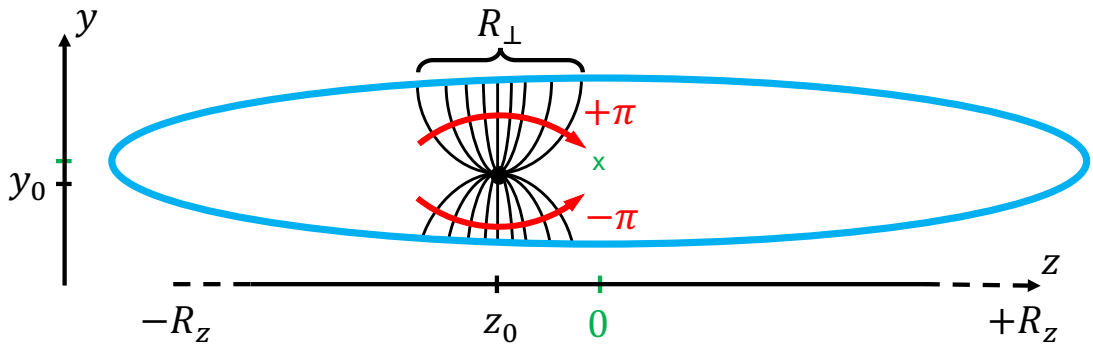


Figure 2.3: Schematic representation of the phase jump around the vortex core, highlighting a phase difference of $\pm\pi$ in the $z$ direction. Due to the anisotropy of the system, the lines of equal phase are bent towards the edges of the condensate, and the phase gradient is only concentrated in a region of size $R_\perp$ around the vortex core.

The canonical momentum of the vortex along the axial direction $z$ is

$$P_z = \frac{m}{m_B}\int d^3r\, mnv_z = \frac{m}{m_B}\int d^3r\, \hbar n(x,y,z)\partial_z\phi. \tag{2.6}$$

By means of the local density approximation, we can substitute $n(x,y,z) \sim n(x,y,z_0)$. Once again we integrate over a cylinder centred in the vortex core

$$P_z = \frac{m}{m_B}\int_0^{R_\perp} dx \int_{y_0}^{R_\perp} dy\, n(x,y,z_0)\int dz\partial_z\phi \tag{2.7}$$

$$= \frac{m}{m_B}\int_0^{R_\perp} dy\, n_{2\mathrm{D}}(y,z_0)\int dz\partial_z\phi. \tag{2.8}$$

Let us now focus on the $\int dz\partial_z\phi$ term. Since our defect is a vortex, the phase around it should undergo a jump of an integer multiple of $2\pi$ (let us assume that it is singly charged). As discussed above, for the peculiar class of the solitonic vortices, the phase gradient is mainly concentrated in a region of the condensate of size $\sim R_\perp$ close to the surface. When we integrate in $z$ from $-R_z$ to $+R_z$, the value of $\Delta\phi$ will depend on whether we perform the linear integration in the $y > y_0$ ($\Delta\phi = +\pi$) or in the $y < y_0$ region ($\Delta\phi = -\pi$), as shown in Figure (2.3). Hence

$$P_z = \hbar\frac{m}{m_B}\left[\pi\int_{-R_\perp}^{y_0} dy - \pi\int_{y_0}^{R_\perp} dy\right] n_{2\mathrm{D}}(y,z_0)$$

$$= \hbar\pi\frac{m}{m_B}\int_{-y_0}^{y_0} dy\, n_{2\mathrm{D}}(y,z_0), \tag{2.9}$$

where we used the symmetry of $n_{2\mathrm{D}}$ in the $y$ direction.

We can now compute the speed of the vortex along the $z$ direction using the Hamil-

ton equation

$$\dot{z}_0 = \frac{\partial E_V}{\partial P_z} = \frac{\partial E_V/\partial y_0}{\partial P_z/\partial y_0}. \tag{2.10}$$

In order to solve (2.10) we need to consider the Thomas-Fermi approximation as in the previous chapter: if the density is slowly varying in the region of interest, the quantum pressure term ($\propto \nabla^2\sqrt{n}$) of the Gross-Pitaevskii equation (1.17) can be neglected (see eq. (1.19)), and the condensate profile assumes the simple shape given by

$$gn(\mathbf{r}) + V_{\mathrm{tr}}(\mathbf{r}) = \mu_0, \tag{2.11}$$

which, in our harmonic trap, is

$$n(\mathbf{r}) = \frac{\mu(\mathbf{r})}{g} = \frac{\mu_0}{g}\left(1 - \frac{x^2+y^2}{R_\perp^2} - \frac{z^2}{R_z^2}\right). \tag{2.12}$$

Here, $\mu_0$ is the (local) chemical potential in the centre of the trap, and $R_\perp = \sqrt{\frac{2\mu_0}{m\omega_\perp^2}}$ and $R_z = \sqrt{\frac{2\mu_0}{m\omega_z^2}}$ are the so-called Thomas-Fermi radii. To generalise the following, let us consider the proportionality of $n$ on $\mu$ as

$$n = A\mu^\gamma \qquad \Rightarrow \qquad \gamma = \frac{\partial n}{\partial \mu}\frac{\mu}{n} = \frac{\partial n}{\partial \mu}\frac{\mu}{n}. \tag{2.13}$$

The noteworthy cases are $\gamma = 1$ for Bose atoms, and $\gamma = 3/2$ for Fermi gases at unitarity[42,43]. Now we can compute the different factors of equation (2.10), and the things get a little messy

$$\begin{aligned}
\frac{\partial E_V}{\partial y_0} &= \pi\hbar^2 \frac{m}{m_B^2}\frac{\partial \mu}{\partial y_0}\frac{\partial n_{2\mathrm{D}}}{\partial \mu}\log\left(\frac{R_\perp}{\xi}\right) \\
&= \pi\hbar^2 \frac{m}{m_B^2}\left(-2\mu_0\frac{y_0}{R_\perp^2}\right)\frac{\partial}{\partial \mu}\left[\int_{-R_\perp}^{R_\perp} dx\, n(x, y_0, z_0)\right]\log\left(\frac{R_\perp}{\xi}\right) \\
&= -2\pi\hbar^2 \frac{m}{m_B^2}\mu_0\frac{y_0}{R_\perp^2}2\left(\int_0^{R_\perp} dx\,\frac{\partial n}{\partial \mu}\right)\log\left(\frac{R_\perp}{\xi}\right) \text{(since } n \text{ is symmetric in } x) \\
&= -2\pi\left(\frac{\hbar m}{m_B}\right)^2 \omega_\perp^2 y_0 \gamma\left[\int_0^{R_\perp} dx\, A\mu_0^{\gamma-1}\left(1 - \frac{x^2+y_0^2}{R_\perp^2} - \frac{z_0^2}{R_z^2}\right)^{\gamma-1}\right]\log\left(\frac{R_\perp}{\xi}\right);
\end{aligned} \tag{2.14}$$

[42] C. Menotti, P. Pedri, and S. Stringari. In: *Phys. Rev. Lett.* 89 (2002), p. 250402.
[43] Hui Hu et al. In: *Phys. Rev. Lett.* 93 (2004), p. 190403.

And

$$\frac{\partial P_z}{\partial y_0} = \pi\hbar \frac{m}{m_B} \frac{\partial}{\partial y_0} \left[ 2 \int_0^{y_0} n_{2\mathrm{D}}(y, z_0) \right] = 2\pi\hbar \frac{m}{m_B} n_{2\mathrm{D}}(y_0, z_0). \tag{2.15}$$

Hence

$$\dot{z_0} = \frac{\partial E_V / \partial y_0}{\partial P_z / \partial y_0} = -\frac{m}{m_B} \hbar\omega^2 y_0 \gamma \log\left(\frac{R_\perp}{\xi}\right) \frac{I}{2}, \tag{2.16}$$

where

$$I = \frac{\int_0^{R_\perp} dx\, \mu_0^{\gamma-1} \left(1 - \frac{x^2+y_0^2}{R_\perp^2} - \frac{z_0^2}{R_z^2}\right)^{\gamma-1}}{\int_0^{R_\perp} dx\, \mu_0^{\gamma} \left(1 - \frac{x^2+y_0^2}{R_\perp^2} - \frac{z_0^2}{R_z^2}\right)^{\gamma}}. \tag{2.17}$$

We can now rename $a = \left(1 - \frac{y_0^2}{R_\perp^2} - \frac{z_0^2}{R_z^2}\right)$ and compute

$$\begin{aligned} \mu_0^{\gamma-1} \int_0^{R_\perp} dx \left(a - \frac{x^2}{R_\perp^2}\right)^{\gamma-1} &= \mu_0^{\gamma-1} \frac{R_\perp}{a} (a - 1^\gamma) \left(\frac{a-1}{a}\right)^{-\gamma} {}_2F^1\left(\frac{1}{2}, 1-\gamma; \frac{3}{2}; \frac{1}{a}\right) \\ &= \mu_0^{\gamma-1} R_\perp a^{\gamma-1} {}_2F^1\left(\frac{1}{2}, 1-\gamma; \frac{3}{2}; \frac{1}{a}\right), \end{aligned} \tag{2.18}$$

where ${}_2F^1\left(\frac{1}{2}, 1-\gamma; \frac{3}{2}; \frac{1}{a}\right)$ is the hypergeometric function.
Analogously

$$\mu_0^{\gamma} \int_0^{R_\perp} dx \left(a - \frac{x^2}{R_\perp^2}\right)^{\gamma} = \mu_0^{\gamma} R_\perp a^{\gamma} {}_2F^1\left(\frac{1}{2}, -\gamma; \frac{3}{2}; \frac{1}{a}\right), \tag{2.19}$$

The properties of the hypergeometric function come to our help, since

$$\frac{{}_2F^1\left(\frac{1}{2}, 1-\gamma; \frac{3}{2}; \frac{1}{a}\right)}{{}_2F^1\left(\frac{1}{2}, -\gamma; \frac{3}{2}; \frac{1}{a}\right)} = \frac{1}{2\gamma} + 1 \tag{2.20}$$

Then we can finally compute equation (2.17):

$$\begin{aligned} I &= \frac{\mu_0^{\gamma-1} R_\perp a^{\gamma-1} {}_2F^1\left(\frac{1}{2}, 1-\gamma; \frac{3}{2}; \frac{1}{a}\right)}{\mu_0^{\gamma} R_\perp a^{\gamma} {}_2F^1\left(\frac{1}{2}, -\gamma; \frac{3}{2}; \frac{1}{a}\right)} \\ &= \frac{1}{\mu_0 a} \left(\frac{2\gamma+1}{2\gamma}\right). \end{aligned} \tag{2.21}$$

Therefore, if we define the planar local chemical potential in the position of the vortex (computed in the Thomas-Fermi approximation without the defect):

$$\tilde{\mu} \equiv \mu_0 a = \mu_0 \left(1 - \frac{y_0^2}{R_\perp^2} - \frac{z_0^2}{R_z^2}\right), \tag{2.22}$$

we get

$$I = \frac{1}{\tilde{\mu}} \frac{2\gamma + 1}{2\gamma}. \tag{2.23}$$

Hence we can finally recover equation (2.10) and write

$$\dot{z}_0 = -\frac{m}{m_B} \frac{2\gamma + 1}{4} \frac{\hbar\omega_\perp}{\tilde{\mu}} \log\left(\frac{R_\perp}{\xi}\right) \omega_\perp y_0, \tag{2.24}$$

which can be rewritten as

$$\boxed{\dot{z}_0 = -\frac{\omega_\perp}{\omega_z} \Omega y_0,} \tag{2.25}$$

where we defined

$$\frac{\Omega}{\omega_z} = \frac{m}{m_B} \frac{2\gamma + 1}{4} \frac{\hbar\omega_\perp}{\tilde{\mu}} \log\left(\frac{R_\perp}{\xi}\right). \tag{2.26}$$

For a Bose gas, as $m_B = m$ and $\gamma = 1$:

$$\frac{\Omega^{\mathrm{BEC}}}{\omega_z} = \frac{3}{4} \frac{\hbar\omega_\perp}{\tilde{\mu}} \log\left(\frac{R_\perp}{\xi}\right). \tag{2.27}$$

Now, it is possible to apply the very same reasoning to the equation for $\dot{y}_0$, which leads to

$$\boxed{\dot{y}_0 = -\frac{\omega_z}{\omega_\perp} \Omega z_0.} \tag{2.28}$$

Equations (2.25) and (2.28) represent an elliptical precession of the defect in the $y$-$z$ plane around the centre of the condensate. The precession will follow orbits of equal chemical potential

$$\tilde{\mu}(n) = \text{const.} \qquad \Rightarrow \qquad \frac{y_0^2}{R_\perp^2} + \frac{z_0^2}{R_z^2} = \text{const.} \tag{2.29}$$

which is indeed an ellipse, whose maximum amplitudes are given by the equipotential condition

$$\frac{z_{\max}^2}{R_z^2} = \frac{y_{\max}^2}{R_\perp^2}. \tag{2.30}$$

The oscillation period is then simply given by

$$\boxed{\frac{T_{\mathrm{SV}}}{T_z} = \frac{\omega_z}{\Omega} = \frac{4}{3} \frac{\tilde{\mu}}{\hbar\omega_\perp} \frac{1}{\log(R_\perp/\xi)},} \tag{2.31}$$

and is expected to be valid with logarithmic accuracy. The period (2.31) can be compared with the results available in the literature, in particular the ones computed using a variational Lagrangian approach in a paper by Fetter et al.[44]. Therein, the period

[44] A. L. Fetter and J.-k. Kim. In: *J. Low Temp. Phys.* 125.5 (2001), pp. 239–248.

of precession for a non-rotating non-axisymmetric 2D condensate is reported to be

$$T_p^{\mathrm{2D}} = \frac{2\pi}{\omega_p} = 2\frac{\tilde{\mu}}{\hbar\omega_\perp}\frac{T_z}{\log(\sqrt{2}R_\perp/\xi)}, \tag{2.32}$$

whereas in a three-dimensional condensate it is

$$T_p^{\mathrm{3D}} = \frac{2\pi}{\omega_p} = \frac{4}{3}\frac{\tilde{\mu}}{\hbar\omega_\perp}\frac{T_z}{\log(\sqrt{2}R_\perp/\xi)}, \tag{2.33}$$

which is compatible with the result (2.31) within logarithmic accuracy.

## 2.3 Time-dependent number of particles

In the previous section we assumed that the condensate maintains its properties in time, and in particular that the number of particles and thus the chemical potential $\mu_0$ are fixed from the beginning. In the real-life experiment, however, two main sources of atom reduction were present: the first, major contribution arose from the imaging process, which implied that at each time interval $\tau$ a fraction $fN(0)$ of the atoms was extracted homogeneously from the condensate; the second source were the natural trap losses, that continually reduced the atoms with time (see Figure (2.4)). Experimentally the typical fraction of the original atoms which was extracted from each shot was $f \sim 2.4\%$.

Let us approximate the step function representing the atom number with a linear relation such that:

$$\begin{aligned} N(t) &= N(0) - \alpha t \\ &= N(0) - f\frac{N(0)}{\tau}t. \end{aligned} \tag{2.34}$$

At the $l$-th imaging shot we have

$$N(l\tau) = N(0)(1 - lf) \qquad \text{with } lf < 1. \tag{2.35}$$

As shown before, in the Thomas-Fermi approximation we have that

$$n(x,y,z) = \frac{\mu_0}{g}\left(1 - \frac{x^2+y^2}{R_\perp^2} - \frac{z^2}{R_z^2}\right), \tag{2.36}$$

hence

$$n(r,z,t) = \frac{\mu_0(t)}{g}\left(1 - \frac{r^2}{R_\perp^2} - \frac{z^2}{R_z^2}\right). \tag{2.37}$$

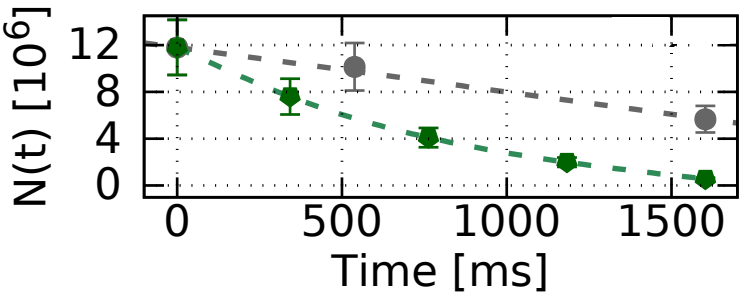


Figure 2.4: [Figure from [27]] Measured atoms in the BEC. The atom reduction only due to trap losses is reported in grey, while the one combined with the imaging extraction is plotted in green.

The normalisation condition for the condensate will then read

$$N(t) = \int dx\, dy\, dz\, n(x, y, z, t), \tag{2.38}$$

where

$$\int dx\, dy\, dz = \int_{-R_z}^{R_z} dz \int_0^{R_\perp(1-z^2/R_z^2)} dr\, r \int_0^{2\pi} d\theta. \tag{2.39}$$

We can compute that

$$\begin{aligned} N(t) &= \int dz \int dr\, r \int d\theta \frac{\mu_0(t)}{g}\left(1 - \frac{r^2}{R_\perp^2} - \frac{z^2}{R_z^2}\right) \\ &= 2\pi\frac{\mu_0(t)}{g}\int dz \int dr \left[\left(1 - \frac{z^2}{R_z^2}\right) r - \frac{r^3}{R_\perp^2}\right] \\ &= 2\pi\frac{\mu_0(t)}{g}\int dz \frac{1}{2}\left(1 - \frac{z^2}{R_z^2}\right)^3 \left[1 - \frac{1}{2}\left(1 - \frac{z^2}{R_z^2}\right)\right] \\ &= 2\pi\frac{\mu_0(t)}{g} R_\perp^2 R_z \frac{16}{63} \\ &= 2\pi\frac{\mu_0(t)}{g}\left(\frac{2\mu_0(t)}{m}\right)^{3/2} \frac{1}{\omega_\perp^2\omega_z}\frac{16}{63}. \end{aligned} \tag{2.40}$$

Hence:

$$\begin{aligned} \mu_0(t) &= \frac{1}{2}\left[\frac{N(t)}{\pi} g m^{3/2}\omega_\perp^2\omega_z \frac{63}{16}\right]^{2/5} \\ &= \frac{\hbar\omega_{\text{ho}}}{2}\left(N(t)\frac{63}{4}\frac{a}{a_{\text{ho}}}\right)^{2/5}, \end{aligned} \tag{2.41}$$

where we recalled the definition (1.6) and we defined

$$\omega_{\rm ho} = (\omega_\perp^2 \omega_z)^{1/3} \qquad \text{and} \qquad a_{\rm ho} = \sqrt{\frac{\hbar}{m\omega_{\rm ho}}}. \tag{2.42}$$

In conclusion we have shown that

$$\mu_0(t) \sim N(t)^{2/5} \quad \Rightarrow \quad \mu_0(l\tau) = \mu_0(0)(1 - lf)^{2/5}. \tag{2.43}$$

Thus in first approximation we derive

$$\boxed{T(l\tau) = \frac{4}{3}\frac{\tilde{\mu}(0)}{\hbar\omega_\perp}(1 - lf)^{2/5}\frac{T_z}{\log\left(2\frac{\mu_0(0)}{\hbar\omega_\perp}(1 - lf)^{2/5}\right)},} \tag{2.44}$$

where we used the fact that

$$\frac{R_\perp(t)}{\xi(t)} = \frac{2\mu_0(t)}{\hbar\omega_\perp}. \tag{2.45}$$

## 2.4 Comparison with the experiment

Due to the relatively good visibility of the defect axial position in the extracted frames, it was possible to follow the orbital motion of a single defect, and compare the results with equation (2.44). The extraction was assumed to be homogeneous, which implied that the gradients of the density and the lines of equal chemical potential remained unchanged throughout the process. As already pointed out, however, $\mu(t) \propto N(t)^{2/5}$ was decreasing with time, and so was the orbital period $T$ (see Figure (2.5)). We defined the period $T(t)$ corresponding to the instant $t$, as the period obtained by fitting a sinusoidal function to the measured position of the vortex. The fit was performed over a time interval centred in $t$, and large enough to include a complete oscillation. In determining the theoretical prediction, we included the consideration of the changing number of particles $N(t)$ as shown in Figure (2.4), both in the value of the chemical potential $\mu$, and of the healing length $\xi$. In particular, we considered the effect of $N(t)$ on the Thomas-Fermi radius $R_z(t)$, so that

$$r_0(t) \equiv \frac{z_{\max}(t)^2}{R_z(t)^2} = \frac{y_{\max}(t)^2}{R_\perp(t)^2}, \tag{2.46}$$

was properly rescaled. Here we extracted $z_{\max}(t)$ by looking at the instantaneous amplitude of the sinusoidal fit of the oscillation.

The reported agreement is quite remarkable, as there are no free parameters in the computation. The main limitation to the accuracy of the prediction arose from the

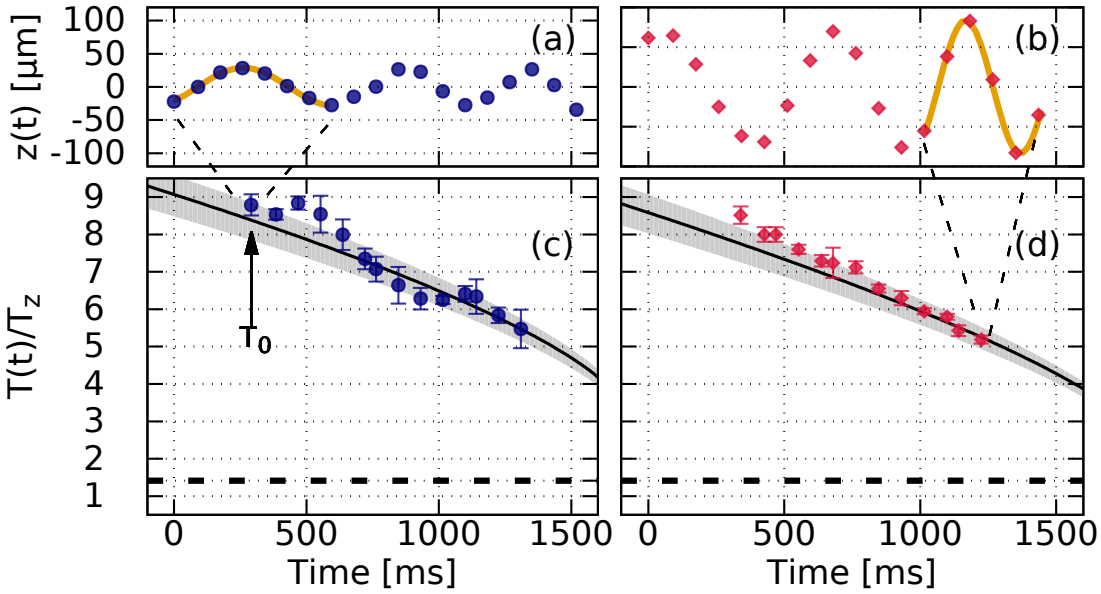


Figure 2.5: [Figure from [27]] (a)-(b) Axial position of the vortex after expansion for the two sets of extraction (b) and (c) of Figure (2.2). (c)-(d) Normalised instantaneous period $T(t)$ fitted on the above data. The theoretical prediction (2.44) is represented by the solid line, and also includes the measured variation of $N(t)$ reported in Figure (2.4). The grey region marks an experimental uncertainty in the number of atoms of 20%. The dashed line shows the prediction for the oscillation of a grey soliton $T_{\mathrm{sol}} = \sqrt{2}T_z$.

uncertainty in the determination of the number of atoms $N(t)$. A famous result[45] concerning the oscillation of a grey soliton in a BEC in a harmonic trap, predicts its period to be $T_{\mathrm{sol}} = \sqrt{2}T_z$, which is reported in Figure (2.5) as a comparison in a black dashed line.

Another test can be performed by looking at the behaviour of the vortex period with the quantity $r_0^2$. For this purpose, for each set of data, we considered the period of the first complete oscillation (marked as $T_0$ in Figure (2.5)). The resulting plot can be seen in Figure (2.6a), where the theoretical prediction (2.31) is reported in a dashed line, and is without free parameters. Once again the agreement is good, and the two are compatible within a 20% uncertainty in the determination of $N(t_0)$.

The result of Figure (2.6a) can be further appreciated by observing the ratio between the period $T_0$, measured at a given $r_0$, and its theoretical counterpart, computed for the same values of $r_0$ and $N$. In Figure (2.6b) are reported the histograms for this quantity, in the presence of a single vortex, and when two vortices are simultaneously oscillating in the condensate. In the single vortex case, the mean value is $\langle T_0/T_{\mathrm{th}}\rangle = 0.97 \pm 0.04$, while in the second case $\langle T_0/T_{\mathrm{th}}\rangle = 0.96 \pm 0.14$, showing an increase in the dispersion

[45] Vladimir V. Konotop and Lev Pitaevskii. In: *Phys. Rev. Lett.* 93 (2004), p. 240403.

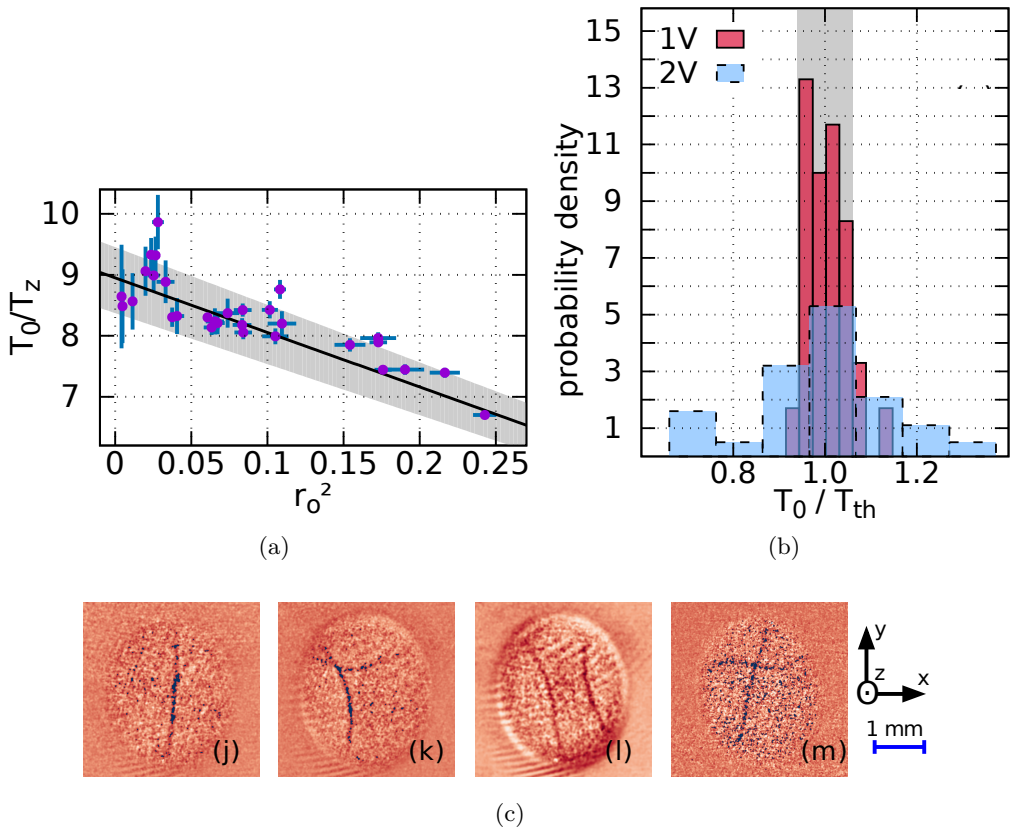


Figure 2.6: [Figure from [27]] (a) Period of the vortex $T(t_0) = T_0$ extracted from the first complete oscillation of 30 different sequences, normalised by $T_z$ and plotted as a function of $r_0^2$. The solid line represents the behaviour $(1 - r_0^2)$ predicted by (2.31), and no free parameters are included. The shaded area allows for an uncertainty in the determination of $N(t_0)$ of 20%. (b) Density of probability for the ratio between the measured period $T_0$ and the theoretical $T_{\rm th}$, computed with the appropriate $N$ and $r_0$. (red) 30 cases of single vortex oscillations; (blue) 27 cases of coexistence of two vortices. The grey area accounts for a 20% uncertainty in the measurement of $N$. (c) Absorption (destructive) images of the BEC in the axial direction, highlighting the presence of one (j) and two (k)-(m) vortices. The vortex lines are not usually straight, and are bent towards the surface of the condensate.

of the data.

The agreement between the theoretical and the experimental results shown above is quite remarkable, especially given the fact that the theory supporting equation (2.31) implies that the vortex behaves as a straight rigid line. In our case, however, where a strong confinement is present, the off-centred vortices are bent towards the surface of the BEC (see Figure (2.6c)).

## 2.5 Vortex interactions

The experiment also addressed the effect of the presence of multiple solitonic vortices all at once. The goal was to investigate the possible effect of interactions between defects. The first quantity to be observed was the vortex lifetime. In a non-rotating BEC this is limited by the scattering of the defect with the thermal fluctuations, which could eventually dissipate the vortex energy into the thermal cloud. Interestingly, as vortices (and solitons) can be mapped to particles with negative effective mass, the dissipation causes an acceleration on their motion, and an *antidamping* effect on their trajectories. When the vortex reaches the edge of the atomic cloud, where the thermal atoms are concentrated, it can dissipate and disappear. The lifetime $\tau$ was measured by counting the number $\langle N_V \rangle_t$ of surviving vortices at time $t$, having started with $N_V(0)$. If $N_V(0) = 1$ a clear exponential decay was measured (Figure (2.7)), and the corresponding lifetime $\tau_1 = (910 \pm 100)$ ms is close to the one available in the literature[37,46].

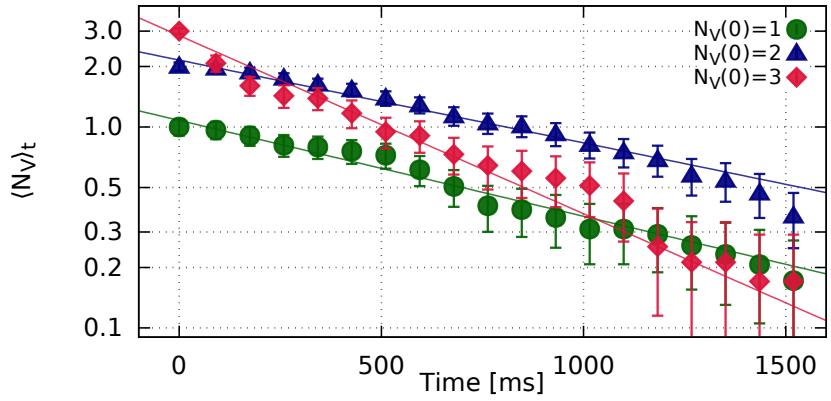


Figure 2.7: [Figure from [27]] Average surviving vortices $\langle N_V \rangle_t$ at time $t$, in logarithmic scale: $N_V(0) = 1$ (green), $N_V(0) = 2$ (blue), $N_V(0) = 3$ (red). The solid lines represent an exponential fit.

In the framework of the Kibble-Zurek mechanism, one could produce a higher number of initial defects in the system (see more on that in Chapter (4)). This simply requires to use a faster evaporation ramp to decrease the temperature and thus accelerate the quench. This way, once the system has grown to the full condensate, it is possible to get up to 5 defects[46]. For the purpose of this work, however, and for visibility reasons, only up to $N_V(0) = 3$ were considered. From the extraction sequences (see Figure (2.2d-i) for some examples) it is again possible to follow the trajectories of the

[37] S. Donadello et al. In: *Phys. Rev. Lett.* 113 (2014), p. 065302.
[46] G. Lamporesi et al. In: *Nat Phys* 9.10 (2013), pp. 656–660.

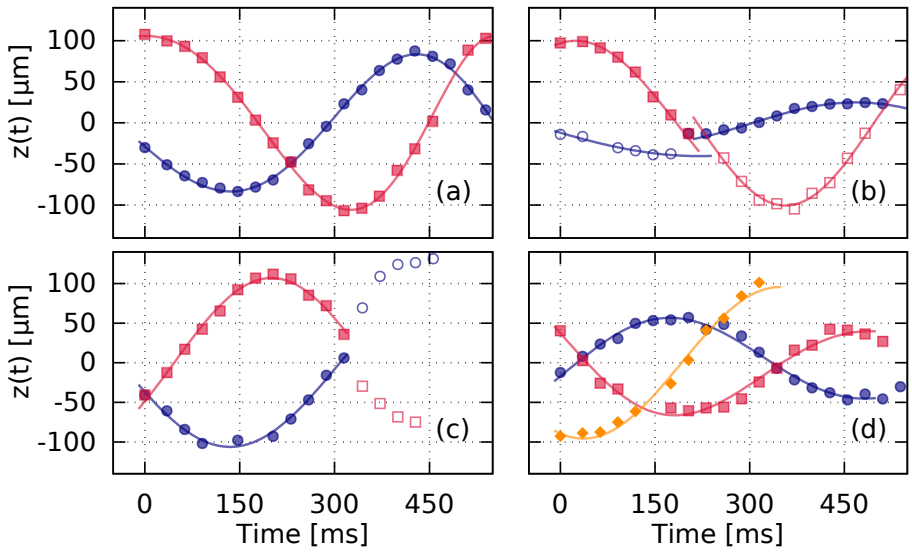


Figure 2.8: [Figure from [27]] Vortex axial position, corresponding to the extraction sequences of Figure (2.2d-g): (a) two vortices crossing with unperturbed trajectories; (b) two vortices crossing with a change in visibility and a phase shift in the trajectory; (c) sudden change in visibility after the crossing; (d) two unperturbed vortices and a third disappearing. Solid and empty symbols represent high and low contrast of the defect, respectively.

vortices. In some cases the path is unperturbed, and the defects seem to cross without effect (see Figure (2.8a)), while in other cases two effects are visible: a phase shift in the trajectories (Figure (2.8b)), or a sudden change in the visibility of the defects (Figure (2.8c)). The phase shift is also responsible for the broadening of the distribution of $T_0/T_{\mathrm{th}}$ for multiple vortices, as seen in Figure (2.6b), whose mean value becomes $0.96 \pm 0.14$. The change in visibility can be associated to a rotation of the vortex line, so that it no longer lies in the $x$-$y$ plane. Due to the observation method that was implemented, which implies that the extracted density is integrated in the $x$ direction, this results indeed in a reduction of the contrast. The lifetimes for the two initial conditions $N_V(0) = 2$ and $N_V(0) = 3$ are $\tau_2 = (1050 \pm 100)$ ms and $\tau_3 = (490 \pm 100)$ ms.

From these results one could argue that whenever only two vortices are present in the system, their interaction is such that it does not influence the lifetime, whereas in the three-vortex case, a clear reduction of the $\tau$ is measured. This led us to formulate the hypothesis that three-body collisions were responsible for the rapid decay in the case $N_V(0) = 3$. The presence of a third defect drastically reduces the chance of three vortices to pass by without crossing. As for the two-vortex case, a possible explanation

for the small effect of the two-body processes was given as follows. When two vortices approach, two outcomes are given: either the defects pass by avoiding each other, or they cross and reconnect. In the first instance, which should be statistically infrequent, the modification to the trajectory could be negligible. When two vortical lines cross, reconnections are predicted to occur[47]: the lines can merge, and locally coplanar sections of them can be exchanged among the defects. This might clearly affect the vortex dynamics, and should cause a change in their motion. The fact that often no appreciable effect is seen was justified by the existence of a double-reconnection process: when the two vortex planes come across, the vortex lines first exchange a section, and, due to the geometry of the system, when the planes separate again, they stretch. The energy cost associated with this elongation favours a second reconnection process when the two vortices are still at close distance, which establishes again the original configuration. Such a mechanism could well explain the trajectory phase shift, and was postulated to be connected with the relative velocity of the incoming defects.

## 2.6 Chapter conclusions and follow-up analysis

In this chapter we described an experiment on the real-time dynamics of vortices generated at random positions by performing a fast quench of the temperature. Solitonic vortices are quantised vortices constrained in a narrow geometry, thus showing some of the properties usually associated with the solitons. In the experiment, their dynamics was followed in real-time by means of a stroboscopic non-destructive technique, outcoupling a small portion of the atoms while leaving the rest of the system only marginally affected. The vortices are predicted to follow equipotential line with constant chemical potential $\mu$. The imaging technique, combined with the natural losses of the trap, were reducing the number of atoms in time, causing the defects to follow elliptical spiral trajectories with decreased period. The theoretical estimation of the period fitted well with the experimental data. We also presented an experimental analysis on the possible effect of vortex interactions, by looking at the lifetime of the defects. It was measured that when the initial number of defects is $N_V(0) = 2$, their lifetime is almost unaffected with respect to the single vortex case. However, when $N_V(0) = 3$, a clear reduction effect was measured. This prompted the idea that vortex reconnection processes might enhance the decay of the defects, in a non-trivial way depending on the initial position and orientation of the vortices. This topic was further addressed in a following paper[39], where a more sophisticated experimental technique has been implemented. This allowed to infer the original mutual orientation of the defects, and

[47] M. S. Paoletti and D. P. Lathrop. In: *Ann. Rev. of Cond. Mat. Phys.* 2.1 (2011), pp. 213–234.
[39] S. Serafini et al. In: *Phys. Rev. X* 7 (2017), p. 021031.

by means of extensive numerical analysis it was possible to identify several unexpected collisional processes, such as double reconnections, rotations, rebounds after a collision and ejection of defects.

# Part II

# Finite-temperature analysis

# Chapter 3

# Stochastic Gross-Pitaevskii theory at finite temperature

In this chapter, we describe the theoretical tools which will be used for the rest of the thesis. Among the finite temperature methods available in the literature (e.g. the Classical-Field approach[48–50]), we give a description of two methods, similar in concept, but coming from different derivations. At first, we introduce the stochastic Gross-Pitaevskii equation (SGPE), and then we review the key aspects of the stochastic projected Gross-Pitaevskii equation (SPGPE).

The SGPE is a theoretical model which allows to describe the non-equilibrium dynamics of a Bose-Einstein condensate, and in particular the condensation process itself. The approach we present is the one introduced by Stoof[51–54], as summarised by Proukakis and Jackson[34], and consists in writing a Fokker-Planck equation for the problem, from which one can then derive an equivalent Langevin equation. This approach is similar to the one applied to the standard treatment of the classical Brownian motion, which is reported for comparison in Appendix A.

Later on, we review the main steps of the stochastic projected Gross-Pitaevskii equation[55], which features a projector explicitly separating low- and high-energy modes. Although having a formulation very close to the SGPE, this method arises from a

[48] A. Sinatra, C. Lobo, and Y. Castin. In: *Phys. Rev. Lett.* 87 (2001), p. 210404.
[49] BV Svistunov. In: *J. Moscow Phys. Soc* 1 (1991), p. 373.
[50] M. Brewczyk, M. Gajda, and K. Rzażewski. In: *J. Phys. B* 40.2 (2007), R1.
[51] H. T. C. Stoof. In: *J. Low Temp. Phys.* 114.1 (1999), pp. 11–108.
[52] H. T. C. Stoof and M. J. Bijlsma. In: *J. Low Temp. Phys.* 124.3 (2001), pp. 431–442.
[53] R. A. Duine and H. T. C. Stoof. In: *Phys. Rev. A* 65 (2001), p. 013603.
[54] HTC Stoof. "Quantum kinetic theory of trapped atomic gases". In: *Dynamics: Models and Kinetic Methods for Non-equilibrium Many Body Systems*. Springer, 2000, pp. 491–502.
[34] N. P Proukakis and B. Jackson. In: *J. Phys. B* 41 (2008), p. 203002.
[55] P. B. Blakie et al. In: *Advances in Physics* 57.5 (2008), pp. 363–455.

different theoretical perspective.

In the second part of the chapter, we outline the numerical implementation of such models for two-dimensional systems, along with some details of their use and of the analysis of the results.

## 3.1 Theoretical description

In Stoof's approach one writes an equation for the evolution of the Wigner probability distribution $P[\phi^*, \phi; t]$, which represents the probability for the system to be in a quantum coherent state

$$|\phi(\mathbf{r}; t)\rangle = e^{\int d\mathbf{r}\, \phi(\mathbf{r})\hat{\Psi}^\dagger(\mathbf{r},t)}|0\rangle, \tag{3.1}$$

where $|0\rangle$ identifies the vacuum state. Then the probability distribution can be computed by means of the initial density matrix $\rho(t_0)$:

$$P[\phi^*, \phi; t] = \mathrm{Tr}\left[\rho(t_0)\frac{|\phi, t\rangle\langle\phi, t|}{\langle\phi, t|\phi, t\rangle}\right] = \int d\phi_0^*\, d\phi_0\, \rho(|\phi_0|^2; t_0)\frac{|\langle\phi, t|\phi_0, t_0\rangle|^2}{\langle\phi, t|\phi, t\rangle}. \tag{3.2}$$

In the above equation, the density matrix $\rho(t_0)$ has been expanded in terms of the coherent states defined in equation (3.1). By means of the Keldysh formalism, it is possible to compute the matrix elements $\langle\phi; t|\phi_0; t_0\rangle$ and $\langle\phi_0; t_0|\phi; t\rangle$ as path integrals over all the possible complex fields $\Phi(\mathbf{r}, t)$ having as their initial state $\Phi(\mathbf{r}, t_0) = \phi_0(\mathbf{r})$. Thus

$$P[\phi^*, \phi, t] = \int d\Phi^*\, d\Phi\, e^{iS_{\mathrm{eff}}(\Phi^*, \Phi)/\hbar}\,, \tag{3.3}$$

where $S_{\mathrm{eff}}(\Phi^*, \Phi)$ is an effective action, as reported by Stoof[56]. Computing $\langle\phi; t|\phi_0; t_0\rangle$ and $\langle\phi_0; t_0|\phi; t\rangle$ means to investigate all the possible paths followed by $\psi$ from the generic time $t$ back to the initial $t_0$ (backward evolution) and back again to $t$ (forward evolution) which then represents a Keldysh contour[57]. From eq. (3.3) it is possible to derive the full Fokker-Planck equation, as is again reported by Stoof[56].

By means of a Hartree-Fock-type approach, the system is separable in two components describing the low-lying modes of the system (the so-called *coherent region*, also known as *c-field*) $\psi$ and the highly energetic thermal modes (*incoherent region*) $\phi'$:

$$P[\phi^*, \phi; t] = P_0[\psi^*, \psi; t]P_1[\phi'^*, \phi'; t]. \tag{3.4}$$

By substituting this ansatz in the full Fokker-Planck equation it is possible to compute

[56] H. T. C. Stoof. In: *Phys. Rev. Lett.* 78 (1997), pp. 768–771.
[57] L. V. Keldysh. In: *JETP* 20 (1965), p. 1515.

a system of two coupled equations for $\psi$ and $\phi'$.

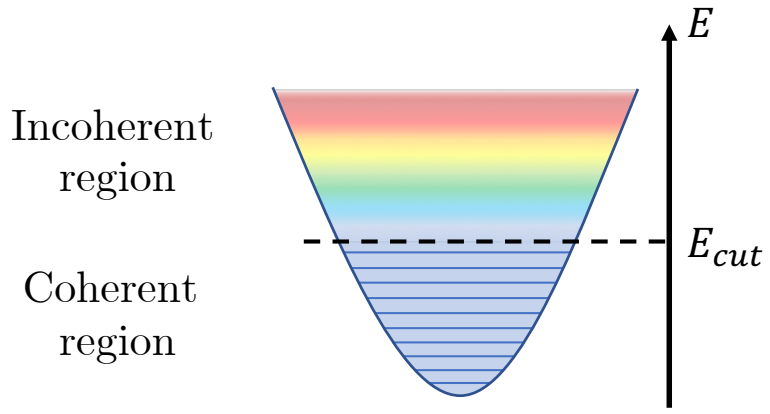


Figure 3.1: Schematic representation of the coherent region included in $\psi$, indicating the highly occupied modes, and of the above lying incoherent region, whose dynamics is not described by $\psi$.

### 3.1.1 Quantum Boltzmann equation for the thermal modes

Let us first give a look at the high-lying modes, whose evolution is governed by the quantum Boltzmann equation:

$$\frac{\partial f}{\partial t} + (\nabla_{\mathbf{p}}\epsilon(\mathbf{r},t)) \cdot (\nabla_{\mathbf{r}} f(\mathbf{r},\mathbf{p},t)) - (\nabla_{\mathbf{r}}\epsilon(\mathbf{r},t)) \cdot (\nabla_{\mathbf{p}} f(\mathbf{r},\mathbf{p},t)) = C_{12}[f] + C_{22}[f], \quad (3.5)$$

where the functions $f(\mathbf{r},\mathbf{p},t)$ are the Wigner phase-space distribution for the thermal particles, constrained by

$$n_t(\mathbf{r},t) = \int \frac{d\mathbf{p}}{(2\pi\hbar)^3} f(\mathbf{r},\mathbf{p},t), \quad (3.6)$$

and the energy of a thermal particle is

$$\epsilon(\mathbf{r},t) = \frac{|\mathbf{p}|^2}{2m} + V(\mathbf{r}) + 2g\big(|\psi(\mathbf{r},t)|^2 + n_t(\mathbf{r},t)\big). \quad (3.7)$$

The two terms on the right side of equation (3.5) represent the binary elastic collisions between particles and refer to two distinct processes.

The exchange between the c-field and the incoherent region is described by the

collisional integral

$$\begin{aligned} C_{12}[f] = \frac{4\pi}{\hbar} g^2 |\psi|^2 \int \frac{d\mathbf{p}_1}{(2\pi\hbar)^3} \int \frac{d\mathbf{p}_2}{(2\pi\hbar)^3} \int \frac{d\mathbf{p}_3}{(2\pi\hbar)^3} \\ \times (2\pi\hbar)^3 \delta(m\mathbf{v}_c + \mathbf{p}_1 - \mathbf{p}_2 - \mathbf{p}_3) \delta(\epsilon_c + \epsilon_1 - \epsilon_2 - \epsilon_3) \\ \times (2\pi\hbar)^3 \left(\delta(\mathbf{p}_c - \mathbf{p}_1) - \delta(\mathbf{p}_c - \mathbf{p}_2) - \delta(\mathbf{p}_c - \mathbf{p}_3)\right) \\ \times \left(f_1(f_2+1)(f_3+1) - (f_1+1) f_3 f_4\right), \end{aligned} \tag{3.8}$$

where the subscript "$c$" indicates the coherent part. Here $(f_1+1)f_3f_4$ accounts for one particle falling into the coherent region, while $f_1(f_2+1)(f_3+1)$ for the promotion of a particle from the low-energy part.

The other collisional integral describes the internal collision involving two thermal atoms, redistributing the population of these modes:

$$\begin{aligned} C_{22}[f] = \frac{4\pi}{\hbar} g^2 \int \frac{d\mathbf{p}_1}{(2\pi\hbar)^3} \int \frac{d\mathbf{p}_2}{(2\pi\hbar)^3} \int \frac{d\mathbf{p}_3}{(2\pi\hbar)^3} \\ \times (2\pi\hbar)^3 \delta(\mathbf{p} + \mathbf{p}_1 - \mathbf{p}_2 - \mathbf{p}_3) \delta(\epsilon + \epsilon_1 - \epsilon_2 - \epsilon_3) \\ \times \left((f+1)(f_1+1) f_2 f_3 - f f_1 (f_2+1)(f_3+1)\right). \end{aligned} \tag{3.9}$$

Note that both in eq. (3.8) and (3.9) the $\delta$ functions ensure the conservation of energy and momentum, for the collisions to be elastic.

### 3.1.2 Fokker-Planck equation for the coherent modes

By integrating out the incoherent part $\phi'$ one gets a Fokker-Planck equation(3.10) for the coherent region $\psi$:

$$\begin{aligned} i\hbar \frac{\partial}{\partial t} P[\psi^*, \psi; t] = \\ - \int d\mathbf{r} \frac{\delta}{\delta\psi(\mathbf{r})} \left( -\frac{\hbar^2\nabla^2}{2m} + V(\mathbf{r}) - iR(\mathbf{r},t) + g|\psi(\mathbf{r},t)|^2 - \mu(t) \right) \psi(\mathbf{r},t) P[\psi^*, \psi; t] \\ + \int d\mathbf{r} \frac{\delta}{\delta\psi^*(\mathbf{r})} \left( -\frac{\hbar^2\nabla^2}{2m} + V(\mathbf{r}) + iR(\mathbf{r},t) + g|\psi(\mathbf{r},t)|^2 - \mu(t) \right) \psi^*(\mathbf{r},t) P[\psi^*, \psi; t] \\ - \frac{1}{2} \int d\mathbf{r} \frac{\delta^2}{\delta\psi(\mathbf{r})\delta\psi^*(\mathbf{r})} \hbar\Sigma^K(\mathbf{r};t) P[\psi^*, \psi; t], \end{aligned} \tag{3.10}$$

where by $\delta/\delta\psi$ we denote a functional derivative in the field $\psi$. Differently from the solution of the Gross-Pitaevskii equation (eq. (1.14)), here $\psi$ does not only represent the condensate wavefunction, but a finite set of low-energy excitations are also included[53].

Let us clarify the role of the elements in (3.10). The two terms $iR(\mathbf{r},t)$ and $\Sigma^K(\mathbf{r},t)$

[53] R. A. Duine and H. T. C. Stoof. In: *Phys. Rev. A* 65 (2001), p. 013603.

have their origin in the coupling with the incoherent region, hence with an infinite reservoir of thermalised atoms with which the c-field can exchange particles due to elastic collisions. In the Hartree-Fock approximation the full expression for the term $R$ is

$$\begin{aligned} R(\mathbf{r},t) =& 2\pi g^2 \int \frac{d\mathbf{p}_1}{(2\pi)^3} \int \frac{d\mathbf{p}_2}{(2\pi)^3} \int \frac{d\mathbf{p}_3}{(2\pi)^3} (2\pi)^3 \delta(\mathbf{p}_1 - \mathbf{p}_2 - \mathbf{p}_3) \\ & \delta(\epsilon_c + \epsilon_1 - \epsilon_2 - \epsilon_3)(f_1(1+f_2)(1+f_4) - (1+f_1)f_2 f_3). \end{aligned} \tag{3.11}$$

In the above equation, the conservation of the energy and momentum in the elastic collisions is ensured again by the $\delta$ terms. The functions $f_i = f_i(\mathbf{r}, \mathbf{p}_i, t)$ represent once again the Wigner distributions for the thermal particles and are the solution of eq. (3.5), and the energies of the thermal particles are

$$\epsilon_i = \frac{|\mathbf{p}|^2}{2m} + V(\mathbf{r}) + 2g\langle|\psi(\mathbf{r},t)|^2\rangle, \tag{3.12}$$

where we assumed that the mean field effect of the incoherent component has a negligible consequence on the properties of the coherent region.
The quantity $\hbar\Sigma^K$ is the so-called *Keldysh self-energy*, determining the strength of the fluctuations:

$$\begin{aligned} \hbar\Sigma^K(\mathbf{r},t) = & -4\pi i g^2 \int \frac{d\mathbf{p}_1}{(2\pi\hbar)^3} \int \frac{d\mathbf{p}_2}{(2\pi\hbar)^3} \int \frac{d\mathbf{p}_3}{(2\pi\hbar)^3} \\ & \times (2\pi\hbar)^3 \delta(\mathbf{p} + \mathbf{p}_1 - \mathbf{p}_2 - \mathbf{p}_3)\delta(\epsilon + \epsilon_1 - \epsilon_2 - \epsilon_3) \\ & \times ((f+1)(f_1+1)f_2 f_3 + f f_1 (f_2+1)(f_3+1)) \,. \end{aligned} \tag{3.13}$$

Equations (3.11) and (3.13) describe respectively the dissipations and the fluctuations in the system[53]. Note that eq. (3.11) and eq. (3.13) are similar but not identical: in one case the Wigner functions, corresponding to "in" and "out" rates in the collisions, are subtracted, while in the other case they are added. This means that at equilibrium, when the particles falling into the coherent region are balanced by the ones extracted from it, the dissipation of the system can be suppressed on average. On the contrary, the fluctuations are always present in the system. The dynamical equilibrium described by this theory is therefore established when these two quantities balance each other out.

[53] R. A. Duine and H. T. C. Stoof. In: *Phys. Rev. A* 65 (2001), p. 013603.

### 3.1.3 The stochastic Gross-Pitaevskii equation

Let us now derive an important tool, following almost exactly the treatment of Duine and Stoof[53]. In order to better treat the problem numerically, it is possible to map the Fokker-Planck equation (3.10) into a Langevin equation describing the same system. The energy $\epsilon_c$ necessary to remove an atom from the low-lying modes described by $\psi$ is

$$\epsilon_c = -\frac{\hbar^2\nabla^2}{2m} + V(\mathbf{r}) + g|\psi(\mathbf{r},t)|^2, \tag{3.14}$$

so that this energy depends on the classical field itself. This has a profound consequence, as both $R$ and $\Sigma^K$ will depend on $\psi$ through $\epsilon_c$. As pointed out by Duine and Stoof[53], this means that the Langevin equation would contain a multiplicative noise term, rather than an additive one, with a prefactor depending on $\psi$. The numerical implementation of this problem is all but trivial. In order to make it more manageable, we will introduce some assumptions. If the thermal cloud is close to equilibrium, it will act as a thermal bath in contact with the coherent region. This way we can neglect the dynamical treatment for the incoherent region associated with the quantum Boltzmann equation (3.5), and instead consider a reduced equation where $C_{22}[f] = 0$ (physically this means that the collisions leading to the thermalisation of the higher modes act much faster than the other dynamical processes). It is possible to show that the solutions for this equation satisfy the Bose-Einstein distribution

$$n_{\mathrm{BE}} = \frac{1}{e^{\beta(\epsilon_i-\mu)}-1}, \tag{3.15}$$

where we introduced $\beta = 1/k_{\mathrm{B}}T$. We will therefore replace the Wigner distributions $f$ with $n_{\mathrm{BE}}$, and this allows us to write a *fluctuation-dissipation* relation[53]

$$iR(\mathbf{r},t) = -\frac{1}{4}\hbar\Sigma^K(\mathbf{r},t)\frac{1}{1/2+n_{\mathrm{BE}}(\epsilon_c)}. \tag{3.16}$$

This relation depends on the particle distribution in the modes (through $n_{\mathrm{BE}}$) plus an average of an extra $1/2$ particle per mode. These indicate respectively the spontaneous and the stimulated scattering processes, underlying the quantum nature of the theory. Equation (3.16) determines the system's equilibrium distribution, and is only valid in the linear regime of the perturbation from equilibrium of the thermal cloud.

We are finally able to write the Langevin equation equivalent to the Fokker-Planck equation (3.10) under the assumptions described above. Its form resembles the one of the Gross-Pitaevskii equation (1.14), with the important addition of the dissipative

[53] R. A. Duine and H. T. C. Stoof. In: *Phys. Rev. A* 65 (2001), p. 013603.

and the fluctuating terms

$$i\hbar\frac{\partial\psi(\mathbf{r},t)}{\partial t}=\left(-\frac{\hbar^2\nabla^2}{2m}+V_{\rm tr}(\mathbf{r},t)-iR(\mathbf{r},t)+g|\psi(\mathbf{r},t)|^2-\mu\right)\psi(\mathbf{r},t)+\eta(\mathbf{r},t). \quad (3.17)$$

Equation (3.16) can be further approximated. For high temperatures ($\beta\ll 1$) or close to equilibrium ($\epsilon_c-\mu\ll 1$) it is possible to Taylor-expand the Bose-Einstein distribution $n_{\rm BE}$

$$\frac{1}{2}+n_{\rm BE}\sim\frac{1}{\beta(\epsilon_c-\mu)}, \quad (3.18)$$

and replace the fluctuation-dissipation relation by its classical counterpart

$$iR(\mathbf{r},t)=-\frac{\beta}{4}\hbar\Sigma^K(\mathbf{r},t)(\epsilon_c-\mu). \quad (3.19)$$

Note that the expansion (3.18) requires that the average occupation number of each mode is larger than one (in practical terms between 1 and 10)[55].

By introducing this approximation it is possible to rewrite the Fokker-Planck equation (3.10) as

$$\begin{aligned}i\hbar\frac{\partial}{\partial t}P[\psi^*,\psi;t]=&\\ &-\frac{\beta}{4}\int d\mathbf{r}\,\hbar\Sigma^K(\mathbf{r},t)\frac{\delta}{\delta\psi(\mathbf{r})}\left(-\frac{\hbar^2\nabla^2}{2m}+V(\mathbf{r})+g|\psi(\mathbf{r},t)|^2-\mu\right)\psi(\mathbf{r},t)P[\psi^*,\psi;t]\\ &-\frac{\beta}{4}\int d\mathbf{r}\,\hbar\Sigma^K(\mathbf{r},t)\frac{\delta}{\delta\psi^*(\mathbf{r})}\left(-\frac{\hbar^2\nabla^2}{2m}+V(\mathbf{r})+g|\psi(\mathbf{r},t)|^2-\mu\right)\psi^*(\mathbf{r},t)P[\psi^*,\psi;t]\\ &-\frac{1}{2}\int d\mathbf{r}\,\hbar\Sigma^K(\mathbf{r},t)\frac{\delta^2}{\delta\psi(\mathbf{r})\delta\psi^*(\mathbf{r})}P[\psi^*,\psi;t], \quad (3.20)\end{aligned}$$

whose solution can be shown[53] to be the correct equilibrium distribution, obeying the time-independent Gross-Pitaevskii equation (1.17). By means of eq. (3.19), the Langevin equation becomes numerically treatable, and can be rewritten as

$$\boxed{i\hbar\frac{\partial\psi(\mathbf{r},t)}{\partial t}=\left(1+\frac{\beta}{4}\hbar\Sigma^K(\mathbf{r},t)\right)\left[-\frac{\hbar^2\nabla^2}{2m}+V_{\rm tr}(\mathbf{r},t)+g|\psi(\mathbf{r},t)|^2-\mu\right]\psi(\mathbf{r},t)+\eta(\mathbf{r},t)} \quad (3.21)$$

which will be referred to as stochastic Gross-Pitaevskii equation (SGPE), and will be one of the main tools used in the following of this thesis. Equations (3.21) and (3.20) show some analogy with the ones for the Brownian motion reported in Appendix A,

[55] P. B. Blakie et al. In: *Advances in Physics* 57.5 (2008), pp. 363–455.
[53] R. A. Duine and H. T. C. Stoof. In: *Phys. Rev. A* 65 (2001), p. 013603.

where we can identify the analogue of the damping term $\gamma$ in eq. (A.27) with

$$i\frac{\beta}{4}\hbar\Sigma^K(\mathbf{r},t)(\epsilon_c-\mu)\equiv\gamma(\mathbf{r},t)(\epsilon_c-\mu). \tag{3.22}$$

Similarly to the noisy term of the Brownian motion (eq. (A.6)) here we have that the correlation is

$$\langle\eta^*(\mathbf{r},t)\eta(\mathbf{r}',t')\rangle=2\gamma(\mathbf{r},t)\hbar k_{\mathrm{B}}T\delta(\mathbf{r}-\mathbf{r}')\delta(t-t'). \tag{3.23}$$

Given the stochastic nature of eq. (3.21), the physical observables are obtained by means of an average over many noise realisations. However, the single realisation still holds information about the fluctuations in the system, and can be linked to a single experimental run[58,59].

**Ultraviolet divergence and cutoff.** The stochastic Gross-Pitaevskii approach described by eq. (3.21) enters the family of the so-called *classical field* (c-field) approximations. The common feature of these methods is to assume a high mode occupation of the low-energy part of the whole quantum Bose operator, and treat it as a classical object. This means that its intrinsic quantised nature is replaced by a continuum of energy levels, so that a classical wave can describe it. This makes the procedure analogous to the one used in electromagnetism, where one can approximate the low-energy limit of the black-body radiation by the classical Rayleigh-Jeans distribution, instead of the quantised Planck distribution. This approximation fails dramatically in the high-energy regime, leading to the so-called *ultraviolet catastrophe*. Thus, a high-energy cutoff is needed in the theory to eliminate the high-energy (large momenta) modes. This also means to introduce an effective theory unaffected by the short-range details of the interaction[55,60]. In order to include all the important dynamics in the system, the cutoff should be much greater than the chemical potential $\mu$ and larger than the thermal energy $k_{\mathrm{B}}T$. In practical terms, this is usually achieved by the natural cutoff introduced by the spatial discretisation needed in treating the equations numerically. However, one could explicitly impose an energy cutoff by means of a projector acting on the system, as explained below.

[58] S. P. Cockburn. "Bose Gases In and Out of Equilibrium within the Stochastic Gross-Pitaevskii Equation". PhD thesis. Newcastle University, 2010.

[59] D. Gallucci. "Ab Initio Modelling of quasi-one-dimensional Bose gas experiments via the Stochastic Gross-Pitaevskii Equation". PhD thesis. Newcastle University, 2013.

[55] P. B. Blakie et al. In: *Advances in Physics* 57.5 (2008), pp. 363–455.

[60] M. J. Davis et al. "C-Field Methods for Non-Equilibrium Bose Gases". In: *Quantum Gases*. Imperial College Press, 2013, pp. 163–175.

### 3.1.4 The stochastic projected Gross-Pitaevskii equation

Among the various *c-field* methods for describing the dynamics of finite temperature condensates, the one which is more closely related to the SGPE approach (3.21) is the stochastic projected Gross-Pitaevskii equation (SPGPE)[61–63]. This method combines the kinetic theory of C. W. Gardiner and co-workers[64–66] with the finite temperature formalism for the Gross-Pitaevskii equation, which was developed by Davis and co-workers[67,68].

Similar to the Stoof approach presented in the previous section, it also assumes the separation of the high- and the low-energy modes of the system, but this separation is carried out in two subsequent steps. At first, the Bose field is coarse-grained by the introduction of a spatial minimum distance (and maximum momentum) to be considered, in order to get an effective coupling in the interaction between atoms. As for the SGPE, this basically consist of recovering the Gross-Pitaevskii equation from the full quantum theory, as an effective field theory, and corresponds to the introduction of a high-energy cutoff to heal the ultraviolet catastrophe. The resulting field is then explicitly separated in two regions

$$\Psi(\mathbf{r}) = \Psi_C(\mathbf{r}) + \Psi_I(\mathbf{r}) \tag{3.24}$$

by means of a projector operator $\hat{\mathcal{P}}_C$, recasting $\Psi$ into the coherent region at each time step

$$\Psi_C(\mathbf{r}, t) = \hat{\mathcal{P}}_C[\Psi(\mathbf{r}, t)] = \sum_{n \in C} a_n \varphi_n(\mathbf{r}, t), \tag{3.25}$$

where $\varphi_n$ are the eigenvectors of the single-particle Hamiltonian belonging to the coherent region $C$.

The Langevin equation (3.21) is indeed very similar to the one for the SPGPE, even though the derivation comes from a quantum optics perspective rather than a Keldysh formalism. The density of the coherent region can be described in terms of a master equation, after introducing a "high-temperature" approximation assuming that the energies of the modes in the coherent region are small compared to the tem-

[61] C. W. Gardiner, J. R. Anglin, and T. I. A. Fudge. In: *J. Phys. B* 35.6 (2002), p. 1555.
[62] M. Davis et al. *Quantum Gases: Finite Temperature and Non-Equilibrium Dynamics.* Imperial College Press, 2013.
[63] C W Gardiner and M J Davis. In: *J. Phys. B* 36.23 (2003), p. 4731.
[64] C. W. Gardiner and P. Zoller. In: *Phys. Rev. A* 55 (1997), pp. 2902–2921.
[65] C. W. Gardiner and P. Zoller. In: *Phys. Rev. A* 58 (1998), pp. 536–556.
[66] C. W. Gardiner and P. Zoller. In: *Phys. Rev. A* 61 (2000), p. 033601.
[67] M. J. Davis, S. A. Morgan, and K. Burnett. In: *Phys. Rev. Lett.* 87 (2001), p. 160402.
[68] M. J. Davis, S. A. Morgan, and K. Burnett. In: *Phys. Rev. A* 66 (2002), p. 053618.

perature. Strictly speaking, this limits the formal validity of the theory to relatively high temperatures, $0.5T_c \lesssim T \lesssim T_c$ in 3D. The master equation can then be mapped into a Fokker-Planck equation for the Wigner distribution of the coherent region. The nonlinear interaction term in the Hamiltonian leads to third order derivatives of the distributions with respect to the phase-space variables, and avoids a direct correspondence of the Fokker-Planck equation with a Langevin equation. By means of the truncated Wigner approximation, however, it is possible to discard the third order derivatives and get a differential equation quite similar in spirit to (3.21). It reads:

$$d\Psi_C(\mathbf{r}) = \hat{\mathcal{P}}_C \left\{ -\frac{i}{\hbar}\left(-\frac{\hbar^2}{2m}\nabla^2 + V_{\rm tr}(\mathbf{r}) + g|\Psi_C(\mathbf{r})|^2\right)\Psi_C(\mathbf{r})\,dt \right. \tag{3.26a}$$

$$+ \frac{G(\mathbf{r})}{k_{\rm B}T}\left[\mu - \left(-\frac{\hbar^2}{2m}\nabla^2 + V_{\rm tr}(\mathbf{r}) + g|\Psi_C(\mathbf{r})|\right)\right]\Psi_C(\mathbf{r}) + dW_G(\mathbf{t},t) \tag{3.26b}$$

$$\left. + \int d\mathbf{r}\, M(\mathbf{r}-\mathbf{r}')\frac{i\hbar\nabla\cdot\mathbf{j}_C(\mathbf{r}')}{k_{\rm B}T}\Psi_C(\mathbf{r})dt + i\Psi_C(\mathbf{r})dW_M(\mathbf{r},t)\right\}, \tag{3.26c}$$

where the noise fields have correlations

$$\langle dW_G^*(\mathbf{r},t)dW_G(\mathbf{r}',t')\rangle = 2G(\mathbf{r})\delta(\mathbf{r}-\mathbf{r}')\delta(t-t'), \tag{3.27a}$$

$$\langle dW_M^*(\mathbf{r},t)dW_G(\mathbf{r}',t')\rangle = 2M(\mathbf{r}-\mathbf{r}')\delta(t-t'). \tag{3.27b}$$

The first line (3.26a) is essentially the $T = 0$ (projected) Gross-Pitaevskii equation. The second line (3.26b) expresses the growth processes, hence the collisions which transfer atoms between the coherent and in the incoherent region. One can draw a direct correspondence between the term $G(\mathbf{r})$ and the $\gamma$ term of eq. (3.22), (eq. (171) of Blakie *et al.*[55]). The "growth" noisy field $dW_G$ corresponds to the noise term $\eta$ in the SGPE, and so do their respective correlations eq. (3.23) and eq. (3.27a). The third line (3.26c) expresses instead the scattering processes that leave the atom number in the two regions unaffected. The amplitude of such collisions is $M(\mathbf{r}-\mathbf{r}')$ and it is usually quite small at equilibrium. Notably, the noise term $dW_M$ associated with this kind of events is multiplicative in $\Psi_C$ and non local, as seen in eq. (3.27b). This fact causes the numerical implementation of the full SPGPE to be quite challenging[1].

To implement the approach in numerical simulations, a simplified version of the stochastic projected GPE is usually applied. This consists in neglecting the terms appearing in (3.26c), postulating that at equilibrium the process they describe is small, and $M(\mathbf{r}-\mathbf{r}') = 0$. This leads to the so-called "simple growth SPGPE", which, apart

[1] A method to treat both the coherent region and the number-conserving scattering processes with the reservoir has been recently implemented in [69].

[55] P. B. Blakie et al. In: *Advances in Physics* 57.5 (2008), pp. 363–455.

from the presence of the projector, is practically equivalent to the SGPE equation (3.21). The two theories have been compared by Proukakis and Jackson[34] to be functionally equivalent, when the projector operator is ignored. The book by Proukakis *et al.*[62], where both these approaches are reviewed, also shows an unpublished comparison (Figure 17.2) between the densities and the correlation functions of a one-dimensional version of both methods. The two quantities are identical, except for a small difference in the thermal wings.

The simulation results reported in the following chapters have been obtained predominantly including the projector term $\hat{\mathcal{P}}$, thus using the stochastic projected Gross-Pitaevskii approach. The main reason for that was to avoid the dependence of the physics included in the theory on the numerical discretisation chosen.

## 3.2 Numerical implementation

Let us now give a description of the way in which the theory developed in the previous section has been adapted to the computational needs of the projects in this thesis. The focus of this work has been the study of low-dimensional systems, and in particular the distinctive 2D case. To this purpose, it is useful to report some of the details of the numerical implementation of the stochastic (projected) Gross-Pitaevskii equation.

### 3.2.1 2D dimensionless formulation

Let us first outline the dimensionless formulation of the equation, in the case of interest of a two-dimensional configuration. Consider a weakly interacting Bose gas in a non-isotropic confinement: $\hbar\omega_z \equiv \hbar\omega_\perp \gg (\mu, k_{\mathrm{B}}T)$ and $\omega_x, \omega_y \ll \omega_z$. In this setting, along the strong confinement direction $z$, the dynamics of the system will be completely suppressed and its wavefunction will simply be the ground-state for the harmonic oscillator. This allows to integrate out the suppressed degree of freedom, and obtain an equation for the two-dimensional problem.

Let us start by writing eq. (3.21), with the addition of the projector $\hat{\mathcal{P}}$, in terms of dimensionless quantities. Let us define

$$\begin{gathered} a_z = \sqrt{\frac{\hbar}{m\omega_z}}; \quad \tau = \frac{1}{\omega_z}; \quad \tilde{\psi}(\mathbf{r},t) = a_z^{3/2}\psi(\mathbf{r},t); \quad \tilde{T} = \frac{k_{\mathrm{B}}T}{\hbar\omega_z}; \\ \tilde{\mathbf{r}} = \frac{\mathbf{r}}{a_z}; \quad \tilde{t} = \frac{t}{\tau}; \quad \tilde{\nabla}^2 = \nabla^2 a_z^2; \quad \alpha_i = \frac{\omega_i}{\omega_z}; \quad \tilde{\mu} = \frac{\mu}{\hbar\omega_z}. \end{gathered} \tag{3.28}$$

[34] N. P Proukakis and B. Jackson. In: *J. Phys. B* 41 (2008), p. 203002.

[62] M. Davis et al. *Quantum Gases: Finite Temperature and Non-Equilibrium Dynamics.* Imperial College Press, 2013.

Then, by ignoring for now the noise term, whose addition has to be considered in the end with the proper dimensionality, we can write

$$i\frac{\partial\tilde{\psi}(\tilde{\mathbf{r}},\tilde{t})}{\partial\tilde{t}} = \hat{\mathcal{P}}\Bigg\{ (1-i\gamma(\tilde{\mathbf{r}},\tilde{t}))\times \\ \times\left[-\frac{\tilde{\nabla}^2}{2}+\frac{1}{2}\left(\alpha_x^2\tilde{x}^2+\alpha_y^2\tilde{y}^2+\tilde{z}^2\right)+\frac{g_{3\mathrm{D}}}{\hbar\omega_z a_z^3}|\tilde{\psi}(\tilde{\mathbf{r}},\tilde{t})|^2-\tilde{\mu}\right]\tilde{\psi}(\tilde{\mathbf{r}},\tilde{t})\Bigg\}. \quad (3.29)$$

By separating the wavefunction into two distinct components it is possible to highlight the ground state form in the direction $z$:

$$\tilde{\psi}(x,y,z,t) = \psi_{2\mathrm{D}}(x,y,t)\phi(z), \quad (3.30)$$

being $\phi(z)_{\mathrm{HO}} = (\pi)^{-1/4}e^{-z^2/2}$ the harmonic oscillator lowest-energy wavefunction. Now, given the fact that $\int_{-\infty}^{\infty}|\phi(z)_{\mathrm{HO}}| = 1$, it is possible to multiply $\phi(z)^*_{\mathrm{HO}}$ on the left and integrate in $z$. The integration of the potential term in $z$ results in a constant that can be reabsorbed in the definition of the chemical potential $\tilde{\mu}$. The resulting equation is (dropping all the tildes):

$$i\frac{\partial\psi}{\partial t} = \hat{\mathcal{P}}\Bigg\{ (1-i\gamma(x,y,t)) \\ \times\left[-\frac{1}{2}\nabla^2+\frac{1}{2}\left(\alpha_x^2x^2+\alpha_y^2y^2\right)+\frac{\sqrt{8\pi}a_s}{a_z}|\psi|^2-\mu\right]\psi+\eta(x,y,t)\Bigg\}. \quad (3.31)$$

In the particular case of a uniform 2D system, $\omega_x = \omega_y = 0$, and

$$i\frac{\partial\psi}{\partial t} = \hat{\mathcal{P}}\Bigg\{ (1-i\gamma)\left[-\frac{1}{2}\nabla^2+g_{2\mathrm{D}}|\psi|^2-\mu\right]\psi+\eta(x,y,t)\Bigg\}, \quad (3.32)$$

where we defined the two-dimensional coupling constant

$$g_{2\mathrm{D}} = \frac{\sqrt{8\pi}a_s}{a_z}, \quad (3.33)$$

and the noise term has the right correlations

$$\langle\eta^*(x,y,t)\eta(x',y',t')\rangle = 2\tilde{T}\gamma\delta(t-t')\delta(x-x')\delta(y-y'). \quad (3.34)$$

The numerical adaptation of equation (3.32) has been performed in two ways during my PhD. At first it was used in a less sophisticated approach based on the use of the Cranck-Nicholson method (see Appendix B.1), and subsequently a more refined approach based on the Adaptive Runge-Kutta method (see Appendix B.2).

### 3.2.2 Energy cutoff and above-cutoff atoms

The theoretical derivation of the stochastic (projected) Gross-Pitaevskii equation assumes that the modes included in the coherent region are all macroscopically occupied. Then, in order for the expansion (3.18) to hold, the occupation number at the last included mode should be in principle very large. In practical terms, this is usually considered to be between 1 and 10, and the cutoff energy $\epsilon_{\rm cut}$ imposed by the projector (3.25) has to be chosen accordingly. In defining $\epsilon_{\rm cut}$ one can consider the distribution of the atoms in the incoherent region to be the Bose-Einstein relation (C.1), so that[2]

$$\epsilon_{\rm cut} \approx k_{\rm B}T\log(2) + \mu. \tag{3.35}$$

The cutoff is explicitly implemented, for example by setting to zero all modes outside a sphere in momentum space of radius $k_{\rm cut} = \sqrt{2m\epsilon_{\rm cut}}$. However, a number of momenta outside the projected region has to be retained in the simulation to avoid aliasing (Appendix B of Blakie *et al.*[55]). In the spatial coordinate, this is achieved by imposing a number of points in the discretised grid such that

$$\Delta x = \frac{L_x}{N_x} \leq \frac{\pi}{2k_{\rm cut}}, \tag{3.36}$$

which is a criterion twice as stringent as the Nyquist sampling requirement, $\Delta x_N = \pi/k_{\rm cut}$.

Another important point concerning the cutoff is that, even though the dynamics of the incoherent region is neglected, in comparing the experimental quantities with the simulations, one should take into account the presence of the *above-cutoff* atoms $n_I$ (meaning the ones in the incoherent region):

$$n_I = \int_{\epsilon_{\rm cut}}^{\infty} d\epsilon\, g(\epsilon) n_{\rm BE}(\epsilon), \tag{3.37}$$

where $g(\epsilon)$ is the appropriate density of states of the system (for uniform and harmonic traps, see Appendix C). This means that, for example, one should consider the *total* number of atoms ($n_{\rm tot} = n_C + n_I$) when determining the simulated density in a uniform system, or in computing other extensive quantities such as the critical

[2] An alternative approach is to simply consider $\epsilon_{\rm cut} - \mu = k_{\rm B}T$ corresponding to an occupation of $\sim 0.6$.

[55] P. B. Blakie et al. In: *Advances in Physics* 57.5 (2008), pp. 363–455.

temperature[58,59].

### 3.2.3 Dissipation term determination

Let us now concentrate on the determination of a relation for the dissipative term in (3.21). In analogy with the classical Brownian motion treatment (Appendix A), in equation (3.22) we have redefined

$$\gamma(\mathbf{r}, T, t) \equiv i\frac{\beta}{4}\hbar\Sigma^K(\mathbf{r}, t), \tag{3.38}$$

which should in principle be computed from the relation for the Keldysh self-energy, eq. (3.13). The term $\gamma$ has the role of parametrising the interaction between the high-lying and the low-lying modes $\psi$, and has the pragmatical role of setting the speed with which the system reaches the equilibrium set by the external parameters $T$ and $\mu$. The larger is $\gamma$, the shorter is the time required for the system to equilibrate, and vice versa. In principle, it should depend both on position and time, but given the uniform nature of the trapping potential we are going to consider, it is possible to use the approximation

$$\gamma \sim \kappa\frac{4mk_{\mathrm{B}}T}{\pi}\left(\frac{a_s}{\hbar}\right)^2, \tag{3.39}$$

first introduced by Penckwitt *et al.*[70], where the value $\kappa \approx 3$ has been found to match the typical experimental growth. Neglecting the spatial dependence in $\gamma$ does generally bear no drastic consequences, as also discussed in the literature[58,71].

It is worth noting that relation (3.39) only gives an effective leading scaling for $\gamma$, and should only be used to express its order of magnitude. Due to its appearance both as the dissipative term as well as in the magnitude of the fluctuation term $\eta$, $\gamma$ is directly related to the speed with which the system will grow to equilibrium, as discussed in the next section. In comparing with experiments, the best match has been found to happen when $\gamma$ is considered as a fitting parameter, and is tuned to reproduce the measured growth to equilibrium in the physical system[72].

[58] S. P. Cockburn. "Bose Gases In and Out of Equilibrium within the Stochastic Gross-Pitaevskii Equation". PhD thesis. Newcastle University, 2010.

[59] D. Gallucci. "Ab Initio Modelling of quasi-one-dimensional Bose gas experiments via the Stochastic Gross-Pitaevskii Equation". PhD thesis. Newcastle University, 2013.

[70] A. A. Penckwitt, R. J. Ballagh, and C. W. Gardiner. In: *Phys. Rev. Lett.* 89 (2002), p. 260402.

[71] S. P. Cockburn et al. In: *Phys. Rev. A* 83 (2011), p. 043619.

[72] C. N. Weiler et al. In: *Nature* 455 (2008), p. 948.

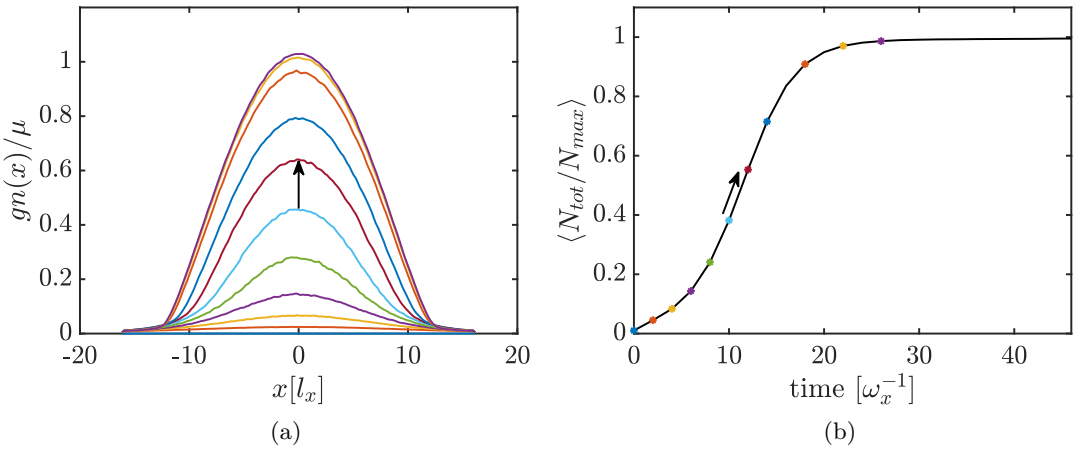


(a) (b)

Figure 3.2: (a) Growth of the profile of the 2D coherent region $\psi$, integrated in one direction and averaged over 100 realisations. (b) Total particle number $N_{\rm tot}$ in time. The points correspond to the density snapshots with the same colour in the figure on the left. The parameters for this simulations are $\omega_x = \omega_y = 2\pi \times 25$Hz, $\omega_\perp = 2\pi \times 1500$Hz, $\mu = 81.72\hbar\omega_x$, $T = 50nK$ and $\gamma = 0.005$.

### 3.2.4 Growth to equilibrium

By "growth" of the system, we mean the spontaneous accumulation of atoms in the low-lying modes until the equilibrium is reached. In our simulations the initial state is effectively represented by the noisy field $\psi(\mathbf{r}, t = 0) = \eta(\mathbf{r}, 0)$, which seeds the growth process randomly. The total atom number will then grow in time until it reaches its final value, fixed by the input chemical potential $\mu$. Figure (3.2) shows the growth process corresponding to the simulation of a two-dimensional isotropic harmonic-trapped gas, at finite temperature. One dimension is integrated out for presentation purposes, and an average over 100 realisations is performed. Figure (3.2a) indicates that, starting from an almost empty initial state, atoms progressively accumulate in the centre of the trap, and the density acquires the inverted parabola shape associated with the Thomas-Fermi profile given by (1.19), plus the broad wings due to the thermal atoms (see eq. (3.45)). Figure (3.2b) shows the equilibration of the total atom number $N_{\rm tot} = N_c + N_I$, given as the sum of the *c-field* atoms and of the above-cutoff ones. The highlighted points in the figure correspond to the density profile with the same colour.

The speed of the growth is determined by the parameter $\gamma$, which sets the rate of collisions between the atoms. Figure (3.3a) shows the different growth rate for the total number of particles when having all the parameters of the simulation identical, except for the scattering value $\gamma$ (which is assumed constant in time and uniform in space). By diminishing the collisional rate, the growth is slowed down significantly, because the bosonic enhancement mechanism leading to the accumulation of atoms in the low-lying

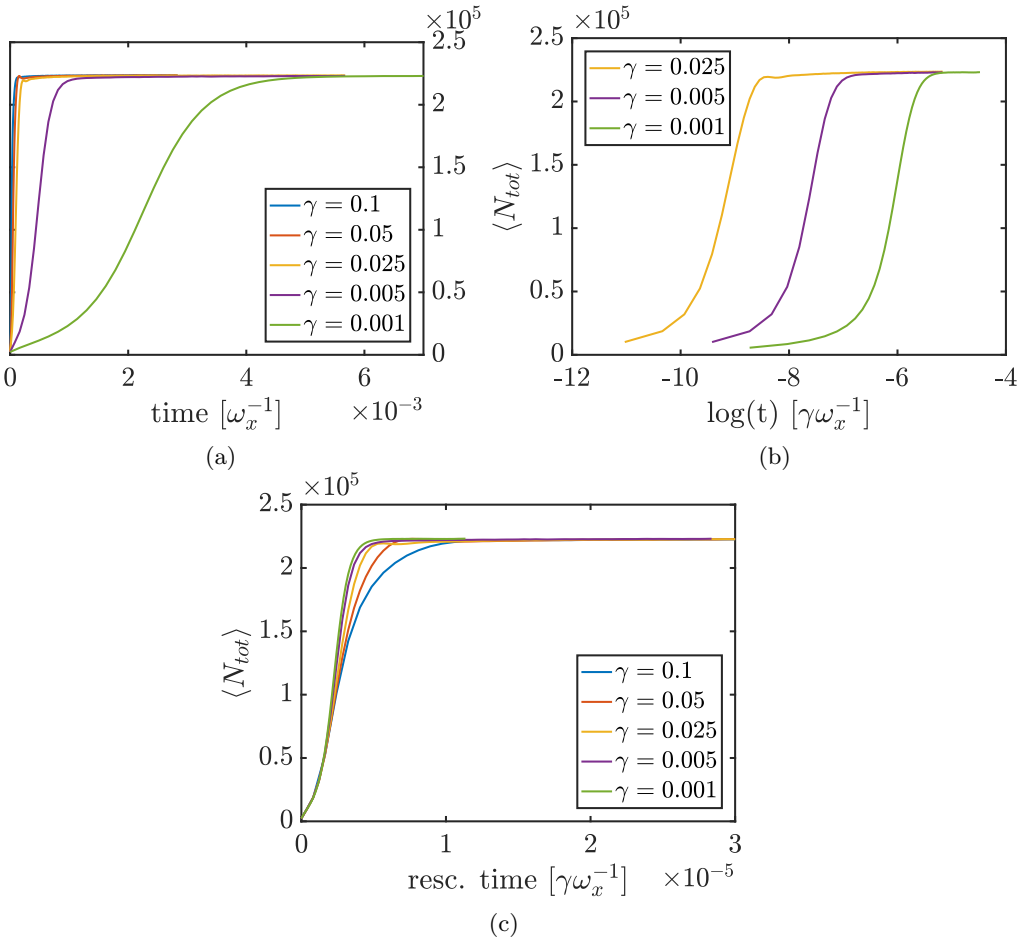


Figure 3.3: Growth processes for different values of gamma. (a)-(b) Reaching of equilibrium for different values of the parameter $\gamma$, in normal and log scale. (c) Same as before, but the time coordinate is rescaled by multiplying $\gamma$. Changing the value of the dissipative factor has little effect aside from rescaling the time needed to reach equilibrium.

modes is reduced. As initially these modes are sparsely populated by the noise, it takes more time for the spontaneous growth to reach a "critical" value when the stimulated process can occur. Since $\gamma$ affects both the spontaneous mechanism (through the noise) and the stimulated one (through the scattering term proportional to $\gamma\epsilon_c$), a small value slows down significantly the equilibration. Figure (3.3b) shows that the growth curves are indeed very similar when the time coordinate is transformed logarithmically, the only difference being an overall shift. Since an added shift in logscale corresponds to a multiplicative factor in normal units, we rescale the time coordinate by $\gamma$ for each simulation, and we find a good agreement between the curves (Figure (3.3c)). Finally, the equilibrium saturation value for $N_{\text{tot}}$ is consistent for all the $\gamma$ considered.

### 3.2.5 Penrose-Onsager diagonalisation

As already stated in Section 3.1.2, the classical field $\psi$ does not represent the condensate as in the $T = 0$ case, but also includes the low-energy excited states. One could therefore ask how to extract information about the condensate. Strictly speaking, in an infinite uniform two-dimensional configuration, Bose-Einstein condensation is not possible, because the long-range order is destroyed by the thermal fluctuations[3]. However, when the system is confined, the coherence range can exceed the physical dimension of the gas, and a "true" condensate can be formed. In an ideal gas, Bose-Einstein condensation occurs when the lowest single-particle mode becomes *macroscopically* occupied with respect to the other modes in the system. In 1956, Penrose and Onsager[13] gave a generalisation of this criterion, in order to also include interacting gases. Its formulation is quite simple: considering a set of $N$ interacting bosons, the single-particle density matrix $\rho$ is defined as:

$$\rho(\mathbf{r}, \mathbf{r}') = |\psi(\mathbf{r})\rangle\langle\psi(\mathbf{r}')|, \tag{3.40}$$

where the average is performed over many different noise realisations. Now, diagonalising the density matrix means to solve the eigenproblem

$$\int d\mathbf{r}'\, \rho(\mathbf{r}, \mathbf{r}')\psi_j(\mathbf{r}') = p_j\psi_j(\mathbf{r}), \tag{3.41}$$

which defines the eigenfunctions $\psi_j$ and the non-negative eigenvectors $p_j$. Then the condensation occurs if the largest eigenvalue

$$N_0 \equiv \sup_j(p_j) \tag{3.42}$$

is *macroscopic*, i.e. if

$$\lim_{N\to\infty} \frac{\sup_j(p_j)}{N} > 0. \tag{3.43}$$

In this case $N_0$ represents the number of condensed particles, and the corresponding eigenvector $\psi_0$ will set the condensed density

$$n_c(\mathbf{r}) = |\psi_0(\mathbf{r})|^2. \tag{3.44}$$

[3] See more about this in Chapter 4.

[13] O. Penrose and L. Onsager. In: *Phys. Rev.* 104 (1956), pp. 576–584.

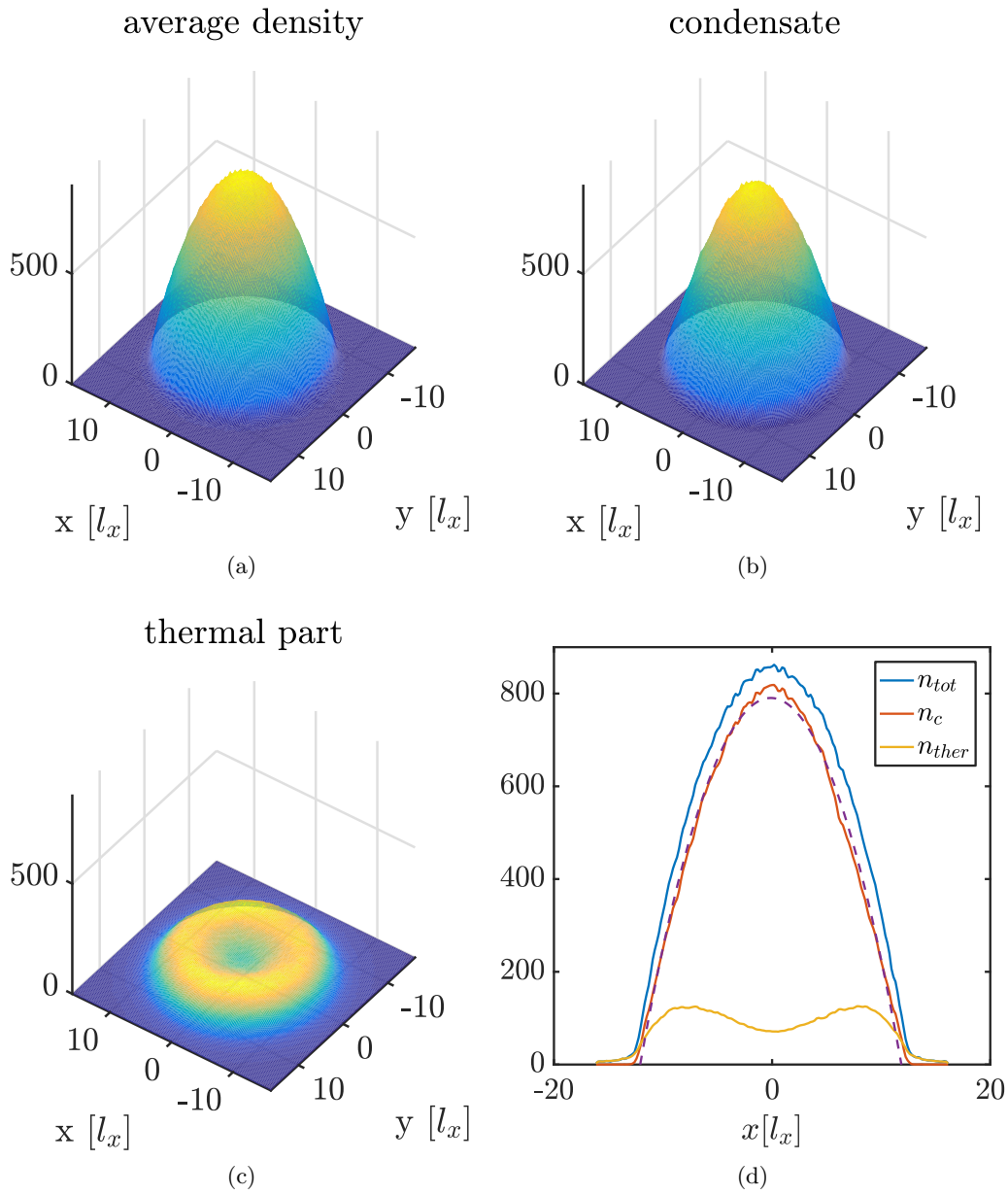


Figure 3.4: (a) Average density for a $^{87}$Rb gas in a harmonic trap, expressed in units of $\mu/g_{2D}$. The parameters for this simulations are $\omega_x = \omega_y = 2\pi(25\text{Hz})$, $\omega_\perp = 2\pi(1500\text{Hz})$, $\mu = 81.52\hbar\omega_x$, $T = 50\text{nK}$, and the average is performed over 1000 noise realisations. (b) Condensed density computed as in (3.44), after performing the Penrose-Onsager diagonalisation.(c) Thermal density computed as in (3.45). Note that, as expected for repulsive interactions $g_{2D} > 0$, the thermal part is repelled by the condensate and pushed towards the edges of the trap. (d) Densities of the total, condensed and thermal atom distributions, obtained as the slice of (a)-(c) in $y = 0$. The dashed line marks a parabolic fit of the condensed density. The resulting concavity $A = 5.5 \pm 0.1$ is close to the one expected in the Thomas-Fermi approximation $A_{\text{TF}} = 5.3$.

The average thermal density[4] is instead recovered by

$$\langle n_t \rangle = \langle n_{\rm tot} \rangle - n_c. \tag{3.45}$$

Figure (3.4) shows the Penrose-Onsager extraction of the condensate for a Bose gas in an isotropic two-dimensional harmonic trap. As expected for a repulsive interaction $g_{\rm 2D} > 0$, the condensate shown in Figure (3.4b) exhibits the Thomas-Fermi inverted parabola profile and mainly occupies the centre of the trap, while the thermal atoms are repelled by the condensate and lie in the external part of the confinement (Figure (3.4c)).

According to the definition, the Penrose-Onsager procedure is only justified when the largest eigenvalue $p_{\rm max}$ is much larger than the others, corresponding to the macroscopic occupation of an eigenmode of the sample. We will therefore consider the extraction for the condensate only valid when $p_{\rm max} > p_{\rm 2max}/0.3$, where $p_{\rm 2max}$ is the second largest eigenvalue. In general, the Penrose-Onsager diagonalisation procedure is computationally quite heavy, and requires large samples of noise realisations to be accurate. However, it has the unique feature to reproduce the equilibrium profile of the condensate and of the thermal cloud. One should also notice that throughout the thesis we perform ensemble averages over many noise realisations, rather than time averages sometimes computed in the literature[73].

### 3.2.6 Order parameter of the SGPE

An alternative method to establish the grade of degeneracy of the system is to compute the order parameter for the stochastic Gross-Pitaevskii equation. This has a great computational advantage with respect to the Penrose-Onsager extraction detailed above, but lacks the possibility to recover the condensed density. The following treatment summarises the approach detailed by Kobayashi *et al.*[74].

The statistical definition for the order parameter associated with breaking a $U(1)$ symmetry is

$$m \equiv \lim_{h \to 0} \langle \psi_h \rangle_{eq}, \tag{3.46}$$

where $h$ represents a perturbation linearly coupled to the field into the Hamiltonian. In the Bose-Einstein condensation process, however, the linear $h$ factor does not have

[4] Strictly speaking, this only represents the density of the thermal atoms inside the coherent region. In comparing to experiments, one should also consider the distribution of the above-cutoff atoms.

[73] I.-K. Liu et al. In: *ArXiv e-prints* (2017). arXiv: 1712.08074.
[74] M. Kobayashi and L. F. Cugliandolo. In: *Phys. Rev. E* 94 (2016), p. 062146.

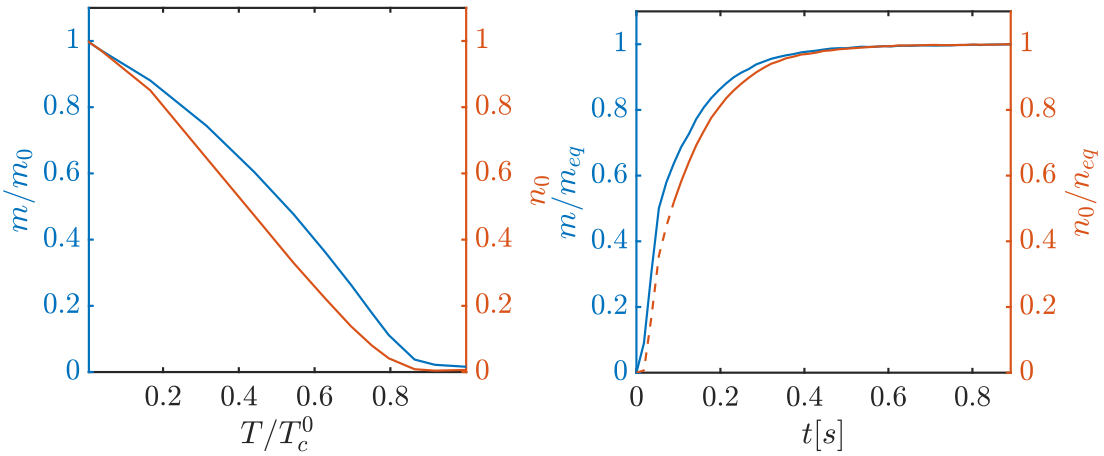


Figure 3.5: (a) Comparison between the order parameter $m$ defined in eq. (3.50) and the condensed fraction $n_0$ defined in eq. (3.51), for a Bose gas in a harmonic confinement. The parameters for this simulations are $\omega_x = \omega_y = 2\pi \times 25\text{Hz}$, $\omega_\perp = 2\pi \times 1500\text{Hz}$, $\mu = 27.17\hbar\omega_x$, the temperature spans a range $(0\text{nK} - 300\text{nK})$ and the averages are performed over 200 noise realisations. $m$ is normalised by its $T = 0$ result $m_0$. (b) Growth of the order parameter $m$ and the condensed fraction $n_0$ defined in eq. (3.51) in time, for a Bose gas in a harmonic confinement, normalised by their equilibrium values for better comparison. The dashed line expresses the time interval for which the relative magnitude of the first and the second eigenvalue is below 0.3, thus the Penrose-Onsager procedure is not well defined (see text). The parameters for this simulations are the same as in (a), and the temperature is $T = 5\text{nK}$. For both plots, we also included the above-cutoff atoms computed as in Section 3.2.2 for the determination of the total atom number.

an easy implementation. Thus, an alternative definition is considered,

$$m \propto \sqrt{|C(r \to \infty)|}, \tag{3.47}$$

where

$$C(r) = \left\langle \frac{1}{4\pi r^2} \int d\Omega \int d\mathbf{r}' \psi^*(\mathbf{r}')\psi(\mathbf{r}+\mathbf{r}') \right\rangle_{eq} \tag{3.48}$$

accounts for the off-diagonal long-range order arising in a BEC.

An equivalent numerical definition, very simple from a computational point of view, can be defined on a discretised two-dimensional grid of $M_x \times M_y$ points

$$L_x \times L_y = (x_1, \ldots, x_i, \ldots, x_{M_x}) \times (y_1, \ldots, y_j, \ldots, y_{M_y}), \tag{3.49}$$

where

$$m \equiv \frac{1}{\sqrt{M_x M_y}} \frac{\langle \left| \sum_{i,j} \psi_{i,j} \right| \rangle}{\sqrt{\langle \sum_{i,j} |\psi_{i,j}|^2 \rangle}}. \tag{3.50}$$

One can show that, using this normalisation, definition (3.50) coincides with the normalised first-order correlation function at the system's limit (see more on that in Chapter 4), as expected from eq. (3.47). In our work we will use definition (3.50).

Figure (3.5a) shows a comparison example between the order parameter defined in (3.50) and the condensed fraction

$$n_0 = \frac{N_0}{N_{\text{tot}}}, \tag{3.51}$$

for a Bose gas in a harmonic trap, over a range of temperatures. Figure (3.5b) shows the growth in time of these two quantities, for a given temperature. Note that, given the non-uniform nature of the sample, the value for the correlation length at the edge of the system is not clearly defined, and $m$ is better compared with the condensed fraction when renormalised by its zero-temperature value $m_0$.

## 3.3 Chapter summary

In this chapter we presented two methods to treat the finite temperature dynamics of atomic Bose gases, similar in spirit but arising from different derivation approaches. The first technique is the stochastic Gross-Pitaevskii equation (SGPE), effectively represented by a Langevin equation describing the combined dynamics of a condensate and of a finite number of thermal modes. It can be seen as an extension to the zero temperature Gross-Pitaevskii approach, where a damping term and a noise term are also included. These two terms represent the collisional processes between the low-lying coherent part and the high-energy incoherent part, which is effectively treated as a bath. The thermal equilibrium is achieved by the establishment of a fluctuation-dissipation theorem in the two collisional terms. The second technique is the stochastic projected Gross-Pitaevskii equation (SPGPE), which explicitly includes a projector to separate the coherent and the incoherent parts. We will make use of both approaches in this thesis. In the following sections, we described the details of the numerical implementation of the methods for the two-dimensional system of our interest. We gave a two-dimensional formulation of the equation and we outlined the selection procedure for the energy cutoff and for the dissipation term $\gamma$. We showed some examples of a harmonically trapped two-dimensional system growing to equilibrium, and we described two methods to extract useful quantities related to the degeneracy of the sample. We introduced the Penrose-Onsager diagonalisation procedure to estimate the condensate

wavefunction and the condensed fraction. We finally compared it with the computation for the order parameter $m$ for the Langevin equation, connected to the establishment of a quasi long-range coherence in the system.

# Chapter 4

# Temperature and interaction quench in a two-dimensional Bose-Einstein condensate

Physics is different in systems with low dimensions, when compared to our canonical three-dimensional world. As strange as it may sound (or as trivial) the dimensionality dramatically affects the properties of a physical system, even more so in the bizarre realm of quantum mechanics. A very clear example of that is the absence of a true condensation in infinite 2D systems at any finite temperature, and in 1D systems altogether. However, not everything is lost. In two dimensions, when the system is confined and has a finite size, the Bose-Einstein transition may still occur: it is sufficient that the coherence length exceeds the boundaries of the trap, and the resulting correlated system becomes indistinguishable from a true BEC. Even in infinite systems a peculiar kind of phase transition still exists, even though it shows some key differences with the Bose-Einstein condensation. In the following I will address the Berezinskii-Kosterlitz-Thouless (BKT) phase transition, reviewing its main properties.

Crossing a phase transition always results in interesting physics. This is both true for the classical as well as for the quantum world. In the second part of the chapter the Kibble-Zurek mechanism for the creation of defects during a phase transition is presented, and its modifications due to dimensionality are also discussed. Finally, a set of numerical results addressing this topic is presented and commented upon.

## 4.1 The Berezinskii-Kosterlitz-Thouless phase transition

Since 1934, when Peierls proposed his argument[75] in solid state physics, it is known that no crystalline order exists in one- or two-dimensional systems for $T > 0$. This is due to the particular form of the relation for the uncertainty of the displacement of an atom from its equilibrium position, $\mathbf{u}_j$. Peierls showed, in fact, that in 1D and in 2D

$$\langle (\mathbf{u}_j - \mathbf{u}_0)^2 \rangle \propto T \log(R_{j0}), \tag{4.1}$$

diverging for large range $R_{j0}$ for any finite temperature $T$ (for the 3D case this quantity only depends on $T$, but is independent from the distance). Peierls conclusion has been generalised by the so-called Mermin-Wagner-Hohenberg theorem, demonstrated by Mermin and Wagner in 1966[76] on the anti- and ferromagnetic order in 1D and 2D systems, and independently by Hohenberg in 1967[77] in Bose liquids and superconductors. The theorem states that for a system of dimension less than or equal to 2 and short range interactions, it is not possible to have the spontaneous breaking of a continuous symmetry at non-zero temperature. In other words, the thermal fluctuations at any temperature are strong enough to destroy the long-range coherence in the system. However, repulsive interactions may induce a quasi long-range order in an atomic gas, leading to an algebraic decrease of the one-body correlation function. This has deep consequences in allowing the formation of a superfluid, even in absence of a true condensation process, and the presence of a topological phase transition, the renowned Berezinskii-Kosterlitz-Thouless (BKT) phase transition, taking the name from Vadim L'vovich Berezinskiĭ, J. Michael Kosterlitz, and David J. Thouless[1]. Let us present the theoretical description of the important quantities related to the transition. We will show the approach given by Dalibard[78], who explicitly follows the original introduction in the seminal paper by Kosterlitz and Thouless[79].

### 4.1.1 Quasi long-range order

A two-dimensional uniform Bose gas at finite temperature cannot condense, apart when it is exactly at $T = 0$ (see Appendix C). Consider a gas confined in a uniform

[1] Kosterlitz and Thouless were awarded the 2016 Nobel Prize in Physics, together with Duncan Haldene, for their studies on topological phase transitions and topological phases of matter.

[75] R. E. Peierls. In: *Helv. Phys. Acta* 7 (1934), p. 24.

[76] N. D. Mermin and H. Wagner. In: *Phys. Rev. Lett.* 17 (1966), pp. 1133–1136.

[77] P. C. Hohenberg. In: *Phys. Rev.* 158 (1967), pp. 383–386.

[78] J. Dalibard. *Lecture notes in "Quantum Fluids in low dimension and Kosterlitz-Thouless transition" (in French).* 2017.

[79] J. M. Kosterlitz and D. J. Thouless. In: *J. Phys. C* 6.7 (1973), p. 1181.

trap of size $L \times L$, with periodic boundary conditions. In this case one can rewrite the wavefunction as $\psi = \sqrt{n}e^{i\theta}$, being $n = N/L^2$ and $\theta$ uniform. From (1.15), its kinetic and interaction energies are

$$E^0_{\rm kin} = 0, \qquad E^0_{\rm int} = \frac{g}{2}L^2 n^2. \tag{4.2}$$

At finite temperature, $n(\mathbf{r})$ and $\theta(\mathbf{r})$ will instead be varying in space due to the thermal fluctuations.

**Suppression of density fluctuations.** It is possible to show that for low temperatures the density fluctuations are suppressed because of the repulsive nature of the atomic interaction. The interaction energy is

$$E_{\rm int} = \frac{g}{2}\int d\mathbf{r}\,|\psi(\mathbf{r})|^4 = \frac{g}{2}L^2\langle n^2(\mathbf{r})\rangle, \tag{4.3}$$

where the average $\langle \dots \rangle$ is performed over the entire sample. Then, the interaction energy surplus is proportional to the density fluctuations

$$\begin{aligned} E_{\rm int} - E^0_{\rm int} \propto (\Delta n)^2 &= \langle n^2(\mathbf{r})\rangle - n^2 \\ &= (g_2(0) - 1)n^2 \end{aligned} \tag{4.4}$$

where

$$g_2(\mathbf{r}) = \frac{\langle n(\mathbf{r})n(0)\rangle}{n^2} \tag{4.5}$$

is the second-order correlation function[2], and $n = \langle n(\mathbf{r})\rangle$.

However, for low enough temperatures, one could write a criterion for which the interaction energy $E_{\rm int}$ becomes dominant with respect to the thermal energy $k_{\rm B}T$:

$$\frac{E_{\rm int}}{k_{\rm B}T} = \frac{gn/2}{k_{\rm B}T} \equiv \frac{g_{\rm 2D}}{4\pi}\mathcal{D}, \tag{4.6}$$

where we recall the definition (3.33) of $g_{\rm 2D}$, and we introduce the *phase-space density* $\mathcal{D}$ as

$$\mathcal{D} = n\lambda_T^2, \tag{4.7}$$

[2] Note that, for a classical field $\psi$, the density correlation function $g_2(0) > 1$ due to the Cauchy-Schwartz inequality

$$L^2\int d^2r\, n(\mathbf{r})^2 \geq \left(\int d^2r\, n(\mathbf{r})\right)^2,$$

so that $E_{\rm int}$ is always greater than $E^0_{\rm int}$.

where

$$\lambda_T = \sqrt{\frac{2\pi\hbar^2}{mk_{\mathrm{B}}T}} \tag{4.8}$$

is the thermal de Broglie wavelength. Hence, for a large phase-space density

$$\mathcal{D} \gg \frac{4\pi}{g_{2\mathrm{D}}} \tag{4.9}$$

any density fluctuation would require an energy much larger than the one available due to the temperature, and it is therefore suppressed. This means that in the uniform system only phase fluctuations can be present for sufficiently low $T$, and that the interaction energy can be considered constant.

**Phase fluctuations.** Let us now treat the case where no vortices are present in the system. We will show that the phase fluctuations, resulting from the thermal excitations as seen above, may result in a disruption of the long-range coherence in the sample. If the density fluctuations are suppressed, one can assume that the gradient

$$\boldsymbol{\nabla}\psi = \boldsymbol{\nabla}\left(\sqrt{n(\mathbf{r})}e^{i\theta(\mathbf{r})}\right) \approx \sqrt{n}(i\boldsymbol{\nabla}\theta)e^{i\theta(\mathbf{r})}, \tag{4.10}$$

and the kinetic energy becomes

$$E_{\mathrm{kin}} = \frac{\hbar^2}{2m}n\int d^2r\,(\boldsymbol{\nabla}\theta)^2. \tag{4.11}$$

The term in front of the integral in (4.11) deserves some discussion. It expresses a certain rigidity of the system: the phase fluctuations are directly related to a cost in kinetic energy. This "rigidity" is a common property of superfluid systems: when one tries to put it in motion, it resists. Then, if one completely neglects the density fluctuations ($T \to 0$), a 2D system described by the Gross-Pitaevskii energy functional is superfluid, and the superfluid density $n_s$ equals the total density $n$. When increasing the temperature, the measured superfluid density decreases, and the association of $n$ with $n_s$ does not hold anymore. However, one could introduce a phenomenological temperature-dependent superfluid density $n_s(T)$, so that

$$E_{\mathrm{kin}} = \frac{\hbar^2}{2m}n_s(T)\int d^2r\,(\boldsymbol{\nabla}\theta)^2. \tag{4.12}$$

This effectively means to renormalise the density so to only take into account the long-range physics we care about, and avoid to treat the short range fluctuations. To

evaluate (4.12) we need to evaluate the first-order correlation function $g_1(\mathbf{r})$

$$g_1(\mathbf{r}) = \frac{\langle \psi(\mathbf{r})\psi^*(0)\rangle}{n} = \langle e^{i(\theta(\mathbf{r})-\theta(0))}\rangle, \tag{4.13}$$

if we consider the suppression of the density fluctuations explained before. The actual computation of the term $g_1$ is quite convoluted, and can be found in detail in the notes of Dalibard[78]. It is possible to show that

$$\langle[\theta(\mathbf{r})-\theta(0)]^2\rangle \sim \frac{2}{\mathcal{D}}\log\left(\frac{r}{\lambda_T}\right), \tag{4.14}$$

which is analogous to the Peierls argument (4.1), and, since for a Gaussian variable $x$ $\langle e^{ix}\rangle = e^{-\langle x^2\rangle/2}$,

$$g_1(r) \sim \left(\frac{\lambda_T}{r}\right)^{1/\mathcal{D}}. \tag{4.15}$$

The decay of the correlation function has then an *algebraic* behaviour, as opposed to the case for an ideal 2D gas, where

$$g_1^{\mathrm{id}}(r) \propto \begin{cases} e^{-\pi r^2/\lambda_T^2} & \text{for non degenerate gases } \left(Z = e^{\mu/k_{\mathrm{B}}T} \ll 1\right) \\ \sqrt{\frac{l}{r}}e^{-r/\zeta} & \text{for degenerate gases } \left(Z = e^{\mu/k_{\mathrm{B}}T} \gg 1\right), \end{cases} \tag{4.16}$$

where $\zeta \sim \frac{\lambda_T}{\sqrt{4\pi}}e^{\mathcal{D}/2}$. The comparison between the two cases is quite striking. As shown in Fig. (4.1), the ideal gas correlation drops to zero much faster than the one for the interacting gas. For the parameters set in the figure, for samples of size less than $1000\lambda_T$ the gas maintains a fairly strong phase coherence in the whole system. This case is usually referred to as *quasi-condensate*[80]. In a system with finite size $L$, this coherence gives rise to a noticeable condensed fraction, which can be defined as the value of $g_1(L)$[81].

Two important conclusions emerge from the above consideration; in a system in two dimensions, both statements below are true:

- according to the Mermin-Wagner theorem, no long-range coherence (hence no condensate) can appear in the thermodynamic limit;
- the interactions between the atoms allow the presence of a quasi-order which, in finite size systems, "simulates" the presence of a true condensate.

Hence the situation is delicate: the Mermin-Wagner theorem has very strong require-

[78] J. Dalibard. *Lecture notes in "Quantum Fluids in low dimension and Kosterlitz-Thouless transition" (in French).* 2017.
[80] Y. Kagan, B. V. Svistunov, and G. V. Shlyapnikov. In: *Sov. Phys. JETP* 66.2 (1987), p. 314.
[81] J. Dalibard. *Lecture notes in "Coherence and superfluidity in atomic gases" (in French).* 2015.

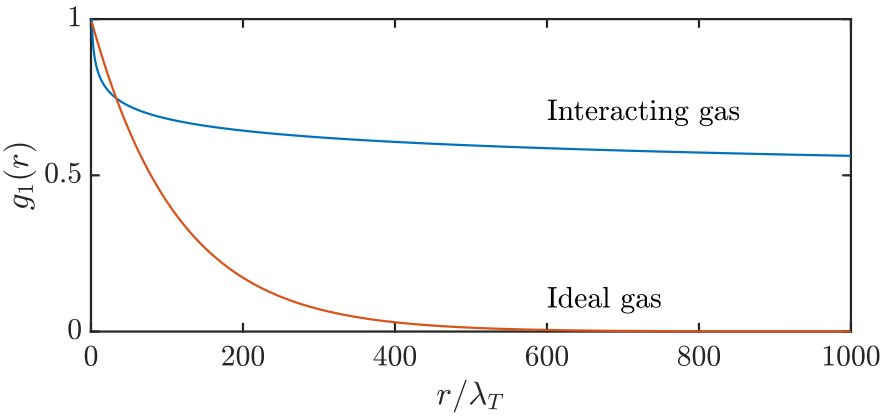


Figure 4.1: Comparison between the first-order correlation functions for an ideal $\left(g_1 \sim e^{-r/\zeta}\right)$ and an interacting $\left(g_1 \sim (\lambda_T/r)^{1/\mathcal{D}}\right)$ Bose gas. The parameters in this example are $\mathcal{D} = 12$, $\zeta = (\lambda_T/\sqrt{4\pi})e^{\mathcal{D}/2} \sim 114\lambda_T$.

ments to be formally established. If we define the limit for which the theorem is fully valid as the one for which the condensed fraction $g_1(L) < 1\%$, for our example in figure (4.1) we find

$$\left(\frac{\lambda_T}{L}\right)^{1/\mathcal{D}} < 0.01 \quad \Rightarrow \quad L > 10^{24}\lambda_T. \tag{4.17}$$

This fact is at the base of the argument made by Bramwell and Holdsworth[82] in the context of the magnetisation of 2D systems: one should need the samples to have the size of Texas to fully apply Mermin-Wagner.

### 4.1.2 Role of vortices

In the previous section we discussed how the role of thermally activated phonons can disrupt the long-range order in a two-dimensional system. Mora and Castin[83] showed that, when no vortices are considered, it is possible to recover a Bogoliubov-like spectrum for the elementary excitations in such a system, similar to the one of eq. (1.60):

$$\omega_q = \frac{\hbar}{2m}\sqrt{q^2(q^2 + 4g_{2\mathrm{D}}n_0)}, \tag{4.18}$$

where $n_0 = N/L$. Such a spectrum, having a linear behaviour at low momenta, implies by itself that the system is superfluid, as can be seen by simply applying the renown Landau criterion[84]. In brief, the criterion states that it exist a minimum velocity for which an impurity moving in a condensate will produce excitations which are ener-

[82] S. T. Bramwell and P. C. W. Holdsworth. In: *Phys. Rev. B* 49 (1994), pp. 8811–8814.
[83] C. Mora and Y. Castin. In: *Phys. Rev. A* 67 (2003), p. 053615.
[84] C. J. Pethick and H. Smith. *Bose–Einstein Condensation in Dilute Gases*. 2nd ed. Cambridge University Press, 2008.

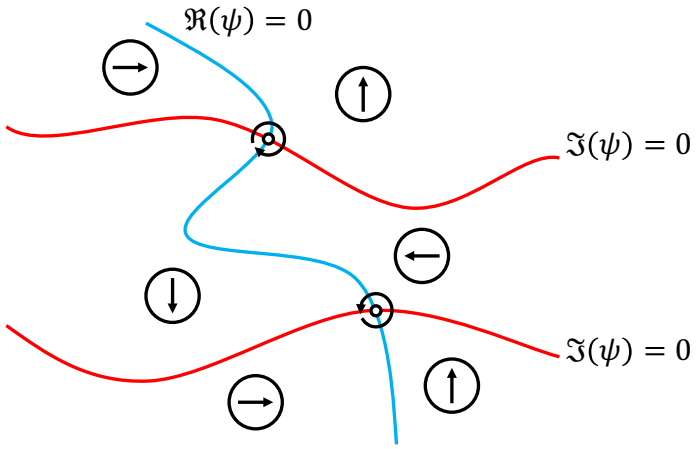


Figure 4.2: Lines of zero value for $\mathcal{R}(\psi)$ (blue) and $\mathcal{I}(\psi)$ (red), showing the presence of a vortex and an antivortex.

getically favourable. If the speed is too low, the excitations produced would actually *increase* the total energy of the system. This allows a flow of the impurity (or of the fluid) without the production of excitations lowering its speed, which remains forever at a constant value. This means that the system has zero viscosity and is a superfluid.

Let us now go beyond the purely phononic approach, and let us also consider vortices in the system. Vortices have the effect of disrupting the phase coherence in a system. This is easily understandable by considering that the phase on two opposite sides of a vortex core has to change by a factor $\pi$. Thus, two points spatially separated by a segment $\bar{AB}$ can have a phase difference $\delta\theta$ which suddenly jumps to $\delta\theta + \pi$ when a vortex randomly passes on the segment. The coherence between A and B will then be lost.

An easy visualisation scheme can be related to the vortex. In our classical field context, a vortex is a zero-density region $|\psi(\mathbf{r})|^2 = 0$, presenting a phase winding[3] around it of $\pm 2\pi$ (charge $q = \pm 1$). Thus, they are simultaneously zero both for the real $\mathcal{R}(\psi)$ and for the imaginary $\mathcal{I}(\psi)$ part of the wavefunction. Both these quantities oscillate in space under the effect of thermal fluctuations, and go from positive to negative. The vortices are then represented as discrete points $\mathbf{r}_i$ such that

$$\mathcal{R}(\psi) = 0 \quad \text{and} \quad \mathcal{I}(\psi) = 0, \tag{4.19}$$

at the same time, hence points where the lines of zero value for the two functions merge (Fig. (4.2)).

The phase winding of a vortex constitutes a topological protection for it: it is not

[3] or any other superposition of the two cases $\pm 2\pi$.

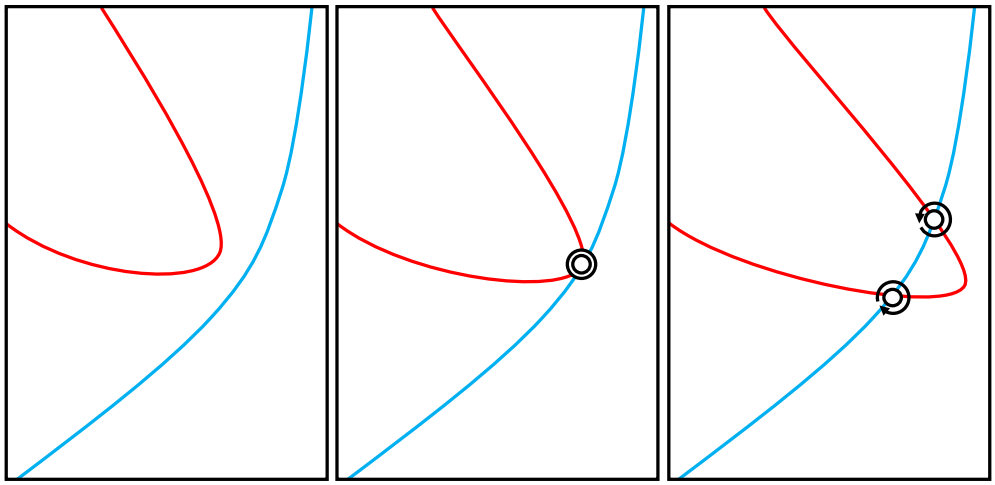

Figure 4.3: Creation of a vortex-antivortex pair from thermal fluctuations. The lines of zero values come toghether (left) and initially form a double zero (middle). Then, as they continue their evolution, a couple of vortices with opposite circulations are formed and start separating (right). The opposite mechanism, leading to the annihilation of two vortices, is also possible.

possible to create or annihilate a single vortex in the bulk of the system, because this would mean to instantly rearrange the phase pattern of the whole sample. Instead, only two cases may happen: either a single vortex is created at the boundaries of the system, where the density is zero, or a vortex-antivortex pair is created from a large density fluctuation. This formation of couples of opposite circulation from a double zero of $\psi(\mathbf{r})$ is pictured in Fig. (4.3).

**Energy of a vortex.** Let us compute the energy of an isolated vortex in the centre of a circular 2D gas of radius $R$. This is going to be useful in determining the probability for single vortices to exist. As already shown in eq. (1.50), the velocity field around a vortex of charge one is

$$\mathbf{v}(r,\theta) = \left(\frac{\hbar}{mr}\right)\hat{\boldsymbol{\theta}}. \tag{4.20}$$

For $\mathbf{r} = 0$ the density goes to zero, while it recovers its bulk value at a distance equal to the healing length defined in eq. (1.23). One can simplify the computation by assuming that the density is a step function such that

$$\begin{aligned} n(\mathbf{r}) &= 0 \quad \text{if } r < \xi, \\ n(\mathbf{r}) &= n \quad \text{if } r > \xi. \end{aligned} \tag{4.21}$$

The kinetic energy of the fluid is then

$$\begin{aligned} E^V_{\rm kin} &= \frac{1}{2} m \int d\mathbf{r}\, n(\mathbf{r}) v^2(\mathbf{r}) \\ &\approx \frac{1}{2} m n \frac{\hbar^2}{2m} \int_\xi^R dr\, \frac{1}{r^2} 2\pi r \\ &= \pi \frac{\hbar^2 n}{m} \log\left(\frac{R}{\xi}\right). \end{aligned} \tag{4.22}$$

Equation (4.22) has a profound consequence: the energy of a *single* vortex diverges logarithmically when the size of the system goes to infinity[4]. Given the suppression of the density fluctuations at low temperatures, the kinetic energy of a vortex is much larger than the phononic one, and $\Delta E_{\rm kin} \approx E^V_{\rm kin}$.

Also the interaction energy is modified by the presence of the vortex, because the density in the bulk changes from $N/(\pi R^2)$ to $n = N/(\pi(R^2 - \xi^2))$. Hence

$$E^V_{\rm int} = \frac{\hbar^2}{2m} g_{\rm 2D} \int dr^2\, n^2(\mathbf{r}). \tag{4.23}$$

The increase in energy from the state without vortices, for which $E_0 = \frac{\hbar^2}{2m} \frac{g_{\rm 2D} N}{\pi R^2}$, is

$$\begin{aligned} \Delta E_{\rm int} &= E^V_{\rm int} - E_0 \\ &= \frac{\hbar^2}{2m} g_{\rm 2D} \left( \frac{N^2}{\pi(R^2 - \xi^2)} - \frac{N^2}{\pi R^2} \right) \approx \frac{\pi}{2} \frac{\hbar^2 n}{2m}, \end{aligned} \tag{4.24}$$

where we used the approximated relation for $\xi^2 \approx \pi R^2 / 2N g_{\rm 2D}$. Since $\Delta E_{\rm int}$ does not depend on the sample size $R$, it becomes negligible when compared to the kinetic energy difference, diverging as $\log(R)$. This is not the case for a vortex-antivortex pair, where the long-range kinetic energy is suppressed (see below).

For finite temperatures, the superfluid density $n_s$ does not coincide with the total density $n$, hence one should consider $n_s$ instead of $n$ in both relations for the kinetic and the interaction energy.

**Probability of an isolated vortex.** If we again consider a circular system of area $\pi R^2$, given that the size of a vortex is $\pi\xi^2$, the number of independent "boxes" to place a vortex will be

$$W \simeq \frac{R^2}{\xi^2}. \tag{4.25}$$

[4] the details of the result do not depend on the model for the density profile, apart from a constant in the logarithm argument, negligible when $R \to \infty$.

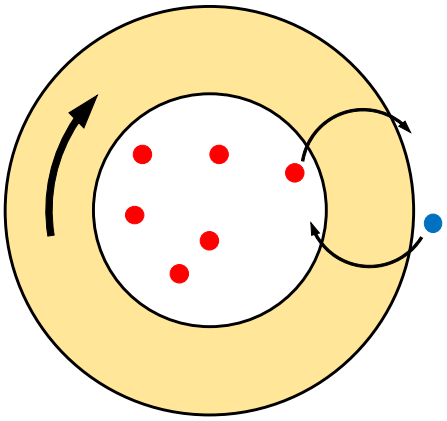

Figure 4.4: Isolated vortices crossing the high-density regions of an atomic ring. The net current is diminished over time, and superfluidity is lost.

The probability for one vortex to appear in the system is given by the Boltzmann law

$$\begin{aligned} p &\approx \exp\left(-E^V_{\text{kin}}/k_{\text{B}}T\right) = \exp\left(-\frac{\pi\hbar^2 n_s}{mk_{\text{B}}T}\log(R/\xi)\right) \\ &\approx \left(\frac{\xi}{R}\right)^{\mathcal{D}_s/2}, \end{aligned} \tag{4.26}$$

where $\mathcal{D}_s = n_s\lambda_T^2$. The total probability is then

$$P_V = pW = \left(\frac{\xi}{R}\right)^{\mathcal{D}_s/2-2}. \tag{4.27}$$

Equation (4.27) presents two cases:

- if the exponent is positive, i.e. if $\mathcal{D}_S > 4$, the probability to form a vortex goes to zero in the thermodynamic limit $R \to \infty$. For large samples it becomes very difficult to have an isolated vortex;
- if the exponent is negative, i.e. if $\mathcal{D}_S < 4$, $P$ diverges in the thermodynamic limit (and thus can no longer be interpreted as a probability). In practice it becomes very likely that the sample has a large number of "isolated" vortices, of random charge. We will show that vortex proliferation disrupts the superfluidity, and we should then consider $\mathcal{D}_S = 0$.

From this basic analysis[5] one recovers the critical point for the BKT phase transition, corresponding to the normal-superfluid transition, which is precisely $\mathcal{D}_s = 4$, independently from the interaction strength $g_{2\text{D}}$.

[5] The same result can be recovered by studying the sign of the free energy $F = E - TS = E - k_{\text{B}}T\log(W)$.

Superfluidity is affected by isolated vortices. Suppose one has a gas in a ring, with a metastable permanent current, so that the phase winding is $2\pi s$ and $s$ is an integer. If $\mathcal{D}_s < 4$, isolated vortices can exist in the high density region of the ring. This means that potentially an isolated vortex can cross from the interior of the ring to the outside (or viceversa), escaping the system and modifying the current. Since there is a higher concentration of vortices of one sign (say positive) in the inside of the ring, the net result of hopping of vortices with random sign will be a reduction of the current, eventually going to zero (Fig. (4.4)). The current is then not metastable, and superfluidity is lost. This is however not the case for *pairs* of vortices, for which the net modification of the current is null.

**Energy and probability of a vortex pair.** The situation just explained for a single vortex is different when computed for a vortex-antivortex pair. Suppose they are separated by a distance $l$. It can be shown[85] that the kinetic energy of a vortex pair is

$$E^{2V}_{\rm kin}(l) \approx 2\pi \frac{\hbar^2 n_s}{m} \log(l/\xi). \tag{4.28}$$

This result, although similar in shape, is instead very different from the isolated case (4.22), because it is not divergent with the size $R$ of the system. The increased interaction energy for a couple of vortices will simply be twice the value computed in eq. (4.24), $\Delta E^{2V}_{\rm int} = 2\Delta E^{V}_{\rm int}$. The probability for a pair is then

$$\begin{aligned} P_{2V}(l) &= \exp\left(-\frac{2\Delta E^{V}_{\rm int} + E^{2V}_{\rm kin}(l)}{k_{\rm B}T}\right) \\ &\approx z_0^2 \left(\frac{\xi}{l}\right)^{\mathcal{D}_s}, \end{aligned} \tag{4.29}$$

where $z_0 = \exp(-\Delta E^{V}_{\rm int}/k_{\rm B}T) \approx \exp(-\mathcal{D}_s/4)$ for a step density profile, is called *fugacity* of the vortex.

Then, up to fairly degenerate gases $\mathcal{D}_s \lesssim 1$ and for vortices not too close ($l \sim$ a few $\xi$), the probability of having a couple of vortices in the system is relevant.

**Average distance.** The average distance between two vortices in a pair is defined as

$$\langle l^2 \rangle = \langle (\mathbf{r}_i - \mathbf{r}_j)^2 \rangle = \frac{\int_\xi^\infty l^2 P_{2V}(l) 2\pi l dl}{\int_\xi^\infty P_{2V}(l) 2\pi l dl}, \tag{4.30}$$

[85] P. Nozieres and D. Pines. *Theory of Quantum Liquids.* Avalon Publishing, 1999.

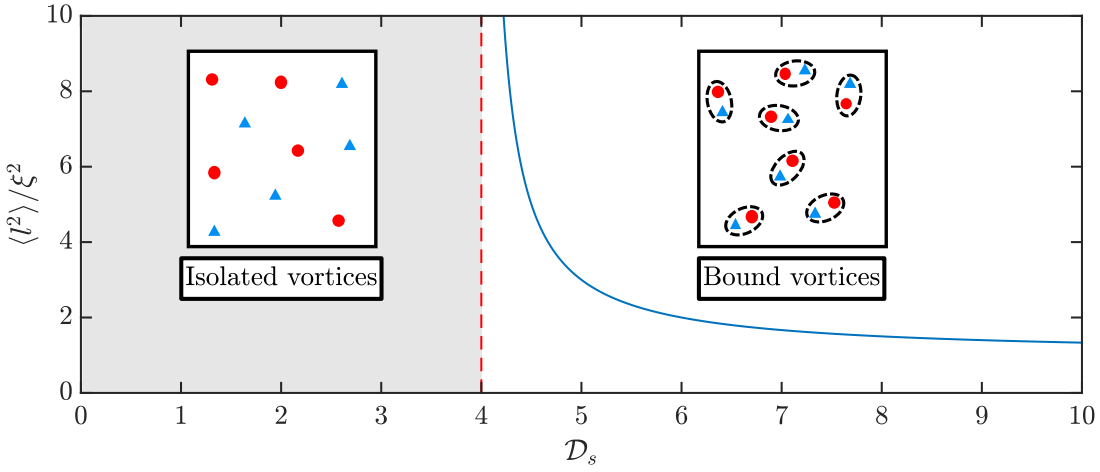


Figure 4.5: Schematic representation of the Berezinskii-Kosterlitz-Thouless phase transition, marked by the divergence of the average normalised distance $\langle l^2\rangle/\xi^2$ (blue line). Depending on the value of the superfluid phase-space density, the vortices in the system are either free ($\mathcal{D}_s < 4$, no superfluidity) or bound in pairs ($\mathcal{D}_s > 4$, superfluid).

whose result is given by Kosterlitz and Thouless[79]:

$$\langle l^2\rangle = \xi^2 \frac{\mathcal{D}_s - 2}{\mathcal{D}_s - 4}. \tag{4.31}$$

From (4.31) we see that the mean distance is only defined for $\mathcal{D}_s > 4$, as it has to be positive, and diverges at the transition point $\mathcal{D}_s = 4$. On the other hand, for increasing $\mathcal{D}_s$ the separation tends to the core size $\xi$.

We can now summarise what we have learnt for the Berezinskii-Kosterlitz-Thouless phase transition. The situation we face is the following (Fig. (4.5)):

- for $\mathcal{D}_s < 4$ we are in the non-degenerate case. The system presents a proliferation of free vortices, and there is no superfluidity: $n_s = 0$.
- for $\mathcal{D}_s > 4$ the system is degenerate. The vortices in the system can only exist in bound pairs, whose average length decreases with increasing $\mathcal{D}_s$. The system is superfluid: $n_s > 0$.

### 4.1.3 Critical temperature

In the previous paragraphs we have seen that the superfluid transition occurs at the critical value $\mathcal{D}_s = 4$ for the phase-space density of the superfluid, which is universal in the sense that it does not depend on the value of the interaction $g$. It is useful to

[79] J. M. Kosterlitz and D. J. Thouless. In: *J. Phys. C* 6.7 (1973), p. 1181.

translate this criterion into one for the critical temperature. Then, once one is able to explicitly calculate the dependence of $n_s$ on the temperature, the critical temperature is defined via

$$n_s(T_c)\lambda_{T_c}^2 = 4. \tag{4.32}$$

Prokof'ev, Ruebenacker *et al.*[86], and Prokof'ev and Svistunov[87] developed a thermodynamic approach to derive the behaviour of the superfluid density on the temperature. This is based on approximating the dynamics of an interacting gas in a $L \times L$ box with a sum of independent oscillators at the Bogoliubov modes $\omega_k$ described by (1.60). This way, one is able to write the chemical potential

$$\mu = \left(\frac{\partial F}{\partial N}\right)_{T,L^2} \tag{4.33}$$

in terms of the free energy

$$F = \frac{\hbar^2}{2mL^2} g_{2\mathrm{D}} N^2 - k_\mathrm{B} T \sum_{\mathbf{k}} \log\left(\frac{k_\mathrm{B} T}{\hbar\omega_k}\right). \tag{4.34}$$

Thus it is possible to write[78] $\mu$ in terms of the phase-space density for the entire gas $\mathcal{D} = n\lambda_T^2$:

$$\frac{\mu}{k_\mathrm{B} T} \approx \frac{g_{2\mathrm{D}}}{2\pi}\left(\mathcal{D} + \log\left(\frac{\pi}{g_{2\mathrm{D}}\mathcal{D}}\right)\right) \tag{4.35}$$

which is an *equation of state* for the interacting gas. If one assumes that the first term on the right side of (4.35) is larger than the logarithmic one, one can invert the previous equation into a relation for the total density of states:

$$\mathcal{D} \approx \frac{2\pi}{g_{2\mathrm{D}}}\frac{\mu}{k_\mathrm{B} T} - \log\left(\frac{k_\mathrm{B} T}{2\mu}\right). \tag{4.36}$$

The superfluid density of states can instead be computed from the Landau relation for the superfluid density[78], and results to be

$$\mathcal{D}_s \approx \mathcal{D} - \log\left(\frac{k_\mathrm{B} T}{2\mu}\right). \tag{4.37}$$

Remembering that the critical point is defined by $\mathcal{D}_s = 4$, after some algebra one arrives to write that

$$\frac{\mu}{k_\mathrm{B} T}\Big|_c \approx \frac{g_{2\mathrm{D}}}{\pi}\log\left(\frac{C_\mu}{g_{2\mathrm{D}}}\right), \tag{4.38}$$

[86] N. Prokof'ev, O. Ruebenacker, and B. Svistunov. In: *Phys. Rev. Lett.* 87 (2001), p. 270402.

[87] N. Prokof'ev and B. Svistunov. In: *Phys. Rev. A* 66 (2002), p. 043608.

[78] J. Dalibard. *Lecture notes in "Quantum Fluids in low dimension and Kosterlitz-Thouless transition" (in French).* 2017.

where $C_\mu$ is a constant depending on the energy cutoff imposed to the model. Analogously, one can write the critical value for the total phase-space density

$$\mathcal{D}_c \approx \log\left(\frac{C_\mathcal{D}}{g_{2\mathrm{D}}}\right). \tag{4.39}$$

The values of $C_\mu$ and $C_\mathcal{D}$ have been determined by Prokof'ev, Ruebenacker and Svistunov[86] by means of classical field simulations, performed in order to correctly match the asymptotic quantum results for a free particle at large $\omega$. The resulting critical values are:

$$\mathcal{D}_c \approx \log\left(\frac{380}{g_{2\mathrm{D}}}\right). \tag{4.40}$$

$$\left.\frac{\mu}{k_\mathrm{B}T}\right|_c \approx \frac{g_{2\mathrm{D}}}{\pi}\log\left(\frac{13.2}{g_{2\mathrm{D}}}\right). \tag{4.41}$$

these results have also been confirmed by quantum Monte Carlo simulations[88].

**Order of the transition.** As the free energy $F$ is continuous in the temperature $T$ at the transition point, and so are all its derivatives, the Berezinskii-Kosterlitz-Thouless is an *infinite order* phase transition. Approaching from $T > T_c$, eq. (4.15) tells us that the correlation function $g_1$ decreases exponentially with the distance

$$g_1(r) \propto e^{-r/\zeta}. \tag{4.42}$$

Differently from what happens in second-order transitions such as Bose-Einstein condensation, in the vicinity of the critical temperature its correlation length diverges *exponentially* rather than algebraically

$$\zeta \sim \lambda_T \exp\left(\frac{\sqrt{\eta}}{\epsilon}\right), \tag{4.43}$$

where $\eta$ is a constant depending on the microphysics of the system and we defined

$$\epsilon = \frac{T - T_c}{T_c} \tag{4.44}$$

as the normalised distance from the critical point.

[86] N. Prokof'ev, O. Ruebenacker, and B. Svistunov. In: *Phys. Rev. Lett.* 87 (2001), p. 270402.
[88] S. Pilati, S. Giorgini, and N. Prokof'ev. In: *Phys. Rev. Lett.* 100 (2008), p. 140405.

## 4.2 Quench across the phase transition

The critical point of a phase transition is critical in the sense that bizarre things may happen. We can observe this aspect in a classical (first-order) phase transition, such as the ice melting process, in which the continuous injection of heat in the system does not cause a change in temperature, but is rather absorbed to drastically modify its physical properties. Continuous (second-order or higher) phase transitions also exhibit interesting features.

It is common knowledge that crossing a phase transition in an abrupt way can result in the production of defects in the system. In statistical physics and condensed matter physics this phenomenon has been addressed theoretically by several authors (see for example [89,90]). In the following we will focus on a particular example of theoretical description for the formation of such impurities, the Kibble-Zurek mechanism. In three dimensions, it describes the formation of defects in a condensed matter system as a result of a relatively fast quench through the critical point. It was first proposed by Kibble[91] in a cosmological context to describe the formation of domain structures in the creation of galaxies, where the relativistic causality imposes a lower bound to the density of defects formed. Its application was later proposed in liquid helium and condensed matter systems by Zurek[92,93]. The mechanism acts both in classical (e.g. in glasses) and in quantum systems (e.g. in superfluid helium[94,95], superconducting films[96] and rings[97], ion chains[98] and recently in quantum gases[46]).

### 4.2.1 Kibble-Zurek mechanism

Let us consider the dynamics of a system undergoing a continuous phase transition. At the critical point, the equilibrium correlation length $\zeta$ and the equilibrium relaxation time $\tau$ will both diverge. The relaxation time is defined as the time interval needed for a system to reach a new equilibrium after being perturbed. In second-order phase

[89] IM Lifshitz. In: *Sov. Phys. JETP* 15 (1962), p. 939. (Original Rus.) Zh, Eksp. Teor. Fiz. 42, 1354 (1962).
[90] Samuel M. Allen and John W. Cahn. In: *Acta Metallurgica* 27.6 (1979), pp. 1085–1095.
[91] T. W. B. Kibble. In: *J. Phys. A* 9.8 (1976), p. 1387.
[92] W. H. Zurek. In: *Nature* 317 (1985), p. 505.
[93] W. H. Zurek. In: *Phys. Rep.* 276.4 (1996), pp. 177–221.
[94] C. Bäuerle et al. In: *Nature* 382 (1996), p. 332.
[95] V. M. H. Ruutu et al. In: *Nature* 382 (1996), p. 334.
[96] R. Carmi and E. Polturak. In: *Phys. Rev. B* 60 (1999), pp. 7595–7600.
[97] R. Carmi, E. Polturak, and G. Koren. In: *Phys. Rev. Lett.* 84 (2000), pp. 4966–4969.
[98] K. Pyka et al. In: *Nature Communications* 4 (2013), p. 2291.
[46] G. Lamporesi et al. In: *Nat Phys* 9.10 (2013), pp. 656–660.

transitions, as the Bose-Einstein condensation, their divergence is algebraic

$$\zeta(\epsilon) = \frac{\zeta_0}{|\epsilon|^\nu} \quad \text{and} \quad \tau(\epsilon) = \frac{\tau_0}{|\epsilon|^{z\nu}}, \tag{4.45}$$

where $\nu$ and $z$ are critical exponents, and $\zeta_0$ and $\tau_0$ depend on the sample. In infinite-order phase transitions such as the BKT, the divergence still occurs, but its form is exponential (eq. (4.43)).

Assume that the quench through the critical point can be considered linear in time $t$. This means that the control parameter $T$ is

$$T(t) = T_c(1 - \epsilon(t)), \tag{4.46}$$

where the reduced parameter $\epsilon$ is symmetric around the critical point

$$\epsilon(t) = t/\tau_q, \tag{4.47}$$

over a time interval $[-\tau_q, \tau_q]$. We imposed the time reference such that $T(0) = T_c$. At any instant, the time distance from the transition is

$$t = |\epsilon/\dot{\epsilon}| \tag{4.48}$$

Both in eqs. (4.43) and (4.45) far away from the transition $|\epsilon| \ll 1$, the equilibrium relaxation time is very small. Conversely, near the transition $\epsilon \to 0$ causing the relaxation time to diverge. The Kibble-Zurek picture is represented by the following approximation[99]:

- The system is assumed to be fully adiabatic when the value of the relaxation time is smaller than $t$. For "adiabatic" we mean having effectively a null relaxation time, and being able to follow instantaneously the equilibrium configuration imposed by the control parameter $\epsilon$.

- When the relaxation time equals the time needed to reach the critical point

$$-\hat{t} = \tau(-\hat{t}), \tag{4.49}$$

  the system will not have enough time to reach a new equilibrium before the transition occurs. The approximation here consists in assuming that after this instant the system dynamics is dramatically slowed down, and is effectively frozen. The instant $-\hat{t}$ is evocatively called *freezing time*.

[99] A. del Campo and W. H. Zurek. In: *Int. J. Mod. Phys. A* 29.08 (2014), p. 1430018.

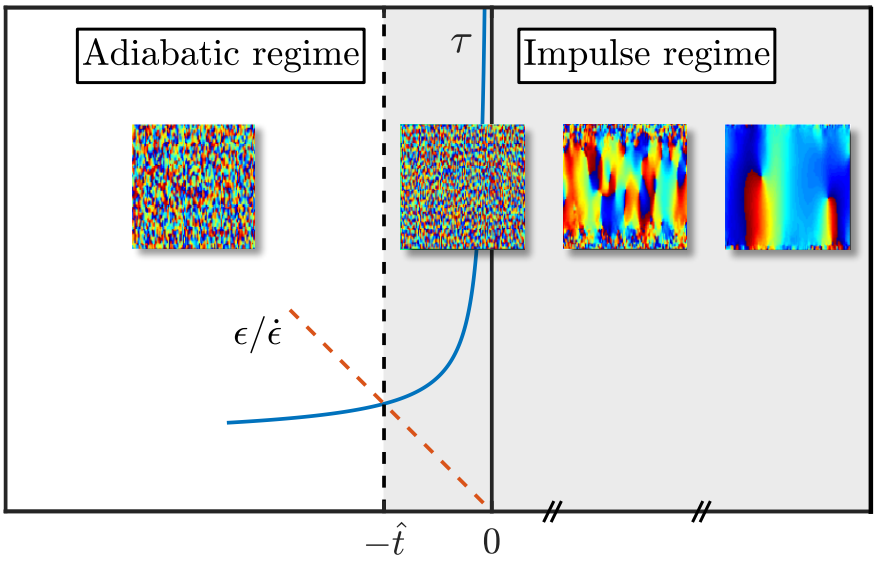


Figure 4.6: Schematic representation of the Kibble-Zurek mechanism. For $t < -\hat{t}$ the system is assumed to be perfectly adiabatic, while for $-\hat{t} > t > 0$ the dynamics is frozen, and the system forms defects. For $t > 0$ the system will eventually recover its dynamics and the defect interaction will slowly lead them to decay.

Figure (4.6) summarises the concepts just introduced. In a second-order phase transition, the degree of freedom relevant for the selection of the symmetry breaking cannot keep up with the externally imposed change of the control $\epsilon$, then it is effectively frozen at the equilibrium value corresponding to $\epsilon(\hat{t})$. This is also true for the correlation length, which is frozen at a value $\hat{\zeta} = \zeta(\hat{\epsilon})$, creating independent domains whenever the system size exceeds $\hat{\zeta}$. These domains are causally disconnected, and the symmetry is independently broken in each one of them. This is cause of the formation of defects at the interface between two domains, where the phase is discontinuous. The usual prediction for the density of defects is given by

$$\rho_{\text{def}} \sim \frac{\hat{\zeta}^d}{\hat{\zeta}^D}, \tag{4.50}$$

where $D$ and $d$ are, respectively, the dimensions of the space and of the defect (e.g. $D = 3$ and $d = 1$ for vortex lines in a 3D superfluid). Usually eq. (4.50) overestimates the density of defects and is only able to provide an order of magnitude indication. The true efficiency of the process is given by

$$\rho_{\text{def}} \sim \frac{1}{f}\frac{\hat{\zeta}^d}{\hat{\zeta}^D}, \tag{4.51}$$

where $f \approx (5 - 10)$ depending on the specific model considered. In the usual picture

of the Kibble-Zurek mechanism for three dimensions, the density of defects depends algebraically on the quench time $\tau_q$, as

$$\rho_{\rm def} \propto \frac{1}{\tau_q^{\alpha}}, \tag{4.52}$$

where $\alpha$ is related to the critical exponents for the transition considered.

## 4.3 Numerical analysis

In the following we will show the results for the numerical analysis on a uniform atomic two-dimensional system, of size $L \times L$, where we also imposed periodic boundary conditions in both directions. The simulations are performed by means of the stochastic projected Gross-Pitaevskii equation described in Chapter 3.

### 4.3.1 Equilibrium results

Before presenting the results on the quench through the phase transition, let us derive some results for the thermal equilibrium of our system. To do so, we run simulations at several temperatures, leaving all the other parameters unchanged. The system size is in this case $L_x \times L_y = (50 \times 50)\mu$m and the chemical potential is $\mu = 20\hbar\omega_{\rm ref}$, where $\omega_{\rm ref} = 2\pi(5\text{Hz})$. After letting the system equilibrate for a very long time we acquired the relevant quantities characterising the equilibrium.

**First-order correlation function.** The first-order correlation function expresses the phase coherence in a quantum system. It is defined as

$$g_1(r) \equiv \frac{\langle \psi^*(\mathbf{x})\psi(\mathbf{x}+\mathbf{r})\rangle_{\mathcal{N}}}{\sqrt{\langle|\psi(\mathbf{x})|^2\rangle_{\mathcal{N}}\langle|\psi(\mathbf{x}+\mathbf{r})|^2\rangle_{\mathcal{N}}}}, \tag{4.53}$$

where the average is performed over the spatial coordinate $\mathbf{x}$, independently on the angle, and over all the stochastic realisations $\mathcal{N}$. In our discretised two-dimensional configuration we define

$$\begin{aligned} g_1(r) &\equiv (g_1^x(r) + g_1^y(r))/2 \\ \text{where } g_1^x(r) &= \frac{1}{N_x N_y}\sum_{i=1}^{N_x}\sum_{j=1}^{N_y} \frac{\langle \psi_{i,j}^*\psi_{i+r,j}\rangle_{\mathcal{N}}}{\sqrt{\langle|\psi_{i,j}|^2\rangle\langle|\psi_{i+r,j}|^2\rangle_{\mathcal{N}}}} \\ \text{and } \quad g_1^y(r) &= \frac{1}{N_x N_y}\sum_{i=1}^{N_x}\sum_{j=1}^{N_y} \frac{\langle \psi_{i,j}^*\psi_{i,j+r}\rangle_{\mathcal{N}}}{\sqrt{\langle|\psi_{i,j}|^2\rangle\langle|\psi_{i,j+r}|^2\rangle_{\mathcal{N}}}}. \end{aligned} \tag{4.54}$$

We also remind that, due to periodic boundary conditions, one should assume that

in the $x$ coordinate $\psi_{i+r,j} = \psi_{i+r-N_x,j}$, and the same is true for the $y$ coordinate. From relations (4.16) and (4.15) one should expect that the correlation function decays exponentially with the distance in the non degenerate case, and progressively grows to an algebraic decay in the low-temperature case. We perform a test of this assumption, by observing the equilibrium profile of $g_1(r)$ as a function of the reduced temperature $T/T_{\mathrm{BKT}}$. Here the critical temperature $T_{\mathrm{BKT}}$ is defined by means of equation (4.41). Figure (4.7a) reports the resulting growth for $g_1(r)$.

It is useful to check the temperature below which the decay turns algebraic. Following the idea in Dagvadorj *et al.*[100], this can be done by fitting the long-range correlation functions with the two relations

$$G_{\mathrm{alg}} \propto (r/r_0)^{\alpha} \quad \text{and} \quad G_{\mathrm{exp}} \propto e^{-r/\lambda}. \tag{4.55}$$

One could then estimate the point at which the two fits apply equally well to the data, and identify it as the crossover between the two regimes. In the Berezinskii-Kosterlitz-Thouless picture, this can be identified with the critical point of the transition. Figure (4.7b) plots the profiles of $g_1(r)$ with the fits defined in eq. (4.55). Figure (4.7c) plots the estimator

$$\Xi = \frac{\mathrm{MSE}_{\mathrm{exp}}}{\mathrm{MSE}_{\mathrm{alg}}}, \tag{4.56}$$

where

$$\mathrm{MSE}(T) = \langle (g(r,T) - G(r,T))^2 \rangle \tag{4.57}$$

is the mean squared error for our fits. The resulting plot shows that one can identify the crossover between an algebraic an an exponential decay of $g_1(r)$ to be shifted by a factor $\sim 0.25$ with respect to the theoretical relation for the transition described in (4.41).

Another test on the same concept concerns the order parameter $m$ defined in (3.50) as a function of the reduced temperature $T/T_{\mathrm{BKT}}$. The result is reported in Fig. (4.8a), together with the square root of the equilibrium result for $|g_1(L_x/2)|$. As described in 3.2.6, the two quantities should coincide at equilibrium. We measure that indeed they show the same qualitative behaviour across the whole temperature range, even though they present a small deviation in the region of the algebraic-to-exponential crossover. Moreover, once again there appears to be a shift of about $\sim 0.25$ in the transition point, as measured in the previous analysis. Finally, following the treatment in [74],

[100] G. Dagvadorj et al. In: *Phys. Rev. X* 5 (2015), p. 041028.

[74] M. Kobayashi and L. F. Cugliandolo. In: *Phys. Rev. E* 94 (2016), p. 062146.

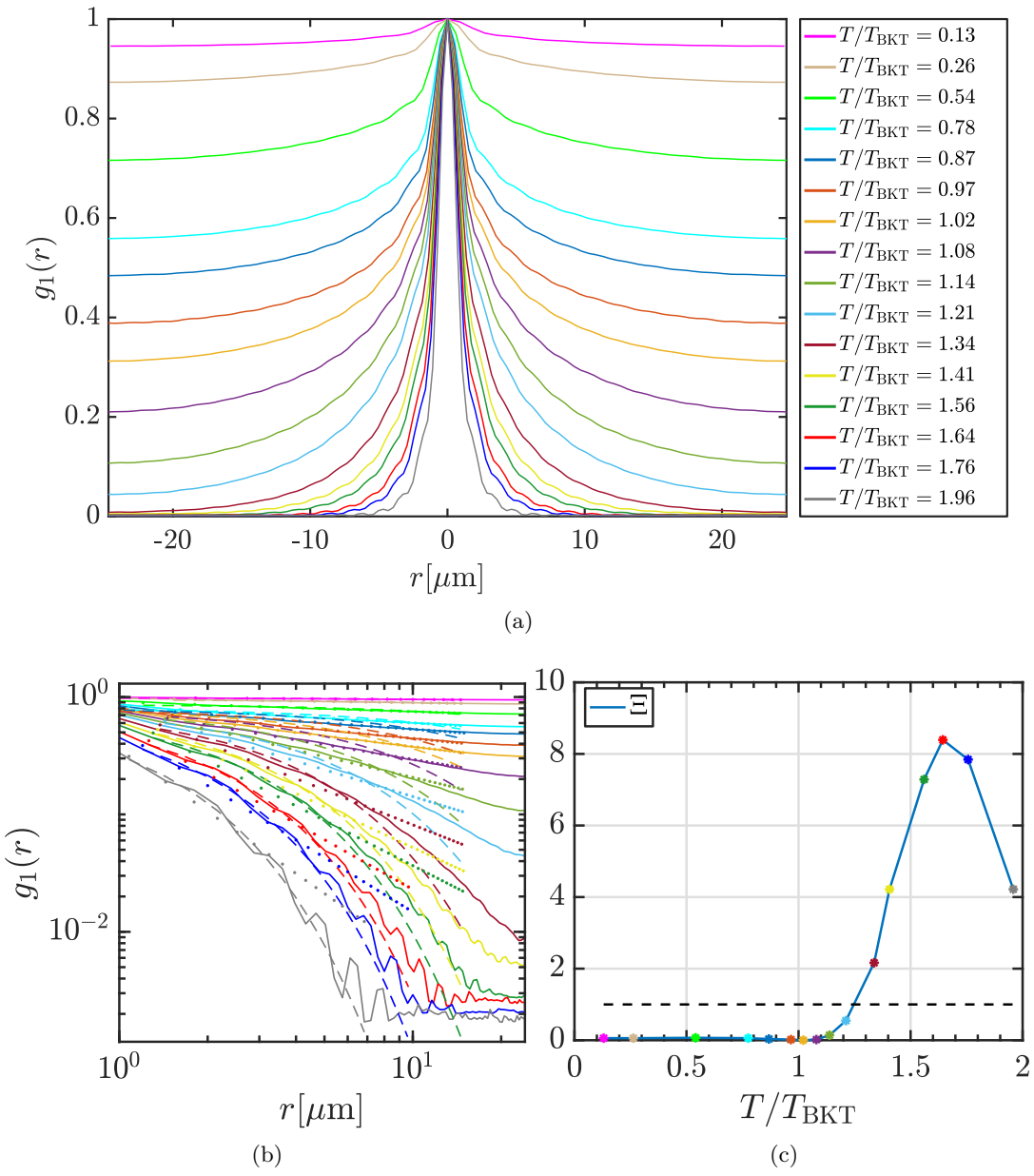


Figure 4.7: Simulation of uniform system in a box of size $L_x \times L_y = (50 \times 50)\mu$m, with periodic boundary conditions. The averages are performed over $\mathcal{N} = 100$ stochastic realisations for each temperature data set. (a) Equilibrium profiles for the first-order correlation function $g_1(r)$ for different temperatures. (b) Correlation function profiles as in the previous figure, in logarithmic scale. The fitted algebraic (dotted lines) and exponential (dashed lines) functions are defined as in (4.55). (c) Ratio $\Xi$ between the mean squared errors for the fits in (b), as defined in (4.56). The dashed line expresses the value of $\Xi$ for which the two fits apply equally well to the data. The resulting critical point presents a shift of about $\sim 0.25$ with respect to the theoretical relation for $T_{\mathrm{BKT}}$, equation (4.41).

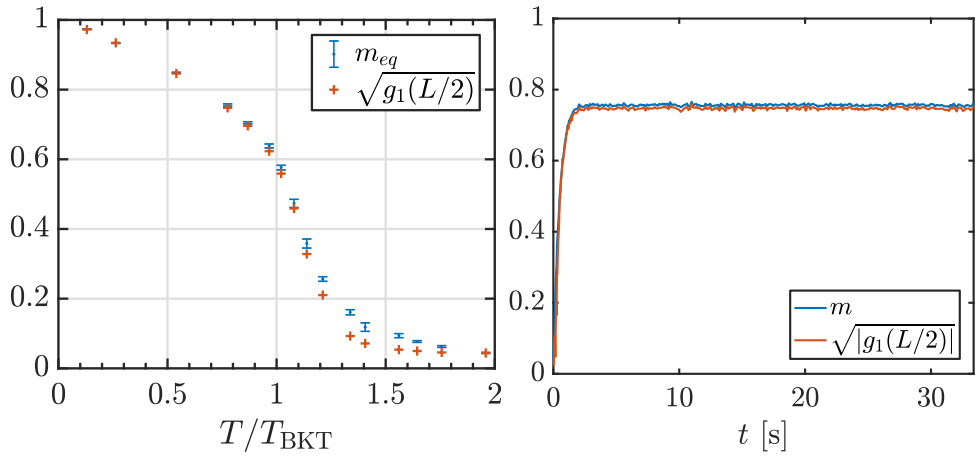


Figure 4.8: (a) Equilibrium order parameter (blue) and square root of the edge correlation function $\sqrt{|g_1(L/2)|}$ (red) for samples at thermal equilibrium at different values of $T/T_{\mathrm{BKT}}$ as in Fig. (4.7). The error bars are indicative of the statistical standard deviation of the different noise realisations. The data show again a shift in the critical point of the order of $\sim 0.25$. (b) Comparison between the time evolution of the order parameter defined as in eq. (3.47) and the one defined as in eq. (3.50) for $T/T_{\mathrm{BKT}} = 0.78$.

we compute the Binder ratio, defined as

$$U = \frac{\langle |\sum_{i,j} \psi_{i,j}|^4 \rangle}{\langle |\sum_{i,j} \psi_{i,j}|^2 \rangle^2}, \tag{4.58}$$

and reported in Fig. (4.9a), which confirms the same trend for the transition temperature.

In Fig. (4.9b) we also plot the value of the quasi-condensate fraction as a function of the temperature. In a uniform Bose system it is possible to compute it as

$$n_{\mathrm{qc}} = \frac{\sqrt{2\langle|\psi|^2\rangle^2 - \langle|\psi|^4\rangle}}{n}, \tag{4.59}$$

where the average is performed over the entire spatial grid and on the different noise realisations. The quasi-condensate has a significant non-zero value also above the critical temperature. At the critical point its value is $\sim 0.7$. In the BKT picture, it is the quasi-condensate which allows the existence of the vortices above the transition, where a superfluid is not present.

The systematic shift in the position of the critical point is a recurrent feature of our analysis, and is currently a matter of investigation. The transition of the order parameter is moreover not very sharp, when compared to the one that can be found

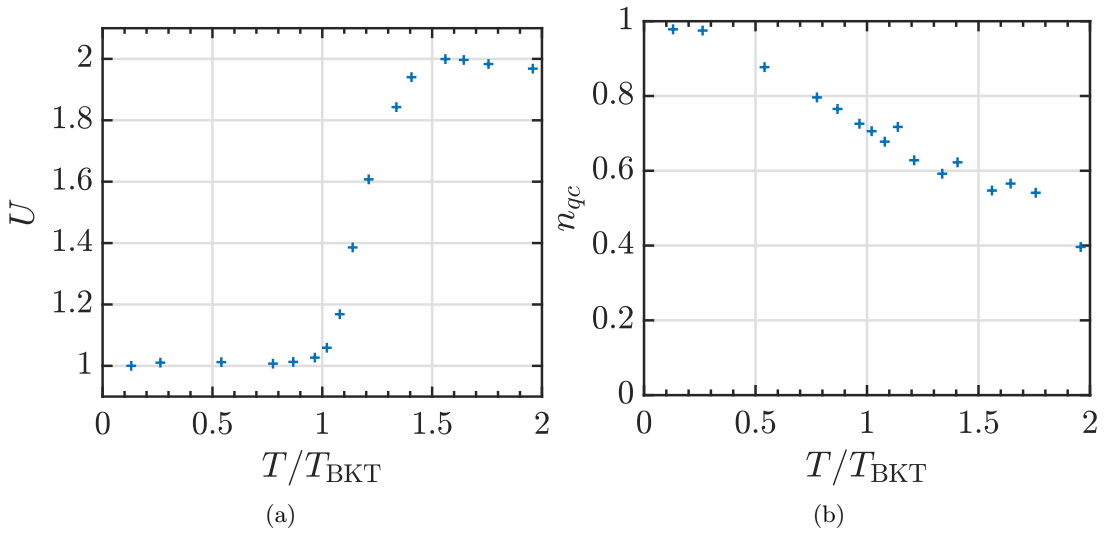


Figure 4.9: (a) Equilibrium Binder ratio $U$ as defined in text, for samples at thermal equilibrium at different values of $T/T_{\mathrm{BKT}}$ as in Fig. (4.7). The data indicate again a shift in the critical temperature position compatible with the one of the previous analysis. (b) Equilibrium quasi-condensate fraction $n_{\mathrm{qc}}$ as a function of the temperature.

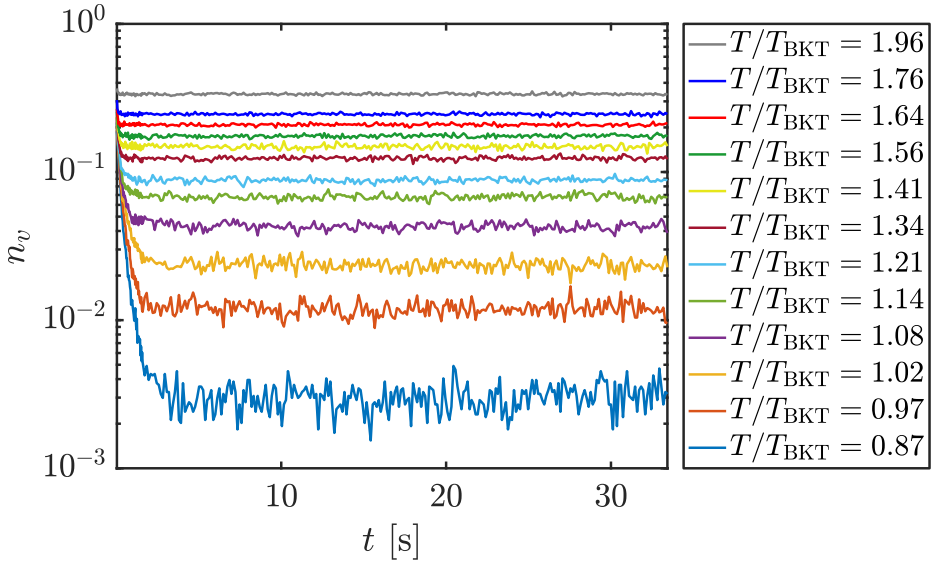


Figure 4.10: Time evolution of the vortex density $n_v$ as a function of the reduced temperature $T/T_{\mathrm{BKT}}$, expressed in natural units of $1/l_{\mathrm{ref}}$, where $l_{\mathrm{ref}} = \sqrt{\hbar/m\omega_{\mathrm{ref}}}$.

in the literature[74]. We believe this effect to be due to the finite size of the system combined with the periodic boundary conditions we imposed, which may enhance the creation of a quasi long-range order, causing the critical point to lose definition. More

[74] M. Kobayashi and L. F. Cugliandolo. In: *Phys. Rev. E* 94 (2016), p. 062146.

discussions on that are reported in Section 4.4.

We also study the equilibrium number of vortices as a function of the temperature. We count the number of vortices $n_v(t)$ at any time step by means of a numerical routine which considers the phase winding around each grid point to identify the vortices in the system, and their circulation[6] (Fig. (4.10)). From the equilibrium value for the vortex density (Fig. (4.11a)) it is possible to estimate an equilibrium correlation length simply defined as $\zeta_v^{eq} = 1/\sqrt{n_v^e q}$ (see the discussion on the next section). The resulting plot in Fig. (4.11b) shows an exponential growth of the correlation length in the proximity of the transition point, as expected from the theory.

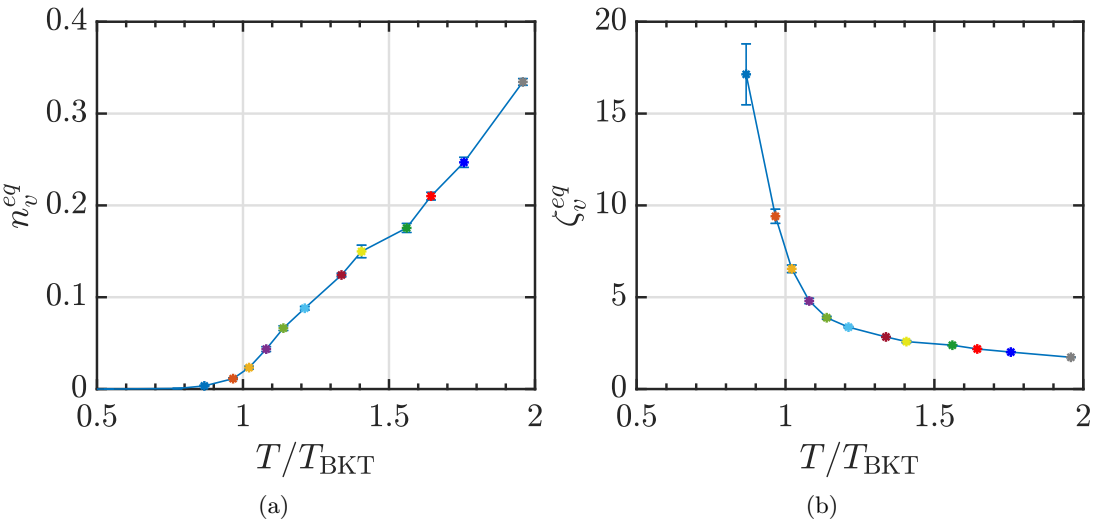


Figure 4.11: (a) Equilibrium vortex density computed by performing a short time average of the final values of $n_v$. For temperatures below $\sim 0.75 T_{\mathrm{BKT}}$, for our parameters, the vortices will completely annihilate. (b) Correlation length $\zeta_v^{eq}$ extracted from the equilibrium values for $n_v$, expressed in natural units of $l_{\mathrm{ref}}$. The coloured points correspond to the temperatures indicated in Fig. (4.10).

### 4.3.2 Quench in temperature and chemical potential

Let us now report some results of quenches performed from a high-temperature $T > T_{\mathrm{BKT}}$ state to a highly degenerate one $T < T_{\mathrm{BKT}}$. In real-life experiments, the atomic cloud is progressively grown into the trap, leading to an accumulation of atoms in the modes of the system and to its thermalisation. This is effectively simulated by first imposing a state at a *negative* value of the chemical potential in equation 3, reproducing an infinite temperature configuration. At a time $t = t_0$ the temperature is suddenly reduced, and the chemical potential assumes a positive value. The system will then grow from a initial state only populated by the Gaussian noise $\eta$ (Fig. (4.12),

[6] The routine follows what is referred to as "Algorithm 5" in George Stagg PhD thesis[101].

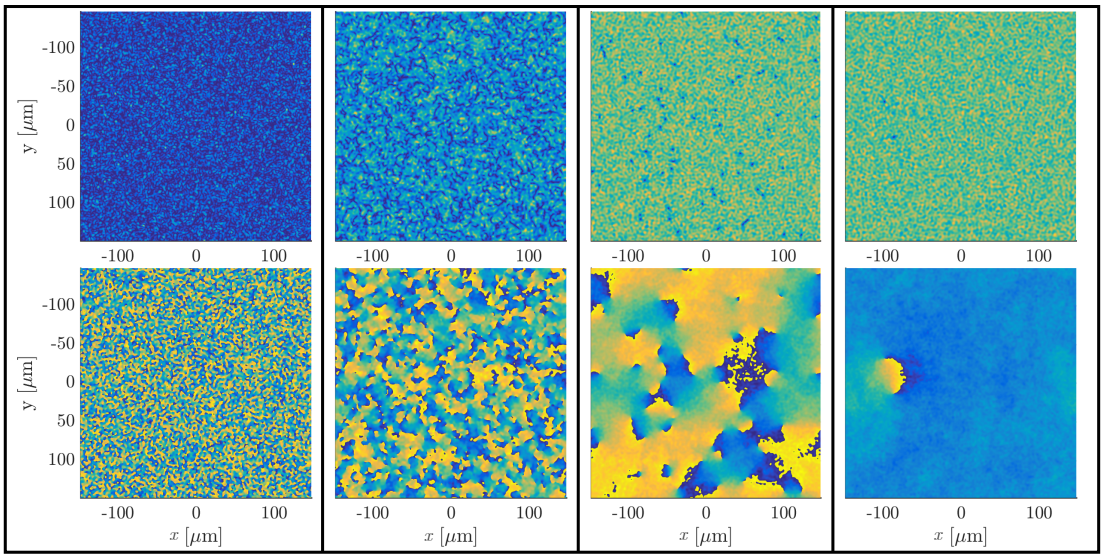


Figure 4.12: Density (above) and phase (below) of a uniform two-dimensional system quenched from a non-degenerate to a degenerate configuration. The initial random state (first panel) grows to an intermediate state where the system shows many soliton-like defects, and the phase is homogeneous in small patches (second panel). They eventually decay into vortex-antivortex pairs due to the snaking instability (third panel), which eventually annihilate if the temperature is low enough (fourth panel). The capture time for these frames is indicated in Fig. (4.14).

first panel), up to its equilibrium configuration set by the final values of $T$ and $\mu$. The equilibration process passes through several phases. At first, immediately after the quench, the system will accumulate atoms in the coherent region $\psi$. Given the random initial distribution of the phase, in the framework of the Kibble-Zurek mechanism, a large number of defects will be formed. The creation of phase domains according to the KZM leads to the formation of soliton-like excitations (Fig. (4.12), second panel, and Fig. (4.13), first panel), which will eventually break due to the snaking instability into pairs of vortices (Fig. (4.12), third panel). If the final temperature is very low, these vortices will eventually lose energy due to the collisions with the thermal excitations, and annihilate (Fig. (4.12), fourth panel). The resulting decay is reported in figure (4.14), where we performed an average over several stochastic realisations.

Figures (4.15a) and (4.15b) report the time evolution of $g_1(r)$ for an instantaneous quench, and show indeed an initial fast spatial decaying profile, progressively growing, after the transition is crossed, to match a slow algebraic decay. Figure (4.15c) shows the simultaneous growth of the function $g_1(L/2)$ at the edge of the system, the condensed fraction $n_c$ extracted via the Penrose-Onsager diagonalisation (see Section 3.2.5) and the order parameter $m$ defined in eq. (3.50). To properly fulfil the Penrose-Onsager prescription, one should only consider the case in which the highest eigenvalue of the

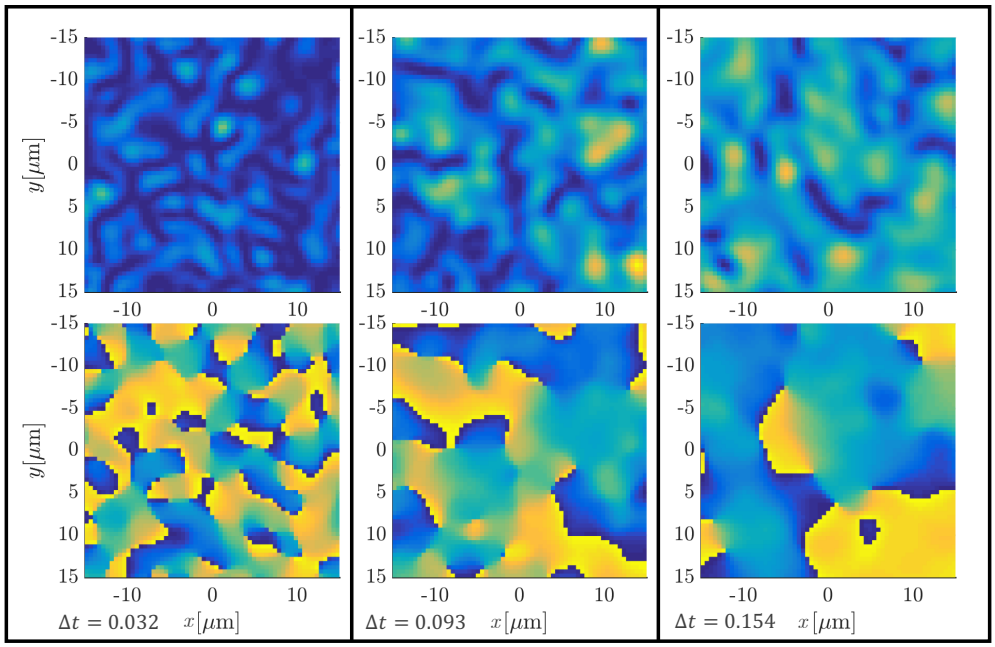


Figure 4.13: Zoom of the central regions of density (above) and phase (below) of the 2D system, captured at a short time after the quench, showing the formation of regions of uniform phase, corresponding, in density, to soliton-like defects at their boundaries. They will eventually undergo a dynamical instability and break into vortex-antivortex pairs.

density matrix $\alpha_{\max} = \alpha(1)$ is *macroscopic* with respect to the others, and this is only true quite far from the transition point, when the system has grown a significant condensed fraction. Here we assume that the Penrose-Onsager extraction holds for each instant in which $p_{2\max} < 0.3 p_{\max}$. As postulated in Sec. 4.1.1, the equilibrium condensed fraction coincides with the edge value of the equilibrium first-order correlation function. The square of the order parameter, after an initial equilibration, also equals $g_1(L/2)$, as one expects from its definition.

### 4.3.3 Dynamical scalings after an instantaneous quench

We now want to study the dynamic scaling of the correlation length when performing an instantaneous quench from a temperature $T > T_{\mathrm{BKT}}$ to $T < T_{\mathrm{BKT}}$. As in the previous section, the gas will initially be in a high-temperature non-degenerate case, and it is suddenly quenched to a degenerate low-temperature configuration. The system is then left to equilibrate for a sufficient time, establishing a quasi long-range order as predicted by (4.15). The procedure reported here is inspired by the one developed for the 2D $XY$ model by Jelić and Cugliandolo[102].

The first-order equal-time space correlation function (4.53) can be can be written

[102] A. Jelić and L. F. Cugliandolo. In: *J. Stat. Mech.* 2011.02 (2011), P02032.

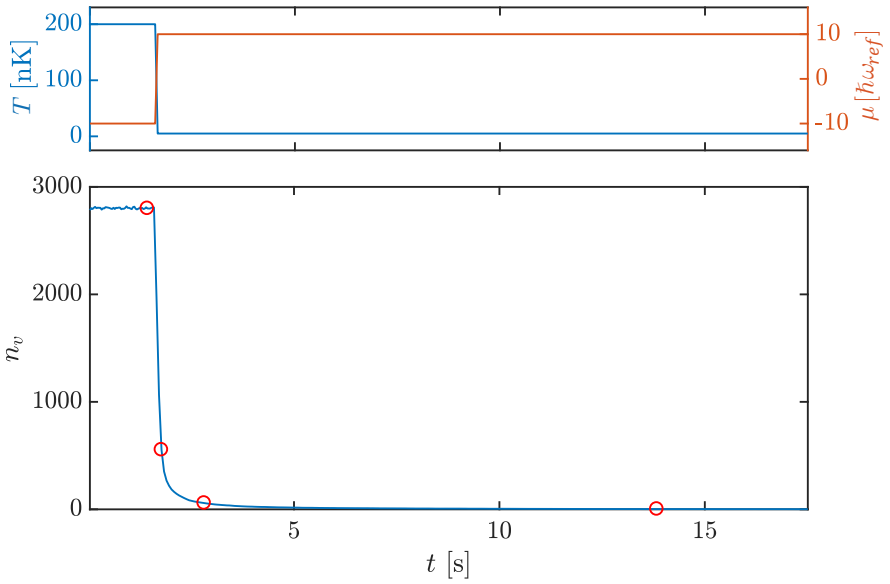


Figure 4.14: (top) Control parameters $T$ and $\mu$, quenched simultaneously. Here $\omega_{\text{ref}} = 2\pi(5\text{Hz})$. (bottom) Measured number of vortices as a function of time, averaged over $\mathcal{N} = 100$ stochastic realisations. The four red points indicate the four instants represented in (4.12).

by means of the scaling relation

$$g_1(r,t) \approx r^{-\eta(T)} f\left(\frac{r}{\zeta(t,T)}\right), \tag{4.60}$$

where $\eta$ is the static critical exponent for the BKT phase transition, $f$ is a *scaling function*, and $\zeta(t,T)$ is the correlation length. The latter is an important quantity, which we will investigate further. Its scaling in time for purely diffusive processes is $\zeta \sim t^{1/2}$. For a quench from a temperature above $T_{\text{BKT}}$ in the $XY$ model, it is predicted[102–104] that it shows instead a small modification

$$\zeta(t,T) \approx \left(\lambda(T)\frac{t}{\log(t/t_0(T))}\right)^{1/z}, \tag{4.61}$$

where $z = 2$ for the $XY$ model, $\lambda(T)$ and $t_0$ are non-universal, since they depend on the way in which $\zeta$ is measured. The difference is considered to be due to the process of vortex annihilation.

We will focus on two ways of measuring $\zeta$. The first is by directly applying eq. (4.60), and by extracting the correlation length $\zeta_g(t)$ from the decay of $g_1(r)$. Figure (4.16) shows the time evolution of the first-order correlation function after an instanta-

[102] A. Jelić and L. F. Cugliandolo. In: *J. Stat. Mech.* 2011.02 (2011), P02032.
[103] B. Yurke et al. In: *Phys. Rev. E* 47 (1993), pp. 1525–1530.
[104] A. J. Bray, A. J. Briant, and D. K. Jervis. In: *Phys. Rev. Lett.* 84 (2000), pp. 1503–1506.

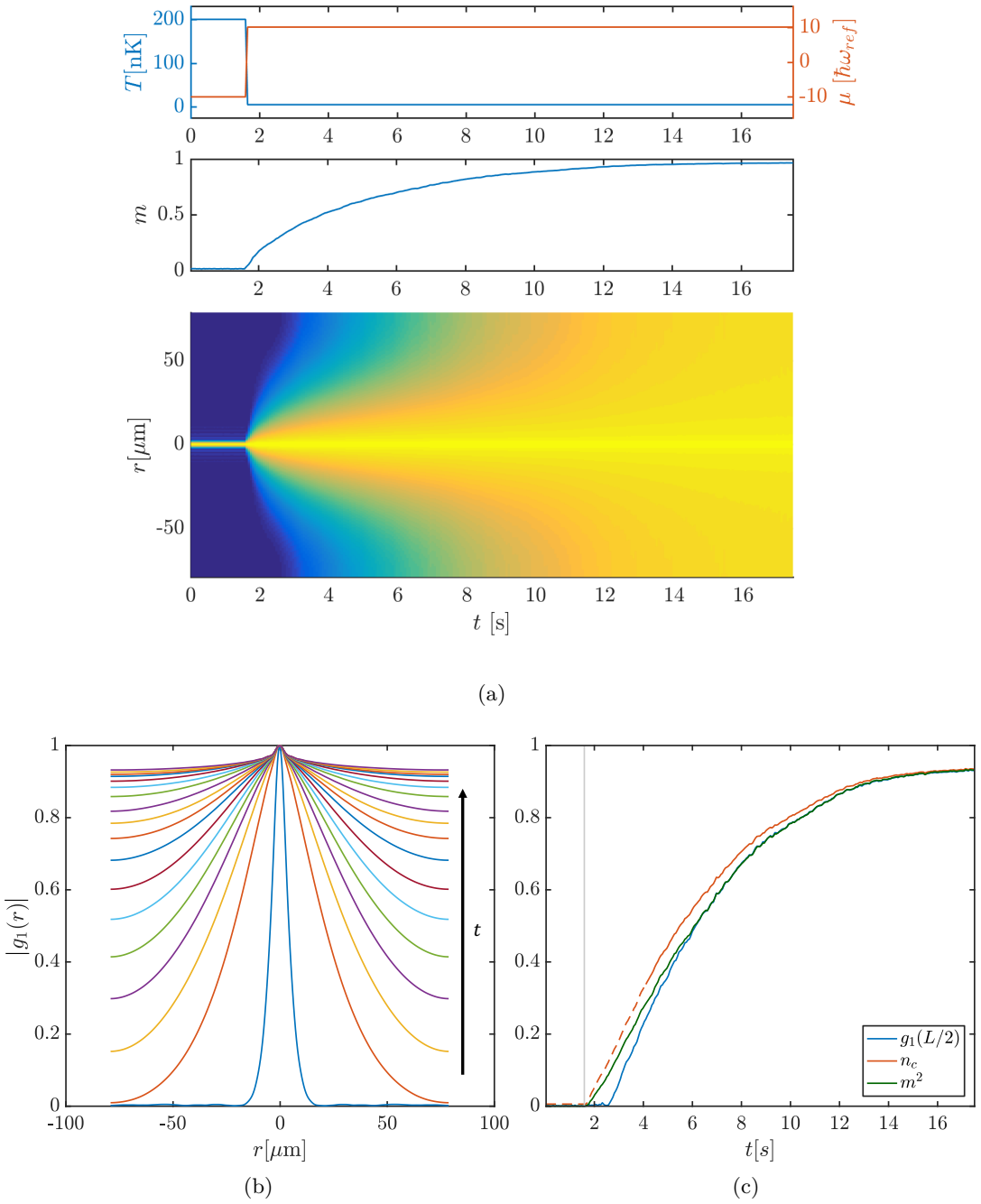


Figure 4.15: (a) (top) Control parameters $T$ and $\mu$, quenched simultaneously. (middle) Growth of the order parameter $m$ (eq. (3.50)). (bottom) Growth of the modulus of the first-order correlation function (4.53) after an instantaneous quench. (b) Evolution of $|g_1(r)|$ from a non degenerate gas to a low-temperature configuration. The shape of the correlation length switches from exponential to algebraic, according to (4.15) and (4.16). (c) Growth of the correlation function at the edge $|g_1(L/2)|$ (blue), of the condensed fraction $n_c$ (red) and of the square of the order parameter $m^2$ (green). $m^2$, $|g_1(L/2)|$, and $n_c$ coincide for long $t$, as postulated in Sections 4.1.1 and 3.2.6. The dashed grey line indicates the instant of the quench. The dashed section of the condensed fraction represents the fact that it is only well defined sufficiently far from the transition (see text).

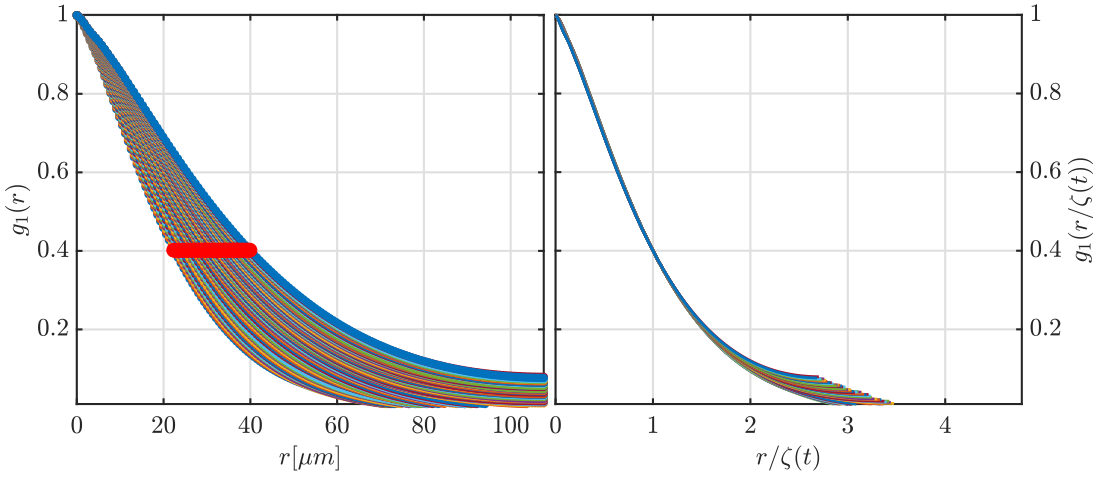


Figure 4.16: (left) Time evolution of the first-order correlation function $g_1(r)$ during an instantaneous quench across the BKT critical point. (right) Correlation function, rescaled according to a function $f(r/\zeta(t))$ as in (4.60). The definition of $\zeta(t)$ is chosen so that, at any $t$, $g_1(\zeta(t), t) = 0.4$. The parameters for this simulation are $\omega_{\text{ref}} = 2\pi(5\text{Hz})$, $\mu = (-10 \to +10)\hbar\omega_{\text{ref}}$, $T = (200 \to 5)\text{nK}$, $\gamma = 0.01$, $L = 216\mu\text{m}$.

neous quench, and its rescaling according to (4.60). This is done by imposing the values of $g_1(\zeta_g(t), t)$ to be equal to a certain cut value $g_{\text{cut}}$ (e.g. $g_{\text{cut}} \equiv 0.4$ in the example), so to get a time-dependent value for $\zeta_g$. The spatial coordinate is then rescaled by the proper $\zeta_g(t)$ for each time. Figure (4.16) (right) shows indeed the predicted dynamic scaling to hold. We checked that the resulting correlation length is only marginally affected by changing the cut value in a sensible range $(0.2 - 0.7)$. The second way of measuring $\zeta$ comes from the study of the density of vortices $\rho_v(t) \equiv n_v(t)/L^2$ in the system. In the fully random infinite temperature limit, at equilibrium, the density of defects is predicted[102] to be $\rho_v \simeq 0.3$. Figure (4.17) (right) reports the decay of the number of defects as a function of time. One can see that for the "infinite" temperature case, we measure a density of defects around 0.4. After the quench is performed, the density of defects decays exponentially. As the vortices disrupt the coherence in a uniform system, one could postulate a correlation length associated with the inverse of the vortex density, as $\zeta_v(t) = 1/\sqrt{\rho_v(t)}$ in two dimensions.

The two correlation lengths are presented in Figure (4.18). The difference in the absolute value for the two quantities is due to the details of how they are computed, and in light of relation (4.61) it can be seen as having determined different values for $t_0$ and $\lambda(T)$. We are interested in investigating the scaling for the growth of $\zeta_g(t)$ and $\zeta_v(t)$. For this purpose we perform several fits for their long-time evolution, according

[102] A. Jelić and L. F. Cugliandolo. In: *J. Stat. Mech.* 2011.02 (2011), P02032.

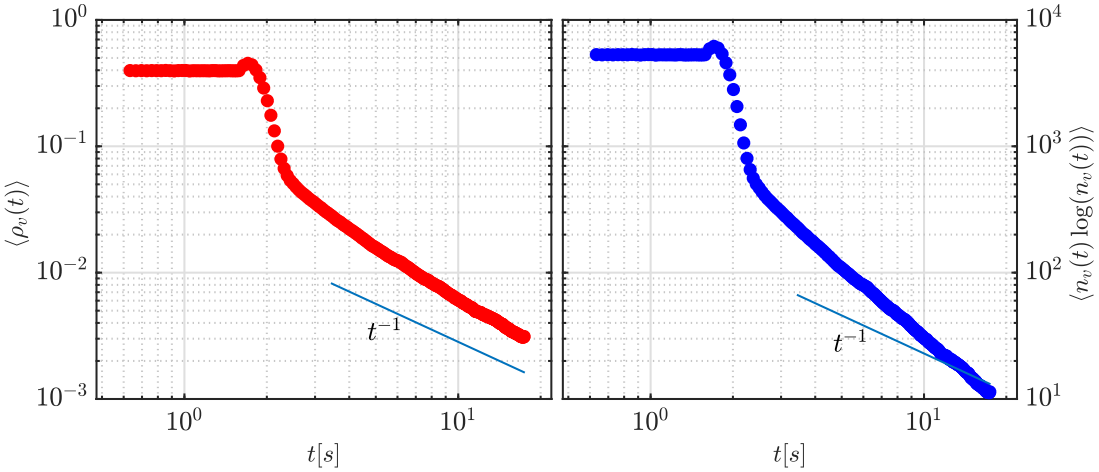


Figure 4.17: (left) Time evolution for the density of defects $\rho_v(t) = n_v(t)/L^2$. Note that the initial value is consistent with the one predicted for an infinite temperature configuration $\sim 0.3$. (right) Decay of $n_v(t)\log(n_v(t))$ as a function of time. The parameters are the same as in Fig. (4.16).

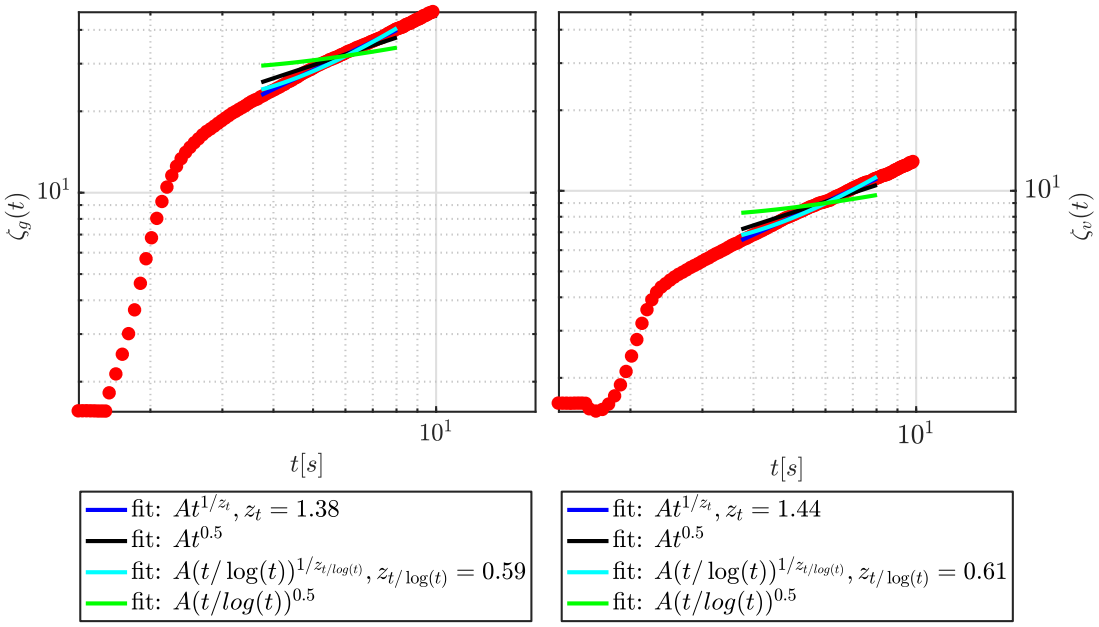


Figure 4.18: (left) Correlation length $\zeta_g(t)$ extracted from the growth of the first-order correlation function $g_1(r)$, reported in Fig. (4.16). The definition of $\zeta_g(t)$ corresponds to the scaling factor for the spatial coordinate $r$, given an intersection of 0.4. (right) Correlation length $\zeta_v(t)$ extracted from the decay of the density of vortices $\rho_v(t)$. The definition is $\zeta_v(t) = 1/\sqrt{\rho_v(t)}$. The difference between the two is given by the different values for the non-universal constants $t_0$ and $\lambda(T)$, due to the different measuring procedure. In both figures several fitted scalings are plotted (see text), giving very similar results for $z$.

to the four relations

$$\begin{aligned}\zeta(t) &\approx A t^{1/z_t} \quad \text{(blue)},\\ &\approx A t^{0.5} \quad \text{(black)},\\ &\approx A(t/\log(t))^{1/z_{t/\log(t)}} \quad \text{(cyan)},\\ &\approx A(t/\log(t))^{0.5} \quad \text{(green)},\end{aligned} \tag{4.62}$$

where we considered as reference the expected value $z_{\text{th}} = 2$. The four fitting relations show respectively a diffusive-type scaling (blue), the diffusive scaling expected from the theory $\sim t^{1/2}$ (black), relation (4.61), with the exponent as a free parameter (cyan), and the one with the expected critical exponent (green).

The plots show indeed a certain internal consistency between the two "independently" computed correlation lengths, but the value for the critical exponent $z$ is not close to the expected one $z_{\text{th}} = 2$. This disagreement is remarkable, especially in the light of previous works[105] in other physical systems showing good agreement with the theory, and remains an open matter for further investigation.

### 4.3.4 Slow quenches and Kibble-Zurek scaling

In this section we study again the evolution of a system from its non-degenerate to its degenerate phase, but instead of performing an instantaneous quench across the transition, we consider slower quenches. In order to simulate this, we follow the prescription by Jelić *et al.*[102]: we first equilibrate the system at a finite temperature above the critical value $T_0 > T_{\text{BKT}}$. Then, at $t_0$ we perform linear ramps in the control parameter, with a finite duration $\tau_q$, up to the final subcritical value:

$$T(t) = T_0 - (T_0 - T_{\text{eq}})\frac{(t - t_0)}{\tau_q}. \tag{4.63}$$

From there, the temperature is kept fixed at $T_{\text{eq}}$, and the system is left to equilibrate. Figure (4.19) summarises the cooling procedure just described, for different quench durations.

According to the Kibble-Zurek picture, after passing $-\hat{t}$, the evolution of the system is dramatically slowed down, and the correlation length $\zeta$ maintains its "frozen" value $\zeta(t > -\hat{t}) = \zeta(-\hat{t}) \equiv \hat{\zeta}$. However, one could argue that this is a rather strong simplification, and that the correlation length evolution is modified but not stopped

[105] P. Comaron et al. In: *ArXiv e-prints* (2017). arXiv: 1708.09199.

[102] A. Jelić and L. F. Cugliandolo. In: *J. Stat. Mech.* 2011.02 (2011), P02032.

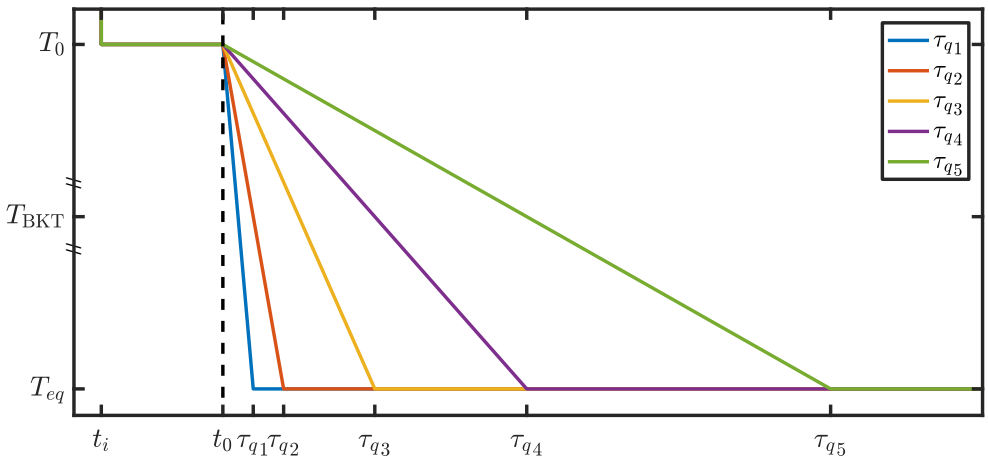


Figure 4.19: Schematic representation of the cooling procedure. The temperature is equilibrated from infinite to a finite value $T_0 > T_{\mathrm{BKT}}$, then, starting at $t_0$, it is quenched with a linear ramp of various durations $\tau_q$ and finally kept fixed at $T_{\mathrm{eq}}$.

after $-\hat{t}$. Jelić *et al.*[102] postulated that, if $\Delta t = \hat{t} + t$:

$$\zeta(t) = \begin{cases} \zeta_{\mathrm{eq}}(T(t)) & \text{for } t < -\hat{t}(\tau_q) \\ \hat{\zeta} + \left(\lambda(T)\frac{\Delta t}{\log(\Delta t/t_0(T(t)))}\right)^{1/z} & \text{for } t > -\hat{t}(\tau_q), \end{cases} \tag{4.64}$$

where $\lambda(T)$ and $t_0(T)$ are assumed to evolve so slowly that one can retain their evolution after an instantaneous quench. Therefore, the correlation length follows its equilibrium value up to $-\hat{t}$, after which its evolution is modified and continues according to (4.61). From (4.61) it is possible to infer a relation for the evolution of the density of defects as a function of the quench time $\tau_q$:

$$\begin{aligned} \rho_v(\tau_q) &\approx \tau_q^{-1} + \left(\lambda(T_{\mathrm{eq}})^{-1}\frac{\log[\Delta t(\tau_q)/t_0(\tau_q)]}{\Delta t(\tau_q)}\right) \\ &= \tau_q^{-1} + \left(\lambda^{-1}\frac{\log[(\hat{t}+\tau_q)/t_0]}{\hat{t}+\tau_q}\right). \end{aligned} \tag{4.65}$$

A very brief analysis has been carried out on the evolution for the density of defects. In the simulation results, due to the choice of the parameters, the growth of the quasi long-range order given by the order parameter $m$ occurs always at the end of the cooling ramp. Hence, the vortex evolutions are always computed after the ramp is completed, therefore in a situation with fixed control parameters $T$ and $\mu$.

This is clearly different from the case studied in [102], where the measurement of the number of defects is done precisely at the end of the ramp, when the temperature

[102] A. Jelić and L. F. Cugliandolo. In: *J. Stat. Mech.* 2011.02 (2011), P02032.

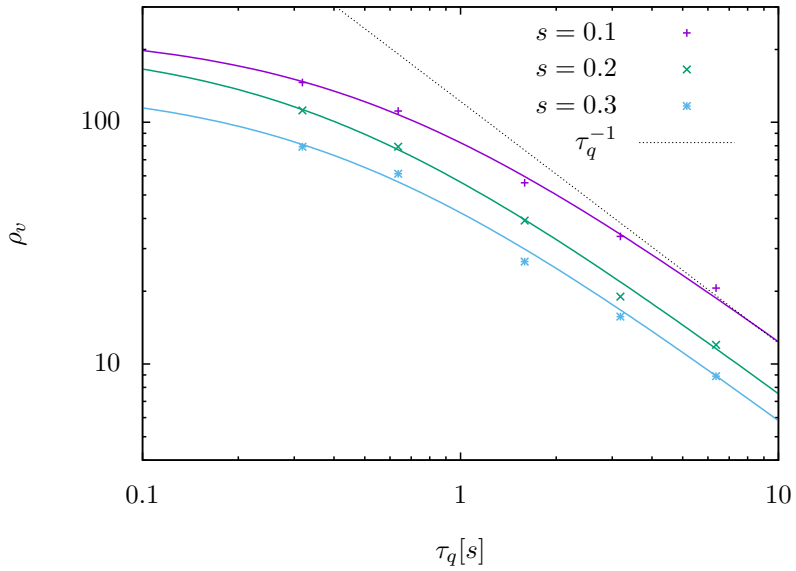


Figure 4.20: Scaling of the vortex density $\rho_v$ as a function of the quench time $\tau_q$. The number of vortices is computed at a time interval $t_{\text{count}} - t_0 = \tau_q(1+s)$ after the cooling ramp is completed. The solid lines correspond to fitting functions of the kind of relation (4.65), where $\lambda$ and $t_0$ are kept as free fitting parameters.

has just reached its final value. To estimate whether this plays a role in the dynamic scaling, we computed the number of vortices at three different fraction $s$ of the ramp time, after the quench is completed. Thus, for any ramp time $\tau_q$ the density of defects is counted at a time

$$\Delta t_{\text{count}} = t_{\text{count}} - t_0 = \tau_q + s\tau_q, \tag{4.66}$$

where we considered the values for the fraction $s = [0.1, 0.2, 0.3]$. The results are shown in Figure (4.20), where indeed the scaling is unaffected by the difference in the fraction $s$, apart from a general shift in the magnitude. The solid lines show a fit for the data according to the relation (4.65), where $\lambda$ and $t_0$ are assumed to be free parameters.

### 4.3.5 Interaction quench

In section 4.3.2 we reported results obtained by quenching both the temperature and the chemical potential in our sample. Dynamically controlling two parameters at the same time causes a certain amount of ambiguity in the determination of the system's critical point. Abruptly changing $\mu$ also causes large atom number fluctuations, which may cause issues in the dynamical evolution to equilibrium, and in the definition of the projector separating the coherent and the incoherent regions. Moreover, one could question whether quenching linearly both $T$ and $\mu$ is seen from the system as a linear overall quench. An alternative approach is easily recognised by looking at equation

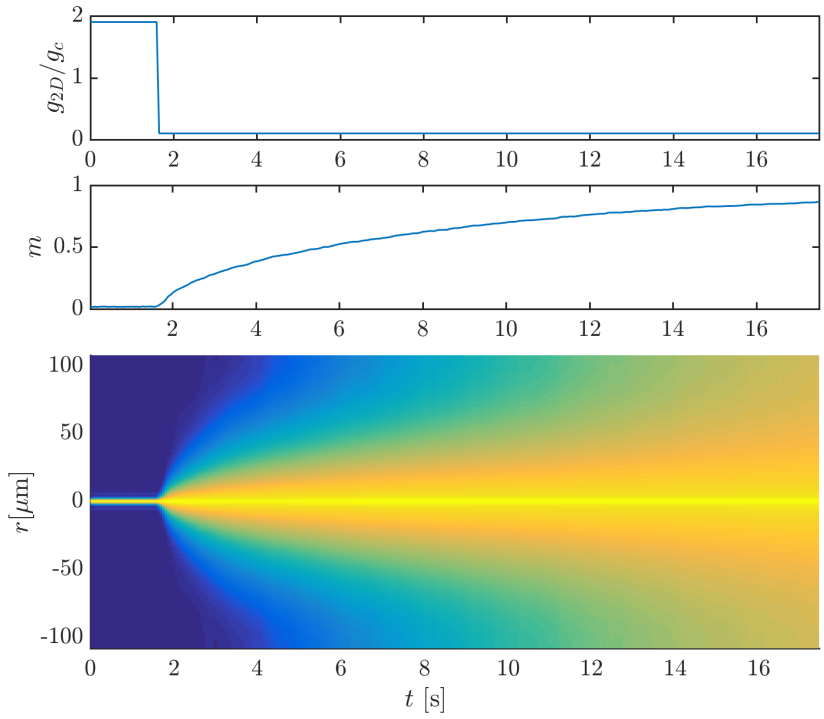


(a)

Figure 4.21: (top) Control parameter $g_{2D}/g_c$. (middle) Growth of the order parameter $m$ (eq. (3.50)). (bottom) Growth of the modulus of the first-order correlation function (4.53) after an instantaneous quench.

(4.41), which sets the critical condition for the Berezinskii-Kosterlitz-Thouless phase transition. Keeping $T$ and $\mu$ fixed, it is still possible to sample the critical region by varying the coupling constant $g_{2D}$ instead. By inverting equation (4.41), its critical value is given by

$$g_{2D}\left(1-\frac{\log(g_{2D})}{\log(13.2)}\right)\Bigg|_c = \frac{\pi\mu}{k_B T}\frac{1}{\log(13.2)}, \tag{4.67}$$

which is a transcendental equation that can be solved numerically. In doing so, one should note that the theory for the classical field approach as the SPGPE used here is only justified for small values of the interaction parameter $g$, and $T$ and $\mu$ have to be chosen accordingly. We repeated the analysis presented in the previous section on instantaneous quenches performed on the interaction constant $g_{2D}$ from $1.9g_c$ to $0.1g_c$, at fixed (and low) temperature and chemical potential. The resulting analysis are reported in Figures (4.21) to (4.24).

The behaviour of the correlation function is once again compatible with a scaling like in eq (4.60), and both the vortex density and the correlation lengths resemble the ones obtained for the temperature quench. In particular, the exponents for the growth of $\zeta$ are again compatible within themselves, and are similar to the ones of the previous

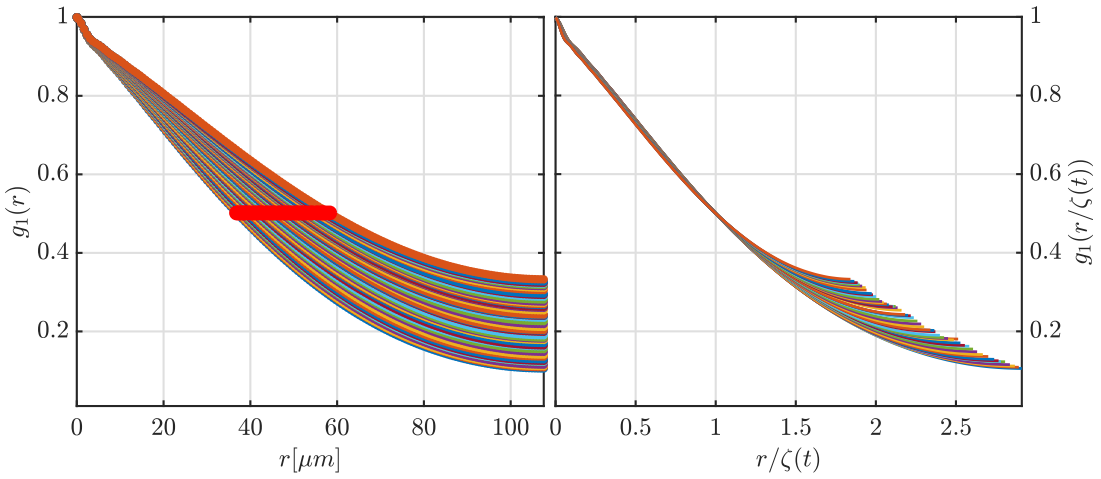


Figure 4.22: (left) Time evolution of the first-order correlation function $g_1(r)$ during an instantaneous quench of $g_{2D}$ across the BKT critical point $g_c$. (right) Correlation function, rescaled according to a function $f(r/\zeta(t))$ as in (4.60). The definition of $\zeta(t)$ is chosen so that, at any $t$, $g_1(\zeta(t), t) = 0.5$. The parameters for this simulation are $\omega_{\text{ref}} = 2\pi 5$ Hz, $\mu = 10\hbar\omega_{\text{ref}}$, $T = 5$nK, $\gamma = 0.01$, $L = 216\mu$m.

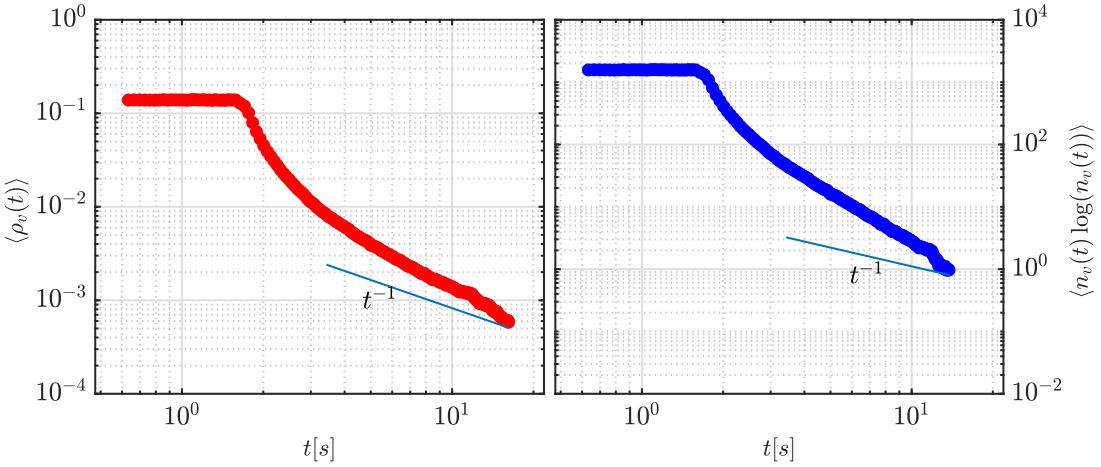


Figure 4.23: (left) Time evolution of the density of defects $\rho_v(t) = n_v(t)/L^2$. (right) Decay of $n_v(t)\log(n_v(t))$ as a function of time. The parameters are the same as in Fig. (4.22).

case, although still far from the predicted values $z = 2$.

Understanding the deviation of the exponents from the theoretical value for the two-dimensional phase transition is the main goal of the future research we intend to carry out in this area.

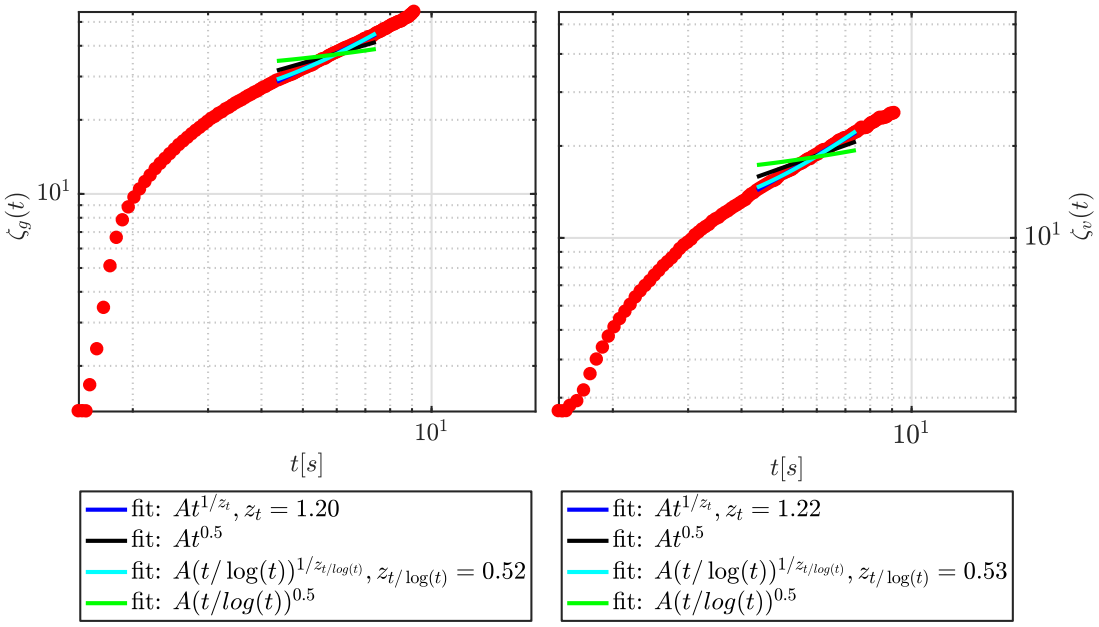


Figure 4.24: (left) Correlation length $\zeta_g(t)$ extracted from the growth of the first-order correlation function $g_1(r)$, reported in Fig. (4.22). The definition of $\zeta_g(t)$ corresponds to the scaling factor for the spatial coordinate $r$, given an intersection of 0.5. (right) Correlation length $\zeta_v(t)$ extracted from the decay of the density of vortices $\rho_v(t)$. The difference between the two is given by the different values for the non-universal constants $t_0$ and $\lambda(T)$, due to the different measuring procedure. On both figures several fitted scalings are plotted (see text).

## 4.4 Chapter conclusions and future outlook

In this chapter we addressed the specificity of the two-dimensional configuration for an atomic Bose gas. At first we reviewed the phase transition occurring in such a system, the Berezinskii-Kosterlitz-Thouless transition. We detailed the derivation of the most important features, such as the establishment of a quasi long-range ordering leading to an algebraic decay of the first-order correlation function, and the role of the vortices in characterising the superfluid transition.

We briefly reviewed the main aspects of the Kibble-Zurek mechanism, responsible for the formation of defects in a three-dimensional system rapidly quenched across a continuous phase transition.

Subsequently, we showed the results for the numerical analysis performed on uniform two-dimensional systems with periodic boundary conditions. At first we concentrated on the equilibrium results. We computed the equilibrium first-order correlation function, at different values of temperature. We then fitted their profile with an algebraic and an exponential law, and we measured the position of the crossover between the two decays. In the BKT framework, this should represent the critical point of the

transition. We measured a shift in its value with respect to the predicted one given by eq. (4.41). We then computed the order parameter as a function of the temperature, and we compared it with the square root of the edge value of the correlation function. We found that they are identical in a broad region of temperatures, as expected from the definition of $m$, and they only show a small deviation in the region of the crossover. Moreover, these quantities seem to confirm the shift in the critical point. This topic is still under investigation, and can be related to the shift in the speed of sound minimum in Chapter (5). Furthermore, the decay region of $m$ and $g_1(L/2)$ was found to be quite large. In [74] a similar behaviour was measured for $m$ when decreasing the system size. We therefore postulated that this could be related to finite size effects. In order to address the issue, we plan to perform the same simulations with different system extensions, and to compute the temperature dependence of the order parameter. In the same paper, the critical temperature for the transition is computed by comparing, for different box size, the first- and the second-order correlation functions, and by producing the so-called *Binder ratio* as in Fig. (4.9a). We plan to perform a similar analysis to precisely characterise the transition. Another issue on the critical point is related to the exact determination of the quantities entering (4.41), and how well the system responds to the input control parameters $T$ and $\mu$.

We are able to count the number of vortices by means of a numerical routine identifying the distribution of the circulation of the phase. We measured an equilibrium value for the vortex density and for the associated correlation length as a function of the temperature. The uncertainty in the determination of the critical temperature for our parameters outlined above also plays a role in the characterisation of the divergence of the correlation length at the transition.

In Section 4.3.2 we reported the results of an instantaneous quench through the phase transition. The quench is performed in both control parameters $T$ and $\mu$, realising a rapid growth of the atoms in the *c-field* and a rapid decay of the number of vortices. For this system, we computed the first-order correlation function defined in equation (4.53). We analysed the dynamical scaling of $g_1(r)$ towards the equilibration, by rescaling the time-dependent profiles by means of a scaling function as in equation (4.60). This allowed us to extract a correlation length $\zeta_g$ associated with the correlation function, which was compared with the one ($\zeta_v$) associated with the time-dependent vortex density. The same procedure can be applied to a slightly different setup. To avoid the issues connected to changing *two* control parameters at the same time, we performed a quench of the coupling constant $g$ across a critical value set by equation (4.41). We performed the same analysis as in the temperature quench, again obtaining two relations for the correlation lengths associated to $g_1(r)$ and to the vortices. An-

other important quantity that we plan to investigate in the future is the growth of the quasi-condensate and link it to the growth of the Penrose-Onsager condensate, as done in Cockburn *et al.*[106].

On the two correlation lengths, one could fit several relations for the dynamical scaling. We found that the predicted logarithmic correction (4.61) produced a critical exponent which is not compatible with the theoretical prediction for the *F-model*, $z_{\mathrm{th}} = 2$, both for the temperature quench as well as for the interaction quench. The values of the critical exponents, however not adherent to the predictions, show a certain degree of internal consistency. In the literature, several values for $z$ are proposed and confirmed for different systems. A recent work on the Kibble-Zurek dynamical scaling for a system in reduced dimensions has been carried out in [107], also showing a significant deviation of the critical exponent from the mean-field prediction (although, in that case, the critical exponent has been found to be *larger* than the theoretical one). For the spin-1 ferromagnetic transition, in certain regimes the value $z = 1$ is predicted by the *model E*[108]. In polariton condensates, it has been recently proposed[109] that the critical exponent can assume value 1 or 2 depending on the physical parameters imposed. Addressing the disagreement between the theoretical and the numerical critical exponent in our simulations will be the core of the future work related to this project.

In Section 4.3.4 we briefly addressed the problem of ramping the control parameters in a finite time interval. We sketched an analysis on the density of defects following different ramps and checked that the predicted scaling including the logarithmic correction can be recovered. Further analysis on that would require to perform a similar analysis on the interaction quenched system, so to better control the definition of the critical point for the transition. Moreover, a crucial point concerns the determination of the *freezing time* $\hat{t}$ entering eq. (4.65), which can be computed as in [102] by comparing the equilibrium correlation length as a function of the control parameter with the one dynamically obtained from the quench system. In the instant for which these two quantities deviate from each other, one can assume that the system is no longer able to adiabatically follow the external control parameter, which provides an operational definition of $\hat{t}$.

[106] S. P. Cockburn et al. In: *Phys. Rev. A* 83 (2011), p. 043619.
[107] R. G. McDonald and A. S. Bradley. In: *Phys. Rev. A* 92 (2015), p. 033616.
[108] L. A. Williamson and P. B. Blakie. In: *Phys. Rev. Lett.* 116 (2016), p. 025301.
[109] Michał Kulczykowski and Michał Matuszewski. In: *Phys. Rev. B* 95 (2017), p. 075306.

# Chapter 5

# Soliton and sound dynamics in two-dimensional Bose-Einstein condensates at finite temperature

In this chapter we will present the results concerning the simulations of two different sets of experiments. The first was performed at the University of Birmingham, by the group of Prof. Kai Bongs, and concerned the generation and the subsequent decay of a soliton, imprinted in an elongated quasi-2D condensate, at various temperatures. The second concerned the measurement of the speed of sound in a uniform two-dimensional Bose gas confined in a box trap, over a temperature range spanning a wide region across the critical point. This experiment has been performed at the Laboratoire Kastler-Brossel at the Collège de France in Paris, under the direction of prof. Jean Dalibard. The results of this analysis have been included in [110], which has been simultaneously submitted with [111] and is currently under review.

## 5.1 Soliton decay in a finite temperature quasi-2D BEC

As presented in Chapter 1, solitons are a nonlinear class of solutions of the one-dimensional Gross-Pitaevskii equation. In two or three dimensions, solitons are known to undergo the so-called *snaking* instability. Kuznetsov and Turitsyn[112] first studied this instability, showing that the dark solitons are prone to transverse modulational instability: for transverse perturbations with long wavelength, the amplitude of a recti-

[110] M. Ota et al. In: *ArXiv e-prints* (2018). arXiv: 1804.04032 [cond-mat.quant-gas].

[111] J. L. Ville et al. In: *ArXiv e-prints* (2018). arXiv: 1804.04037 [cond-mat.quant-gas].

[112] E. A. Kuznetsov and Turitsyn S. K. In: *JETP* 67.8 (1988). (original Rus.) Zh. Eksp. Teor. Fiz. 94 (1988) p. 119.

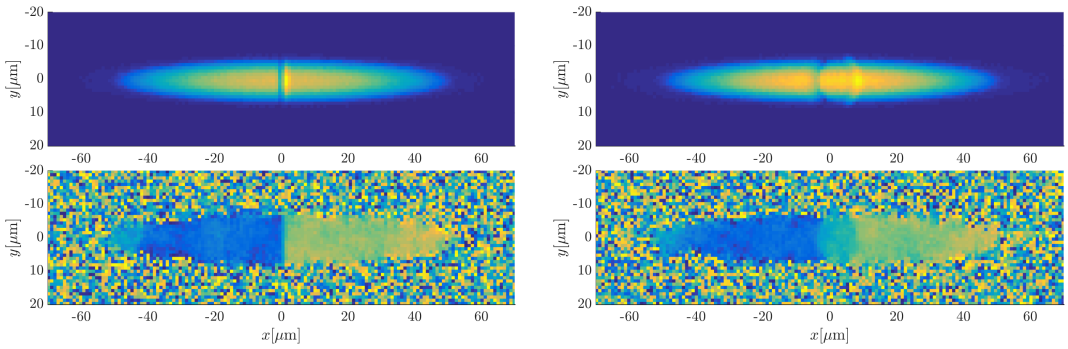


(a) (b)

Figure 5.1: (a) Presence of a solitonic defect a short time interval $\Delta t = 0.6$ms after the phase jump is imprinted in the system at $T = 17$nK. (above) Density profile averaged over $\mathcal{N} = 100$ stochastic realisations. (below) Phase of a single noise realisation. (b) Bending of the soliton line due to the spatial inhomogeneities of the trapped system after $\Delta t \simeq 6$ms. (above) Density profile averaged over $\mathcal{N} = 100$ stochastic realisations. (below) Phase of a single noise realisation.

linear (or planar) soliton will grow exponentially in the transverse direction. The decay process results[113] in the creation of topologically protected defects such as vortex-antivortex pairs (in 2D) or vortex rings (in 3D). A stabilisation of the defect and an increase of its lifetime can be achieved by confining the system in a narrow channel. Unstable grey solitons, hence defects with velocity $v > 0$ and whose density depletion is not complete, may not decay into vortices, dispersing instead in a finite time by the emission of phonons.

An experiment at the University of Birmingham, in the group of Prof. Kai Bongs, wanted to address the possibility that the thermal excitations naturally present in a system with finite temperature might have an effect on the lifetime of a grey soliton in a quasi-2D geometry. This prompted the work presented in the following section, in which we simulate the phase imprinting of a solitonic defect and its successive decay, by means of the stochastic Gross-Pitaevskii equation addressed in Chapter 3. The parameters for the system are set to match the experimental ones, and are

$$\omega_x = 2\pi(5\text{Hz}) \quad \omega_y = 2\pi(40\text{Hz}) \quad \omega_\perp = 2\pi(250\text{Hz}) \tag{5.1}$$

for the trapping frequencies, and

$$\begin{aligned} \mu &= 63\hbar\omega_x, \quad N \simeq 41500, \quad T = 17\text{nK}, \quad T/T_c^0 = 0.15 \\ \mu &= 59\hbar\omega_x, \quad N \simeq 45000, \quad T = 50\text{nK}, \quad T/T_c^0 = 0.41. \end{aligned} \tag{5.2}$$

[113] P.G. Kevrekidis, D.J. Frantzeskakis, and R. Carretero-González. *The Defocusing Nonlinear Schrödinger Equation: From Dark Solitons to Vortices and Vortex Rings*. SIAM, 2015.

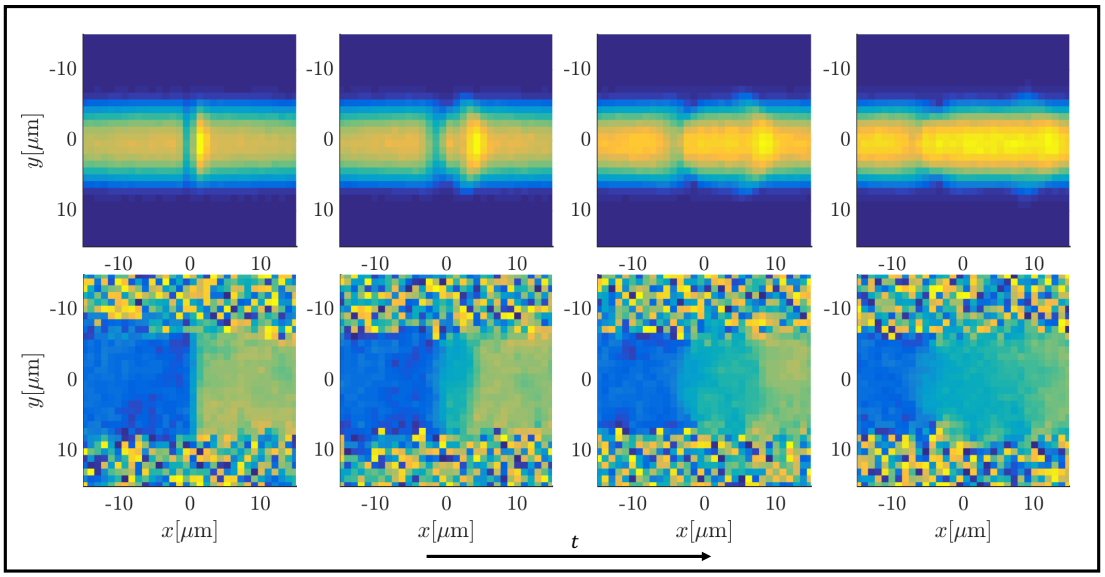


Figure 5.2: Zoomed density (above) and phase (below) evolution after the imprinting of the phase step. During its propagation, the soliton will bend due to the density inhomogeneity. The frames are taken respectively at $\Delta t = [0.6, 3.12, 6.27, 9.11]$ms after the perturbation is imposed.

where $T_c^0$ is the critical temperature for the ideal gas in a 2D harmonic trap[84]:

$$k_{\mathrm{B}} T_c^0 = \hbar \sqrt{6\omega_x \omega_y \frac{N}{\pi^2}}. \tag{5.3}$$

Once the sample is grown to thermal equilibrium, a phase jump of $\Delta\varphi = \pi$ is imprinted along the $x$ direction, centred in the origin. This is achieved by multiplying the wavefunction by a hyperbolic factor

$$\psi_{\Delta\varphi}(\mathbf{r}) = e^{i\Delta\varphi(1+\tanh(x/\xi))/2}\psi(\mathbf{r}), \tag{5.4}$$

where $\xi$ is the healing length. This causes the system to develop a density defect in the centre, which will move with a velocity set by its depth. In its motion, it will eventually bend due to the inhomogeneous spatial profile of the system in the trap (Figures (5.1) and (5.2)).

The decay of the soliton is then characterised in terms of the normalised depth

$$\Delta n = n_{\mathrm{sol}}/n_0, \tag{5.5}$$

where $n_{\mathrm{sol}}$ marks the density depletion in the soliton core, while $n_0$ is the equilibrium

[84] C. J. Pethick and H. Smith. *Bose–Einstein Condensation in Dilute Gases*. 2nd ed. Cambridge University Press, 2008.

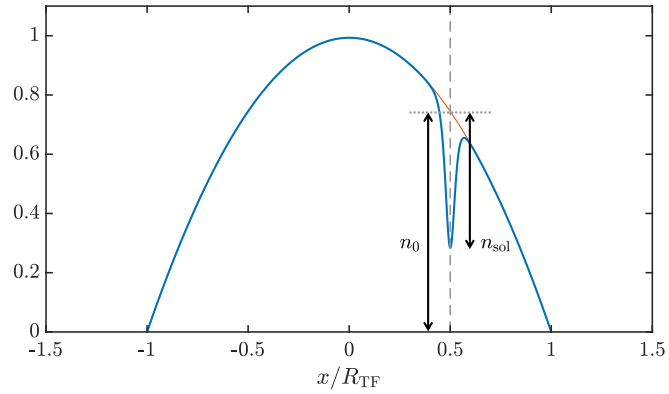


Figure 5.3: Schematic definition of the normalised depth $\Delta n = n_{\rm sol}/n_0$.

density in the absence of a defect (see Fig. (5.3)). The depth of the defect $n_{\rm sol}$ is measured by subtraction in the central region of the atomic cloud, by comparing the unperturbed density with the one in the presence of the soliton. At first, for each stochastic realisation, we integrate the density profile over a very narrow region in the central part of the trap in the $y$ direction, to increase the visibility of the defect. We then produce the unperturbed result by averaging the density profile over all the random samples and by further performing a short time-average over several equilibrium time steps. We subtract the first quantity from the second, obtaining samples of density difference as in Fig. (5.4b).

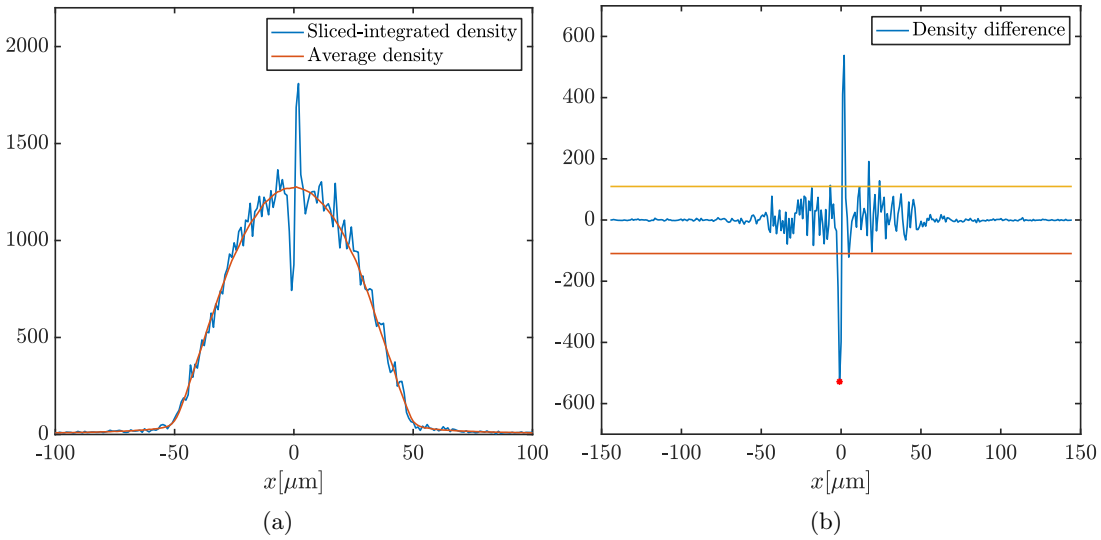


Figure 5.4: (a) Slice-integrated density of a single noise realisation (see text) and corresponding integrated average density. (b) Difference between the sliced-integrated density and the average density. The red point marks the minimum as recognised by the tracking routine, while the coloured lines indicate the standard deviation of the background noise.

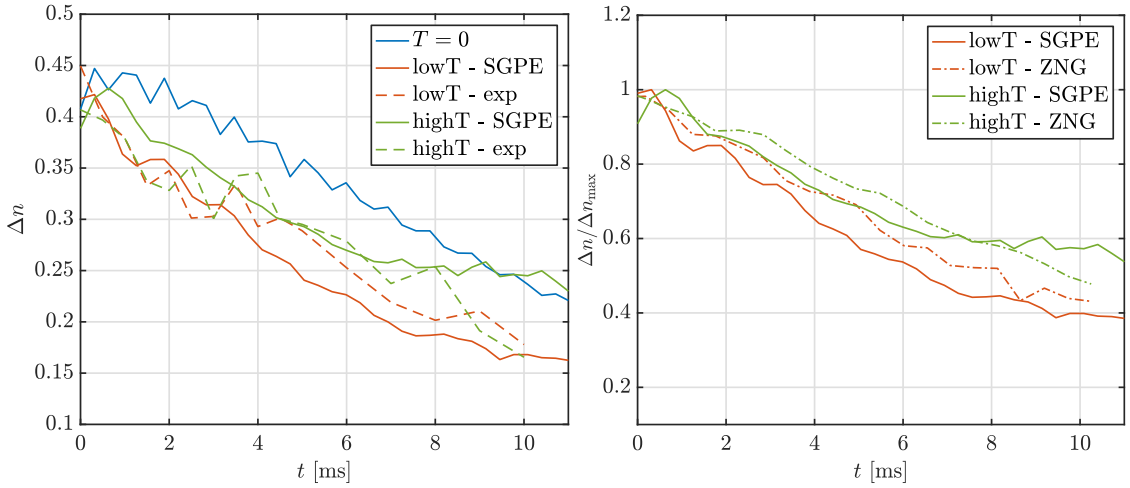


Figure 5.5: (a) Decay of the normalised depth of the soliton, as a function of time. The solid lines report the numerical results from the GPE ($T = 0$) and the SGPE simulations (lowT, highT), while the dashed lines represent the experimental data from Birmingham [Courtesy of Giovanni Barontini, *unpublished*]. (b) Numerical results for the simulations performed with SGPE and with ZNG method [Courtesy of Kean Loon Lee, *unpublished*]. The normalised depth is rescaled by its maximum value for better comparison.

We identify the presence of the soliton with the minimum of the density difference, when this exceeds twice the standard deviation of the background noise. Otherwise, the defect is considered to be completely decayed. The resulting decay of the soliton depth as a function of time is reported in Fig. (5.5a), where we also add the resulting behaviour for a $T = 0$ simulation performed by solving the Gross-Pitaevskii equation (1.14).

They appear to show a remarkable qualitative agreement with the experimental data also plotted in the same figure, even though a closer quantitative comparison would require a higher resolution. We also report the results of numerical simulations with the same physical parameters, performed by Kean-Loon Lee using the Zaremba-Nikuni-Griffin (ZNG) method[114]. This is a self-consistent treatment describing the coupled dynamics of the condensate, by means of a dissipative Gross-Pitaevskii equation, and the thermal cloud, through a quantum Boltzmann equation. The data obtained with the SGPE and with the ZNG approach also show a good qualitative agreement (Fig. (5.5b)). We perform an exponential fit on the data of the kind

$$\Delta n(t) = A(T)e^{-t/\tau(T)}, \tag{5.6}$$

[114] E. Zaremba, T. Nikuni, and A. Griffin. In: *J. Low Temp. Phys.* 116.3-4 (1999), pp. 277–345.

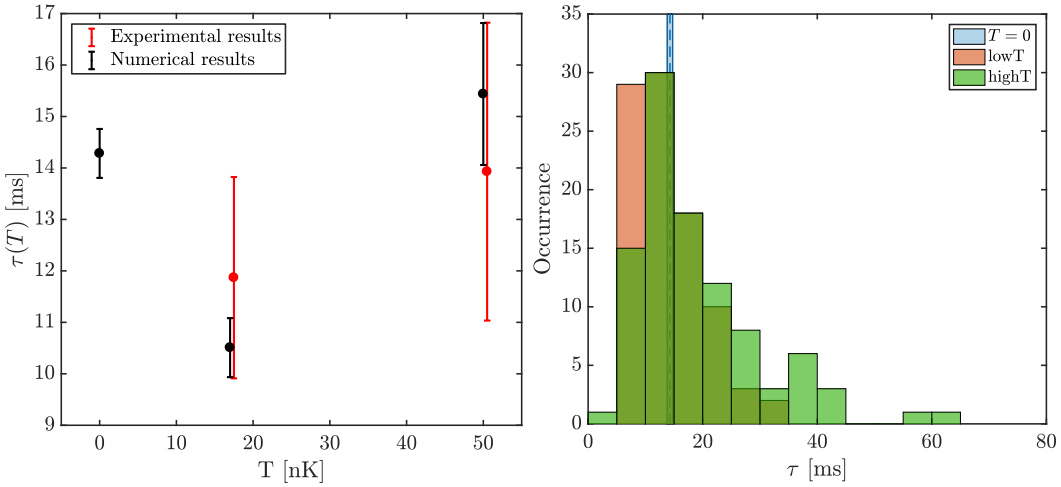


Figure 5.6: (a) Resulting lifetime extracted from a fit of the normalised depth according to equation (5.6). The resulting numerical values for the SGPE approach (in black) are qualitatively compatible with the experimental ones (in red) within the errorbars. The latter are slightly shifted in temperature to better display the errorbars. (b) Distribution of the occurrences of the fitted lifetime $\tau(T)$. The effect of the temperature is a slight widening of the distribution corresponding to the highest case.

to extract the lifetime as a function of the temperature $\tau(T)$. The result is plotted in Fig. (5.6), and again the SGPE simulations are compatible with the experiments within the error bars. Finally, we include the distribution of the occurrences of $\tau$ for the two different temperature cases, showing a wider distribution for the higher temperature case.

The analysis reported above shows that there is a rather good agreement between the numerical simulations and the experimental data. The results give a qualitative indication that the main mechanism for the dispersion of a grey soliton in an inhomogeneous atomic sample is scarcely influenced by the temperature, and that it is likely to be connected with the geometry of the system. However, the situation might be different in different systems, such as a purely two-dimensional sample, where the defect is confined in a narrow channel and bounces on the rigid walls of a box trap.

## 5.2 Sound propagation in a thermal uniform 2D Bose gas

In this section we will present the simulations concerning the experiment performed at the Collège de France, on the measurement of the speed of sound in a finite temperature uniform 2D BEC. We will first introduce some of the theoretical background related to the subject, and then show the numerical results with a comparison to the experimental data.

### 5.2.1 Theoretical background: hydrodynamic sound

The topic of the speed of sound at the Berezinskii-Kosterlitz-Thouless phase transition, in a configuration at which the collisions are strong enough to sustain a hydrodynamic regime, has been addressed in a paper by Ozawa and Stringari[115]. Therein, the temperature dependence of the first and the second sound velocities has been computed by solving Landau's equations for the two-fluid model. We will now introduce the relevant relations following the treatment given in the book by Pitaevskii and Stringari[26], which is independent from the dimensionality.

The hydrodynamic equations for a finite temperature sample are identical in form to the ones for the zero-temperature case, equations (1.51) and (1.52). If we only concentrate on the small-amplitude oscillations in a uniform system, we can neglect the $v^2$ term and rewrite equation (1.52) for the superfluid velocity as

$$m\frac{\partial \mathbf{v}_s}{\partial t} + \boldsymbol{\nabla}\mu = 0, \tag{5.7}$$

where one can no longer consider the zero temperature relation $\mu = gn$ to hold, but should also include a temperature dependence in the chemical potential. The equation for the density is the usual continuity equation

$$\frac{\partial n}{\partial t} + \boldsymbol{\nabla}\cdot\mathbf{j} = 0, \tag{5.8}$$

where, according to the two-fluid picture, one can separate the current into the normal and the superfluid component

$$\mathbf{j} = n_s\mathbf{v}_s + n_n\mathbf{v}_n. \tag{5.9}$$

When no external fields are present, the time derivative of the momentum density $m\mathbf{j}$ is the force per unit volume, which can be approximated by the gradient of the pressure

[115] T. Ozawa and S. Stringari. In: *Phys. Rev. Lett.* 112 (2014), p. 025302.

[26] L. Pitaevskii and S. Stringari. *Bose-Einstein Condensation and Superfluidity.* Oxford University Press, 2016.

$P$, then

$$m\frac{\partial \mathbf{j}}{\partial t} + \boldsymbol{\nabla} P = 0. \tag{5.10}$$

One can finally derive an equation for the entropy per unit volume, $s$. If all dissipation processes are absent in the system, the entropy is conserved, and one can associate a continuity equation to it. The entropy is however only transported by the normal part of the fluid, hence

$$\frac{\partial s}{\partial t} + \boldsymbol{\nabla} \cdot (s\mathbf{v}_n) = 0. \tag{5.11}$$

Equations (5.8) and (5.10) can be combined to eliminate $\mathbf{j}$ and get an equation relating the time and the space variations of the density and of the pressure:

$$m\frac{\partial^2 n}{\partial t^2} = \nabla^2 P. \tag{5.12}$$

Now we need another equation, relating the time and space variations of the temperature and of the entropy. If one rewrites equation (5.11) in terms of the entropy per unit mass, $\tilde{s} = s/(mn)$:

$$m\left(\frac{\partial \tilde{s}}{\partial t}\right) n + m\tilde{s}\left(\frac{\partial n}{\partial t}\right) + m\tilde{s}n\boldsymbol{\nabla} \cdot \mathbf{v}_n = 0, \tag{5.13}$$

by means of eq. (5.10) one can further write

$$\frac{\partial \tilde{s}}{\partial t} + \tilde{s}\frac{n_s}{n}\boldsymbol{\nabla} \cdot (\mathbf{v}_n - \mathbf{v}_s). \tag{5.14}$$

The Gibbs-Duhem equation connects some of the intensive thermodynamic quantities we are studying:

$$n\boldsymbol{\nabla}\mu = -s\boldsymbol{\nabla}T + \boldsymbol{\nabla}P. \tag{5.15}$$

Then, by means of eq. (5.15), one can rewrite eq. (5.10) as

$$m\frac{\partial}{\partial t}(n_s\mathbf{v}_s + n_n\mathbf{v}_n) + (n_s + n_n)\boldsymbol{\nabla}\mu + m\tilde{s}n\boldsymbol{\nabla}T. \tag{5.16}$$

Now, eq. (5.7) allows us to eliminate the chemical potential $\mu$ and get

$$n_n\frac{\partial}{\partial t}(\mathbf{v}_n - \mathbf{v}_s) + n\tilde{s}\boldsymbol{\nabla}T = 0. \tag{5.17}$$

Combining equations (5.14) and (5.17), in the linear regime, we get the equation we were searching for:

$$\frac{\partial^2 \tilde{s}}{\partial t^2} = \tilde{s}^2\frac{n_s}{n}\nabla^2 T. \tag{5.18}$$

The two equations (5.12) and (5.18) provide coupled equations for the pressure and the

temperature. Indeed, let us search for plane-wave solutions of the kind

$$\begin{aligned} P = P_0 e^{-i\omega(t-x/c)} \rightarrow \nabla^2 P = -\frac{\omega^2}{c^2} P, \quad \frac{\partial^2 P}{\partial t^2} = -\omega^2 P; \\ T = T_0 e^{-i\omega(t-x/c)} \rightarrow \nabla^2 T = -\frac{\omega^2}{c^2} T, \quad \frac{\partial^2 T}{\partial t^2} = -\omega^2 T. \end{aligned} \tag{5.19}$$

Then, given that the two thermodynamic coordinates under consideration are $T$ and $P$, the two relations for the differential hold

$$dn = \left.\frac{\partial n}{\partial P}\right|_T dP + \left.\frac{\partial n}{\partial T}\right|_P dT, \tag{5.20}$$

$$d\tilde{s} = \left.\frac{\partial \tilde{s}}{\partial P}\right|_T dP + \left.\frac{\partial \tilde{s}}{\partial T}\right|_P dT. \tag{5.21}$$

The relations (5.21) allow us to expand the derivatives $\partial^2 n/\partial t^2$ and $\partial^2 \tilde{s}/\partial t^2$, and by substituting (5.19) and only retaining the real part of the resulting equations, one obtains the system of equations

$$\begin{cases} \left(\frac{1}{c^2} - m\frac{\partial n}{\partial P}\right) P & = m\frac{\partial n}{\partial T} T \\ \left(\frac{n_s}{n_n}\frac{\tilde{s}^2}{c^2} - \frac{\partial \tilde{s}}{\partial T}\right) T & = \frac{\partial \tilde{s}}{\partial P} P \end{cases} \tag{5.22}$$

By substitution, one gets to the following relation for the velocity of sound

$$m\left(\frac{\partial \tilde{s}}{\partial T}\frac{\partial n}{\partial P} - \frac{\partial \tilde{s}}{\partial P}\frac{\partial n}{\partial T}\right) c^4 - \left(\frac{\partial \tilde{s}}{\partial T} + m\tilde{s}^2\frac{n_s}{n_n}\frac{\partial n}{\partial P}\right) c^2 + \tilde{s}^2\frac{n_s}{n_n} = 0 \tag{5.23}$$

In his original paper[11] about the two-fluid model for Helium-II, Landau showed that it is possible to rewrite this equation by means of thermodynamic relations, in a more convenient form

$$\boxed{c^4 - \left(\frac{1}{m}\left.\frac{\partial P}{\partial n}\right|_{\tilde{s}} + \frac{n_s T \tilde{s}^2}{n_n \tilde{C}_v}\right) c^2 + \frac{n_s T \tilde{s}^2}{n_n \tilde{C}_v m}\left.\frac{\partial P}{\partial n}\right|_T = 0}, \tag{5.24}$$

where we introduced the specific heat at constant volume per unit mass

$$\tilde{C}_v = T\left.\frac{\partial \tilde{s}}{\partial T}\right|_n. \tag{5.25}$$

One can immediately see that, whenever $n_s \neq 0$, equation (5.24) gives rise to two different sound velocities. These are associated with the two degrees of freedom given

[11] L. D. Landau. In: *Phys. Rev.* 60 (1941), pp. 356–358. (original Rus.) Zh. Eksp. Teor. Fiz. 11 (1941) p. 592.

by the presence of the normal and of the superfluid component. An easy solution is found in the limit of $T \to T_c$ where the superfluid density can be neglected. The larger velocity is in this case

$$c_{10}^2 = \frac{1}{m}\frac{\partial P}{\partial n}\bigg|_{\tilde{s}} \equiv \frac{1}{mn\kappa_s}, \tag{5.26}$$

where

$$\kappa_s = \frac{1}{n}\frac{\partial n}{\partial P}\bigg|_{\tilde{s}} \tag{5.27}$$

is the isoentropic (adiabatic) compressibility. By neglecting the $c^4$ term in equation (5.24), and in the same regime $n_s \to 0$, one gets the smaller solution

$$c_{20}^2 = \frac{T}{m}\frac{\tilde{s}^2 n_s}{\tilde{C}_p n_n}, \tag{5.28}$$

where $\tilde{C}_v = T(\partial\tilde{s}/\partial T)|_P$ is the specific heat at constant pressure. The quantity $c_{10}$ is associated with isoentropic oscillations in the system, while $c_{20}$ with isobaric oscillations.

For systems with a small thermal expansion coefficient $\alpha = -(\partial n/\partial T)|_P/n = T^{-1}(\tilde{C}_p/\tilde{C}_v - 1)$, showing therefore almost identical isothermal and adiabatic compressibility, as in superfluid Helium or 3D Fermi gases at unitarity, the two solutions (5.26) and (5.28) represent an accurate estimation of the two sound speeds. In particular, the first sound is related to the in-phase oscillation of the normal and the thermal components, leading to an overall total density fluctuation. The second sound is conversely connected to the propagation of entropy perturbations, while the two components oscillate out of phase, leaving the total density unperturbed.

However, this is not the case for dilute Bose gases, where $\alpha$ is indeed quite large. One can instead develop an alternative approach by considering that for temperatures $k_{\mathrm{B}}T \gg \mu = gn$ the thermodynamic functions of the weakly interacting Bose gas, apart from the isothermal compressibility, are not very sensitive to the interactions. Therefore, it is possible to use the ideal Bose gas model, which gives the following result

$$\frac{1}{m}\frac{\partial P}{\partial n}\bigg|_{\tilde{s}} + \frac{n_s T\tilde{s}^2}{n_n\tilde{C}_v} = \frac{nT\tilde{s}^2}{n_n\tilde{C}_v} \tag{5.29}$$

for the coefficient of the $c^2$ term in eq. (5.24). Then one can compute the second sound speed by discarding the larger term $c^4$, and get

$$c_2^2 = \frac{n_s}{nm}\frac{\partial P}{\partial n}\bigg|_T = \frac{n_s}{n}\frac{1}{nm\kappa_T}. \tag{5.30}$$

In 3D one can safely replace the superfluid density $n_s$ by the condensate density. In

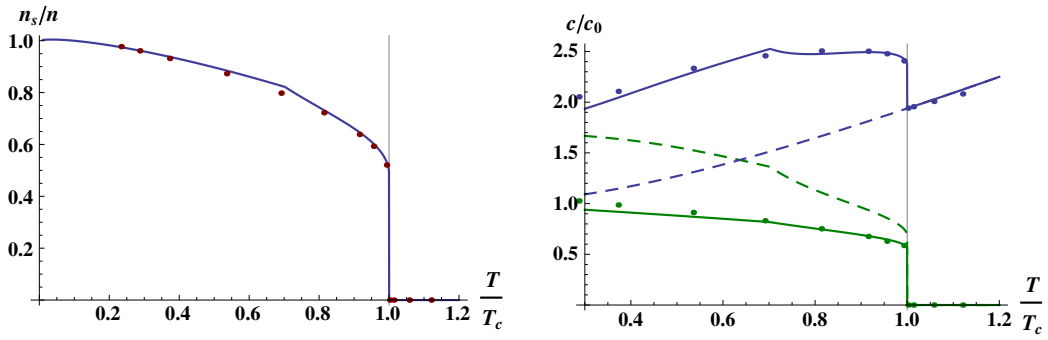


(a) (b)

Figure 5.7: [Figure from [115]] (a) Relative superfluid density for $g = 0.1$. The line is calculated for the two approximated analytical expressions from [87], for high and low temperatures, resulting in an unphysical kink at $T/T_c \sim 0.7$. The dots are calculated from the numerical data from [87]. (b) Velocities of first (blue solid line) and second (green solid line) sound as computed by solving equation (5.24), rescaled by the zero temperature Bogoliubov sound velocity $c_0 = \sqrt{gn/m}$. The dashed lines correspond to $c_{10}$ and $c_{20}$ defined in equations (5.26) and (5.28). The dots correspond again to numerical values extracted from the results in [87].

two dimensions, relation (5.30) still describes the behaviour of the second sound, in the limit of small interactions. The first sound velocity is solved by means of the equation (5.24). In searching for large sound speed, one can neglect the last term and obtain

$$\begin{aligned} c_1^2 &= \frac{1}{mn\kappa_s} + \left(\frac{T}{m}\frac{\tilde{s}^2}{\tilde{C}_p}\frac{n_s}{n}\right)\frac{\tilde{C}_p}{\tilde{C}_v} \\ &= c_{10}^2 + c_{20}^2(T\alpha + 1) \\ &\approx c_{10}^2 + c_{20}^2 T\alpha. \end{aligned} \tag{5.31}$$

Prokof'ev and Svistunov[87] gave an approximate analytic equation for the ratio $n_s/n$ below the critical point. Ozawa and Stringari[115] plotted the resulting curves (Fig. (5.7a)) showing a sharp discontinuity at the transition. This discontinuity has an effect on both sound speeds, as can be seen from Fig. (5.7b). The second sound is predicted to show a sudden drop at the transition point, while the first sound should discontinuously reach the value set by $c_{10}$.

### 5.2.2 Experimental setup at the Collège de France

The experimental group at the Laboratoire Kastler-Brossel at the Collège de France is able to realise a two-dimensional configuration for a $^{87}$Rb gas by means of an "optical

[87] N. Prokof'ev and B. Svistunov. In: *Phys. Rev. A* 66 (2002), p. 043608.
[115] T. Ozawa and S. Stringari. In: *Phys. Rev. Lett.* 112 (2014), p. 025302.

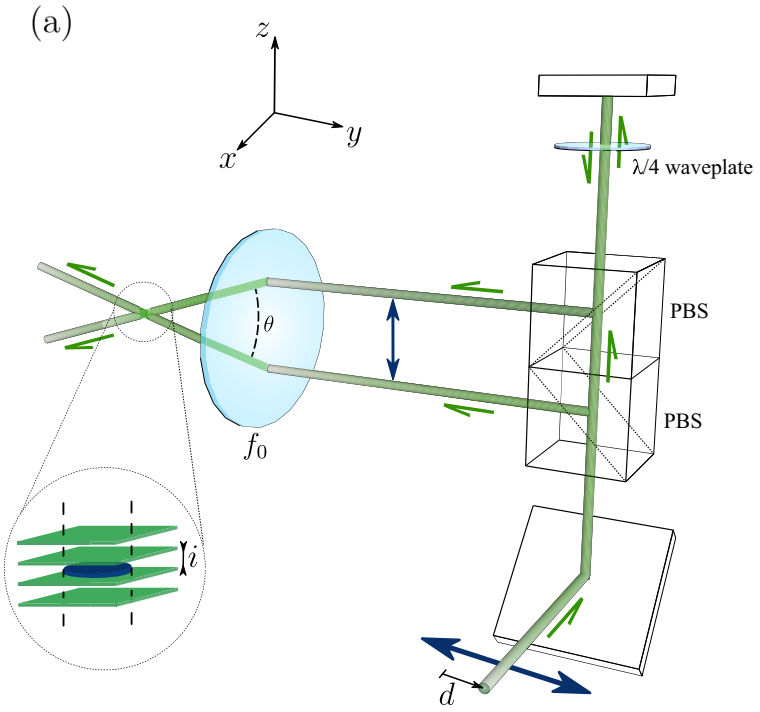


Figure 5.8: [Figure from [116]] Sketch of the setup of the "optical accordion". By moving the initial beam by a distance $d$ it is possible to change the angle between the two final beams, which results in an increased trapping frequency $\omega_z$ along the vertical direction.

accordion"[116]. This mainly consists in realising a one-dimensional optical lattice in the gravity direction $z$, thanks to the focussing of two copies of a single laser beam of wavelength $\lambda = 532$nm. The distance between the interference fringes can be tuned by changing the angle between the two beams, and results in a trapping frequency $\omega_z$ inversely proportional to the spacing itself (see Fig. (5.8)). The atomic cloud can therefore be cooled down in a magneto-optical trap by using standard techniques, obtaining a 3D ultracold gas. This can be compressed in the $z$ direction into a pancake-shaped distribution. The power of the accordion beam can then be increased to trap the atoms in a single node of the optical lattice, and the dipole trap can be turned off. At this point, an adiabatic change in the angle between the accordion beams further compresses the gas, up to the point in which the thermal and the interaction energy are smaller than $\hbar\omega_z$, effectively freezing the motion in the vertical direction, and achieving the two-dimensional regime. The in-plane confinement is implemented by a digital micromirror device (DMD), a spatial light modulator allowing to imprint traps of any shape, without perturbing the flat bottom of the resulting confinement. The cloud can be imaged *in-situ* along the $z$ and the $y$ directions by absorption techniques.

[116] J. L. Ville et al. In: *Phys. Rev. A* 95 (2017), p. 013632.

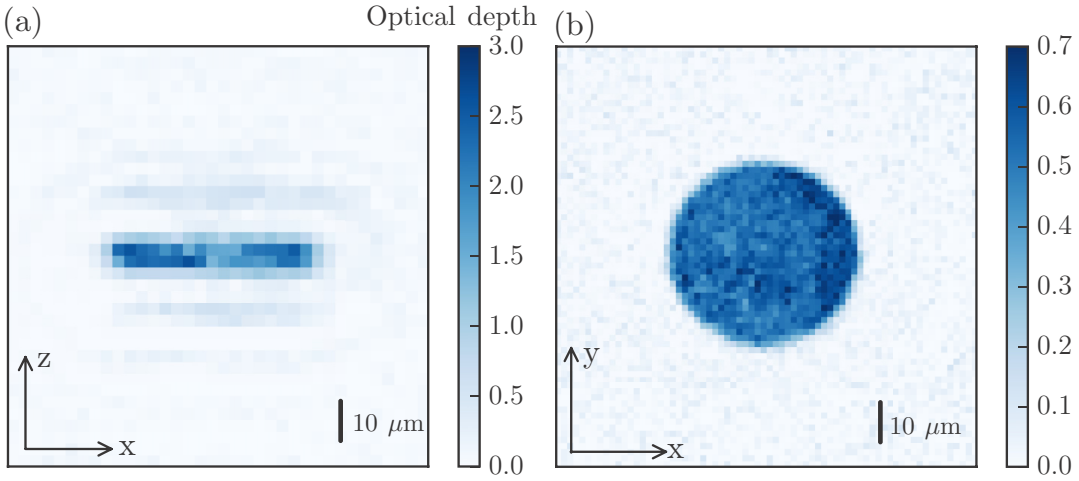


Figure 5.9: [Figure from [116]] *In-situ* absorption images of the trapped atomic cloud at $T = 800$nK, before the compression of the accordion. (a) Side view of the atoms, acquired along the $y$ direction. The fringes are due to the propagation of light through the sample, and do not represent an atomic distribution. (b) Top view for a circular trapping realised by the DMD.

An example of the loaded atomic cloud before compression is provided by Fig. (5.9), where the DMD has been set to imprint a circular trapping.

The temperature of the sample is measured by outcoupling a small fraction of the atoms (small enough to avoid the formation of a condensate) and by comparing its expanded radial profile with the one of an ideal gas, initially Bose-Einstein distributed and uniform in the trap, expanded for the same time. The resulting temperature estimation is given with an uncertainty between 3% and 25%.

### 5.2.3 Measurement of the speed of sound

According to Ozawa and Stringari[115] the first sound is hardly achievable in experiments involving density perturbations as a source. The first difficulty is the necessity to reach the collisional hydrodynamic regime, so that $\omega\tau \ll 1$, where $\omega$ is the frequency of the sound and $\tau$ the typical time interval between the collisions. Given the high frequencies involving the first sound, this regime is difficult to achieve experimentally. Even if this is the case, the authors proved that the second sound contribution dominates the inverse weighted energy moment $\int_{-\infty}^{\infty} S(\mathbf{q},\omega)/\omega$, where $S(\mathbf{q},\omega)$ is the dynamical structure function with momentum $\mathbf{q}$ and frequency $\omega$. This will effectively mean that it is much more favourable to excite the second sound via density perturbations.

[115] T. Ozawa and S. Stringari. In: *Phys. Rev. Lett.* 112 (2014), p. 025302.

### Step potential

The purpose of the experimental measurements, as well as the one of our simulations, is hence to study the propagation of the second sound in a uniform 2D gas in a box, and to investigate the effect of temperature on its speed. We consider a rectangular flat-bottom trap of size $L_x \times L_y = 40 \times 30\mu$m, containing about 33000 atoms. The atomic sample is initially equilibrated into the trap, in the presence of a step potential

$$V(x,y) = \begin{cases} V_{\text{step}} & \text{for } -(L_x/2) < x < -(L_x/2) + \Delta x \\ 0 & \text{otherwise,} \end{cases} \tag{5.32}$$

which increases the bottom of the box in a region of $\Delta x = 10\mu$m in the $x$ direction. The step height is set to be a fraction of the chemical potential $V_{\text{step}} = 0.25\mu$ (Fig. (5.10a)). The effect of the step potential is to induce a density perturbation on the side of the trap (Fig. (5.10b)). Once the system has reached the equilibrium, the coupling with the thermal reservoir is removed by setting $\gamma$ and $\eta$ to zero, and the subsequent time evolution is performed according to the (projected) Gross-Pitaevskii equation. At the same time, the step is suddenly removed, releasing the density perturbation which starts its propagation in the trap. After reaching the other edge of the trap it bounces back, and depending on the dissipation magnitude determined by the temperature, is able to perform several complete oscillations before disappearing (Fig. (5.11)).

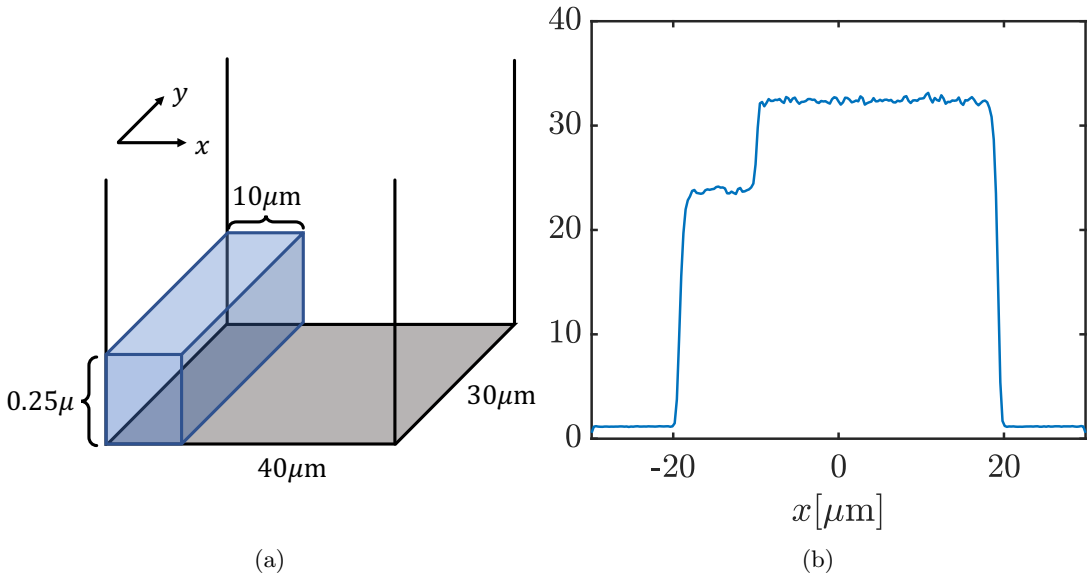


(a) (b)

Figure 5.10: (a) Sketch of the 2D uniform box trap, with the step potential $V_{\text{step}}$ inducing a density depletion in one side of the atomic sample. (b) Average density integrated in the $y$ direction, at equilibrium in the presence of the step potential. The temperature of this simulation is $T \simeq 0.19 T_{\text{BKT}}$.

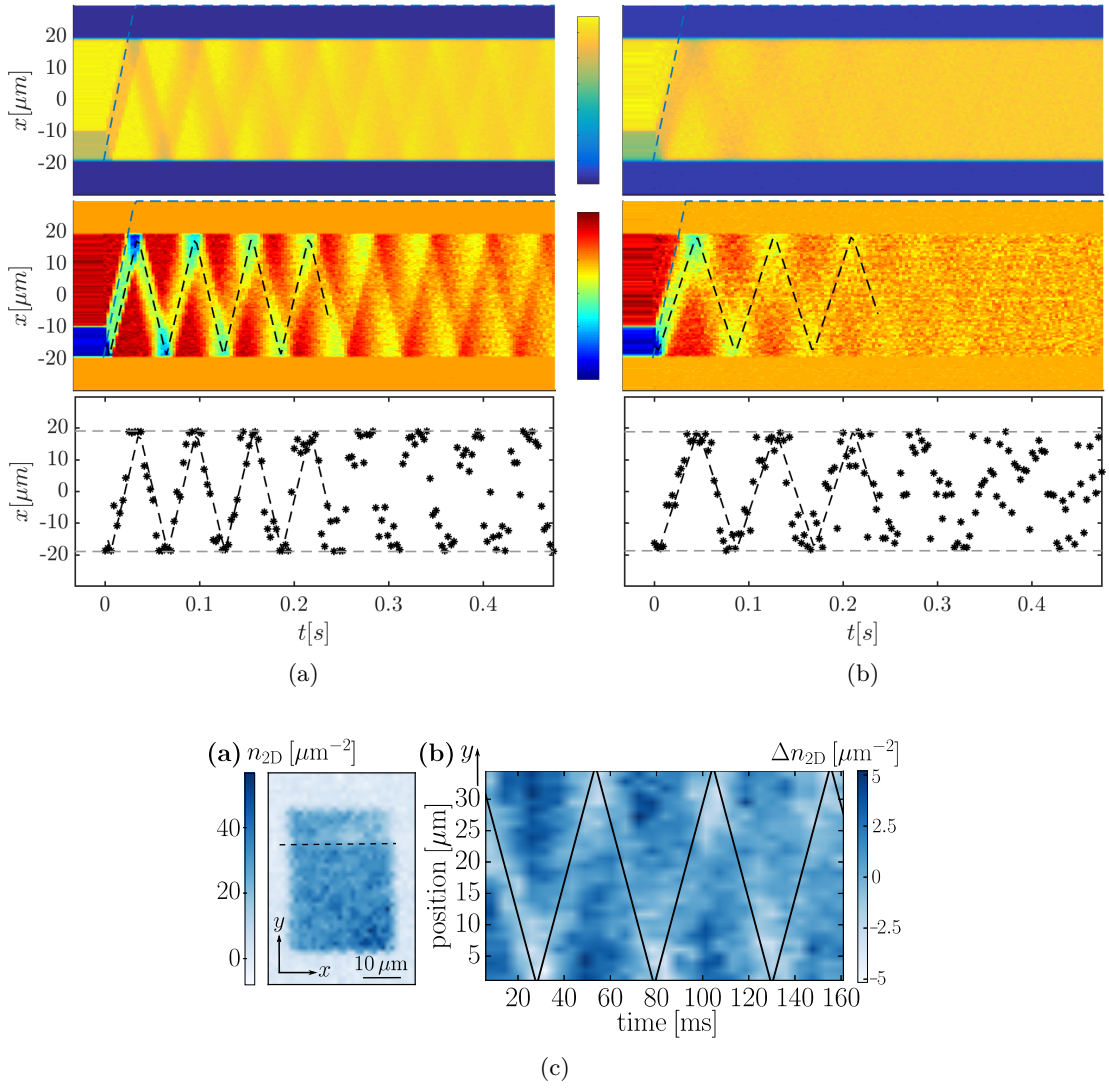


Figure 5.11: (top) Time propagation of a density perturbation generated at $t = 0$ in a $^{87}$Rb gas with scattering length $a_s = 5.27$nm. The density is integrated in the $y$ direction to enhance visibility of the defect, and is averaged over a variable number $\mathcal{N} = (30 - 100)$ of stochastic realisations. Depending on the temperature, the perturbation is able to bounce several times off the system walls. The blue dashed line corresponds to the computed Bogoliubov speed of sound at $T = 0$, $c_{\rm bog} = \sqrt{ng/m}$. (middle) Integrated differential density, obtained by subtracting the integrated density above by its time-averaged value at equilibrium, after the perturbation has completely dissipated. The black dashed line is the triangular fit extracted from the data of the bottom panel. (bottom) Trace of the minimum density as a function of time. The dashed black line represents a triangular fit, while the grey line marks the boundaries of the system. (a) Data for $T \simeq 0.19 T_{\rm BKT}$. (b) Data for $T \simeq 0.60 T_{\rm BKT}$. (c) [Figure from [111]] (left) Absorption imaging of the *in-situ* density profile of the experiment at Collège de France, perturbed by a step potential whose size is marked by the dashed line. (right) Experimental data for the time propagation of the density perturbation. The density is integrated in the $y$ direction to enhance the visibility of the defect, and $T/T_{\rm BKT} = 0.37$.

We perform numerical simulations by means of the stochastic projected Gross-Pitaevskii equation described in Chapter 3. Some results for low- and high-temperature data are shown in Fig. (5.11). In order to enhance the visibility of the density perturbation propagating towards $x$, we integrate the averaged density of our stochastic realisations in the $y$ direction. The resulting profile shows the motion of the defect as it bounces back and forth in the trap, for an amount of time depending on the temperature (Figures (5.11a) and (5.11b), top panel), and it closely resembles the experimental data (Fig. (5.11c)). This feature is even more evident when we subtract from the integrated density profile its time-averaged value at equilibrium, when the system has completely dissipated the density perturbation (Figures (5.11a) and (5.11b), middle panel). From this, it is possible to extract the defect trajectory by following the minima of the differential density. One could also fit on this data a triangular wave

$$f_{\Delta}(t) = \frac{4A}{\tilde{T}}\left((t-\theta) - \frac{1}{2}\tilde{T}F(t-\theta)\right)(-1)^{F(t-\theta)}, \tag{5.33}$$

where

$$F(x) = \left\lfloor \frac{2x}{\tilde{T}} + \frac{1}{2} \right\rfloor, \tag{5.34}$$

$\lfloor\cdot\rfloor$ is the floor function, $\tilde{T}$ is the period of the wave, $A$ is the amplitude, and $\theta$ is a phase in time (Figures (5.11a) and (5.11b), bottom panel). Then one could extract from it the speed of sound as

$$c_{\Delta} = \frac{4A}{T}. \tag{5.35}$$

Although the analysis above is in principle correct, a more accurate estimation of the speed of sound can be performed by studying the motion of the centre of mass of the system. The displacement of the centre of mass with respect to the centre of the trap is defined as

$$\Delta x_{\mathrm{cm}}(t) = \frac{\int dx'\, dy\, x' n(x', y, t)}{\int dx'\, dy\, n(x', y, t)}, \tag{5.36}$$

and is an oscillating function whose amplitude is decaying in time, as the perturbation progressively dissipates (see Fig. (5.12)).

Thus, by imposing a fitting function of the kind of a damped harmonic oscillator

$$\mathcal{F}_{\mathrm{cm}}(t) = Fe^{-t/\tau}\left(\cos(\omega t) + \frac{1}{\omega\tau}\sin(\omega t)\right), \tag{5.37}$$

where $F$ is the amplitude, $\omega/2\pi$ is the frequency of the oscillating wave, and $\tau$ is a decay time, one could extract the speed of sound as

$$c_{\mathrm{cm}} = \frac{L_x\omega}{\pi}. \tag{5.38}$$

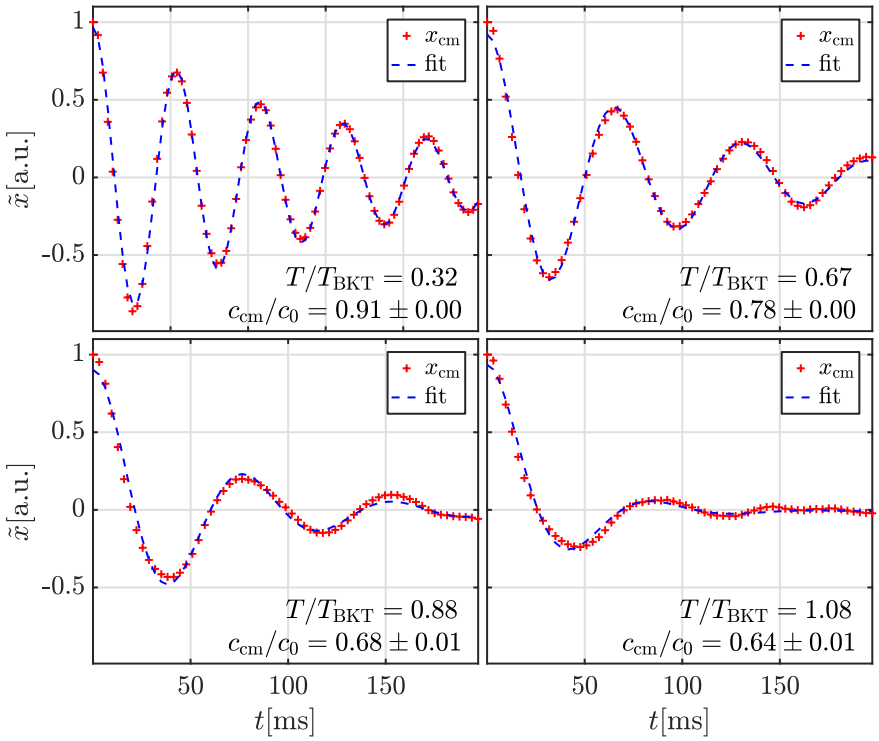


Figure 5.12: Oscillation of the centre of mass, as defined in text, for the different values of temperature indicated in the figures. The centre of mass position is normalised by its value at $t = 0$, hence $\tilde{x}_{\mathrm{cm}}(t) = x_{\mathrm{cm}}(t)/x_{\mathrm{cm}}(0)$. The dashed line indicates the damped oscillating fit according to the relation (5.37). The resulting speed of sound, computed as in equation (5.38), is normalised according to the Bogoliubov speed of sound. The uncertainty in the measurement is simply the relative error of the fit.

Figure (5.12) reports the resulting oscillatory behaviour of the centre of mass in four cases at different temperatures, and the corresponding fits according to equation (5.37). The speed of sound computed according to eq. (5.38) is normalised by the zero-temperature Bogoliubov speed of sound $c_0 = \sqrt{ng/m}$.

A third method, which was implemented in [111], consists in studying the decay of the first Fourier mode associated with the collective oscillation of the atoms. One could decompose the integrated density profile in the sine basis as[1]

$$n(x,t) = \bar{n} + \sum_{n=1}^{\infty} A_n(t) \sin(\tilde{k}_n x), \tag{5.39}$$

where $\tilde{k}_n = \pi/L_x$ is the wavelength corresponding to the $n$th mode of the box, and $\bar{n}$ is

[1] Note that, in [111] this is instead expanded in the cosine basis, because of a different definition of the spatial coordinate $x$: in our case $x \in [-L_x/2, L_x/2]$, while in the reference $x \in [0, L_x]$.

[111] J. L. Ville et al. In: *ArXiv e-prints* (2018). arXiv: 1804.04037 [cond-mat.quant-gas].

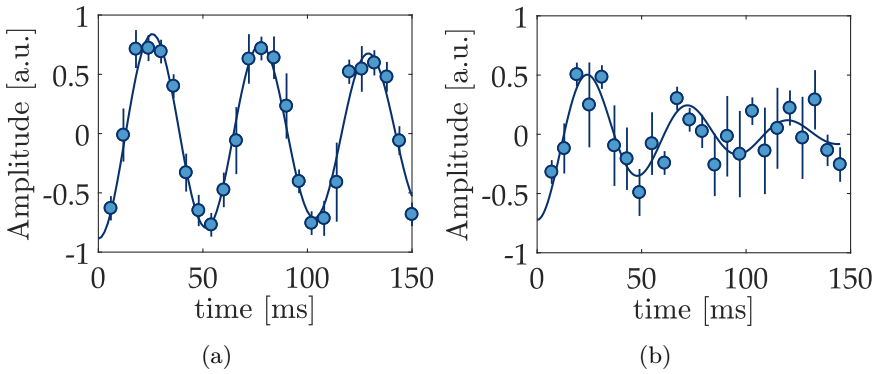


Figure 5.13: [Courtesy by the group of Jean Dalibard at the Collège de France, *unpublished*] Decay of the amplitude of the Fourier mode corresponding to the collective mode $\sin(k_1 x)$, with $k_1 = \pi/L_x$. (a) Data corresponding to a temperature $T/T_{\mathrm{BKT}} \simeq 0.37$. (b). Data corresponding to a temperature $T/T_{\mathrm{BKT}} \simeq 0.95$.

the average density along $x$. Some examples of the experimental analysis can be seen in Fig. (5.13). By studying the time decay of the amplitude of the first mode $A_1(t)$ with a fitting procedure analogous to eq. (5.37), at different temperatures, it is possible to extract the speed of sound. We applied this approach to the following treatment, where we detached from the experimental configuration described so far, to study a similar but different system more suited to this kind of analysis.

### Oscillation and decay of single standing waves

The aim of the previous analysis has been to reproduce the experimental configuration of the Dalibard's group. However, from a purely theoretical perspective, one would want to excite a single standing wave (SSW) to study its decay. Therefore, instead of a step density perturbation, one could engineer the initial potential to mainly couple with one oscillation mode of the system, and study the decay of its amplitude in time. We performed numerical simulations of a two-dimensional system with periodic boundary conditions in both directions. The size of the computational box was set to match the experimental trap, so once again we considered $L_x \times L_y = 40 \times 30 \mu$m, and the chemical potential was tuned to reproduce the experimental atom number. The system is grown to thermal equilibrium in the presence of a stationary sinusoidal perturbation of the trap bottom,

$$V_p(x, y, t) = V_p(x) = -0.1\mu \sin(k_n x), \tag{5.40}$$

where

$$k_n = \frac{2\pi}{L_x} n \tag{5.41}$$

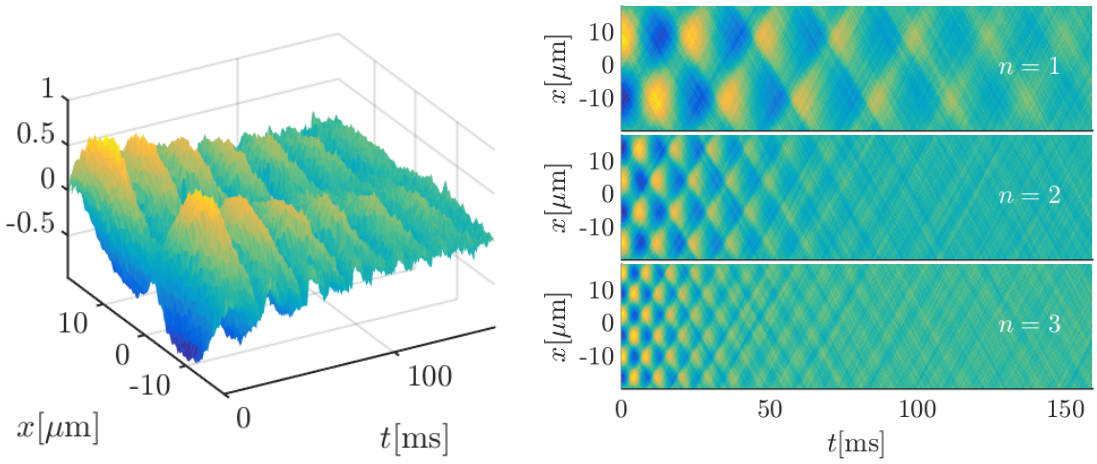


Figure 5.14: Oscillation and decay of a single standing wave (SSW) for a temperature of $T/T_{\mathrm{BKT}} = 0.29$. The two-dimensional density is integrated in the $y$ direction to enhance visibility, and its average equilibrium value is subtracted from it. (a) Decay of the $n = 1$ mode. (b) Carpet plot of the decay for the three modes $n = 1, 2, 3$.

and $n$ is a positive integer number. For the periodicity imposed by the boundary conditions to be non singular, we can only consider those values of $k_n$ such that the box contains an integer number of wavelengths. Different values for the amplitude of the perturbation have been considered, and the value of $0.1\mu$ has been found to be sufficiently strong to generate a good signal but low enough to minimise the coupling of the standing wave with other modes of the system.

Once the system has equilibrated, the coupling with the thermal reservoir is switched off, and the sinusoidal perturbation is removed. The real-time evolution is then performed according to the (projected) Gross-Pitaevskii equation. As in the previous case, we integrate along the $y$ direction to enhance the visibility. The density profile of the system oscillates in time, maintaining its initial sinusoidal shape if only one collective mode was originally excited (see Fig. (5.14)). We extract the values of the amplitude at each time by fitting to the integrated density a sinusoidal function[2]

$$f_{\mathrm{fit}} = A \sin(k_n x) \tag{5.42}$$

where the amplitude is the fitting parameter. Figure (5.15) shows the resulting damped oscillations for $A$. Analogously to what has been done in eq. (5.37), we fit the oscilla-

[2] An alternative approach consists in a Fourier analysis of the integrated density similar to what has been done in [111]. We checked that the results are identical to the ones obtained as explained in the text.

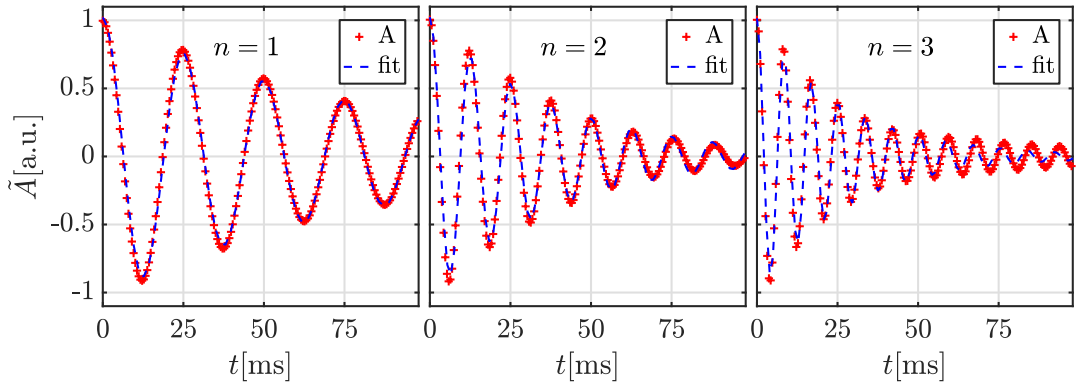


Figure 5.15: Oscillation of the normalised amplitude $\tilde{A} = A(t)/A(0)$, as defined in text, for the different values of the mode index $n$ indicated in the figures. The dashed line indicates the damped oscillating fit according to the relation (5.43). The temperature for these data is $T/T_{\mathrm{BKT}} = 0.32$.

tions with the damped harmonic oscillator relation

$$\mathcal{F}_{\mathrm{osc}} = Fe^{-t/\tau_n}\left(\cos(\omega_n t) + \frac{1}{\omega_n \tau_n}\sin(\omega_n t)\right), \tag{5.43}$$

where the index $n$ corresponds again to the collective mode $k_n$. Thus, we are able to get different values of the oscillation frequency and of the decay time for up to three collective modes of the system ($n = 1, 2, 3$), as a function of the temperature.

In the next subsection we will show the resulting behaviour of these quantities, and how they are related among themselves and with the literature.

### Results and comments

In the following we report the results of the analysis performed in the previous sections. The results for the fit of the sound speed extracted from the study of the step perturbation are reported in Fig. (5.16a). The blue points correspond to the velocity computed by analysing the motion of the centre of mass, as explained above. The red points correspond to the decay of the coefficient $A_1(t)$ for the first Fourier mode as in equation (5.39), and resemble the analysis performed for the experimental data[111], plotted in green. The two sets of theoretical data show an identical trend, but present a small shift. In particular, the Fourier decay points are systematically smaller than the centre of mass ones, and do not converge to unity in the low-temperature limit. We believe that this effect might be due to the coupling of the lowest collective mode with the ones of higher order, caused by the step potential perturbation. Having a coupling with modes of higher order and lower wavelength could result in a lowering of

[111] J. L. Ville et al. In: *ArXiv e-prints* (2018). arXiv: `1804.04037 [cond-mat.quant-gas]`.

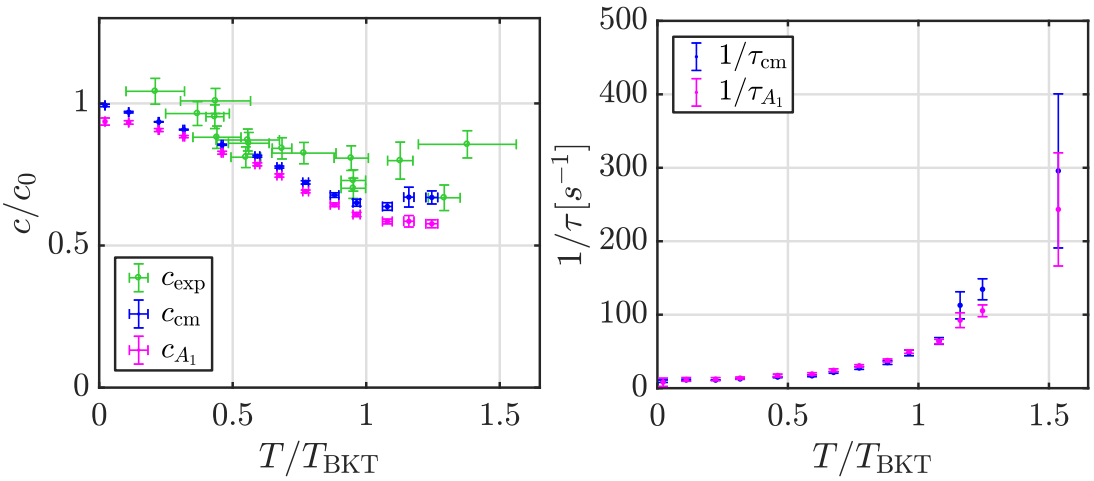


(a) (b)

Figure 5.16: (a) Speed of sound computed from the propagation of a density depletion produced by a step potential, as described in Fig. (5.10a), normalised by the zero-temperature Bogoliubov speed of sound $c_0 = \sqrt{ng/m}$. The green data correspond to the experimental values of [111]. The blue and red points are the result of the analysis performed on the simulations described in the previous subsection. The blue data report the sound computed from the oscillation of the centre of mass, while the red ones correspond to the decay of the first Fourier component $A_1$, as done in [111]. We measure a small systematic shift between these two methods, which could be explained by the coupling of the first mode with the ones at higher order. The errorbars in $c$ are indicative of the error of the fit, while the ones in temperature account for a small uncertainty in the value of the density $n$, arising from statistical fluctuations. (a) Decay rates $1/\tau$ for the oscillation of the centre of mass and of the first Fourier component.

the sound speed.

Both the experimental and the numerical results show that, above $T_{\mathrm{BKT}}$, the values of $c$ do not fall to zero, as expected for the second sound in the hydrodynamic regime[115]. However, the theoretical prediction for the first sound would require the values of the velocity to be much larger than the measured ones. Thus, one could wonder if the measured speeds of sound arise from a non hydrodynamic process. Indeed, the experimental parameter of [111] are such, that the collisional rate[117]

$$\Gamma_{\mathrm{coll}} = \frac{\hbar n g_{2\mathrm{D}}^2}{m} \tag{5.44}$$

is of the same order of the frequency of the excited mode, meaning that the collisions are not frequent enough for the system to be in the collisional hydrodynamic regime.

[115] T. Ozawa and S. Stringari. In: *Phys. Rev. Lett.* 112 (2014), p. 025302.
[111] J. L. Ville et al. In: *ArXiv e-prints* (2018). arXiv: `1804.04037 [cond-mat.quant-gas]`.
[117] D. S. Petrov and G. V. Shlyapnikov. In: *Phys. Rev. A* 64 (2001), p. 012706.

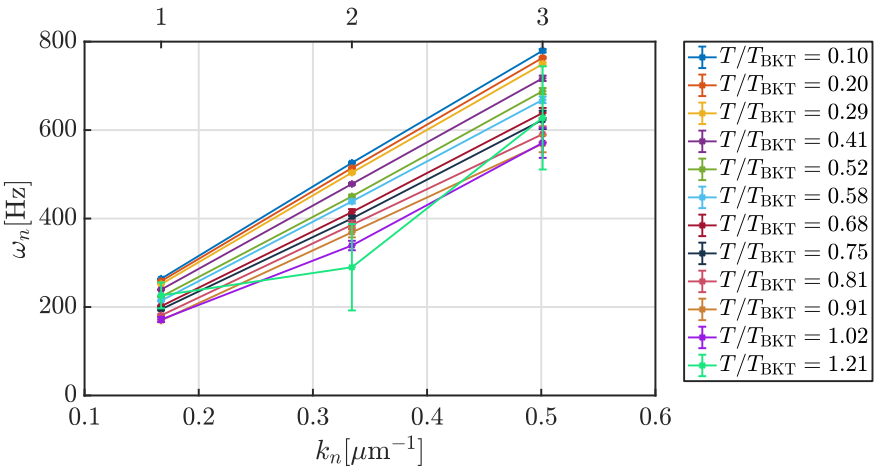


Figure 5.17: Distribution of $\omega_n$ as a function of $k_n$ for the three modes $n = 1, 2, 3$, at various temperatures indicated in the legend.

In order to avoid the coupling with more modes, we performed the analysis on the decay of a single collective mode, imprinted by a proper sinusoidal density perturbation, as explained above. The fit procedure according to eq. (5.43) gives different sets of frequencies $\omega_n$ and decay time $\tau_n$ for each temperature, and for the modes $n = 1, 2, 3$. With them, two interesting quantities can be computed. The first is the speed of sound, obtained by performing linear fits of the distributions of $\omega_n$ as a function of the wavevectors $k_n$, as in Fig. (5.17) and Fig. (5.18a). The data obtained this way agree remarkably well with the experiment, and show once again the same features as the results of Fig. (5.16a), such as the finite value of the sound speed for temperatures higher than $T_{\mathrm{BKT}}$. In [110], the data have been found to agree very well with the theoretical prediction of the Random Phase Approximation (RPA) formalism, which is a method to describe the dynamic behaviour of a Bose gas in the absence of collisions[118], which is also reported in Fig. (5.18a). Note that, below the BKT transition, the measured speed of sound agrees well with the theoretical prediction for the second sound $c_2$ defined in eq. (5.30), reported as a dashed line in Fig. (5.18a). This is understood by considering that in weakly interacting Bose gases close to the transition, relation (5.30) approximates well the second sound. Moreover, it only differs from the isothermal sound $c_{\mathrm{T}} = 1/\sqrt{mn\kappa_{\mathrm{T}}}$ by a factor $\sqrt{n_s/n}$, depending on the superfluid fraction, which remains fairly large even in the vicinity of the transition. The isothermal (collisionless) sound actually serves as a good approximation for the measured speed of sound (see [110] for a more detailed treatment of this aspect).

[110] M. Ota et al. In: *ArXiv e-prints* (2018). arXiv: `1804.04032 [cond-mat.quant-gas]`.

[118] L.P. Kadanoff and G. Baym. *Quantum statistical mechanics: Green's function methods in equilibrium and nonequilibrium problems.* W.A. Benjamin, 1962.

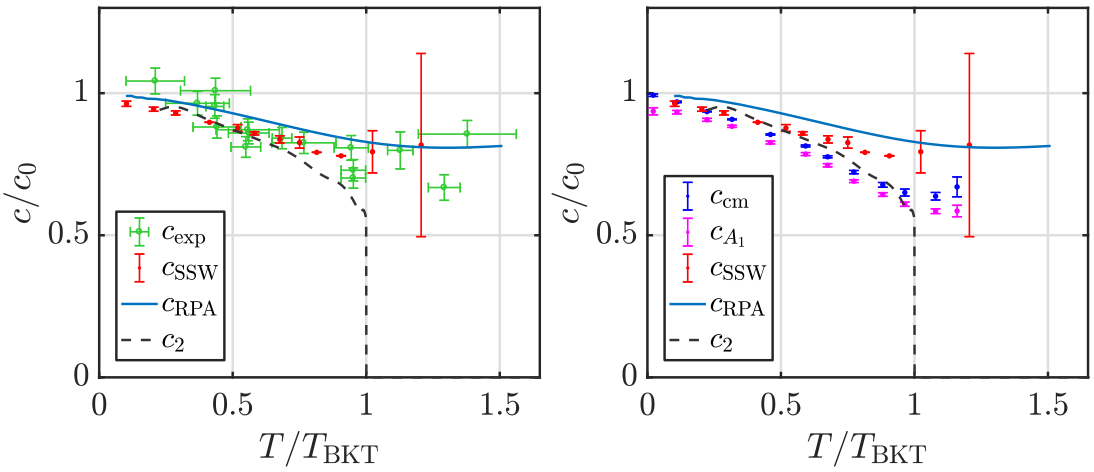


Figure 5.18: (a) Resulting speed of sound as a function of temperature, normalised by the zero-temperature Bogoliubov speed of sound $c_0 = \sqrt{ng/m}$. The red points are the speed of sound of the single standing wave (SSW) computed from a linear fit of the distribution of $\omega_n$ in Fig. (5.17), while the green points are the experimental data from [111]. The blue solid line corresponds to the theoretical data obtained with the RPA approach., while the grey dashed line corresponds to the result for the second sound speed as in [115]. (b) Theoretical and numerical results for the speed of sound, as defined in (a) and in Fig. (5.16).

A second interesting quantity is the quality factor $Q$ of the damped harmonic oscillator, which expresses the energy loss in a single cycle of the oscillator, relative to the total energy stored in the system. In our definition of the parameters in eq. (5.43), the quality factor is

$$Q = \omega_n \tau_n. \tag{5.45}$$

Fig. (5.19a) shows the resulting quality factor for the temperature range considered, and for the three modes $n = 1, 2, 3$. From it, one could deduce that the quality factor does not depend on which mode is considered, nor on the associated oscillation frequencies (inset). This is a clear feature indicating that the damping mechanism of the system is collisionless. If it were collisional, in fact, the damping rate $1/\tau_n$ would show a quadratic dependence on the oscillation frequency $\omega_n$, which should also be reflected in a strong frequency dependence for the quality factor[119].

Finally, since it does not depend on $n$, we can average the quality factor over the oscillation modes and compare it to the experimental one, from [111]. The result is shown in Fig. (5.19b), also including the theoretical curve obtained by the RPA approach.

[119] I.M. Khalatnikov. *An introduction to the theory of superfluidity.* W.A. Benjamin, 1965.
[111] J. L. Ville et al. In: *ArXiv e-prints* (2018). arXiv: `1804.04037 [cond-mat.quant-gas]`.

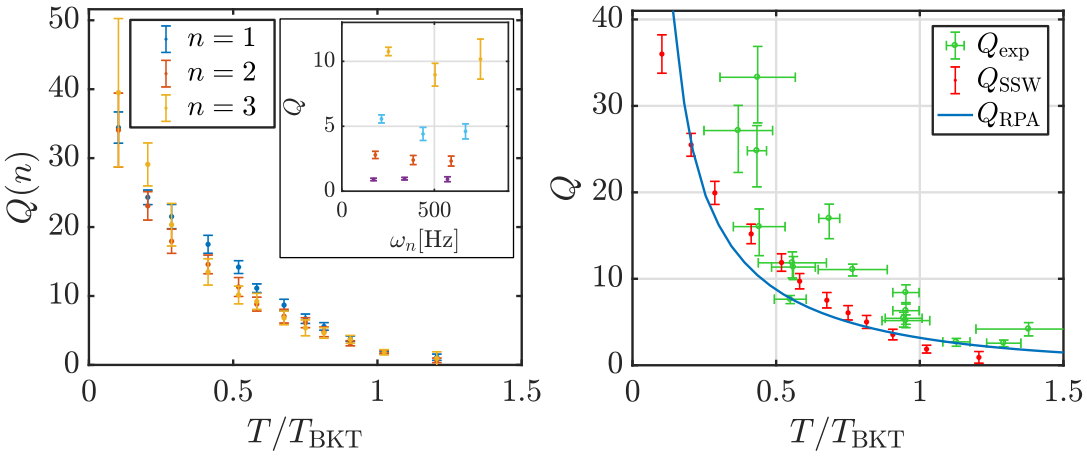


(a) (b)

Figure 5.19: (a) Resulting quality for the three modes $n = 1, 2, 3$, as a function of temperature. (inset) Quality factor as a function of the fitted frequency $\omega_n$ for the three modes, for different values of temperature. From top to bottom, $T/T_{\mathrm{BKT}} = 0.29, 0.58, 0.81, 1.02$. Both plot show that the quality factor does not show a strong dependence on the mode considered, nor on its frequency. (b) Quality factors for numerical and experimental data. The red data correspond to the quality factor for the single standing wave (SSW), averaged over the three modes $n = 1, 2, 3$. The green points are the experimental data from [111], and the blue solid line corresponds to the theoretical result for the RPA approach, as in [110].

The experimental analysis performed in [111], and the theoretical investigation in [110] agree well with each other, and both seem to indicate that indeed, for the parameters in the experiment, the system is not in the collisional hydrodynamic regime. The measured speed of sound, then, does not correspond to one of the hydrodynamic sounds described in section 5.2.1, but has rather to be related to a collisionless sound propagation, which can exist even at temperatures above the critical value, in the absence of superfluidity.

## 5.3 Chapter conclusions and future outlook

In this chapter we described the collaboration with two distinct experiments on the dynamics of excitations in a finite temperature gases in reduced dimensions. In the first section we report the analysis performed on the decay of a soliton in an elongated quasi-2D condensate. After equilibrating the sample at two different temperatures, a phase difference is imprinted in the soliton, leading to the creation of a grey soliton.

[111] J. L. Ville et al. In: *ArXiv e-prints* (2018). arXiv: 1804.04037 [cond-mat.quant-gas].
[110] M. Ota et al. In: *ArXiv e-prints* (2018). arXiv: 1804.04032 [cond-mat.quant-gas].

This propagates in the condensate bending due to the inhomogeneity of the density profile, and eventually decaying into sound waves. The progressive reduction of the defect density depletion is measured as a function of time, and a lifetime is estimated by means of an exponential fit. The simulations are compared with the experimental results of the group at Birmingham University and with ZNG simulations performed in Newcastle, showing good agreement. It is possible to get a qualitative indication about the effect of temperature on the soliton decay, which seems to be marginal, apart from a slight widening of the distribution for the lifetimes of the single noise realisations. The main mechanism for the decay of the defect appears to be the geometry of the system, at least in this configuration. A further analysis would involve the determination of the same quantities in a 2D homogeneous system, where the soliton can be confined in a narrow channel to increase its stability.

In the second section we reviewed the theoretical derivation of the equation for the two branches of the speed of sound in a two-dimensional gas at finite temperature, in the hydrodynamic regime, as done in [115]. We summarised the experimental realisation of a 2D ultracold Bose gas in a uniform trap by the laboratory at the Collège de France, by means of an "optical accordion" and a digital mirror device, and we described the mechanism used to create sound waves in the experimental sample. We presented our numerical simulations, with two different sound excitation protocols: the initial step potential in a rectangular box as used in the experiments, and a single standing wave (SSW) excitation potential in a periodic system. We detailed the analysis leading to the extraction of the speed of sound as a function of temperature for the two protocols. In both cases, we are able to reproduce the main features of the experimental findings. In particular, we are able to confirm the absence of a sudden drop of the sound speed at the transition, as predicted for the hydrodynamic second sound. Instead, we observe a finite velocity even above the critical point. This is compatible with the propagation of sound in a collisionless regime, which is sustained by interactions even above the transition by the fairly large presence of the quasi-condensate. Most of the analysis related to this part of the chapter have been included in [110], together with an investigation of the same system with the Random Phase Approximation and with some more analysis on the equation of state of a two-dimensional Bose gas across the Berezinskii-Kosterlitz-Thouless phase transition. The paper has now been simultaneously submitted with [111], and is currently under review.

[110] M. Ota et al. In: *ArXiv e-prints* (2018). arXiv: `1804.04032 [cond-mat.quant-gas]`.
[111] J. L. Ville et al. In: *ArXiv e-prints* (2018). arXiv: `1804.04037 [cond-mat.quant-gas]`.

# General conclusions

At the end of a long journey, it is always useful to sum up the travelled path and the gathered experience. In this work we presented some analysis on the dynamics of excitations in low-dimensional Bose gases. The thesis is divided in two parts: the first is devoted to the theoretical description and the following analysis of zero temperature results, while the second addresses finite temperature, which allows us to explore interesting phenomena such as the phase transitions and the effect of the thermal fluctuations on the dynamics of excitations in low dimensions. This section is a brief recap of the more detailed conclusions that can be found at the end of each chapter.

In Chapter 1 we outlined the theoretical framework related to the treatment of zero temperature Bose-Einstein condensates. We reviewed the Gross-Pitaevskii equation governing their dynamics, and the Thomas-Fermi approximation for its solution in the low-temperature stationary regime. We looked at the concept of solitons, a class of dynamical solutions for the equation, and we described their main features. We introduced the concepts of superfluidity in a BEC, the associated quantisation of vorticity, and we outlined the hydrodynamic equations for a condensate. We also reported the Bogoliubov approach for the first-order excitations in the system.

Most of these concepts were used in the subsequent Chapter 2, where we described the results related to an experiment[27] in which, by means of a stroboscopic technique, it was possible to follow the dynamics of solitonic vortices in an elongated, quasi one-dimensional condensate. The defects in this distinctive trapping configuration are called solitonic vortices, because they share some of the properties of solitons. Experimentally, it was possible to follow their oscillations by means of a stroboscopic non-destructive technique. We detailed the theoretical analysis predicting a motion of the vortices following equipotential lines in the condensate, and we accounted for the atom losses due to the imaging and the trap imperfection to produce a fitting relation for the experimental data. This constituted my main contribution to this work. Theory and experiment resulted to be in good agreement.
This work was the starting point of further studies on the decay and interaction of

[27] S. Serafini et al. In: *Phys. Rev. Lett.* 115 (2015), p. 170402.

vortices. A preliminary experimental result investigated the presence of more than one vortex in the system, and how the lifetime of the defects is reduced in the $N_V(0) = 3$ configuration, while it remains almost unaffected in the $N_V(0) = 2$ one. The properties of vortex interactions were further addressed in a subsequent paper[39], where a more sophisticated imaging technique was implemented, that also allowed to infer the vortex orientation. A larger insight was possible thanks to numerical simulations of the vortex dynamics, that indeed showed the occurrence of double reconnection processes, as well as other unexpected phenomena such as rebounds, vortex rotations, and ejections of defects.

In Chapter 3 we reviewed the theoretical derivation of two models allowing to treat the finite temperature dynamics of atomic gases, similar in spirit but arising from different derivation approaches. At first we described the stochastic Gross-Pitaevskii equation, a Langevin equation describing the combined time evolution of a condensate and a finite number of thermal modes. The coupling between the low-lying modes and a heat bath representing the high-energy thermal modes is effectively realised by means of a dissipation term and a stochastic term added to the zero temperature Gross-Pitaevskii equation. The second method we outlined is the stochastic projected Gross-Pitaevskii equation, which explicitly introduces a projector to separate the high-energy modes from the coherent region. We detailed the numerical implementation of such methods in the two-dimensional case, and we outlined the constraints on the physical input parameters. We produced some example of the result analysis by simulating a harmonically trapped two-dimensional sample, on which we applied two methods to estimate the degeneracy at finite temperature: the Penrose-Onsager diagonalisation, allowing for the determination of the condensate wave function, and the computation of the order parameter of the equation, related to the quasi long-range ordering in the system.

Chapter (4) is devoted to the analysis of a two-dimensional uniform system with periodic boundary conditions going through the topological Berezinskii-Kosterlitz-Thouless (BKT) phase transition. We started the chapter by reviewing the main features of the BKT. We introduced the concept of quasi long-range ordering and the role of vortices in the breakdown of the superfluidity in the system. We presented the picture for the Kibble-Zurek mechanism (KZM) leading to the creation of defects as a result of fast quenches across continuous phase transitions. Then, we reported some results on the thermal equilibration of the 2D system. At first we measured the equilibrium first-order correlation function $g_1(r)$ for a temperature range spanning the critical region. We studied its transition from an exponential to an algebraic decay, and we measured

[39] S. Serafini et al. In: *Phys. Rev. X* 7 (2017), p. 021031.

a systematic shift in the critical point of about $\sim 0.25$ with respect to the theoretical relation for the BKT. We also computed the temperature dependence of the equilibrium order parameter, measuring again the same shift in the critical point. The data also showed a widening of the decay region, which might be due to finite size effect. We counted the number of vortices in the system by means of a numerical routine accounting for the circulation of the phase. From it, we got an equilibrium result for the number of vortices as a function of temperature, and the associated correlation length $\zeta_v$. The uncertainty in the determination of the critical point is also reflected here, and we plan to address the problem by performing a precise characterisation of these quantities as a function of the system size, similarly to what has been done in [74].

We then described the dynamics of a two-dimensional Bose gas instantaneously driven across the BKT phase transition. At first we performed quenches in *two* control parameters ($T$ and $\mu$). This might conceptually present some issues in the precise control of the system status, therefore we chose to perform further simulations, implementing a quench in the interaction strength $g$. For both quench protocols, we performed an analysis on the time growth of the first-order correlation function $g_1(r)$, from which a correlation length $\zeta_g$ can be extracted by applying a scaling argument. This can be compared with the correlation length extracted from the decay in time of the vortex density, and both can be fitted with a relation including a logarithmic correction accounting for the coupling of vortices below $T_{\mathrm{BKT}}$. The resulting critical exponent shows a degree of self consistency, for both quench protocols, but is not compatible with the theoretical prediction for the BKT transition. Addressing this disagreement will be the core of the future work on this project. We also reported a brief analysis on the dynamics following ramped quenches, with finite time durations. We checked that the predicted scaling for the density of defects is recovered. Further analysis would require a precise characterisation of the important quantities related to the Kibble-Zurek mechanism, such as the freezing time $\hat{t}$.

The final chapter reported the results of the collaboration with two experimental groups, on the dynamical properties of excitations in finite temperature gases confined in reduced dimension. In the first section we analysed an experiment carried out at the University of Birmingham, on the decay of a phase imprinted grey soliton in a quasi-2D condensate. The propagation of the defect was traced by looking at the motion of the density depletion, whose progressive reduction characterises the decay of the soliton. We extracted the lifetimes for two different temperatures and we compared them with the experimental results, as well as with numerical results obtained with a different theoretical approach (ZNG). We found good agreement between the data, leading to the formulation of the hypothesis that the main contribution in the decay mechanism

for this geometry is not given by the temperature, but rather by the inhomogeneity of the density. A further analysis would require to simulate 2D uniform systems with a greater aspect ratio, so to increase the stability of the defect.

The second section reported the analysis of an experiment performed at the Collège de France, on the sound propagation in a two-dimensional uniform gas at different temperatures. At first we reviewed the theoretical background related to this problem, as presented in [115]. We then presented the experimental setup at the Collège, and we performed numerical simulations in the same conditions. The speed of sound was then estimated by looking at the oscillations of the centre of mass, and was compared to the experimental result, finding a good qualitative agreement. We then investigated a second excitation protocol, able to better couple with a single mode of the system. We found again a good agreement with the experimental data. A notable feature measured both by the experiment and by the simulation is the finite value of the speed of sound above the critical temperature for the BKT transition. This is in contrast with the theoretical approach for the sound speed in the hydrodynamic regime, which predicts its sudden drop to zero at the critical point. We obtained a strong indication that the sound propagation measured in [111] is related to a collisionless regime. The results of this investigation have been included in [110], which is currently under revision for the publication, and has been simultaneously submitted with [111].

[111] J. L. Ville et al. In: *ArXiv e-prints* (2018). arXiv: `1804.04037 [cond-mat.quant-gas]`.
[110] M. Ota et al. In: *ArXiv e-prints* (2018). arXiv: `1804.04032 [cond-mat.quant-gas]`.

# Appendices and References

# Appendix A

# Stochastic analysis of the Brownian motion

Among the discoveries of modern Physics, the Brownian motion occupies a very relevant place. First observed by Robert Brown[120] at a time at which the debate on the existence of atoms was still open, once it was correctly interpreted as due to molecular motion by Albert Einstein[121] in 1905 it quickly became a typical model for many physical processes. In the following is reported a derivation of the Langevin equation for the Brownian motion, largely taken from the book by Risken and Frank[122]. In the subsequent section the Fokker-Planck equation for the Brownian motion is derived, mimicking the procedure contained in the book by Reif[123].

## A.1 Stochastic (Langevin) equation for the Brownian motion

The problem is first approached by means of the Newton laws. Take a particle of mass $m$, immersed in a fluid. Deterministically, a friction force of expression

$$F = m\frac{dv}{dt} = -\alpha v, \tag{A.1}$$

[120] R. Brown. In: *Philosophical Magazine* 4 (1828), pp. 161–173.

[121] A. Einstein. In: *Annalen der Physik* 17 (1905), pp. 549–560.

[122] H. Risken and T. Frank. *The Fokker-Planck Equation: Methods of Solution and Applications.* Springer-Verlag Berlin Heidelberg, 1996.

[123] Reif F. *Fundamentals Of Statistical And Thermal Physics.* McGraw-Hill Science/Engineering/Math, 1965.

will act on the particle. The solution of this equation is simply

$$v(t) = v(0)e^{-\gamma t}. \tag{A.2}$$

An initial velocity $v(0)$ will then dissipate within the relaxation time $\tau = 1/\gamma = m/\alpha$. Equation (A.1), however, is only valid in the regime for which $m$ is large enough that its velocity associated with the thermal fluctuations can be neglected. If we also consider temperature in the picture, we can say that, thanks to the equipartition theorem, in one dimension

$$\frac{1}{2}m\langle v^2\rangle = \frac{1}{2}k_{\mathrm{B}}T. \tag{A.3}$$

The average thermal velocity is then

$$v_t = \sqrt{\frac{k_{\mathrm{B}}T}{m}} \tag{A.4}$$

which can assume significant values for large temperatures $T$ or small masses $m$, and can no longer be neglected. One should therefore modify eq. (A.1) so that it leads to the correct thermal energy, eq. (A.3). This is achieved by the addition of a *random* force $F_f(t) = m\Gamma(t)$

$$\frac{dv(t)}{dt} = -\gamma v(t) + \Gamma(t), \tag{A.5}$$

which represents the combined action of the fluid particles. The random force varies from system to system, depending in principle on the initial conditions of the fluid, and the meaningful results can only be computed *on average*. Equation (A.5) is a stochastic differential equation usually named *Langevin equation*, and it should recover the *mean* findings of the deterministic equation (A.1), when averaged. The force should not impose a bias towards any direction, hence the average effect should be null. Moreover, it is reasonable to assume that the collisions of different fluid molecules with the probe particle are independent. This means that

$$\langle\Gamma(t)\rangle = 0 \quad \text{and} \quad \langle\Gamma(t)\Gamma(t')\rangle = q\delta(t-t') \tag{A.6}$$

where $\sqrt{q}$ represents the strength of the Langevin force. The second (autocorrelation) condition is derived by assuming that the typical collision time $\tau_0$ is much smaller than the relaxation time $\tau$ of the velocity of the probe. The resulting force $\Gamma$ is simply white noise, as can be easily seen by computing its power spectral density

$$S(w) = \int_{-\infty}^{\infty} d\tau\, e^{-i\omega\tau} q\delta(\tau) = \frac{q}{2}, \tag{A.7}$$

which is indeed uniform.

Let us now compute the mean square velocity of the particle. The solution of (A.5), assuming that $v(0) = v_0$, is

$$v(t) = v_0 e^{-\gamma t} + \int_0^t e^{-\gamma(t-t')}\Gamma(t')dt'. \tag{A.8}$$

By using eq. (A.6) we can compute

$$\langle v(t_1)v(t_2)\rangle = v_0^2 e^{-\gamma(t_1+t_2)} + \int_0^{t_1}\int_0^{t_2} e^{t_1+t_2-t'-t''} q\delta(t'-t'')dt'dt''. \tag{A.9}$$

Which results in

$$\langle v(t_1)v(t_2)\rangle = v_0^2 e^{-\gamma(t_1+t_2)} + \frac{q}{2\gamma}\left(e^{-\gamma|t_1-t_2|} - e^{-\gamma|t_1+t_2|}\right). \tag{A.10}$$

For large times $\gamma t_1 \gg 1$ and $\gamma t_2 \gg 1$ the correlation in velocity only depends on the time difference

$$\langle v(t_1)v(t_2)\rangle \to \frac{q}{2\gamma} e^{-\gamma|t_1-t_2|}. \tag{A.11}$$

If we now substitute this into eq. (A.3), assuming $t_1 = t_2$, we find the magnitude of the noise

$$q = \frac{2\gamma k_{\mathrm{B}} T}{m}. \tag{A.12}$$

Interestingly, eq. (A.12) represents a fluctuation-dissipation relation, connecting the amplitude of the noisy force with the damping magnitude. The two quantities act on the opposite: while the first agitates the system, the second dissipates such effect, and when these two mechanism balance an equilibrium is established.

Let us now compute the mean square displacement of the particle, at equilibrium. This is simply

$$\langle (x(t) - x_0)^2\rangle = \langle \int_0^t v(t_1)dt_1 \int_0^t v(t_2)dt_2\rangle, \tag{A.13}$$

By means of eq. (A.11) we can compute it to be

$$\langle (x(t) - x_0)^2\rangle = 2Dt, \tag{A.14}$$

where

$$D = \frac{q}{2\gamma^2} = \frac{k_{\mathrm{B}}T}{m\gamma} \tag{A.15}$$

is the famous Einstein relation for the diffusion coefficient $D$.

## A.2 The Fokker-Planck equation for the Brownian motion

By considering the problem in a more probabilistic way, it is possible to show that the Langevin equation for the Brownian motion can be mapped into a Fokker-Planck equation. Instead of investigating the time behaviour of the mean value of the velocity, tha Fokker-Planck equation governs the evolution of the probability $P(v,t)dv$ that the particle possesses, at time $t$, a velocity lying between $v$ and $v+dv$. It is reasonable to consider that this probability should not depend on the entire history of the particle, but that it can be computed knowing simply the velocity $v_0$ at a certain past instant $t_0$. This is usually referred to as the "Markovian approximation". Therefore, $P$ can be written as a conditional probability

$$Pdv = P(v,t|v_0,t_0)\,dv = P(v,s|v_0)\,dv, \tag{A.16}$$

where we make explicit that $P$ does not depend on the origin at which the time is computed, and that only the time interval $s = t - t_0$ is relevant. There are two regimes for the previous equation. In the case $s \to 0$, of course $v = v_0$, thus

$$P(v,s|v_0) \to \delta(v - v_0). \tag{A.17}$$

In case $s \to \infty$, instead, we should assume that the particle equilibrates with the background medium at temperature $T$, and the past history is forgotten. In this case $P$ should not any more depend on the value of $v_0$ and of time, and the system should get a Boltzmann distribution

$$P(v,s|v_0) \to \sqrt{\frac{m\beta}{2\pi}} e^{\frac{-\beta}{2}mv^2} dv. \tag{A.18}$$

Let us now consider a general condition on the evolution of the probability $P(v,s|v_0)$. In any small interval $\tau$, the variation of the probability that a particle has velocity between $v$ and $v+dv$ is negative for the particles whose velocity changes to one outside this interval, let us say in another interval between $v_1$ and $v_1 + dv_1$; it is instead positive for the particles that originally had a velocity outside the range, but which end up having a final velocity inside $[v,(v+dv)]$. In mathematics

$$\frac{\partial P}{\partial s}\,dv\,\tau = -\int_{v_1} \left(P(v,s|v_0)\,dv\right)\left(P(v_1,\tau|v_0)\,dv_1\right) + \int_{v_1} \left(P(v_1,s|v_0)\,dv_1\right)\left(P(v,\tau|v_0)\,dv\right). \tag{A.19}$$

Here the integrals run over all the possible values of the velocity $v_1$ and $\int_{v_1} P(v_1,s|v)\,dv_1 = 1$. If we assume to treat *macroscopic* particles, over the small time increment $\tau$ the

change in the velocity can be postulated to be small. Thus, the probability distribution will be very peaked in a small velocity interval $|\xi| = |v - v_1|$, and we can rewrite

$$\frac{\partial P}{\partial s}\tau = -P(v, s|v_0) + \int_{-\infty}^{\infty} P(v-\xi, s|v_0)P(v, \tau|v-\xi)\, d\xi, \tag{A.20}$$

and Taylor expand it in powers of $\xi$

$$\frac{\partial P}{\partial s}\tau = -P(v, s|v_0) + \sum_{n=0}^{\infty} \frac{(-1)^n}{n!}\frac{\partial^n}{\partial v^n}\left(P(v, \tau|v_0)\int_{-\infty}^{\infty} d\xi\, \xi^n P(v+\xi, \tau|v)\right). \tag{A.21}$$

The $n = 0$ term is simply $P(v, s|v_0)$, while we can rewrite the other terms as moments of the velocity increment

$$M_n \equiv \frac{1}{\tau}\int_{-\infty}^{\infty} d\xi\, \xi^n P(v+\xi, \tau|v) = \frac{\langle (v(\tau) - v(0))^n \rangle}{\tau}, \tag{A.22}$$

so that

$$\frac{\partial P}{\partial s}\tau = \sum_{n=1}^{\infty} \frac{(-1)^n}{n!}\frac{\partial^n}{\partial v^n}(P(v, \tau|v_0)M_n). \tag{A.23}$$

It is possible to show that, for $\tau \to 0$, the moments $\langle (v(\tau) - v(0))^n \rangle \to 0$ more quickly that $\tau$, if $n > 2$. Then we can neglect all terms beyond the two lowest orders in eq. (A.23), for small time increment $\tau$ (which are, however, still large compared to the correlation time of the noisy Langevin force):

$$\frac{\partial P}{\partial s}\tau = -\frac{\partial}{\partial v}(M_1 P) + \frac{1}{2}\frac{\partial^2}{\partial v^2}(M_2 P), \tag{A.24}$$

which is finally the "Fokker-Planck equation".

We can associate eq. (A.24) with the Brownian motion and its relative Langevin equation by computing the moments $M_1$ and $M_2$. By simply taking a discretised version of eq. (A.5), by performing the average and considering (A.6), we can write

$$M_1 = \frac{\langle v(\tau) - v(0) \rangle}{\tau} = -\gamma \langle v(\tau) \rangle, \tag{A.25}$$

where we assumed for simplicity that $v(0) = 0$. We already computed $M_2$ in eq. (A.11), hence

$$M_2 = \frac{\langle (v(\tau) - v(0))^2 \rangle}{\tau} = \frac{2\gamma k_B T}{m}. \tag{A.26}$$

Thus, finally, the Fokker-Planck equation for the Brownian motion is

$$\frac{\partial P}{\partial s}\tau = \gamma\frac{\partial}{\partial v}(vP) + \gamma\frac{k_B T}{m}\frac{\partial^2}{\partial v^2}P. \tag{A.27}$$

# Appendix B

# Numerical tools

In the following are reported the main numerical tools used to solve the Stochastic Gross-Pitaevskii equation (3.32). At first the Cranck-Nicholson method to solve partial differential equations is shown, then the Runge-Kutta method is explained.

## B.1 Cranck-Nicholson method

Let us start by sketching the reasoning behind the solution of the Gross-Pitaevskii equation, followed by the detailed application to the stochastic Gross-Pitaevskii equation.

### B.1.1 Gross-Pitaevskii equation

Consider the Gross-Pitaevskii equation (1.14):

$$i\hbar\frac{\partial\psi(\mathbf{r},t)}{\partial t} = (\mathcal{H}_{\rm GP} - \mu)\psi(\mathbf{r},t) \tag{B.1}$$

Let us discretise the time coordinate by means of an index $m = 0, 1, 2, ..., m_{\max}$ dividing the interval into equal segments of magnitude $\Delta t = t/m_{\max}$, so that

$$t_m = m\Delta t. \tag{B.2}$$

The solution of equation (B.1) is

$$\psi(\mathbf{r}, t_{m+1}) = e^{-i(\mathcal{H}_{\rm GP}-\mu)\Delta t/\hbar}\psi(\mathbf{r}, t_m). \tag{B.3}$$

If we apply Cayley's relation for the exponential

$$\exp\left(-i(\mathcal{H}_{\rm GP} - \mu)\frac{\Delta t}{\hbar}\right) = \frac{1 - i\Delta t(\mathcal{H}_{\rm GP} - \mu)/2\hbar}{1 + i\Delta t(\mathcal{H}_{\rm GP} - \mu)/2\hbar} + \mathcal{O}(\Delta t^2), \tag{B.4}$$

the equation to solve becomes

$$[1 + i\Delta t(\mathcal{H}_{\rm GP}^{m+1/2} - \mu)/2\hbar]\psi(\mathbf{r}, t_{m+1}) = [1 - i\Delta t(\mathcal{H}_{\rm GP}^{m+1/2} - \mu)/2\hbar]\psi(\mathbf{r}, t_m), \tag{B.5}$$

where we introduced

$$\mathcal{H}_{\rm GP}^{m} = -\frac{\hbar^2\nabla^2}{2m} + V_{\rm tr}(\mathbf{r}) + g|\psi(\mathbf{r}, t_m)|^2, \tag{B.6}$$

and

$$\mathcal{H}_{\rm GP}^{m+1/2} \equiv \frac{\mathcal{H}_{\rm GP}^{m} + \mathcal{H}_{\rm GP}^{m+1}}{2}. \tag{B.7}$$

The introduction of $\mathcal{H}_{\rm GP}^{m+1/2}$ has the purpose to give a self-consistent average of the non-linear term, evaluated at the midpoint of the time step. The solution of (B.5) at time $m+1$ then passes through the following steps:

- Solve (B.5) using $\psi^m \equiv \psi(\mathbf{r}, t_m)$ in the non-linear term, obtaining the intermediate solution $\tilde{\psi}^m$.
- Solve (B.5) again, using the combination $(\tilde{\psi}^m + \psi^m)/2$ in the non-linear term, getting the solution $\psi^{m+1}$.

### B.1.2 Stochastic Gross-Pitaevskii equation

The reasoning with the Stochastic Gross-Pitaevskii equation (3.21) is similar. As pointed out by Bijlsma and Stoof[52], the solution for the SGPE is

$$\begin{aligned}\psi(\mathbf{r}, t_{m+1}) = {} & e^{i\Gamma(\mathcal{H}_{\rm GP}-\mu)\Delta t/\hbar}\,(\psi(\mathbf{r}, t_m) + \\ & - \frac{i}{\hbar} e^{i\Gamma(\mathcal{H}_{\rm GP}-\mu)t_m/\hbar} \int_{t_m}^{t_{m+1}} dt'\, e^{i\Gamma(\mathcal{H}_{\rm GP}-\mu)t'/\hbar}\eta(\mathbf{r}, t),\end{aligned} \tag{B.8}$$

where $\Gamma \equiv 1 - i\gamma(\mathbf{r})$, and we can define

$$\xi_m(\mathbf{r}) \equiv e^{i\Gamma(\mathcal{H}_{\rm GP}-\mu)t_m/\hbar} \int_{t_m}^{t_{m+1}} dt'\, e^{i\Gamma(\mathcal{H}_{\rm GP}-\mu)t'/\hbar}\eta(\mathbf{r}, t) \tag{B.9}$$

as a new noisy field, having correlations

$$\langle \xi_m^*(\mathbf{r})\xi_m(\mathbf{r}')\rangle = 2\gamma(\mathbf{r})k_{\rm B}T\delta(\mathbf{r} - \mathbf{r}')\delta_{mn}\Delta t + \mathcal{O}(\Delta t^2). \tag{B.10}$$

[52] H. T. C. Stoof and M. J. Bijlsma. In: *J. Low Temp. Phys.* 124.3 (2001), pp. 431–442.

Let us consider for now the one-dimensional case. Again by using Cayley's relation, we will have to solve

$$\underbrace{[1+i\Gamma\Delta t(\mathcal{H}_{\rm GP}-\mu)]}_{B}\psi^{m+1}(x)=\underbrace{[1-i\Gamma\Delta t(\mathcal{H}_{\rm GP}-\mu)]}_{A}\underbrace{\left(\psi^m(x)-\frac{i}{\hbar}\xi(x,t_m)\right)}_{\equiv\phi^m(x_i)=\phi_i^m}, \quad \text{(B.11)}$$

where we also discretised the spatial coordinate into segments $\Delta x$ by means of an index $j=0,1,2,...,N_x$.

The operator $A$ can be made adimensional:

$$\begin{aligned}A&=1-i\frac{\Delta t}{2}(1-i\gamma)\left(-\frac{1}{2}\frac{\partial^2}{\partial x^2}+V+g|\psi|^2-\mu\right)\\&\equiv 1-i\frac{\Delta t}{2}(1-i\gamma)\left(-\frac{1}{2}\frac{\partial^2}{\partial x^2}+\mathcal{V}\right)\\&=1-\gamma\frac{\Delta t}{2}\left(-\frac{1}{2}\frac{\partial^2}{\partial x^2}+\mathcal{V}\right)-i\frac{\Delta t}{2}\left(-\frac{1}{2}\frac{\partial^2}{\partial x^2}+\mathcal{V}\right)\end{aligned} \quad \text{(B.12)}$$

Now, the discretised version of the Laplacian is

$$\frac{\partial^2\phi}{\partial x^2}=\frac{\phi_{j+1}-2\phi_j+\phi_{j-1}}{\Delta x^2}, \quad \text{(B.13)}$$

so that

$$\frac{\Delta t}{2}\left(-\frac{1}{2}\frac{\partial^2}{\partial x^2}+\mathcal{V}\right)\phi_j^m=\underbrace{\frac{\Delta t}{2\Delta x^2}}_{\alpha_x}\left(-\frac{\phi_{j-1}^m}{2}+(1+\mathcal{V}\Delta x^2)\phi_j^m-\frac{\phi_{j+1}^m}{2}\right). \quad \text{(B.14)}$$

Thus

$$\begin{aligned}A\phi_j^m=\phi_j^m\underbrace{\left[1-\gamma\alpha_x(1+\mathcal{V}\Delta x^2)-i\alpha_x(1+\mathcal{V}\Delta x^2)\right]}_{\equiv b_{\rm rhs}}+\\+\phi_{j-1}^m\underbrace{\frac{\alpha_x}{2}(\gamma+i)}_{\equiv a_{\rm rhs}}+\phi_{j+1}^m\underbrace{\frac{\alpha_x}{2}(\gamma+i)}_{\equiv c_{\rm rhs}}.\end{aligned} \quad \text{(B.15)}$$

Similarly, for $B$:

$$B=1+\gamma\frac{\Delta t}{2}\left(-\frac{1}{2}\frac{\partial^2}{\partial x^2}+\mathcal{V}\right)+i\frac{\Delta t}{2}\left(-\frac{1}{2}\frac{\partial^2}{\partial x^2}+\mathcal{V}\right), \quad \text{(B.16)}$$

hence

$$\begin{aligned}B\phi_j^m=\phi_j^m\underbrace{\left[1+\gamma\alpha_x(1+\mathcal{V}\Delta x^2)+i\alpha_x(1+\mathcal{V}\Delta x^2)\right]}_{\equiv b_{\rm lhs}}\\+\phi_{j-1}^m\underbrace{\frac{\alpha_x}{2}(-\gamma-i)}_{\equiv a_{\rm lhs}}+\phi_{j+1}^m\underbrace{\frac{\alpha_x}{2}(-\gamma-i)}_{\equiv c_{\rm lhs}}.\end{aligned} \quad \text{(B.17)}$$

The problem can now be reduced to the solution of a tridiagonal linear system. Indeed we can rewrite eq. (B.11) as

$$B\Psi^{m+1} = \Phi^m_{\text{rhs}}, \tag{B.18}$$

where $B$ is a tridiagonal matrix and we defined

$$\Psi^{m+1} = \begin{pmatrix} \psi_1^{m+1} \\ \vdots \\ \psi_{N_x}^{m+1} \end{pmatrix} \qquad \text{and} \qquad \Phi^m_{\text{rhs}} = \begin{pmatrix} A\phi_1^m \\ \vdots \\ A\phi_{N_x}^m \end{pmatrix}. \tag{B.19}$$

Several effective methods exist to solve a tridiagonal linear system, and can be easily found in the literature[124].

## B.2 Runge-Kutta method

Let us now shortly review the idea behind the Runge-Kutta method to solve differential equations. The Runge-Kutta algorithm is based on the simple Euler method, which is now sketched.

### B.2.1 Euler method

Suppose to have the generic first-order[1] differential equation

$$\frac{dy}{dt} = f(t, y). \tag{B.20}$$

Consider, as above, the coordinate discretisation $\Delta t$, so that $t_{m+1} = t_m + \Delta t$ and $m = 0, ...m_{\max}$. the simple Euler approach predicts

$$y_{m+1} = y_m + \Delta t f(t_m, y_m). \tag{B.21}$$

Equation (B.21) is non symmetric, in that only uses information on the function $f(t_m, y_m)$ evaluated at one side of the interval $[t_m, t_{m+1}]$, and it is accurate up to a

[1] Any ordinary differential equation, of any order $n$, can be rewritten into a system of $n$ first-order differential equations. For example, $h'' + q(t)h' = r(t)$ can be rewritten into

$$\begin{cases} y_1' = y_2(t) \\ y_2' = r(t) - q(t)y_2(t), \end{cases}$$

where $h(t) = y_1(t)$ and $y_2(t)$ is a new independent variable.

[124] W. H. Press et al. *Numerical Recipes in Fortran 77: the art of Scientific Computing.* 2nd ed. Cambridge University Press, 1993.

correction $\mathcal{O}(\Delta t^2)$. The Euler method is poorly accurate for finite size $\Delta t$ and shows a large region of instability.

### B.2.2 Runge-Kutta algorithm

In order to improve the accuracy of the Euler method, the simpler solution is to consider the so-called *midpoint approximation*. In practice, once the Euler method has been applied, its solution is used as the trial function for the subsequent iteration:

$$\begin{aligned} k_1 &= \Delta t f(t_m, y_m) \\ k_2 &= \Delta t f(t_m + \frac{1}{2}\Delta t, y_m + \frac{1}{2}k_1) \\ y_{m+1} &= y_m + k_2 + \mathcal{O}(\Delta t^3). \end{aligned} \tag{B.22}$$

Equation (B.22) is called the *second order Runge-Kutta* method (RK2), and has order 2. Of course nothing prevents us from using the solution of RK2 to increase the precision of a successive iteration, and this is exactly the principle behind the subsequent orders of the algorithm. It can be shown that any successive addition eliminates approximation errors of growing order.

The most used configuration is the fourth-order Runge-Kutta algorithm (RK4), which is

$$\begin{aligned} k_1 &= \Delta t f(t_m, y_m) \\ k_2 &= \Delta t f(t_m + \frac{1}{2}\Delta t, y_m + \frac{1}{2}k_1) \\ k_3 &= \Delta t f(t_m + \frac{1}{2}\Delta t, y_m + \frac{1}{2}k_2) \\ k_4 &= \Delta t f(t_m + \Delta t, y_m + k_3) \\ y_{m+1} &= y_m + \frac{k_1}{6} + \frac{k_2}{3} + \frac{k_3}{3} + \frac{k_4}{6} + \mathcal{O}(\Delta t^5). \end{aligned} \tag{B.23}$$

In equation (B.23), the different terms represent increments based on the slope of the function at different points, and, in the averaging of the contributions, a larger influence is given to the midpoint.

A good practice is to also include in the algorithm a way to adaptively control its progress, by making frequent changes in the stepsize $\Delta t$. The principle is that when the function exhibits roughness, the step should be smaller to better capture it, while in smooth, uninteresting regions it can be assumed to be larger. This is usually achieved by comparing, with a fixed frequency in time, the results of the algorithm with a step $\Delta t_1$ and $\Delta t_2 = \Delta t_1/2$. When the difference falls below a certain imposed threshold, the larger $\Delta t_1$ can be considered, otherwise the interval is reduced. Other more refined methods imply to use different orders of Runge-Kutta to evaluate the step size. In this

thesis, depending on the problem faced, several of these techniques have been used.

## B.3 The XMDS2 software package

The numerical simulations of this thesis have been performed mainly by using two approaches:

1. A in-house solver of the SGPE, developed by the group of Prof. Nick Proukakis, and specifically by Dr. Stuart Cockburn[58,59,125], based on the Cranck-Nicholson algorithm summarised above.

2. XMDS2[2], a partial and ordinary differential equation solver, originally developed by Peter Drummond and Greg Collecutt and subsequently rewritten by Graham Dennis[126].

[2] `www.xmds.org/index.html`

[58] S. P. Cockburn. "Bose Gases In and Out of Equilibrium within the Stochastic Gross-Pitaevskii Equation". PhD thesis. Newcastle University, 2010.

[59] D. Gallucci. "Ab Initio Modelling of quasi-one-dimensional Bose gas experiments via the Stochastic Gross-Pitaevskii Equation". PhD thesis. Newcastle University, 2013.

[125] S. P. Cockburn and N. P. Proukakis. In: *Phys. Rev. A* 86 (2012), p. 033610.

[126] Dennis G. R., Hope J. J., and Johnsson M. T. In: *Computer Physics Communications* 184.1 (2013), pp. 201–208.

# Appendix C

# Two-dimensional ideal Bose gas

The very basis of the theory of Bose-Einstein condensation is represented by the study of a gas of non-interacting particles[1]. For these gases, the mean occupation number of a single-particle mode $s$ is the Bose-Einstein distribution already described in (2)

$$n(E_s) = n_s = \frac{1}{e^{\beta(E_s-\mu)} - 1}, \tag{C.1}$$

where $\beta = 1/k_{\mathrm{B}}T$ and $E_s$ denotes the energy of the state $s$. The chemical potential is determined by assuming that

$$\sum_s n_s = N. \tag{C.2}$$

Equation (C.1) tells us a very important fact. The chemical potential $\mu$ can never exceed the minimum energy $E_{\mathrm{min}}$ (usually set to be 0), otherwise the occupation of the state would become negative, and therefore unphysical. This means that the mean occupation $n_s$ can never exceed the value

$$n_s^{\mathrm{max}} = \frac{1}{e^{\beta(E_s-E_{\mathrm{min}})} - 1}, \tag{C.3}$$

which is fixed and determined by the physical parameters (and is decreasing when lowering the temperature). Thus, the number of particles that can be allocated to the excited states

$$N_{\mathrm{ex}} = \sum_{s>0} n_s \tag{C.4}$$

is finite and determined by the temperature. In very cold systems, $N_{\mathrm{ex}}$ can be less than the total number of particles $N$, leading to an accumulation of atoms in the only available state: the ground state. The particles are then said to *condense*. The critical temperature $T_c$ is defined as the last temperature for which a condensate still exists.

[1] The following treatment is largely taken from [84].

## C.1 Density of states

Let us now consider the limitations to condensation that can arise from dimensionality. In order to do this, it is useful to introduce the *density of states*. This is a usual concept in treating the thermodynamics of gases, when the sums are replaced by integrals and the quantum level structure is replaced by a continuum. For this reason, this approach fails in describing a condensed system, but it is still a sensible approximation for the excited state contribution. Given a quantum system, if $\Gamma(E)$ is the total number of states with energy less than $E$, the density of states is defined as

$$g(E) = \frac{d\Gamma(E)}{dE}. \tag{C.5}$$

### C.1.1 Uniform system

Let us now consider the relevant case of a uniform two-dimensional atomic system. Assume that a particle of mass $m$ is confined in a 2D box of dimension $L$ in the $x-y$ plane:

$$V_{\text{tr}} = \begin{cases} 0 \text{ inside the box,} \\ \infty \text{ outside.} \end{cases} \tag{C.6}$$

The solution of the Schrödinger equation for such potential is

$$\psi_{s_x,s_y} = \frac{2}{L} \sin\left(\frac{\pi}{L} s_x x\right) \sin\left(\frac{\pi}{L} s_y y\right) \tag{C.7}$$

where $s_x, s_y = 1, 2, 3, \ldots$, and the corresponding eigenenergies are

$$E = \frac{hbar^2}{2m} \frac{\pi s^2}{L^2} \equiv \frac{\hbar^2 k^2}{2m}, \tag{C.8}$$

where $s = \sqrt{s_x^2 + s_y^2}$ and $k_i = s_i \pi / L$. Hence, a unit change in the level index $s_x$ or $s_y$ corresponds to the smallest change in energy $\Delta E$. Assuming that $L \gg 1$ we can consider these quantities to be infinitesimal. Since $E \propto s^2$, all the states in the phase space lying on the circle of radius $s$ will have the same energy. Then, the number of states whose energy lies in between $E$ and $E + dE$ is an annulus of area

$$dA = 2\pi s \, ds. \tag{C.9}$$

However, since necessarily $s_x, s_y > 0$ we are only interested in a quadrant of the disk, and

$$g(E)dE = \frac{dA}{4} = \frac{\pi}{2} s \, ds. \tag{C.10}$$

Thanks to eq. (C.8) we can say that

$$\frac{ds}{dE} = \frac{1}{2}\sqrt{\frac{2m}{E}}\frac{L}{\pi\hbar}, \tag{C.11}$$

hence

$$g(E) = \frac{\pi}{2}s\frac{ds}{dE} = \frac{mL^2}{2\pi\hbar^2}. \tag{C.12}$$

An important point is that the density of states (C.12) does not depend on $E$. This is a peculiarity of the two-dimensional system, and it is possible to prove that

$$g(E) \propto E^{d/2-1} \tag{C.13}$$

for a free particle in a $d$-dimensional state.

The dependence of $g$ on $E$ has a strong consequence on the possibility for the system to present condensation. In fact, by assuming a continuum of states, eq. (C.4) becomes

$$N_{\text{ex}} = \int_0^\infty dE\, g(E)n(E). \tag{C.14}$$

Considering that, if $E_{\min} = 0$,

$$n_s^{\max} = \frac{1}{e^{\beta E} - 1} \xrightarrow[E\to 0]{} \frac{k_{\text{B}}T}{E}, \tag{C.15}$$

let us now see the different cases, from eq. (C.13):

- 3D: $g(E) \propto \sqrt{E}$, hence $N_{\text{ex}} \propto \int_0^\infty dE\,(1/\sqrt{E})$ which is convergent in $E \to 0$. The number of particles allocable to the excited modes is therefore finite, and in the thermodynamic limit $N \to \infty$ condensation is possible.
- 2D: $g(E) \propto$ const., and the integral $N_{\text{ex}} \propto \int_0^\infty dE\,(1/E)$ does not converge in $E \to 0$. There is no upper limit for the excited atoms, and condensation does not occur.

### C.1.2 Harmonic trap.

Let us now briefly present the case for an atomic gas confined in a harmonic potential

$$V(x, y) = \frac{1}{2}m(\omega_x^2 x^2 + \omega_y^2 y^2). \tag{C.16}$$

The eigenstates of the Schrödinger equation will be the Hermite-Gauss functions, and the spectrum

$$E(s_x, s_y) = \left(s_x + \frac{1}{2}\right)\hbar\omega_x + \left(s_y + \frac{1}{2}\right)\hbar\omega_y, \tag{C.17}$$

where $s_x, s_y = 0, 1, 2, \ldots$ Once again we want to compute the number of states $\Gamma(E)$ with energy less than $E$. For large energies we can treat the index $s$ as a continuous variable, and we can neglect the zero-point energy $\hbar\omega_i/2$. Then:

$$\Gamma(E) = \frac{1}{\hbar^2\omega_x\omega_y}\int_0^E dE_x \int_0^{E+E_x} dE = \frac{E^2}{2\hbar^2\omega_x\omega_y}. \tag{C.18}$$

Then, the density of states is

$$g(E) = \frac{d\Gamma(E)}{dE} = \frac{E}{\hbar^2\omega_x\omega_y}. \tag{C.19}$$

For a generic $d$-dimensional harmonic oscillator, it can be shown that

$$g(E) = \frac{E^{d-1}}{(d-1)!\prod_i \hbar\omega_i}. \tag{C.20}$$

From eq. (C.19) one can immediately see that when confined in a harmonic trap, a two-dimensional system can still exhibit Bose-Einstein condensation[2].

[2] An important note is that this is only valid for an ideal gas. In fact, even though the integral (C.14) remains finite, the density profile in the centre of the trap[78]

$$\rho(r) \overset{r\to 0}{\approx} -\frac{1}{\lambda_T^2}\log(r^2) + \text{const.}$$

is divergent, and this is not achievable for atoms with repulsive interaction. This makes the experimental realisation of atomic 2D BECs in harmonic traps challenging. However, photons in a cavity are shown to behave like a nearly ideal 2D Bose gas, with a very small effective mass. Some recent experiments[24,127,128] showed indeed that it is possible to reach Bose-Einstein condensation for an ideal gas of photons in a 2D harmonic trap.

# References


[1] F. Dalfovo, S. Giorgini, L. P. Pitaevskii, and S. Stringari. "Theory of Bose-Einstein condensation in trapped gases". In: *Rev. Mod. Phys.* 71 (3 Apr. 1999), pp. 463–512.

[2] I. Bloch, J. Dalibard, and W. Zwerger. "Many-body physics with ultracold gases". In: *Rev. Mod. Phys.* 80 (3 July 2008), pp. 885–964.

[3] S. Giorgini, L. P. Pitaevskii, and S. Stringari. "Theory of ultracold atomic Fermi gases". In: *Rev. Mod. Phys.* 80 (4 Oct. 2008), pp. 1215–1274.

[4] A. A. Starobinsky. "Dynamics of phase transition in the new inflationary universe scenario and generation of perturbations". In: *Physics Letters B* 117.3 (1982), pp. 175–178.

[5] M. Delbruck. "Was Bose-Einstein statistics arrived at by serendipity?" In: *J. Chem. Ed.* 57.7 (July 1980), p. 467.

[6] Bose. "Plancks Gesetz und Lichtquantenhypothese". In: *Zeitschrift für Physik* 26.1 (Dec. 1924), pp. 178–181.

[7] A. Einstein. "Quantentheorie des einatomigen idealen Gases". In: *Sitz. der Preus. Akad. der Wiss.* (1924).

[8] A. Einstein. "Quantentheorie des einatomigen idealen Gases - Zweite Abhandlung". In: *Sitz. der Preus. Akad. der Wiss.* (1925).

[9] P. Kapitza. "Viscosity of Liquid Helium below the $\lambda$-Point". In: *Nature* 141 (Jan. 1938), p. 74.

[10] F. London. "The $\lambda$-Phenomenon of Liquid Helium and the Bose-Einstein Degeneracy". In: *Nature* 141 (Apr. 1938), p. 643.

[11] L. D. Landau. "Theory of the Superfluidity of Helium II". In: *Phys. Rev.* 60 (4 Aug. 1941), pp. 356–358. (original Rus.) Zh. Eksp. Teor. Fiz. 11 (1941) p. 592.

[12] N. N. Bogoliubov. "On the theory of superfluidity". In: *J. Phys U.S.S.R.* 11.1 (1947), p. 23.

[13] O. Penrose and L. Onsager. "Bose-Einstein Condensation and Liquid Helium". In: *Phys. Rev.* 104 (3 Nov. 1956), pp. 576–584.

[14] L. Onsager. "Statistical hydrodynamics". In: *Il Nuovo Cimento* 6 (Mar. 1949), pp. 279–287.

[15] R.P. Feynman. *Chapter II Application of Quantum Mechanics to Liquid Helium*. Ed. by C. J. Gorter. Vol. 1. Progress in Low Temperature Physics Supplement C. Elsevier, 1955, pp. 17–53.

[16] H. E. Hall and W. F. Vinen. "The rotation of liquid helium II II. The theory of mutual friction in uniformly rotating helium II". In: *Proceedings of the Royal Society of London A: Mathematical, Physical and Engineering Sciences* 238.1213 (1956), pp. 215–234.

[17] C. E. Hecht. "The possible superfluid behaviour of hydrogen atom gases and liquids". In: *Physica* 25.7 (1959), pp. 1159–1161.

[18] Isaac F. Silvera and J. T. M. Walraven. "Stabilization of Atomic Hydrogen at Low Temperature". In: *Phys. Rev. Lett.* 44 (3 Jan. 1980), pp. 164–168.

[19] Dale G. Fried, Thomas C. Killian, Lorenz Willmann, David Landhuis, Stephen C. Moss, Daniel Kleppner, and Thomas J. Greytak. "Bose-Einstein Condensation of Atomic Hydrogen". In: *Phys. Rev. Lett.* 81 (18 Nov. 1998), pp. 3811–3814.

[20] M. H. Anderson, J. R. Ensher, M. R. Matthews, C. E. Wieman, and E. A. Cornell. "Observation of Bose-Einstein Condensation in a Dilute Atomic Vapor". In: *Science* 269.5221 (1995), pp. 198–201.

[21] K. B. Davis, M. -O. Mewes, M. R. Andrews, N. J. van Druten, D. S. Durfee, D. M. Kurn, and W. Ketterle. "Bose-Einstein Condensation in a Gas of Sodium Atoms". In: *Phys. Rev. Lett.* 75 (22 Nov. 1995), pp. 3969–3973.

[22] C. A. Regal, M. Greiner, and D. S. Jin. "Observation of Resonance Condensation of Fermionic Atom Pairs". In: *Phys. Rev. Lett.* 92 (4 Jan. 2004), p. 040403.

[23] Fang Fang, Ryan Olf, Shun Wu, Holger Kadau, and Dan M. Stamper-Kurn. "Condensing Magnons in a Degenerate Ferromagnetic Spinor Bose Gas". In: *Phys. Rev. Lett.* 116 (9 Mar. 2016), p. 095301.

[24] J. Klaers, J. Schmitt, F. Vewinger, and M. Weitz. "Bose–Einstein condensation of photons in an optical microcavity". In: *Nature* 468 (Nov. 2010), p. 545.

[25] J. Kasprzak, M. Richard, S. Kundermann, A. Baas, P. Jeambrun, J. M. J. Keeling, F. M. Marchetti, M. H. Szymańska, R. André, J. L. Staehli, V. Savona, P. B. Littlewood, B. Deveaud, and Le Si Dang. "Bose–Einstein condensation of exciton polaritons". In: *Nature* 443 (Sept. 2006), p. 409.

[26] L. Pitaevskii and S. Stringari. *Bose-Einstein Condensation and Superfluidity.* Oxford University Press, 2016.

[27] S. Serafini, M. Barbiero, M. Debortoli, S. Donadello, F. Larcher, F. Dalfovo, G. Lamporesi, and G. Ferrari. "Dynamics and Interaction of Vortex Lines in an Elongated Bose-Einstein condensate". In: *Phys. Rev. Lett.* 115 (17 Oct. 2015), p. 170402.

[28] E. P. Gross. "Structure of a quantized vortex in boson systems". In: *Il Nuovo Cimento* 20 (1961), pp. 454–457.

[29] L. P. Pitaevskii. "Vortex lines in an imperfect Bose gas". In: *Soviet Physics JETP-USSR* 13.2 (1961). (original Rus.) Zh. Eksp. Teor. Fiz. 40 (1961) p. 646.

[30] Y. Castin. "Bose-Einstein Condensates in Atomic Gases: Simple Theoretical Results". In: *Coherent atomic matter waves.* Ed. by R. Kaiser, C. Westbrook, and F. David. 2001, p. 1.

[31] W. Thomson (Lord Kelvin). "Vibrations of a columnar vortex". In: *Philos. Mag.* 10 (1880), p. 155.

[32] V. Bretin, P. Rosenbusch, F. Chevy, G. V. Shlyapnikov, and J. Dalibard. "Quadrupole Oscillation of a Single-Vortex Bose-Einstein Condensate: Evidence for Kelvin Modes". In: *Phys. Rev. Lett.* 90 (10 Mar. 2003), p. 100403.

[33] Alexander L. Fetter. "Kelvin mode of a vortex in a nonuniform Bose-Einstein condensate". In: *Phys. Rev. A* 69 (4 Apr. 2004), p. 043617.

[34] N. P Proukakis and B. Jackson. "Finite-temperature models of Bose–Einstein condensation". In: *J. Phys. B* 41 (Oct. 2008), p. 203002.

[35] T. D. Lee and C. N. Yang. "Many-Body Problem in Quantum Mechanics and Quantum Statistical Mechanics". In: *Phys. Rev.* 105 (3 Feb. 1957), pp. 1119–1120.

[36] T. D. Lee, Kerson Huang, and C. N. Yang. "Eigenvalues and Eigenfunctions of a Bose System of Hard Spheres and Its Low-Temperature Properties". In: *Phys. Rev.* 106 (6 June 1957), pp. 1135–1145.

[37] S. Donadello, S. Serafini, M. Tylutki, L. P. Pitaevskii, F. Dalfovo, G. Lamporesi, and G. Ferrari. "Observation of Solitonic Vortices in Bose-Einstein condensates". In: *Phys. Rev. Lett.* 113 (6 Aug. 2014), p. 065302.

[38] D. V. Freilich, D. M. Bianchi, A. M. Kaufman, T. K. Langin, and D. S. Hall. "Real-Time Dynamics of Single Vortex Lines and Vortex Dipoles in a Bose-Einstein Condensate". In: *Science* 329.5996 (2010), pp. 1182–1185.

[39] S. Serafini, L. Galantucci, E. Iseni, T. Bienaimé, R. N. Bisset, C. F. Barenghi, F. Dalfovo, G. Lamporesi, and G. Ferrari. "Vortex Reconnections and Rebounds in Trapped Atomic Bose-Einstein Condensates". In: *Phys. Rev. X* 7 (2 May 2017), p. 021031.

[40] L. P. Pitaevskii. "Hydrodynamic theory of motion of quantized vortex rings in trapped superfluid gases". In: *ArXiv e-prints* (Nov. 2013). arXiv: `1311.4693 [cond-mat.quant-gas]`.

[41] M. J. H. Ku, W. Ji, B. Mukherjee, E. Guardado-Sanchez, L. W. Cheuk, T. Yefsah, and M. W. Zwierlein. "Motion of a Solitonic Vortex in the BEC-BCS Crossover". In: *Phys. Rev. Lett.* 113 (6 Aug. 2014), p. 065301.

[42] C. Menotti, P. Pedri, and S. Stringari. "Expansion of an Interacting Fermi Gas". In: *Phys. Rev. Lett.* 89 (25 Dec. 2002), p. 250402.

[43] Hui Hu, A. Minguzzi, Xia-Ji Liu, and M. P. Tosi. "Collective Modes and Ballistic Expansion of a Fermi Gas in the BCS-BEC Crossover". In: *Phys. Rev. Lett.* 93 (19 Nov. 2004), p. 190403.

[44] A. L. Fetter and J.-k. Kim. "Vortex Precession in a Rotating Nonaxisymmetric Trapped Bose-Einstein Condensate". In: *J. Low Temp. Phys.* 125.5 (Dec. 2001), pp. 239–248.

[45] Vladimir V. Konotop and Lev Pitaevskii. "Landau Dynamics of a Grey Soliton in a Trapped Condensate". In: *Phys. Rev. Lett.* 93 (24 Dec. 2004), p. 240403.

[46] G. Lamporesi, S. Donadello, S. Serafini, F. Dalfovo, and G. Ferrari. "Spontaneous creation of Kibble-Zurek solitons in a Bose-Einstein condensate". In: *Nat Phys* 9.10 (Oct. 2013), pp. 656–660.

[47] M. S. Paoletti and D. P. Lathrop. "Quantum Turbulence". In: *Ann. Rev. of Cond. Mat. Phys.* 2.1 (2011), pp. 213–234.

[48] A. Sinatra, C. Lobo, and Y. Castin. "Classical-Field Method for Time Dependent Bose-Einstein Condensed Gases". In: *Phys. Rev. Lett.* 87 (21 Nov. 2001), p. 210404.

[49] BV Svistunov. "Highly nonequilibrium Bose condensation in a weakly interacting gas". In: *J. Moscow Phys. Soc* 1 (1991), p. 373.

[50] M. Brewczyk, M. Gajda, and K. Rzażewski. "Classical fields approximation for bosons at nonzero temperatures". In: *J. Phys. B* 40.2 (2007), R1.

[51] H. T. C. Stoof. "Coherent Versus Incoherent Dynamics During Bose-Einstein Condensation in Atomic Gases". In: *J. Low Temp. Phys.* 114.1 (Jan. 1999), pp. 11–108.

[52] H. T. C. Stoof and M. J. Bijlsma. "Dynamics of Fluctuating Bose–Einstein Condensates". In: *J. Low Temp. Phys.* 124.3 (Aug. 2001), pp. 431–442.

[53] R. A. Duine and H. T. C. Stoof. "Stochastic dynamics of a trapped Bose-Einstein condensate". In: *Phys. Rev. A* 65 (1 Dec. 2001), p. 013603.

[54] HTC Stoof. "Quantum kinetic theory of trapped atomic gases". In: *Dynamics: Models and Kinetic Methods for Non-equilibrium Many Body Systems*. Springer, 2000, pp. 491–502.

[55] P. B. Blakie, A. S. Bradley, M. J. Davis, R. J. Ballagh, and C. W. Gardiner. "Dynamics and statistical mechanics of ultra-cold Bose gases using c-field techniques". In: *Advances in Physics* 57.5 (2008), pp. 363–455.

[56] H. T. C. Stoof. "Initial Stages of Bose-Einstein Condensation". In: *Phys. Rev. Lett.* 78 (5 Feb. 1997), pp. 768–771.

[57] L. V. Keldysh. "Diagram Technique for Nonequilibrium Processes". In: *JETP* 20 (4 Apr. 1965), p. 1515.

[58] S. P. Cockburn. "Bose Gases In and Out of Equilibrium within the Stochastic Gross-Pitaevskii Equation". PhD thesis. Newcastle University, 2010.

[59] D. Gallucci. "Ab Initio Modelling of quasi-one-dimensional Bose gas experiments via the Stochastic Gross-Pitaevskii Equation". PhD thesis. Newcastle University, 2013.

[60] M. J. Davis, T. M. Wright, P. B. Blakie, A. S. Bradley, R. J. Ballagh, and C. W. Gardiner. "C-Field Methods for Non-Equilibrium Bose Gases". In: *Quantum Gases*. Imperial College Press, 2013, pp. 163–175.

[61] C. W. Gardiner, J. R. Anglin, and T. I. A. Fudge. "The stochastic Gross-Pitaevskii equation". In: *J. Phys. B* 35.6 (2002), p. 1555.

[62] M. Davis, N. Proukakis, S. Gardiner, and M. Szymańska. *Quantum Gases: Finite Temperature and Non-Equilibrium Dynamics*. Cold atoms. Imperial College Press, 2013. ISBN: 9781848168121.

[63] C W Gardiner and M J Davis. "The stochastic Gross–Pitaevskii equation: II". In: *J. Phys. B* 36.23 (2003), p. 4731.

[64] C. W. Gardiner and P. Zoller. "Quantum kinetic theory: A quantum kinetic master equation for condensation of a weakly interacting Bose gas without a trapping potential". In: *Phys. Rev. A* 55 (4 Apr. 1997), pp. 2902–2921.

[65] C. W. Gardiner and P. Zoller. "Quantum kinetic theory. III. Quantum kinetic master equation for strongly condensed trapped systems". In: *Phys. Rev. A* 58 (1 July 1998), pp. 536–556.

[66] C. W. Gardiner and P. Zoller. "Quantum kinetic theory. V. Quantum kinetic master equation for mutual interaction of condensate and noncondensate". In: *Phys. Rev. A* 61 (3 Feb. 2000), p. 033601.

[67] M. J. Davis, S. A. Morgan, and K. Burnett. "Simulations of Bose Fields at Finite Temperature". In: *Phys. Rev. Lett.* 87 (16 Sept. 2001), p. 160402.

[68] M. J. Davis, S. A. Morgan, and K. Burnett. "Simulations of thermal Bose fields in the classical limit". In: *Phys. Rev. A* 66 (5 Nov. 2002), p. 053618.

[69] S. J. Rooney, P. B. Blakie, and A. S. Bradley. "Numerical method for the stochastic projected Gross-Pitaevskii equation". In: *Phys. Rev. E* 89 (1 Jan. 2014), p. 013302.

[70] A. A. Penckwitt, R. J. Ballagh, and C. W. Gardiner. "Nucleation, Growth, and Stabilization of Bose-Einstein Condensate Vortex Lattices". In: *Phys. Rev. Lett.* 89 (26 Dec. 2002), p. 260402.

[71] S. P. Cockburn, A. Negretti, N. P. Proukakis, and C. Henkel. "Comparison between microscopic methods for finite-tempe rature Bose gases". In: *Phys. Rev. A* 83 (4 Apr. 2011), p. 043619.

[72] C. N. Weiler, T. W. Neely, D. R. Scherer, A. S. Bradley, M. J. Davis, and B. P. Anderson. "Spontaneous vortices in the formation of Bose-Einstein condensates". In: *Nature* 455 (Oct. 2008), p. 948.

[73] I.-K. Liu, S. Donadello, G. Lamporesi, G. Ferrari, S.-C. Gou, F. Dalfovo, and N. P. Proukakis. "Dynamical Equilibration Across a Quenched Phase Transition in a Trapped Quantum Gas". In: *ArXiv e-prints* (Dec. 2017). arXiv: 1712.08074.

[74] M. Kobayashi and L. F. Cugliandolo. "Quench dynamics of the three-dimensional U(1) complex field theory: Geometric and scaling characterizations of the vortex tangle". In: *Phys. Rev. E* 94 (6 Dec. 2016), p. 062146.

[75] R. E. Peierls. "Über die statistischen Grundlagen der Elektronentheorie der Metalle". In: *Helv. Phys. Acta* 7 (1934), p. 24.

[76] N. D. Mermin and H. Wagner. "Absence of Ferromagnetism or Antiferromagnetism in One- or Two-Dimensional Isotropic Heisenberg Models". In: *Phys. Rev. Lett.* 17 (22 Nov. 1966), pp. 1133–1136.

[77] P. C. Hohenberg. "Existence of Long-Range Order in One and Two Dimensions". In: *Phys. Rev.* 158 (2 June 1967), pp. 383–386.

[78] J. Dalibard. *Lecture notes in "Quantum Fluids in low dimension and Kosterlitz-Thouless transition" (in French)*. 2017.

[79] J. M. Kosterlitz and D. J. Thouless. "Ordering, metastability and phase transitions in two-dimensional systems". In: *J. Phys. C* 6.7 (1973), p. 1181.

[80] Y. Kagan, B. V. Svistunov, and G. V. Shlyapnikov. "Influence on inelastic processes of the phase transition in a weakly collisional two-dimensional Bose gas". In: *Sov. Phys. JETP* 66.2 (1987), p. 314.

[81] J. Dalibard. *Lecture notes in "Coherence and superfluidity in atomic gases" (in French)*. 2015.

[82] S. T. Bramwell and P. C. W. Holdsworth. "Magnetization: A characteristic of the Kosterlitz-Thouless-Berezinskii transition". In: *Phys. Rev. B* 49 (13 Apr. 1994), pp. 8811–8814.

[83] C. Mora and Y. Castin. "Extension of Bogoliubov theory to quasicondensates". In: *Phys. Rev. A* 67 (5 May 2003), p. 053615.

[84] C. J. Pethick and H. Smith. *Bose–Einstein Condensation in Dilute Gases*. 2nd ed. Cambridge University Press, 2008.

[85] P. Nozieres and D. Pines. *Theory of Quantum Liquids*. Advanced Books Classics. Avalon Publishing, 1999. ISBN: 9780813346533.

[86] N. Prokof'ev, O. Ruebenacker, and B. Svistunov. "Critical Point of a Weakly Interacting Two-Dimensional Bose Gas". In: *Phys. Rev. Lett.* 87 (27 Dec. 2001), p. 270402.

[87] N. Prokof'ev and B. Svistunov. "Two-dimensional weakly interacting Bose gas in the fluctuation region". In: *Phys. Rev. A* 66 (4 Oct. 2002), p. 043608.

[88] S. Pilati, S. Giorgini, and N. Prokof'ev. "Critical Temperature of Interacting Bose Gases in Two and Three Dimensions". In: *Phys. Rev. Lett.* 100 (14 Apr. 2008), p. 140405.

[89] IM Lifshitz. "Kinetics of ordering during second-order phase transitions". In: *Sov. Phys. JETP* 15 (1962), p. 939. (Original Rus.) Zh, Eksp. Teor. Fiz. 42, 1354 (1962).

[90] Samuel M. Allen and John W. Cahn. "A microscopic theory for antiphase boundary motion and its application to antiphase domain coarsening". In: *Acta Metallurgica* 27.6 (1979), pp. 1085–1095.

[91] T. W. B. Kibble. "Topology of cosmic domains and strings". In: *J. Phys. A* 9.8 (1976), p. 1387.

[92] W. H. Zurek. "Cosmological experiments in superfluid helium?" In: *Nature* 317 (Oct. 1985), p. 505.

[93] W. H. Zurek. "Cosmological experiments in condensed matter systems". In: *Phys. Rep.* 276.4 (1996), pp. 177–221.

[94] C. Bäuerle, Y. M. Bunkov, S. N. Fisher, H. Godfrin, and G. R. Pickett. "Laboratory simulation of cosmic string formation in the early Universe using superfluid 3He". In: *Nature* 382 (July 1996), p. 332.

[95] V. M. H. Ruutu, V. B. Eltsov, A. J. Gill, T. W. B. Kibble, M. Krusius, Y. G. Makhlin, B. Plaçais, G. E. Volovik, and W. Xu. "Vortex formation in neutron-irradiated superfluid 3He as an analogue of cosmological defect formation". In: *Nature* 382 (July 1996), p. 334.

[96] R. Carmi and E. Polturak. "Search for spontaneous nucleation of magnetic flux during rapid cooling of $YBa_2Cu_3O_{7-\delta}$ films through $T_c$". In: *Phys. Rev. B* 60 (10 Sept. 1999), pp. 7595–7600.

[97] R. Carmi, E. Polturak, and G. Koren. "Observation of Spontaneous Flux Generation in a Multi-Josephson-Junction Loop". In: *Phys. Rev. Lett.* 84 (21 May 2000), pp. 4966–4969.

[98] K. Pyka, J. Keller, H. L. Partner, R. Nigmatullin, T. Burgermeister, D. M. Meier, K. Kuhlmann, A Retzker, M. B. Plenio, W. H. Zurek, A. del Campo, and T. E. Mehlstäubler. "Topological defect formation and spontaneous symmetry breaking in ion Coulomb crystals". In: *Nature Communications* 4 (Aug. 2013), p. 2291.

[99] A. del Campo and W. H. Zurek. "Universality of phase transition dynamics: Topological defects from symmetry breaking". In: *Int. J. Mod. Phys. A* 29.08 (2014), p. 1430018.

[100] G. Dagvadorj, J. M. Fellows, S. Matyja śkiewicz, F. M. Marchetti, I. Carusotto, and M. H. Szyma ńska. "Nonequilibrium Phase Transition in a Two-Dimensional Driven Open Quantum System". In: *Phys. Rev. X* 5 (4 Nov. 2015), p. 041028.

[101] G. W. Stagg. "A Numerical Study of Vortices and Turbulence in Quantum Fluids". PhD thesis. Newcastle University, 2016.

[102] A. Jelić and L. F. Cugliandolo. "Quench dynamics of the 2d XY model". In: *J. Stat. Mech.* 2011.02 (2011), P02032.

[103] B. Yurke, A. N. Pargellis, T. Kovacs, and D. A. Huse. "Coarsening dynamics of the XY model". In: *Phys. Rev. E* 47 (3 Mar. 1993), pp. 1525–1530.

[104] A. J. Bray, A. J. Briant, and D. K. Jervis. "Breakdown of Scaling in the Nonequilibrium Critical Dynamics of the Two-Dimensional *XY* Model". In: *Phys. Rev. Lett.* 84 (7 Feb. 2000), pp. 1503–1506.

[105] P. Comaron, G. Dagvadorj, A. Zamora, I. Carusotto, N. P. Proukakis, and M. H. Szymańska. "Dynamical critical exponents in driven-dissipative quantum systems". In: *ArXiv e-prints* (Aug. 2017). arXiv: 1708.09199.

[106] S. P. Cockburn, A. Negretti, N. P. Proukakis, and C. Henkel. "Comparison between microscopic methods for finite-temperature Bose gases". In: *Phys. Rev. A* 83 (4 Apr. 2011), p. 043619.

[107] R. G. McDonald and A. S. Bradley. "Reservoir interactions during Bose-Einstein condensation: Modified critical scaling in the Kibble-Zurek mechanism of defect formation". In: *Phys. Rev. A* 92 (3 Sept. 2015), p. 033616.

[108] L. A. Williamson and P. B. Blakie. "Universal Coarsening Dynamics of a Quenched Ferromagnetic Spin-1 Condensate". In: *Phys. Rev. Lett.* 116 (2 Jan. 2016), p. 025301.

[109] Michał Kulczykowski and Michał Matuszewski. "Phase ordering kinetics of a nonequilibrium exciton-polariton condensate". In: *Phys. Rev. B* 95 (7 Feb. 2017), p. 075306.

[110] M. Ota, F. Larcher, F. Dalfovo, L. Pitaevskii, N. P. Proukakis, and S. Stringari. "Collisionless sound in a uniform two-dimensional Bose gas". In: *ArXiv e-prints* (Apr. 2018). arXiv: 1804.04032 [cond-mat.quant-gas].

[111] J. L. Ville, R. Saint-Jalm, É. Le Cerf, M. Aidelsburger, S. Nascimbène, J. Dalibard, and J. Beugnon. "Sound propagation in a uniform superfluid two-dimensional Bose gas". In: *ArXiv e-prints* (Apr. 2018). arXiv: 1804.04037 [cond-mat.quant-gas].

[112] E. A. Kuznetsov and Turitsyn S. K. "Instability and collapse of solitons in media with a defocusing nonlinearity". In: *JETP* 67.8 (1988). (original Rus.) Zh. Eksp. Teor. Fiz. 94 (1988) p. 119.

[113] P.G. Kevrekidis, D.J. Frantzeskakis, and R. Carretero-González. *The Defocusing Nonlinear Schrödinger Equation: From Dark Solitons to Vortices and Vortex Rings*. Other Titles in Applied Mathematics. SIAM, 2015. ISBN: 9781611973945.

[114] E. Zaremba, T. Nikuni, and A. Griffin. "Dynamics of trapped Bose gases at finite temperatures". In: *J. Low Temp. Phys.* 116.3-4 (1999), pp. 277–345.

[115] T. Ozawa and S. Stringari. "Discontinuities in the First and Second Sound Velocities at the Berezinskii-Kosterlitz-Thouless Transition". In: *Phys. Rev. Lett.* 112 (2 Jan. 2014), p. 025302.

[116] J. L. Ville, T. Bienaimé, R. Saint-Jalm, L. Corman, M. Aidelsburger, L. Chomaz, K. Kleinlein, D. Perconte, S. Nascimbène, J. Dalibard, and J. Beugnon. "Loading and compression of a single two-dimensional Bose gas in an optical accordion". In: *Phys. Rev. A* 95 (1 Jan. 2017), p. 013632.

[117] D. S. Petrov and G. V. Shlyapnikov. "Interatomic collisions in a tightly confined Bose gas". In: *Phys. Rev. A* 64 (1 June 2001), p. 012706.

[118] L.P. Kadanoff and G. Baym. *Quantum statistical mechanics: Green's function methods in equilibrium and nonequilibrium problems*. Frontiers in physics. W.A. Benjamin, 1962.

[119] I.M. Khalatnikov. *An introduction to the theory of superfluidity*. W.A. Benjamin, 1965.

[120] R. Brown. "A brief account of microscopical observations made on the particles contained in the pollen of plants". In: *Philosophical Magazine* 4 (1828), pp. 161–173.

[121] A. Einstein. "Über die von der molekularkinetischen Theorie der Wärme geforder te Bewegung von in ruhenden Flüssigkeiten suspendierten Teilchen". In: *Annalen der Physik* 17 (1905), pp. 549–560.

[122] H. Risken and T. Frank. *The Fokker-Planck Equation: Methods of Solution and Applications*. Springer Series in Synergetics. Springer-Verlag Berlin Heidelberg, 1996.

[123] Reif F. *Fundamentals Of Statistical And Thermal Physics*. McGraw-Hill Series in Fundamentals of Physics. McGraw-Hill Science/Engineering/Math, 1965.

[124] W. H. Press, Flannery B. P., Teukolsky S. A., and Vetterling W. T. *Numerical Recipes in Fortran 77: the art of Scientific Computing*. 2nd ed. Cambridge University Press, 1993. ISBN: 0521437164.

[125] S. P. Cockburn and N. P. Proukakis. "*Ab initio* methods for finite-temperature two-dimensional Bose gases". In: *Phys. Rev. A* 86 (3 Sept. 2012), p. 033610.

[126] Dennis G. R., Hope J. J., and Johnsson M. T. "XMDS2: Fast, scalable simulation of coupled stochastic partial differential equations". In: *Computer Physics Communications* 184.1 (2013), pp. 201–208.

[127] J. Marelic and R. A. Nyman. "Experimental evidence for inhomogeneous pumping and energy-dependent effects in photon Bose-Einstein condensation". In: *Phys. Rev. A* 91 (3 Mar. 2015), p. 033813.

[128] J. Marelic, L. F Zajiczek, H. J Hesten, K. H Leung, E. Y X Ong, F. Mintert, and R. A Nyman. "Spatiotemporal coherence of non-equilibrium multimode photon condensates". In: *New Journal of Physics* 18.10 (2016), p. 103012.